4D crust-mantle evolution of the Western Superior Craton: implications for Archaean granite-greenstone petrogenesis and geodynamics

Katarina Edith Bjorkman

HBsc, Lakehead University, Canada

This thesis is presented for the degree of Doctor of Philosophy of The University of Western Australia

Centre for Exploration Targeting
School of Earth and Environment
Geology

2017

Supervisors: Dr Anthony I. S. Kemp
Dr T. Campbell McCuaig
Dr Yongjun Lu
Dr Peter N. Hollings
Dr Marco Fiorentini

Of old, Lord, you laid the foundations of the earth,
and the heavens are the work of your hands.
They will perish, but you remain;
they will all wear out like a garment.
You will roll them up like a robe;
like a garment they will be changed.
But you remain the same,
and your years will never end.
Hebrews 1:10-12

For my parents,

Karl and Veronique,

THESIS DECLARATION

I, Katarina Edith Bjorkman, certify that:

This thesis has been substantially accomplished during enrolment in the degree.

This thesis does not contain material that has been accepted for the award of any other degree or diploma in my name, in any university or other tertiary institution.

No part of this work will, in the future, be used in a submission in my name for any other degree or diploma in any university or other tertiary institution without the prior approval of The University of Western Australia and where applicable, any partner institution responsible for the joint-award of this degree.

This thesis does not contain any material previously published or written by another person, except where due reference has been made in the text.

The work(s) are not in any way a violation or infringement of any copyright, trademark, patent, or other rights whatsoever of any person.

The work described in this thesis was funded by the Australian Research Council (ARC) Centre of Excellence for Core to Crust Fluid Systems (CCFS), Flagship Program 2 – Genesis, transfer and focus of fluids and metals. UWA SIRF, UIS and UIS top-up scholarships funded Katarina Bjorkman during the PhD Candidature.

Technical assistance was kindly provided by Hao Gao, Dr Cristina Talavera and Dr Allen Kennedy for U-Pb isotope determination on the SHRIMP II at the John De Laeter Centre, Curtin University that is described in Chapter 3, Dr Heejin Jeon and Dr Matt Kilburn for O isotope measurements in zircons using the Cameca 1280, CMCA, UWA that is described in Chapters 4 and 6, and Dr Yi Hu for Hf isotope collection by laser ablation at Advanced Analytical Centre, James Cook University, Townsville that is described in Chapters 4 and 6.

This thesis contains published work and/or work prepared for publication, some of which has been co-authored.

Signature: 

Date: March 20th 2017

ABSTRACT

New, spatially constrained, U-Pb, Lu-Hf and O isotopic measurements on igneous-hosted zircons challenge the paradigm of exotic pre-Kenoran terranes in the Western Superior Craton. The Western Superior Craton comprises two parallel Paleo – Meso – Neoarchaean south-younging sequences, the Hudson Bay – North Caribou – Uchi and Winnipeg River – Marmion – (Western Wabigoon, Eastern Wabigoon and Wawa) terranes respectively. Hafnium isotope-time arrays, spanning 600 m.y. of magmatism, display an outstanding unity across these alternating volcanic-plutonic terranes and intervening sedimentary basins. This isotopic coherence is therefore consistent with linked, rather than exotic, growth of terranes.

Hafnium isotope compositions form three coherent and diachronous segments across all terranes. Zircon Hf is (I) unradiogenic at 3.26 – 3.02 Ga, (II) superchondritic at 3.02 – 2.76 Ga, and (III) trends steeply to less radiogenic Hf compositions from 2.76 – 2.67 Ga. Oxygen isotopes in zircons are mantle-like until 2.7 Ga, when they rise sharply to heavier compositions. A model reconciling the isotopic record involves Paleoarchaean rifting and basin development during Segments I & II, and subsequent basin closure and collision in Segment III. Craton-wide, high-flux magmatism during Segment III reworked and recycled a portion of Segment I & II crust, but mixing with a mantle-derived endmember masks this contribution. Structural repetition reconciles an original along-strike arrangement of the two parallel Paleo – Meso – Neoarchaean south-younging sequences by late dextral displacement on craton-wide strike-slip faults during transpression accompanying the late stages of the Kenoran Orogeny.

The $^{176}Hf/^{177}Hf$ of the Mesoarchaean mantle source inferred from these data is lower than the hypothetical depleted MORB mantle typically used in model crust formation age calculations. This disparity translates into Hf depleted mantle model ages that overestimate crustal residence times and Early Archaean crustal volumes. Depleted mantle model ages are even more erroneously old for the high flux event of Segment III, which sourced an enriched, metasomatised mantle. Thus, Hf model ages do not faithfully represent a major crust-forming event at 2.7 Ga in the Superior Craton.

Secular whole rock geochemical trends corresponding to the isotopic work presented herein, suggest that the Hf-O isotope time array represents a TTG-sanukitoid progression. A shift in whole rock chemistry at 2.75 Ga involves increased variation in major oxide compositions and some incompatible trace elements. This reflects changing magma source compositions and greater ranges in melting and fractionation depths, corroborating isotopic evidence for a change in magma petrogenesis at 2.76 Ga. A shift to higher abundances of both highly compatible and incompatible elements at 2.7 Ga reflects sanukitoid and late voluminous granite-granodiorite magmatism.

Elemental variations show that sanukitoids are highly differentiated mantle-derived melts. Their peculiar enrichments in LILE, LREE, transition elements and PGE-Au reflects combined fractional crystallisation, melt replenishment and magma mixing with sediment-derived melt. Elevated PGE patterns in sanukitoid and coeval mantle-derived mafic intrusions resemble those of local sedimentary rocks, with the implication that sediment-derived melts contributed to the PGE budget. A sediment-derived contribution is corroborated by elevated zircon $\delta^{18}O$ and by modelling of Hf-O isotope arrays. The appearance of sanukitoids reflects (i) the sudden widespread availability of sedimentary material, (ii) transport of this material to depth by subduction and thrusting, (iii) preferential melting of sedimentary rock in a high thermal regime, and (iv) horizontal compression that trapped magmas at great crustal depths where extreme differentiation could proceed.

The Western Superior Hf-O arrays and TTG-sanukitoid transitions are typical of Archaean cratons globally. Accordingly, this magmatic and isotopic pattern likely reflects a global Archaean process. This process involved the local onset of subduction and collision, which in turn, required rigid plates, allowing for thick crust, extensive sedimentation and mixing of originally bimodal magmatism. The sanukitoids therefore mark the end of bimodal granite-greenstone assemblages and the beginning of widespread andesitic magmatism and clastic sedimentation.

TABLE OF CONTENTS

Table of contents

Table of contents

TABLE OF FIGURES

Table of figures

Table of figures

ACKNOWLEDGEMENTS

I thank my supervisors, Anthony Kemp, Campbell McCuaig, Yongjun Lu, Peter Hollings and Marco Fiorentini. I am grateful for their contribution to my project and their impact on my growth.

Cam's vision to map the lithospheric architecture for mineral systems targeting was the inspiration for this PhD. I thank Cam for entrusting this project to me. His time in the field, together with Yongjun, was instructive, intense and remains a highlight. I aspire to his ability to grasp key features within complexity and readily communicate the essence to others. Yongjun radiates energy; he is full of ideas. I thank him for the early months of training for imaging and isotopic analytical techniques. He made himself available and approachable in the early season of my PhD. Pete encouraged me to embark on this journey. His feedback and communication are always rapid, concise and cheerful. I am so thankful for his help and support near the end of my PhD. A vivacious Marco was influential in shaping my written communication via my proposal. I thank him for supporting my endeavours throughout my PhD.

Tony bore the lion's share of my supervision. He gave me the freedom to work through my data and develop ideas. I thank him for his patience and direction. Through his supervision, granite petrogenesis and crustal growth has transformed from a vague enigma to an intriguing concept for me. Tony brightens conversation with his sincerity and humorous illustrations. His scientific rigour and innovation are an inspiration to me. I will miss his guidance.

I thank the Ontario Geological Survey for support. Jack Parker agreed to fund geochemical analyses through GeoLabs. Gary Beakhouse spent two days giving me a whirlwind field trip of the Western Wabigoon terrane, through the lens of his experience. Folks at the Ministry of Northern Development and Mines were cheerful and supportive, and Rob Cundari aided in early fieldwork.

Dr Janet Muhling (SEM, Centre for Microscopy, Characterisation and Analysis, UWA), Hao Gao, Dr Cristina Talavera and Dr Allen Kennedy (SHRIMP II, John De Laeter Centre, Curtin University), Dr Heejin Jeon and Dr Matt Kilburn (Cameca 1280, CMCA, UWA) and Dr Yi Hu (Laser, Advanced Analytical Centre, James Cook University, Townsville) provided friendly and professional technical assistance.

Michael Djohan provided extraordinary IT service. His generosity was legendary. Estelle Dawes, Cindi Dunjey, Wendy Carter, Susie Cass, Gillian Evans and Hayley Newberry at the CET have made administrative life easy. Luis Para-Avila, Linda Iaccheri, Jessica Bogossian, Johannes

Hammerli, Quentin Maserel, Dave Stevenson, Natalie Yeung, Denis Fougerouse, Crystal Laflamme and Heta Lampinen made office life light and fun.

I owe much of my love for the outdoors and rocks to my prospecting family. My family provided company in the field. They also lent trucks, boats and ATVs for access. Karla provided ongoing field assistance, making camping excursions memorable. I am so grateful for Ruth and Jessica's help with the arrangement of my tables and appendices. I thank my dad for his love and curiosity for truth and for his wisdom in my distresses. My dad's songs were so often the melody in my heart and tune on my lips, encouraging me that as 'The earth is spinning towards the sunshine', 'I am in the hollow of his hand' 'And he loves me', and 'His name is Jesus', to name a few. My mom shines joy, light and love into so many lives. Her voice on the phone is the one of sweetest things I can imagine. I love you Mom, Dad, Jess, Bjorn, Ruth, Veronique and Karla. Thank you for caring for my horse and for visiting me Down Under! I thank my Opa for his support and love. I also thank my uncles and aunts for their support, especially Uncle Eric and Aunt Bonnie.

To all the Aussies who welcomed me into your life, thank you. You are a quality crew, and made Perth home during these last four years. I treasure the music, dinner and southern adventures we shared: Scott Davies, Mark Davies, Wendy Green, Rob Westenhaver, Boyd Zurg, Lorne McCrum, Truc Pham, Kim Reynolds, Louise Stan-Bishop, Scott Hardie, Annette Fraser, Sarah and Matt MacDonald, Aaron and Ellie Mitchell, Ziech and Caroline Van Onselen, Arlene Gregory, Grace and Leonard Ochieng and Rita Rizzeri. You are truly my brothers and sisters and I will always love you as such.

Drs Jennifer and Neil Turner shared their home, breaking all their tenant rules and allowing me to stay in paradise much longer than planned. Neil is a great scientist and, like Jennifer, an excellent mentor. I have gained much from our many shared dinner conversations.

I thank Jesus, the Rock of my soul. As my Shepherd, he has walked with me through the hills and valleys. It is such joy and strength to know my Heavenly Father loves me.

AUTHORSHIP DECLARATION: CO-AUTHORED PUBLICATIONS

This thesis contains work that has been prepared for publication.

Details of the work: Late Archaean geodynamic changes in the Southwestern Superior Craton implied from secular geochemistry of felsic intrusions *(U-Th-Pb isotope measurements in zircons and interpretation of whole rock geochemistry)*
Location in thesis: Chapter 3
Student contribution to work: 90%
Co-author signatures and dates: (signed on Yongjun Lu Anthony I. S. Kemp [redacted] (signed on behalf of all co-authors 20-3-17) T. Campbell McCua Peter N. Hollings

Details of the work: Autochthonous growth of the Western Superior Craton inferred from Hf-O isotopes *(Oxygen and hafnium isotope measurements in igneous zircons)*
Location in thesis: Chapter 4
Student contribution to work: 90%
Co-author signatures and dates: Anthony I. S. Kemp [redacted] (signed on behalf of all co-authors 20-3-17) Yongjun Lu Peter N. Hollings T. Campbell McCuaig

Details of the work: Enrichment in Late Archaean sanukitoids by partial melting, fractionation, replenishment and magma mixing *(Field and petrographic investigations and interpretation of whole rock geochemistry)*
Location in thesis: Chapter 5
Student contribution to work: 90%
Co-author signatures and dates: Anthony I. S. Kemp [redacted] (signed on behalf of all co-authors 20-3-17) Yongjun Lu Peter N. Hollings T. Campbell McCuaig

Details of the work: Zircon O and Hf isotope evidence for widespread supracrustal recycling during sanukitoid formation in the Western Superior Craton *(Trace element measurements in zircons)*
Location in thesis: Chapter 6
Student contribution to work: 90%
Co-author signatures and dates: Anthony I. S. Kemp [redacted] (signed on behalf of all co-authors 20-3-17) Yongjun Lu Peter N. Hollings T. Campbell McCuaig

I, Anthony I.S. Kemp certify that the student statements regarding their contribution to each of the works listed above are correct

Coordinating supervisor signature: [redacted]

Date: 20 March 2017

Chapter 1: Introduction

1.1. CONTEXT AND PROBLEM IDENTIFICATION

The formation of Archaean crust is contentious (Dhuime et al., 2011; Hawkesworth et al., 2016; Kemp and Hawkesworth, 2013). Did Archaean oceanic lithosphere possess the negative buoyancy and stiffness to subduct (see van Hunen and Moyen, 2012), thereby producing preserved continents? Thin, dense Phanerozoic oceanic crust is recycled back into the mantle within 200 m.y. of formation (Rudnick and Gao, 2003), but subduction, like other crust formation processes, leaves a physiochemical fingerprint in the continental crust. Remnants of the continental crust have survived for billions of years, making it the physiochemical record to Earth's ancient past (Kemp and Hawkesworth, 2013). Nevertheless, this partial rock record allows for non-unique geodynamic scenarios. Accordingly, Archaean crustal growth models range widely between Phanerozoic-like plate tectonics (Percival et al., 2012) and subductionless variations (Bédard et al., 2013; Johnson et al., 2014). As the largest coherent Archaean craton, the Superior Craton in Canada has the potential to shed light on this debate.

1.1.1. Continental crust

Earth's continental crust is a rich storehouse of metals and nutrients vital for humanity. The growth of continents in the Archaean concentrated critical ore reserves (Barley et al., 1998; Champion and Huston, 2016; Robert et al., 2005), and influenced the development and nature of the atmosphere, hydrosphere and biosphere (Campbell and Allen, 2008). Consequently, the mechanisms and timing of Archaean crustal growth is central to Earth science. However, the inferred once-voluminous Archaean crustal volumes (~70% of current volumes; Belousova et al., 2010; Dhuime et al., 2011; Figure 1-1) now comprise a small fraction of exposed continents (Bleeker, 2002; Figure 1-1), resulting in a biased record and various conflicting interpretations.

The growth of continents reflects the chemical differentiation of the silicate Earth (mantle and crust) (Hawkesworth and Kemp, 2006) driven by secular cooling (Ashwal et al., 1987; Labrosse and Jaupart, 2007). Proto-Earth underwent extreme chemical segregation into core-mantle-crust by 4.45 Ga (Allègre et al., 2008). The timeline and means of the silicate Earth's evolution from a postulated magma ocean to its current configuration is speculative. Most models invoke an evolution from continent-free mafic crust and involve a stagnant lid to mobile lid transition (Hamilton, 2011; Harris and Bédard, 2014; Hawkesworth et al., 2016; Johnson et al., 2017; Kamber, 2015; Kemp et al., 2010).

Crustal growth involves mass transfer from the mantle to the crust. Mantle-derived magmas are, however, basaltic, whereas bulk continental crust is andesitic and enriched in incompatible elements (Taylor and McLennan, 1985; Weaver and Tarney, 1984). Therefore, mass balance requires that

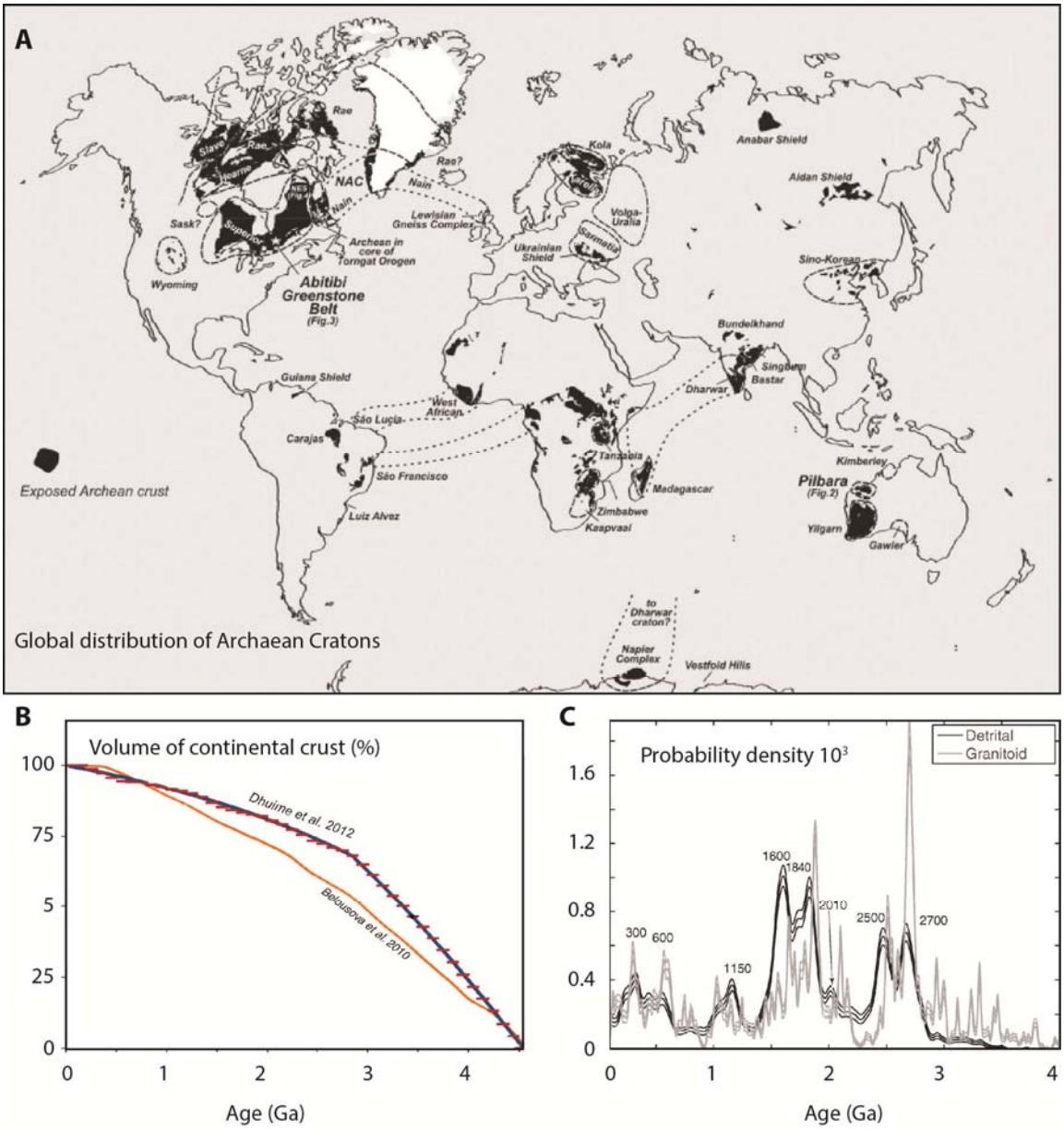

Figure 1-1: A. Global distribution of Archaean cratons from Bleeker (2002) and modified by Bédard et al. (2013). B. Crustal growth curves estimated from Hf isotopes in detrital zircons (Belousova et al., 2010; Dhuime et al., 2012). C. Peaks in the U-Pb zircon record in detrital and granite-hosted zircons (Condie and Aster, 2010).

mantle-derived basalts are reworked, such that differentiated material is added to the crust and residual material is returned to the mantle (Ellam and Hawkesworth, 1988; Herzberg et al., 1983; Rudnick, 1995). Reworking is the 'physical reprocessing of continental material by magmas, metamorphism, or fluids within the crust, or by alteration, weathering, erosion, or sedimentation processes at Earth's surface' (Kemp and Hawkesworth, 2013).

Phanerozoic continental evolution largely reflects magmatic extraction and distillation at convergent margins, for example, along the Pacific Rim (Cawood et al., 2009; Davidson and Arculus, 2006; Jagoutz and Kelemen, 2015; Kemp et al., 2009; Rudnick, 1995). Differentiation of arc magmas shifts their composition to andesitic and enriches them in incompatible elements (DeBari and Greene, 2011; Ducea et al., 2015; Kelemen, 1995). Thickened depleted mafic lower arc crust delaminates into the mantle (Ducea, 2002; Jull and Kelemen, 2001; Kay and Mahlburg-Kay, 1991).

Phanerozoic subduction is largely driven by the negative buoyancy of old, cold oceanic lithosphere and metamorphic transformation of oceanic crust to eclogite (Hamilton, 2007). In many models, the Archaean mantle and crust was hotter and less viscous (Bickle, 1978; Herzberg et al., 2010; Korenaga, 2008; Labrosse and Jaupart, 2007). Thus, Archaean oceanic crust may have lacked the necessary density and rigidity to sink into the mantle (Sizova et al., 2010; van Hunen and van den Berg, 2008). Accordingly, interpretations remain divided between Archaean subduction settings and plume or mantle upwelling.

1.1.2. Archaean crustal growth

Archaean cratons preserve peaks in igneous emplacement and mantle extraction ages (Condie, 1998; Figure 1-1). Episodic mantle depletion events corroborate the inferred pulses of crust formation (Parman, 2007; Pearson et al., 2007). Because subduction is continuous, the periodicity of the Archaean record may reflect emplacement of mantle plumes (Condie, 1998; Stein and Hofmann, 1994), episodic subduction (O'Neill et al., 2007) or biased preservation imposed on continuous growth (Belousova et al., 2010; Cawood et al., 2013; Hawkesworth et al., 2016; Spencer et al., 2015; Voice et al., 2011). Because interpretations of age peaks guide models of crustal growth, clarifying their origin by analysis of the rock record is important for crustal growth models. Chapters 3 and 4 address the origin of crustal growth peaks and implications for the crust-mantle evolution using U-Pb geochronology and Hf-O isotope compositions in zircons.

Archaean crust typically comprises contemporaneous bimodal tonalite-trondhjemite-granodiorite (TTG) – greenstone (subaqueous komatiitic basalt) sequences (Arndt, 1999; Condie, 1994; Nisbet et al., 1993; Wilson et al., 1978). Calc-alkaline and boninitic signatures (Polat and Kerrich, 2000; Smithies et al., 2005; Wyman et al., 2000) and horizontal shortening (Card, 1990; Percival et al., 2006) underpin key arguments for an uniformitarian interpretation. However, calc-alkaline and boninitic signatures can be created without subduction by partial melting of basaltic lower crust with residual garnet, amphibole and rutile, and localised fluxing of refractory mantle respectively (Bédard et al., 2013; Smithies et al., 2009). Moreover, greenstone belts contain basalt and komatiite

with an enriched chemistry most akin to oceanic plateaux (Arndt, 1999; Condie, 1994; Hollings and Kerrich, 1999). Thus, subduction models require widespread plume-arc interaction to explain plateau-like chemistry (e.g., Hollings and Wyman, 1999).

There is some agreement that TTG generation requires a two-step process whereby enriched basaltic magma extracted from the mantle is subsequently chemically modified by melting or crystal fractionation in the presence of garnet ± amphibole (Arth and Barker, 1976; Barker and Arth, 1976; Drummond and Defant, 1990; Foley et al., 2002; Martin, 1987; Moyen, 2011; Moyen and Martin, 2012; Rapp et al., 1991). However, there are competing views on the nature of the mechanism affording chemical modification. Models include: (i) direct melting of subducting oceanic crust (Barker and Arth, 1976; Martin, 1987; Rapp et al., 1991), (ii) remelting the base of a thickened volcanic pile by underplating with new hot magma, possibly coupled with magmatic fractionation of the new magma (Bédard, 2006; Johnson et al., 2017; Polat, 2012; Smithies et al., 2009), (iii) infracrustal differentiation by fractional crystallisation (Barker and Arth, 1976; Kamber et al., 2002), or (iv) delamination and dripping of the lower mafic crust into the mantle in combination with local crustal thickening and overturns (Sizova et al., 2015). Whether the bimodal character of TTG and basalt-komatiite can be explained by formation in similar or contrasting settings has much to bear on the favoured models of TTG genesis. This conundrum is addressed in Chapters 3 and 4.

1.1.3. When did plate tectonics begin?

A fundamental question concerns the onset of plate tectonics on Earth. Herein, plate tectonics involves global mantle convection where deformation is concentrated along plate boundaries (van Hunen and Moyen, 2012). Models range from as early as the Hadean (Armstrong and Harmon, 1981; Hastie et al., 2016; Hopkins et al., 2008) through the Archaean (Dhuime et al., 2012; Næraa et al., 2012; Shirey and Richardson, 2011; Smart et al., 2016; Smithies et al., 2005; Van Kranendonk, 2011) and Proterozoic (Bédard, 2006; Brown, 2006; Hamilton, 1998). Many workers envision a transition involving episodic subduction between a stagnant lid and modern plate tectonics (O'Neill et al., 2007; van Hunen and Moyen, 2012). Major shifts in Earth's physicochemical record are candidates for the timing of the onset of plate tectonics. Therefore, recognising these shifts, and the processes they reflect, is critical.

The late Archaean (3.0 to 2.5 Ga) was a time of isotopic and geochemical shifts (Dhuime et al., 2015; Keller and Schoene, 2012; Laurent et al., 2014; Martin et al., 2005). A global peak in precious and base mineral systems is contemporaneous with a major peak in crustal growth at 2.7 Ga (Barley et al., 1998; Campbell and Allen, 2008). This time also corresponds with the beginning

of major changes in the hydrosphere and atmosphere as recorded in O, C and S and Sr isotopes (Campbell and Allen, 2008; Jaffrés et al., 2007; Kump and Barley, 2007; Lyons et al., 2014; Shields, 2007). The shifts may reflect changes in Archaean geodynamics and the nature of the continental crust and lithosphere, making this time period an exciting candidate for investigating long debated ambiguities of Archaean geology.

Late Archaean diversification of magmatism manifests in the TTG-sanukitoid transition. Prolonged sodic TTG magmatism culminated in emplacement of large potassic crustal melts and the potassic mantle-derived sanukitoid suite (Beakhouse, 2007; Bédard, 2006; Corfu and Stone, 1998; Frost et al., 2006; Laurent et al., 2014). This transition followed a similar sequence in all Archaean terranes, but occurred at different times in different cratons, suggesting a global Archaean process (Heilimo et al., 2013; Laurent et al., 2011; Smithies and Champion, 2000). Clarifying this process has global implications for Archaean geodynamics and crustal growth and is addressed in Chapters 3-6.

High compatible and fluid-mobile elements in sanukitoid magmatism suggests the involvement of a subduction-modified mantle wedge, and may provide concrete evidence for subduction (Laurent et al., 2014; Martin et al., 2010; Rapp et al., 2010; Shirey and Hanson, 1984; Smithies and Champion, 2000). Understanding the petrogenesis of sanukitoid rocks is therefore important for understanding the transition in the late Archaean to modern potassic magmatism. Detailed petrogenetic investigation in Chapters 5 and 6 investigate the sources, differentiation processes and conditions that contributed to the unique physiochemistry of the sanukitoid suite, and its significance for crustal growth and geodynamics.

1.1.4. Geological setting of the Western Superior Craton

In spite of decades of detailed characterisation, the geodynamic evolution of Earth's largest preserved Archaean craton, (1.4x10-6 km2; >3.7 – 2.6 Ga; Figure 1-2; Hoffman, 1988) remains contentious (Bédard, 2013; Bédard et al., 2013; Hamilton, 2011; Hansen, 2015; Maurice et al., 2009; Parmenter et al., 2006; Percival et al., 2006; Wyman, 2013b). The Western Superior Craton is a collage of linear volcano-plutonic terranes separated by sedimentary basins with a prominent east-west orientation (Card and Ciesielski, 1986; Stott, 2011). Widespread sedimentation and compression during the 2.7 Ga Kenoran Orogeny records the progressive north to south assembly of linear terranes into a coherent craton (Card, 1990; Percival et al., 2006; and references therein).

Langford and Morin (1976) proposed that the volcano-plutonic and sedimentary subprovinces represent island arcs and accretionary prisms, respectively. Geochronological (Beakhouse et al., 1988; Corfu, 1988; Corfu et al., 1998; Davis et al., 1988; Krogh et al., 1976; Melnyk et al., 2006)

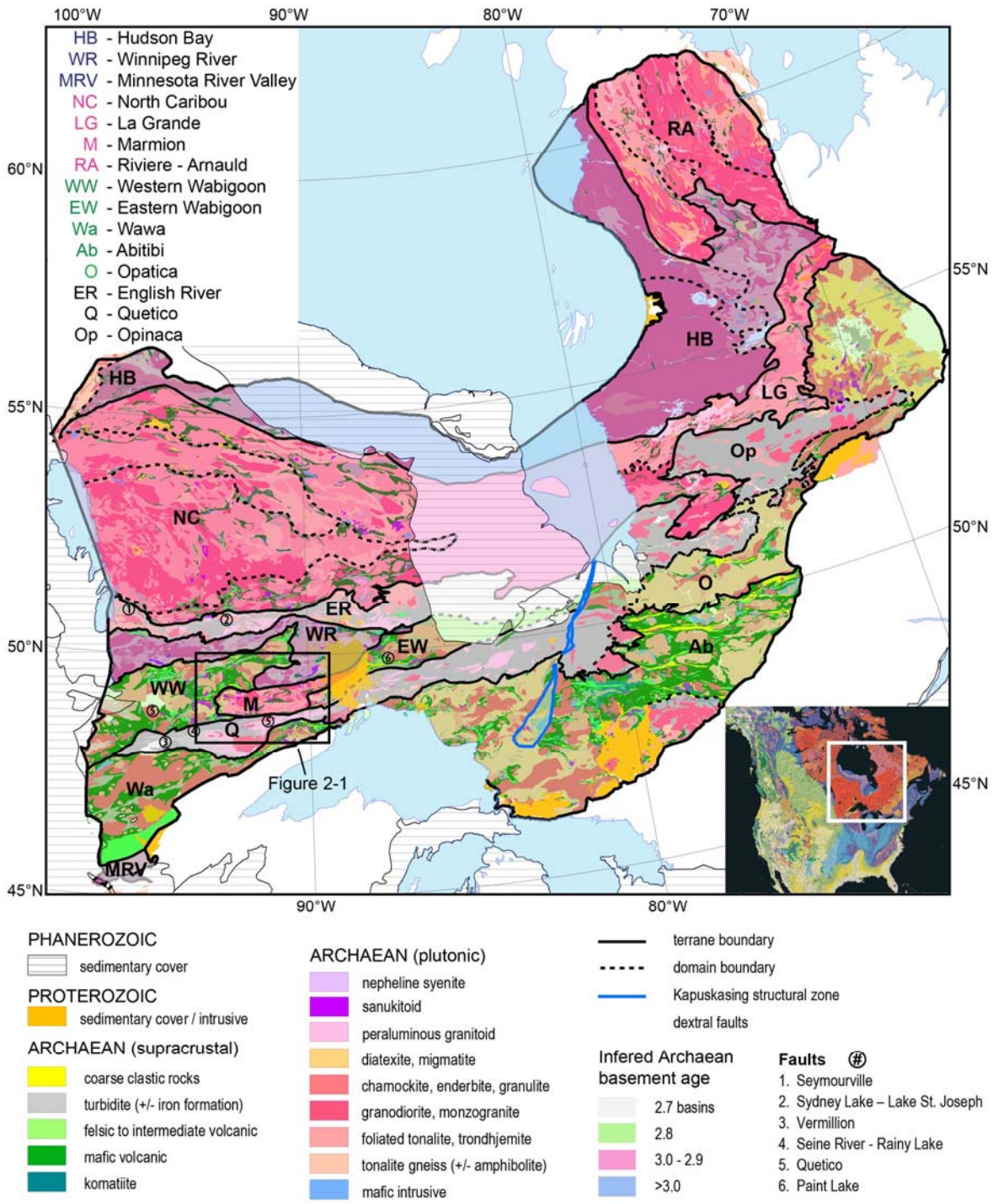

Figure 1-2: Geology of the Superior Craton, illustrating the east-west trend of volcano-plutonic terranes and intervening sedimentary basins in the Western Superior. Geology is compiled from provincial and state digital maps from Manitoba (Viljoen et al., 1999), Minnesota (Jirsa et al., 2011), Ontario (Ontario Geological Survey, 2003), and from a digitized version of Quebec (MRN (Ministère des Ressources naturelles), 2002). Tectonic subdivisions adopted from (Stott, 2011), (Percival et al., 2012) and Chapter 3; basement ages are emphasised by colour for clarity. Black box indicates extent of

Figure 2-1. Inset: Tectonic map of North America outlining the figure extent. Terrane abbreviations listed at top left. Faults listed at bottom right.

and Nd isotopic studies (Henry et al., 1998; Henry et al., 2000; Tomlinson et al., 2004) recognised a Mesoarchaean heritage for five of the volcano-plutonic terranes. These include, from north to south, the >3.8 Ga Hudson Bay (Böhm et al., 2000; Böhm et al., 2003), 3.0 Ga North Caribou (Stott, 1997; Stott and Corfu, 1991), 3.4 Ga Winnipeg River (Beakhouse, 1991; Henry et al., 1998), 3.0 Ga Marmion (Davis and Jackson, 1988; Tomlinson et al., 2003), and 3.6 Ga Minnesota River Valley (Bickford et al., 2006; Satkoski et al., 2013) terranes.

Seismic profiles image south-dipping structures north of the North Caribou terrane and north-dipping structures south of it (Figure 1-3; White et al., 2003). This has been used to support the idea of Thurston et al. (1991) that the North Caribou terrane formed the nucleus to which the Hudson Bay terrane was accreted from the north, and Winnipeg River – Marmion terrane from the south (Percival et al., 2006).

Distinct isotope-age domains within older fragments bolstered a plate tectonic interpretation (e.g., Henry et al., 1998; Tomlinson et al., 2004). However, the boundaries between terranes are commonly cryptic in both geological and geophysical datasets, and so the natures of the boundaries remain unresolved. Moreover, a Hf isotopic study by Davis et al. (2005) highlighted similarities between the North Caribou and Marmion terranes, suggesting a shared history. As the Paleoarchaean Winnipeg River terrane and 2.7 Ga English River basin (Corfu et al., 1995; Davis, 1996) separate the North Caribou and Marmion, their relationship is enigmatic (Davis et al., 2005). Other workers have noted stratigraphic (Ayer et al., 2002; Fralick et al., 2008; Thurston, 2002) and geophysical (Bédard and Harris, 2014) continuity or similarity across terrane boundaries. Resolving the nature of isotopic, geologic and geophysical boundaries is imperative for understanding the crustal evolution of the craton, and for geodynamic models of the Superior Craton.

Tectonic models of the Western Superior Craton favour accretionary settings involving subduction (Percival et al., 2012; Wyman, 2013a) or subcretion (Bédard et al., 2013) during the Neoarchaean, but models for the Paleo to Mesoarchaean evolution are divided. The widespread occurrence of non-arc basalt (Hollings and Kerrich, 1999; Tomlinson et al., 1999) and platformal sequences (Thurston and Chivers, 1990) suggests intraplate magmatism involving plumes or rifting. Accordingly, Mesoarchaean tectonic models favour either plume-related intraplate settings (Fralick et al., 2008) or plume-arc interaction (Wyman and Hollings, 1998).

The Wabigoon superterrane contains four isotopically distinct terranes (Henry et al., 1998; Tomlinson et al., 2004). It records a Paleoarchean history in the Winnipeg River terrane in the north (Corfu, 1988; Davis et al., 1988; Henry et al., 1998), and a protracted Mesoarchaean record in the Marmion terrane in the south, with events not commonly preserved in other parts of the craton (Stone and Davis, 2006). Internal margins based on Nd isotopes (Tomlinson et al., 2004) are cryptic in geology (Stott et al., 2010) and geophysics (Musacchio et al., 2004; Figure 1-3). The Wabigoon superterrane records extended TTG magmatism culminating in sanukitoid magmatism, but otherwise lacks an obvious chemical evolution (Stone, 2010). Oxygen isotopes measured in zircons across the Western Superior Craton highlight a marked transition from mantle-like to heavy compositions with the intrusion of the Sanukitoid suite at 2.7 Ga, hinting at a change in magma source compositions (King et al., 1998). Together, this makes the Wabigoon superterrane an ideal natural laboratory from which to interrogate the Archaean record.

1.2. AIMS

This study applies an in-situ isotopic inquiry of igneous rock-hosted zircons combined with whole rock major and trace element geochemistry to address key controversies of Archaean crustal growth and geodynamic evolution. Principal objectives include to:

(i) develop the chronological and stratigraphic framework of the Western Superior Craton;
(ii) investigate secular and spatial chemical variations and their causes;
(iii) constrain magma sources and differentiation histories through time and space;
(iv) illuminate the significance of the transient sanukitoid suite and the origin of their peculiar geochemistry;
(v) map lithospheric blocks through time and space and unravel the nature of isotopic boundaries;
(vi) unravel the geodynamic evolution of the Superior Craton to clarify the meaning of TTG-sanukitoid transitions globally, and
(vii) to contribute to models of late Archaean crust and mantle evolution.

1.3. APPROACH

Isotopic systems are powerful tracers of crustal growth and, when applied to granites, yield information not only about the continental crust they largely constitute, but also the lesser known lower crust and mantle lithosphere that they commonly sample. Apart from zircon U-Pb geochronology, previous work in the Western Superior Craton has largely focussed on whole rock chemical, isotopic, petrologic and belt to terrane scale geophysical signatures to investigate the crust (Corfu and Stone, 1998; Tomlinson et al., 2004; White et al., 2003). Deformation and

metamorphism commonly overprint these features after emplacement, and magmatic differentiation can obscure deeper level processes and the identity of magma sources.

This thesis integrates in-situ zircon isotope and trace element analyses with field observations, petrography and whole-rock geochemistry of felsic to intermediate intrusive rocks of the southwestern Superior Craton (see Figure 1-3). Isotopic and chemical variations in igneous rocks reflect magma sources and the conditions of partial melting and differentiation (Adam and Green, 1994; DePaolo, 1981; DePaolo and Wasserburg, 1979; Green, 1995; Langmuir et al., 1978). As

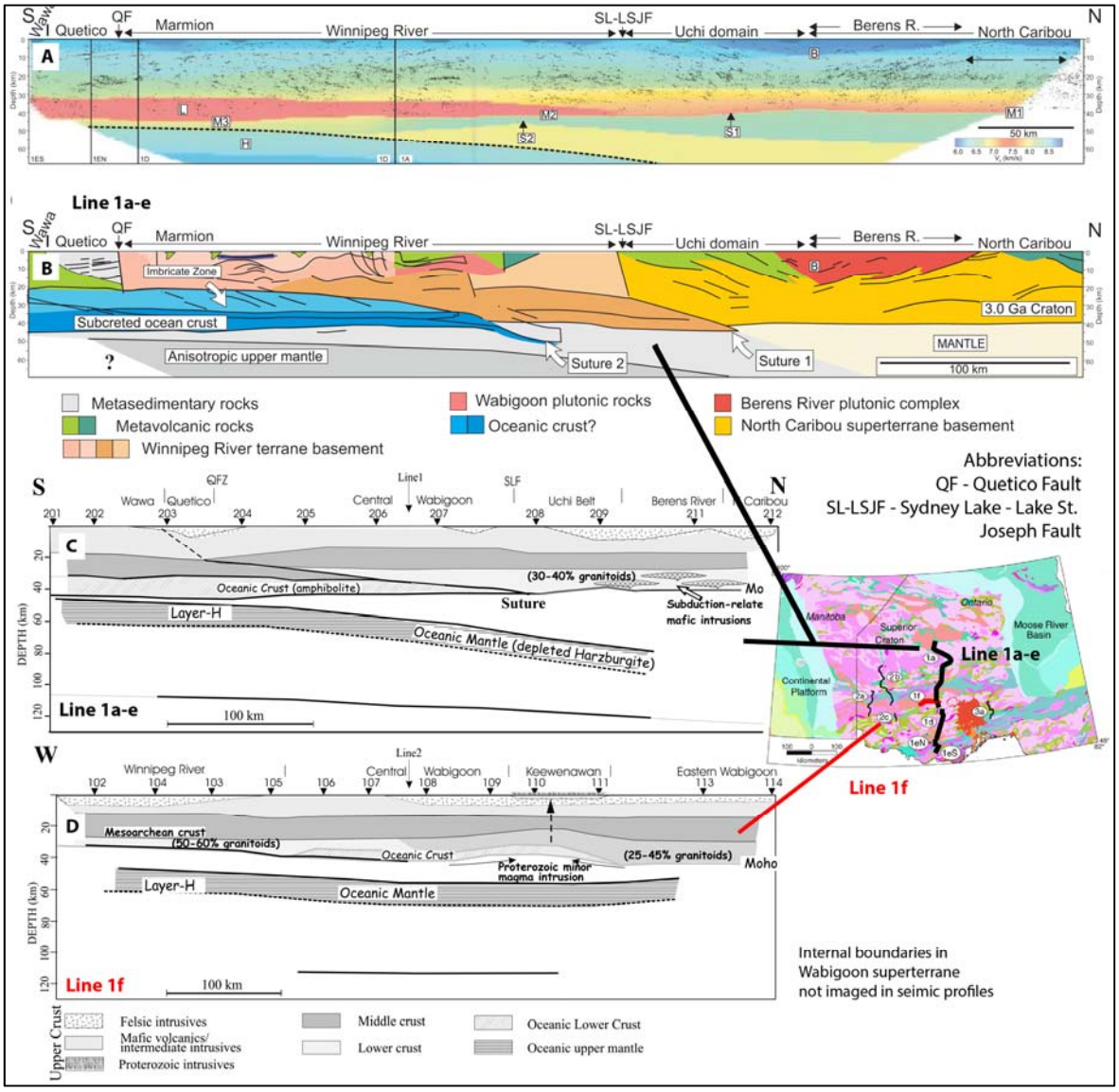

Figure 1-3: A. Seismic image of Lithoprobe WS Line 1 a-e (N-S; black) and B. interpretations from White et al. (2003) modified by Percival et al. (2006) and C. interpretation from Musacchio et al., 2004. D. Interpretation of line f (E-W; red) across the Wabigoon superterrane, where internal boundaries are not recognised (Musacchio et al., 2004).

tectonic setting influences sources and the depth of melting and differentiation, the isotopic and chemical variations can potentially unravel the geodynamic evolution (e.g., Andonaegui et al., 2016; Draut and Clift, 2001; Loucks, 2014; Lu et al., 2015; Murphy and Nance, 2002; Yogodzinski et al., 2010).

Felsic to intermediate intrusive rocks were the focus of the sampling effort because they represent the largest volume of Archaean crust preserved, and they are likely to contain zircons. A relatively evenly spaced sampling density allowed for spatial analysis of chemical and isotopic data. Representatives of all felsic to intermediate compositions were taken to better understand secular variations of the crust as recorded by trace elements and isotope systems.

Trace elements are particularly useful as petrogenetic tracers because they tend to partition into particular mineral phases as a function of P, T, composition and redox conditions (Adam and Green, 1994; Drake and Weill, 1975; Green, 1994; Irving, 1978; Nash and Crecraft, 1985). Due to their low abundance, trace elements approximate Henry's law behaviour of proportionality, making them relatively easy to model given the distribution coefficients (Irving, 1978; McIntire, 1963). Strongly compatible elements are sensitive to the extent of differentiation because they partition into early-crystallising phases. Strongly incompatible elements provide insight into the degree of partial melting and the residual and early-crystallising mineral assemblage. However, magmatic processes during differentiation, particularly involving accessory phases in granites, can strongly affect trace elements (Allègre et al., 1978; DePaolo, 1981; Hildreth and Moorbath, 1988). Isotopic variations are sensitive to contamination, with potential to identify, but also see through, the modifying effects of crystallisation and contamination (Bennett et al., 1993; DePaolo, 1981; Hawkesworth and Vollmer, 1979; Langmuir et al., 1978; Taylor, 1980).

Zircon resists isotopic and elemental disturbance through many tectono-thermal and sedimentary processes (Cherniak and Watson, 2003). The zircon lattice concentrates valuable radiogenic (U-Pb, Lu-Hf) and stable (O) isotope systems and trace elements such as REE (rare earth elements: La to Lu) and HFSE (high field strength elements: Zr-Hf, Ti) (Cherniak and Watson, 2003; Watson and Cherniak, 1997). In-situ analytical methods permit spatially resolved analyses of various zircon growth domains. This enables dating of zircon core and rims with potential to unravel a multistage thermal and metamorphic evolution, and subsequent isotopic and trace element analyses in the same zircon domains (Kemp and Hawkesworth, 2013).

Lutetium is more compatible in residual mantle peridotite phases than Hf, so over time the mantle evolves to higher Lu/Hf, and consequently higher $^{176}Hf/^{177}Hf$ (Patchett et al., 1981) in accordance

with the ^{176}Lu decay constant (Söderlund et al., 2004). Meanwhile, the crust evolves to less radiogenic Hf, along a trajectory defined by its Lu/Hf (Vervoort and Patchett, 1996). Putative evolution lines determined for the hypothetical depleted MORB mantle (Griffin et al., 2002) and the Chondritic Uniform Reservoir (Bouvier et al., 2008), allow comparison with the evolution of silicate reservoirs and estimates of crustal residence age (Payne et al., 2016). Calculated crustal residence ages are fraught with significant uncertainties over (i) the veracity of the hypothetical depleted MORB mantle curve in ^{176}Hf/^{177}Hf –time space and (ii) the estimation of the Lu/Hf of the crustal source, which can only be calculated if a number of determinations form a coherent trend in ^{176}Hf/^{177}Hf-time space (Vervoort and Kemp, 2016). This investigation applies ^{176}Hf/^{177}Hf-age relations to qualify, rather than quantify, variations in source age and composition.

Oxygen isotopes fingerprint a contribution from a supracrustal source. Near-surface hydrosphere-rock interaction enriches ^{18}O in the solid, imparting a heavy signature to supracrustal rocks compared with the relatively homogenous mantle (Eiler, 2001). Magmatic fractionation in zircons during crystallisation is largely offset by the co-crystallisation of ^{18}O-rich mineral phases such as quartz. Therefore, zircons that crystallise from magmas in equilibrium with the mantle have a very narrow range in $\delta^{18}O_{zrc}$ of 5.3 ± 0.6 (2σ) ‰ (Valley et al., 1998). Together, Hf and O isotopes in zircons have potential to resolve the extent of recycling and reworking versus juvenile magmatic addition, provided basement rocks have a contrasting isotopic composition (Kemp et al., 2007; Scherer et al., 2007; Yang et al., 2007).

Zircon elemental variations can illuminate a dynamic magmatic evolution (Claiborne et al., 2006; Claiborne et al., 2010; Dilles et al., 2015). Key insights gained from trace elements in zircons include: (i) magmatic oxidation states and water contents from Ce and Eu anomalies (Ballard et al., 2002; Burnham and Berry, 2012; Dilles et al., 2015; Hoskin and Schaltegger, 2003; Lu et al., 2016), (ii) the temperature of zircon crystallisation from Ti concentration (Ferry and Watson, 2007; Watson and Harrison, 2005), and (iii) evolving magma composition from variations in Zr/Hf, U, Th and REE patterns (Claiborne et al., 2006; Kemp et al., 2007).

Neodymium and Hf isotope maps can be used to provide a spatial picture of juvenile growth and reworking through time and map the architecture of the deep crust and mantle lithosphere (Champion and Cassidy, 2007; Champion and Huston, 2016; Mole et al., 2014; Wang et al., 2016). This thesis applies spatial mapping to complement graphical representations.

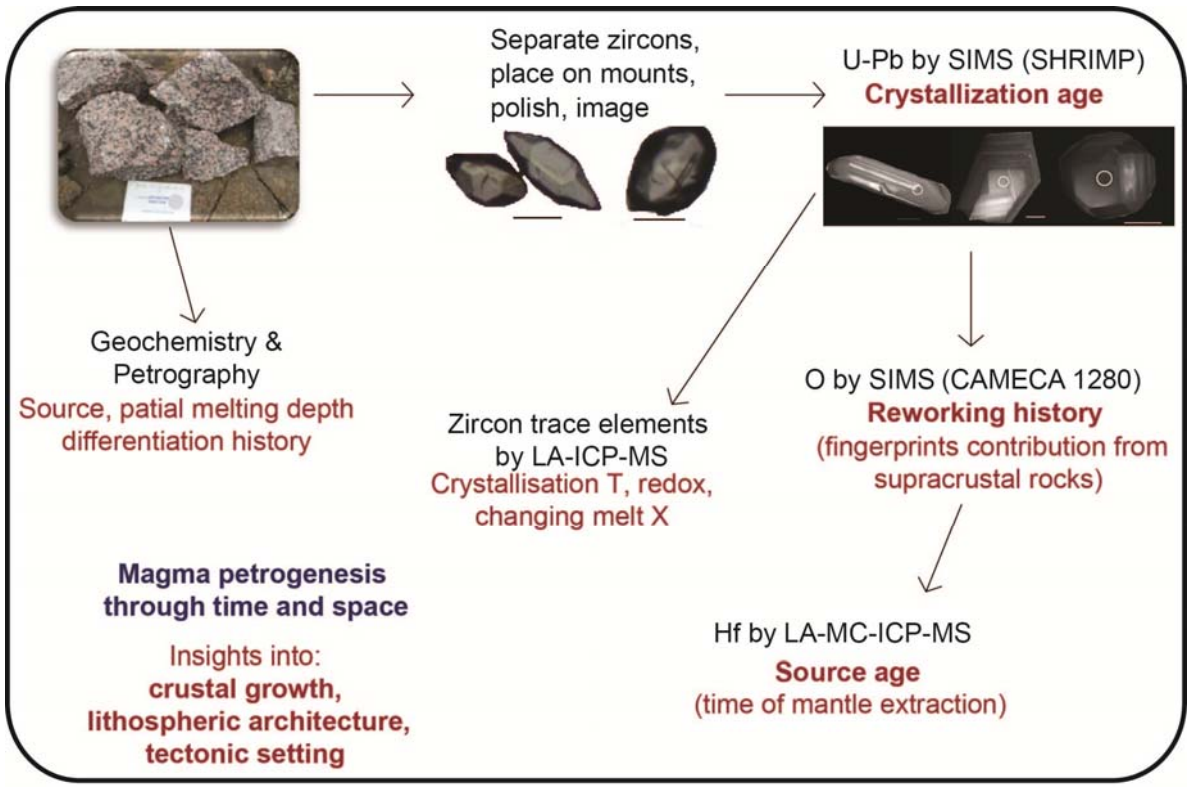

Figure 1-4: Schematic illustration of approach employed in this investigation.

1.4. SIGNIFICANCE AND INNOVATION

This thesis has added high quality original data, including:

- In-situ measurements of igneous rock-hosted zircons in the form of
  - U-Th-Pb isotopes, 55 rock samples
  - Lu-Hf isotopes, 45 rock samples
  - O isotopes, 45 rock samples
  - and trace elements, 15 rock samples
- Whole rock geochemistry, 230 samples

This thesis adds to the current understanding of Archaean crustal growth, as follows -

- Secular whole rock geochemistry (Chapter 3) highlights **two temporally discrete shifts in magmatism** in the southwestern Superior Craton. The most striking shift corresponds to a transition from TTG to sanukitoid magmatism at 2.7 Ga. An earlier shift relates to increased variation in major oxide abundances and greater variation in Sr/Y and La/Lu. This suggests a change in melt sources and melting depths respectively, and sheds new light into granite petrogenesis and geodynamics.

- **Hafnium isotopes record extended autochthonous growth within the Western Superior Craton** (Chapter 4). This requires a fundamental paradigm shift from an assembly of exotic fragments.
- This thesis presents two possible models for the growth of the Superior Craton and global late Archaean TTG-granite sequences (Chapter 4). **Early magmatism reflects intraplate rifting, whereas the late stage magmatism reflects arc-back arc magmatism during a subduction-collision cycle**.
- The significance of sanukitoid magmatism is clarified by detailed petrogenetic investigation. The major outcomes include:
    - **Sanukitoids of the Superior Craton have significant sediment (10-50%) input;**
    - **Sanukitoids are highly differentiated**, mantle-derived products of fractionation, melt replenishment and magma mixing. These processes were instrumental in generating the enrichments in highly compatible and highly incompatible elements.
    - Sanukitoids reflect (i) Kenoran compression, which caused magma ponding and evolution at depth, (ii) the widespread availability of sediment due to uplift during collision, and the transport of that sediment to depth during subduction and underthrusting, and (iii) elevated geotherms causing lower crustal anatexis and magma mingling.
    - **Sanukitoid PGEs were sourced from Archaean sedimentary rocks**, and
    - They are prospective hosts of Cu-Ni-PGE-Au mineralisation.

1.5. ORGANISATION OF THESIS

This thesis comprises seven chapters. It is organised by introductory and methodology chapters, followed by four independent manuscripts intended for journal publication, and synthesised in a concluding chapter. The common thread of Archaean crustal and geodynamic evolution links each chapter. Early chapters evaluate broad patterns in chemical and isotopic data whereas successive chapters build on this foundation to explore detailed petrogenesis of the sanukitoid suite.

Six appendices present analytical data collected throughout this project. Unpublished data from a parallel study of the Wabigoon superterrane conducted at The University of Western Australia by Dr. Yongjun Lu are included for context as supplementary data. All thesis chapters and appendices clearly distinguish data acquired by myself.

Chapter 1: Introduction

Chapter 1 introduces general concepts central to Archaean geology and the Western Superior Craton. This chapter highlights problems and knowledge gaps for Archaean crustal growth and geodynamics, identifies specific project aims and discusses the approach adopted by the thesis.

Chapter 2: Methods

Chapter 2 details the sampling methodology, analytical techniques and data evaluation employed for this investigation.

Chapter 3 (Manuscript 1): Late Archaean geodynamic changes in the Southwestern Superior Craton implied from secular geochemistry of felsic intrusions

This contribution presents new paired, spatially constrained, in-situ U-Pb zircon geochronology and whole rock geochemistry of felsic to intermediate intrusions in the southwestern Superior Craton. These data are integrated with compiled U-Pb geochronological data compiled from previous studies.

Using this large dataset, a comprehensive geochronological and stratigraphic framework for the Western Superior Craton is outlined. The nature and significance of broad geochemical shifts through time and space are explored. This provides new insight into (i) magma petrogenesis of lithological groups, (ii) granite-greenstone petrogenesis, (iii) terrane relationships and lithospheric architecture, and (iv) tectonic setting. The U-Pb geochronology presented in this chapter forms the basis of Hf-O and trace element investigations presented in Chapters 4 and 6.

Chapter 4 (Manuscript 2): 600 m.y. of autochthonous growth of the Superior Craton from Hf – O isotopes in igneous zircons

Chapter 4 builds on the geochronological study of Chapter 3. New Hf – O isotope measurements in igneous zircons previously dated using U-Pb geochronology are presented from across five terranes and one intervening sedimentary basin. These data are augmented by zircon Hf isotopic data collected from three additional terranes.

The broad isotopic patterns across time and space are used to: (i) provide insight into the variation of magma sources through time and space, (ii) build a tectonic model for the Superior Craton, and (iii) discuss broader implications for Archaean geodynamics and crust-mantle evolution.

Introduction

Chapter 5 (Manuscript 3): *Elemental enrichment by fractionation, replenishment and magma mixing in the Late Archaean sanukitoid suite*

Chapter 5 address the petrogenesis of sanukitoid magmatism from whole rock geochemistry and petrography of 19 sanukitoid intrusions across five terranes and one sedimentary basin. It includes contemporaneous and gabbroic and pyroxenite intrusive phases within and external to sanukitoid intrusions. Aims included: (i) investigating consanguinity between sanukitoid, gabbro and pyroxenite, (ii) unravelling differentiation histories and source contributions, thereby (iii) illuminating the cause of their unusual enrichments in highly compatible and incompatible elements, including economic Ni-Cu-PGE, and (iv) adding clarity to their tectonic setting.

Chapter 6 (Manuscript 4): *Sanukitoids record the widespread onset of supracrustal recycling*

Chapter 6 address the petrogenesis of sanukitoid magmatism from zircon in-situ Lu-Hf and O isotopic and trace elemental results. Chapter 6 builds on the petrogenetic results of Chapter 5 to quantify endmember contributions and investigate differentiation histories. This enables greater constraint on tectonic models for their genesis and reveals the significance of their transient appearance in the late Archaean rock record.

Chapter 7: Synthesis and future directions

This chapter summarises the major outcomes of this study and discusses future research.

Appendix A provides detailed descriptions of the samples for which isotopic measurements were undertaken.

Appendix B lists whole rock geochemical analytical results from this study.

Appendix C provides tables of U-Pb, O and Lu-Hf isotopic and trace element measurements in zircons undertaken throughout the course of this study.

Appendix D lists U-Pb, O and Lu-Hf isotopic and trace element measurements on standard reference materials measured throughout the same sessions as unknowns listed in Appendix C.

Appendix E provides tables of unpublished U-Pb, O and Lu-Hf isotopic and trace element measurements in zircons and reference materials collected by Dr Yongjun Lu. These results were interpreted, organised and compiled by KEB.

Appendix F presents two Summary of Field Work articles for the Ontario Geological Survey written by KEB and co-authored by supervisors and Ontario Geological Survey collaborators. The extended abstract for the SGA biennial conference in Nancy, France, August 2015 is also included here.

1.6. JUSTIFICATION OF THESIS FORMAT AND AUTHORSHIP

This section clearly outlines the contributions of the candidate and co-authors to each manuscript presented in Chapters 3, 4, 5 and 6.

The manuscript presented in Chapter 3 is first-authored by the candidate (Katarina E. Bjorkman) and co-authored by Yongjun Lu, Anthony I.S. Kemp, T. Campbell McCuaig and Peter N. Hollings. The candidate undertook sample collection and preparation, zircon imagery, U-Pb isotope determination, analysis, interpretation and presentation of geochronological and geochemical data, collation of previous geochronology and stratigraphic column construction. Prof McCuaig and Dr Lu accompanied the initial stages of the first field season, where they contributed to sample planning and collection and to structural and stratigraphic field observations. Dr Lu provided training in imagery techniques and U-Pb analytical procedures using the SHRIMP II, and in interpretation of geochronological data. The candidate wrote the manuscript. Editorial comments and revisions provided by Dr Kemp, Prof McCuaig, Dr Hollings and Dr Lu added focus and clarity.

The manuscript presented in Chapter 4 is first-authored by KEB and co-authored by Anthony I.S. Kemp, Yongjun Lu, T. Campbell McCuaig and Peter N. Hollings. The candidate undertook O isotope measurements by SIMS (with technical support from Heejin Jeon of the CMCA, UWA , see acknowledgements), Lu-Hf isotope measurements by LA-MC-ICP-MS (with technical support from Dr Kemp and Dr Yi Hu), and interpretation of data herein and previously collected by Dr Lu (supplementary material), in addition to collation of previous isotopic work. The candidate wrote the manuscript. Dr Kemp provided detailed conceptual feedback throughout manuscript preparation, which contributed to data interpretation, organisation and presentation of the manuscript. Dr Hollings and Dr Lu provided editorial comments and revisions that improved the quality of the manuscript.

The manuscript presented in Chapter 5 is first-authored by KEB and co-authored by Anthony I.S. Kemp, Yongjun Lu, Peter N. Hollings and T. Campbell McCuaig. The candidate undertook petrographic and field observations and wrote the manuscript. Dr Kemp provided critical ongoing feedback. Dr Hollings provided feedback on early and late versions, improving the organisation and clarity of the manuscript. Prof McCuaig and Dr Lu provided editorial comments and revisions.

Introduction

The manuscript presented in Chapter 6 is first-authored by KEB and co-authored by Anthony I.S. Kemp, Yongjun Lu and Peter N. Hollings. The candidate undertook in-situ trace element measurement by LA- ICP-MS (with technical support from Dr Kemp), interpretation of data and wrote the manuscript. Dr Kemp provided ongoing feedback and revision, which contributed to data interpretation and idea development. Dr Hollings provided editorial comments and revisions, and Dr Lu provided discussion.

1.7. SUPPORTING REFERENCES

2013

Geological survey publication

Bjorkman, K.E., McCuaig, T.C., Lu, Y.J., Beakhouse, G.P., Hollings, P., Smyk, M.C., 2013. Project Unit 13-030. Preliminary observations of the Marmion Terrane four-dimensional crust-mantle evolution and mineral systems. Summary of Field Work and other Activities 2013, Ontario Geological Survey, Open File Report 6290, p. 8-1 to 8-10.

Published Conference Abstract

Bjorkman, K.E., McCuaig, T.C., Lu, Y.J., Hollings, P., Fiorentini, M.L., Kemp, A., 2013. The 4D crust-mantle evolution and mineral system distribution of the 3.0 Ga Marmion Terrane, Western Superior Province, Canada: Preliminary observations and interpretations. CCFS Lithosphere Dynamics Workshop, 4-6th Nov., Perth. P.52-53.

2014

Geological survey publication

Bjorkman, K.E., McCuaig, T.C., Lu, Y.J., Beakhouse, G.P., Hollings, P. and Smyk, M.C. 2014. The Marmion terrane four-dimensional crust–mantle evolution and mineral systems: An update; *in* Summary of Field Work and Other Activities 2014, Ontario Geological Survey, Open File Report 6300, p.12-1 to 12-13.

2015

Refereed conference abstract

Bjorkman, K.E., McCuaig, T.C., Lu, Y.J., Hollings, P., and Beakhouse, G.P. 2015. Linking crustal evolution to mineral systems using U-Pb geochronology in zircons from the Marmion Terrane (3.02–2.68 Ga), western Superior Craton, Canada. In: *Proceedings: 13th Biennuel Meeting, Society for Geology Applied to Ore Deposits. 23-27 Aug, Nancy, France.*

Published conference abstract

Bjorkman, K.E., Lu, Y.J., McCuaig, T.C., Hollings, P. 2015. Using U-Pb, Lu-Hf and O Isotopes in Zircons to Unlock the Crust-Mantle Evolution and Relationships to Mineral Systems of

the Marmion Terrane (3.02-2.68 Ga), Superior Province, Canada. In: GAC-MAC 2015 Joint Assembly: Canadian Cratons Through Time: 4.0 Ga of Chemical Evolution and Tectonism, 3-6th May, Montreal, Canada.

Bjorkman, K.E., Lu, Y.J., McCuaig, T.C., Hollings, P., Beakhouse, G.P. 2015. Linking Crustal Growth to Orogenic Gold and Ni-Cu-PGE Mineralisation using U-Pb Geochronology in Zircons in the Marmion Terrane (3.0 Ga), Western Superior Craton, Canada. In: SEG 2015: World-Class Ore Deposits: Discovery to Recovery. 27-30th Sept. 2015, Hobart, TAS, Australia.

Björkman, K.E., McCuaig, T.C., Lu, Y.J., Kemp, A.I.S., Hollings, P. 2015. Unravelling crustal growth and geodynamics in the Meso to Neoarchaean using U-Pb-O isotopes in zircons and stratigraphic reconstructions from the Marmion Terrane (3.0 Ga). In: CCFS 2nd Lithosphere Workshop, 19-20th Nov., Perth.

2016

Published conference abstract

Bjorkman, K.E., Kemp, A.I., Lu, Y.J., McCuaig, T.C., Hollings, P.N., 2016. Sanukitoids record the onset of widespread Neoarchean supracrustal recycling. In: 2016 AGU Fall Meeting: Tectonochemistry II, 12-16th December, San Francisco, USA.

1.8. FINANCIAL SUPPORT

The Australian Research Council Centre of Excellence for Core to Crust Fluid Systems funded this project. It was part of Research Program 2: Genesis, transfer and focus of fluids and metals. The Scholarship for International Research Students (SIRF) covered The University of Western Australian tuition fees, the University International Stipend (UIS) and UIS top-up scholarships funded living costs for KEB.

The Ontario Geological Survey funded all whole rock geochemical analyses performed over the course of the PhD. A Graduate Research fellowship granted by the Society of Economic Geologists Foundation Inc. supported 2014 fieldwork.

1.9. REFERENCES

Adam, J. and Green, T.H., 1994. The effects of pressure and temperature on the partitioning of Ti, Sr and REE between amphibole, clinopyroxene and basanitic melts. Chemical Geology, 117(1–4): 219-233.

Allègre, C.J., Hart, S.R., Allègre, C.J. and Minster, J.F., 1978. Trace Elements in Igneous PetrologyQuantitative models of trace element behavior in magmatic processes. Earth and Planetary Science Letters, 38(1): 1-25.

Allègre, C.J., Manhès, G. and Göpel, C., 2008. The major differentiation of the Earth at ~ 4.45 Ga. Earth and Planetary Science Letters, 267(1–2): 386-398.

Andonaegui, P., Arenas, R., Albert, R., Sánchez Martínez, S., Díez Fernández, R. and Gerdes, A., 2016. The last stages of the Avalonian–Cadomian arc in NW Iberian Massif: isotopic and igneous record for a long-lived peri-Gondwanan magmatic arc. Tectonophysics, 681: 6-14.

Armstrong, R.L. and Harmon, R.S., 1981. Radiogenic Isotopes: The Case for Crustal Recycling on a Near-Steady-State No-Continental-Growth Earth [and Discussion]. Philosophical Transactions of the Royal Society of London A: Mathematical, Physical and Engineering Sciences, 301(1461): 443-472.

Arndt, N., 1999. Why was flood volcanism on submerged continental platforms so common in the Precambrian? Precambrian Research, 97(3–4): 155-164.

Arth, J.G. and Barker, F., 1976. Rare-earth partitioning between hornblende and dacitic liquid and implications for the genesis of trondhjemitic-tonalitic magmas. Geology, 4(9): 534-536.

Ashwal, L.D., Morgan, P., Kelley, S.A. and Percival, J.A., 1987. Heat production in an Archean crustal profile and implications for heat flow and mobilization of heat-producing elements. Earth and Planetary Science Letters, 85(4): 439-450.

Ayer, J., Amelin, Y., Corfu, F., Kamo, S., Ketchum, J., Kwok, K. and Trowell, N., 2002. Evolution of the southern Abitibi greenstone belt based on U–Pb geochronology: autochthonous volcanic construction followed by plutonism, regional deformation and sedimentation. Precambrian Research, 115(1–4): 63-95.

Ballard, J.R., Palin, M.J. and Campbell, I.H., 2002. Relative oxidation states of magmas inferred from Ce(IV)/Ce(III) in zircon: application to porphyry copper deposits of northern Chile. Contributions to Mineralogy and Petrology, 144(3): 347-364.

Barker, F. and Arth, J.G., 1976. Generation of trondhjemitic-tonalitic liquids and Archean bimodal trondhjemite-basalt suites. Geology, 4(10): 596-600.

Barley, M.E., Krapez, B., Groves, D.I. and Kerrich, R., 1998. The Late Archaean bonanza: metallogenic and environmental consequences of the interaction between mantle plumes, lithospheric tectonics and global cyclicity. Precambrian Research, 91(1): 65-90.

Beakhouse, G.P., 1991. Winnipeg River subprovince. In: H.R.W. P.C. Thurston, R.H. Sutcliffe and G.M Stott (Editor), Geology of Ontario. Ontario Geological Survey, Special Volume 4, Part 1, pp. 279-301.

Beakhouse, G.P., 2007. Structurally controlled, magmatic hydrothermal model for Archean lode gold deposits: a working hypothesis, Open File Report 6193. Ontario Geological Survey, 133 pp.

Beakhouse, G.P., McNutt, R.H. and Krogh, T.E., 1988. Comparative Rb-Sr and U-Pb zircon geochronology of late- to post-tectonic plutons in the Winnipeg River belt, Northwestern Ontario, Canada. Chemical Geology: Isotope Geoscience section, 72(4): 337-351.

Bédard, J.H., 2006. A catalytic delamination-driven model for coupled genesis of Archaean crust and sub-continental lithospheric mantle. Geochimica et Cosmochimica Acta, 70(5): 1188-1214.

Bédard, J.H., 2013. How many arcs can dance on the head of a plume?: A 'Comment' on: A critical assessment of Neoarchean 'plume only' geodynamics: Evidence from the Superior province, by Derek Wyman, Precambrian Research, 2012. Precambrian Research, 229(0): 189-197.

Bédard, J.H. and Harris, L.B., 2014. Neoarchean disaggregation and reassembly of the Superior craton. Geology, 42(11): 951-954.

Bédard, J.H., Harris, L.B. and Thurston, P.C., 2013. The hunting of the snArc. Precambrian Research, 229(0): 20-48.

Belousova, E.A., Kostitsyn, Y.A., Griffin, W.L., Begg, G.C., O'Reilly, S.Y. and Pearson, N.J., 2010. The growth of the continental crust: Constraints from zircon Hf-isotope data. Lithos, 119(3–4): 457-466.

Bennett, V.C., Nutman, A.P. and McCulloch, M.T., 1993. Nd isotopic evidence for transient, highly depleted mantle reservoirs in the early history of the Earth. Earth and Planetary Science Letters, 119(3): 299-317.

Bickford, M.E., Wooden, J.L. and Bauer, R.L., 2006. SHRIMP study of zircons from Early Archean rocks in the Minnesota River Valley: Implications for the tectonic history of the superior province. Geological Society of America Bulletin, 118(1-2): 94-108.

Bickle, M.J., 1978. Heat loss from the earth: A constraint on Archaean tectonics from the relation between geothermal gradients and the rate of plate production. Earth and Planetary Science Letters, 40(3): 301-315.

Bleeker, W., 2002. Archaean tectonics: a review, with illustrations from the Slave craton. Geological Society, London, Special Publications, 199(1): 151-181.

Böhm, C.O., Heaman, L.M., Creaser, R.A. and Corkery, M.T., 2000. Discovery of pre-3.5 Ga exotic crust at the northwestern Superior Province margin, Manitoba. Geology, 28(1): 75-78.

Böhm, C.O., Heaman, L.M., Stern, R.A., Corkery, M.T. and Creaser, R.A., 2003. Nature of Assean Lake ancient crust, Manitoba: a combined SHRIMP–ID-TIMS U–Pb geochronology and Sm–Nd isotope study. Precambrian Research, 126(1–2): 55-94.

Bouvier, A., Vervoort, J.D. and Patchett, P.J., 2008. The Lu–Hf and Sm–Nd isotopic composition of CHUR: Constraints from unequilibrated chondrites and implications for the bulk composition of terrestrial planets. Earth and Planetary Science Letters, 273(1–2): 48-57.

Brown, M., 2006. Duality of thermal regimes is the distinctive characteristic of plate tectonics since the Neoarchean. Geology, 34(11): 961-964.

Burnham, A.D. and Berry, A.J., 2012. An experimental study of trace element partitioning between zircon and melt as a function of oxygen fugacity. Geochimica et Cosmochimica Acta, 95: 196-212.

Campbell, I.H. and Allen, C.M., 2008. Formation of supercontinents linked to increases in atmospheric oxygen. Nature Geosci, 1(8): 554-558.

Card, K.D., 1990. A review of the Superior Province of the Canadian Shield, a product of Archean accretion. Precambrian Research, 48(1): 99-156.

Card, K.D. and Ciesielski, A., 1986. Subdivisions of the Superior Province of the Canadian Shield. Geoscience Canada, 13: 5-13.

Cawood, P.A., Hawkesworth, C.J. and Dhuime, B., 2013. The continental record and the generation of continental crust. Geological Society of America Bulletin, 125(1-2): 14-32.

Cawood, P.A., Kröner, A., Collins, W.J., Kusky, T.M., Mooney, W.D. and Windley, B.F., 2009. Accretionary orogens through Earth history. Geological Society, London, Special Publications, 318(1): 1-36.

Champion, D.C. and Cassidy, K., F., 2007. An overview of the Yilgarn Craton and its crustal evolution: Geoscience Australia Record, pp. 8-13.

Champion, D.C. and Huston, D.L., 2016. Radiogenic isotopes, ore deposits and metallogenic terranes: Novel approaches based on regional isotopic maps and the mineral systems concept. Ore Geology Reviews, 76: 229-256.

Cherniak, D.J. and Watson, E.B., 2003. Diffusion in Zircon. Reviews in Mineralogy and Geochemistry, 53(1): 113-143.

Claiborne, L.L., Miller, C.F., Walker, B.A., Wooden, J.L., Mazdab, F.K. and Bea, F., 2006. Tracking magmatic processes through Zr/Hf ratios in rocks and Hf and Ti zoning in zircons: An example from the Spirit Mountain batholith, Nevada. Mineralogical Magazine, 70(5): 517-543.

Claiborne, L.L., Miller, C.F. and Wooden, J.L., 2010. Trace element composition of igneous zircon: a thermal and compositional record of the accumulation and evolution of a large silicic batholith, Spirit Mountain, Nevada. Contributions to Mineralogy and Petrology, 160(4): 511-531.

Condie, K.C., 1994. Greenstones through time. Developments in Precambrian Geology, 11: 85-120.

Condie, K.C., 1998. Episodic continental growth and supercontinents: a mantle avalanche connection? Earth and Planetary Science Letters, 163(1–4): 97-108.

Condie, K.C. and Aster, R.C., 2010. Episodic zircon age spectra of orogenic granitoids: The supercontinent connection and continental growth. Precambrian Research, 180(3–4): 227-236.

Corfu, F., 1988. Differential response of U-Pb systems in coexisting accessory minerals, Winnipeg River Subprovince, Canadian Shield: implications for Archean crustal growth and stabilization. Contributions to Mineralogy and Petrology, 98(3): 312-325.

Corfu, F., Davis, D.W., Stone, D. and Moore, M.L., 1998. Chronostratigraphic constraints on the genesis of Archean greenstone belts, northwestern Superior Province, Ontario, Canada. Precambrian Research, 92(3): 277-295.

Corfu, F. and Stone, D., 1998. Age structure and orogenic significance of the Berens River composite batholiths, western Superior Province. Canadian Journal of Earth Sciences, 35(10): 1089-1109.

Corfu, F., Stott, G. and Breaks, F., 1995. U-Pb geochronology and evolution of the English River Subprovince, an Archean low P-high T metasedimentary belt in the Superior Province. Tectonics, 14(5): 1220-1233.

Davidson, J.P. and Arculus, R., 2006. The significance of Phanerozoic arc magmatism in generating continental crust. In: M. Brown and T. Rushmer (Editors), Evolution and Differentiation of the Continental Crust. Cambridge University Press, Cambridge, pp. 135–172.

Davis, D.W., 1996. Provenance and depositional age constraints on sedimentation in the western Superior transect area from U–Pb ages of zircons, Western Superior Lithoprobe Transect 2nd Annual Workshop. Lithoprobe Secretariat, The University of British Columbia, Vancouver, BC, Lithoprobe Report, pp. 18-23.

Davis, D.W., Amelin, Y., Nowell, G.M. and Parrish, R.R., 2005. Hf isotopes in zircon from the western Superior province, Canada: Implications for Archean crustal development and evolution of the depleted mantle reservoir. Precambrian Research, 140(3–4): 132-156.

Davis, D.W. and Jackson, M.C., 1988. Geochronology of the Lumby Lake greenstone belt: A 3 Ga complex within the Wabigoon subprovince, northwest Ontario. GSA Bulletin, 100(6): 818-824.

Davis, D.W., Sutcliffe, R.H. and Trowell, N.F., 1988. Geochronological constraints on the tectonic evolution of a late Archaean greenstone belt, Wabigoon Subprovince, Northwest Ontario, Canada. Precambrian Research, 39(3): 171-191.

DeBari, S.M. and Greene, A.R., 2011. Vertical Stratification of Composition, Density, and Inferred Magmatic Processes in Exposed Arc Crustal Sections, Arc-Continent Collision. Springer Berlin Heidelberg, Berlin, Heidelberg, pp. 121-144.

DePaolo, D.J., 1981. Trace element and isotopic effects of combined wallrock assimilation and fractional crystallization. Earth and Planetary Science Letters, 53(2): 189-202.

DePaolo, D.J. and Wasserburg, G.J., 1979. Petrogenetic mixing models and Nd-Sr isotopic patterns. Geochimica et Cosmochimica Acta, 43(4): 615-627.

Dhuime, B., Hawkesworth, C. and Cawood, P., 2011. When Continents Formed. Science, 331(6014): 154-155.

Dhuime, B., Hawkesworth, C.J., Cawood, P.A. and Storey, C.D., 2012. A Change in the Geodynamics of Continental Growth 3 Billion Years Ago. Science, 335(6074): 1334-1336.

Dhuime, B., Wuestefeld, A. and Hawkesworth, C.J., 2015. Emergence of modern continental crust about 3 billion years ago. Nature Geosci, 8(7): 552-555.

Dilles, J.H., Kent, A.J.R., Wooden, J.L., Tosdal, R.M., Koleszar, A., Lee, R.G. and Farmer, L.P., 2015. Zircon compositional evidence for sulfur-degassing from ore-forming arc magmas. Economic Geology, 110(1): 241-251.

Drake, M.J. and Weill, D.F., 1975. Partition of Sr, Ba, Ca, Y, Eu2+, Eu3+, and other REE between plagioclase feldspar and magmatic liquid: an experimental study. Geochimica et Cosmochimica Acta, 39(5): 689-712.

Draut, A.E. and Clift, P.D., 2001. Geochemical evolution of arc magmatism during arc-continent collision, South Mayo, Ireland. Geology, 29(6): 543-546.

Drummond, M.S. and Defant, M.J., 1990. A model for Trondhjemite-Tonalite-Dacite Genesis and crustal growth via slab melting: Archean to modern comparisons. Journal of Geophysical Research: Solid Earth, 95(B13): 21503-21521.

Ducea, M.N., 2002. Constraints on the bulk composition and root foundering rates of continental arcs: A California arc perspective. Journal of Geophysical Research: Solid Earth, 107(B11): ECV 15-1-ECV 15-13.

Ducea, M.N., Saleeby, J.B. and Bergantz, G., 2015. The Architecture, Chemistry, and Evolution of Continental Magmatic Arcs. Annual Review of Earth and Planetary Sciences, 43(1): 299-331.

Eiler, J.M., 2001. Oxygen Isotope Variations of Basaltic Lavas and Upper Mantle Rocks. Reviews in Mineralogy and Geochemistry, 43(1): 319-364.

Ellam, R.M. and Hawkesworth, C.J., 1988. Is average continental crust generated at subduction zones? Geology, 16(4): 314-317.

Ferry, J.M. and Watson, E.B., 2007. New thermodynamic models and revised calibrations for the Ti-in-zircon and Zr-in-rutile thermometers. Contributions to Mineralogy and Petrology, 154(4): 429-437.

Foley, S., Tiepolo, M. and Vannucci, R., 2002. Growth of early continental crust controlled by melting of amphibolite in subduction zones. Nature, 417(6891): 837-840.

Fralick, P., Hollings, P. and King, D., 2008. Stratigraphy, geochemistry, and depositional environments of Mesoarchean sedimentary units in western Superior Province: Implications for generation of early crust. In: K.C. Condie and V. Pease (Editors), When Did Plate Tectonics Begin on Planet Earth. Geological Society of America Special Papers, pp. 77-96.

Frost, C.D., Frost, B.R., Kirkwood, R. and Chamberlain, K.R., 2006. The tonalite-trondhjemite-granodiorite (TTG) to granodiorite-granite (GG) transition in the late Archean plutonic rocks of the central Wyoming Province1. Canadian Journal of Earth Sciences, 43(10): 1419-1444.

Green, T.H., 1994. Experimental studies of trace-element partitioning applicable to igneous petrogenesis — Sedona 16 years later. Chemical Geology, 117(1–4): 1-36.

Green, T.H., 1995. Significance of Nb/Ta as an indicator of geochemical processes in the crust-mantle system. Chemical Geology, 120(3–4): 347-359.

Griffin, W.L., Wang, X., Jackson, S.E., Pearson, N.J., O'Reilly, S.Y., Xu, X. and Zhou, X., 2002. Zircon chemistry and magma mixing, SE China: In-situ analysis of Hf isotopes, Tonglu and Pingtan igneous complexes. Lithos, 61(3–4): 237-269.

Hamilton, W.B., 1998. Archean magmatism and deformation were not products of plate tectonics. Precambrian Research, 91(1): 143-179.

Hamilton, W.B., 2007. Driving mechanism and 3-D circulation of plate tectonics. Geological Society of America Special Papers, 433: 1-25.

Hamilton, W.B., 2011. Plate tectonics began in Neoproterozoic time, and plumes from deep mantle have never operated. Lithos, 123(1–4): 1-20.

Hansen, V.L., 2015. Impact origin of Archean cratons. Lithosphere.

Harris, L.B. and Bédard, J.H., 2014. Crustal Evolution and Deformation in a Non-Plate-Tectonic Archaean Earth: Comparisons with Venus. In: Y. Dilek and H. Furnes (Editors), Evolution of Archean Crust and Early Life. Modern Approaches in Solid Earth Sciences. Springer Netherlands, pp. 215-291.

Hastie, A.R., Fitton, J.G., Bromiley, G.D., Butler, I.B. and Odling, N.W.A., 2016. The origin of Earth's first continents and the onset of plate tectonics. Geology, 44(10): 855-858.

Hawkesworth, C., Cawood, P. and Dhuime, B., 2016. Tectonics and crustal evolution. GSA Today, 26(09): 4-11.

Hawkesworth, C.J. and Kemp, A.I.S., 2006. Evolution of the continental crust. Nature, 443(7113): 811-817.

Hawkesworth, C.J. and Vollmer, R., 1979. Crustal contamination versus enriched mantle: 143Nd/144Nd and 87Sr/86Sr evidence from the Italian volcanics. Contributions to Mineralogy and Petrology, 69(2): 151-165.

Heilimo, E., Halla, J., Andersen, T. and Huhma, H., 2013. Neoarchean crustal recycling and mantle metasomatism: Hf–Nd–Pb–O isotope evidence from sanukitoids of the Fennoscandian shield. Precambrian Research, 228(0): 250-266.

Henry, P., Stevenson, R.K. and Gariepy, C., 1998. Late Archean mantle composition and crustal growth in the Western Superior Province of Canada: Neodymium and lead isotopic evidence from the Wawa, Quetico, and Wabigoon subprovinces. Geochimica Et Cosmochimica Acta, 62(1): 143-157.

Henry, P., Stevenson, R.K., Larbi, Y. and Gariépy, C., 2000. Nd isotopic evidence for Early to Late Archean (3.4–2.7 Ga) crustal growth in the Western Superior Province (Ontario, Canada). Tectonophysics, 322(1–2): 135-151.

Herzberg, C., Condie, K. and Korenaga, J., 2010. Thermal history of the Earth and its petrological expression. Earth and Planetary Science Letters, 292(1–2): 79-88.

Herzberg, C.T., Fyfe, W.S. and Carr, M.J., 1983. Density constraints on the formation of the continental Moho and crust. Contributions to Mineralogy and Petrology, 84(1): 1-5.

Hildreth, W. and Moorbath, S., 1988. Crustal contributions to arc magmatism in the Andes of Central Chile. Contributions to Mineralogy and Petrology, 98(4): 455-489.

Hoffman, P.F., 1988. United Plates of America, The birth of a craton - Early Proterozoic assembly and growth of Laurentia. Annual Review of Earth and Planetary Sciences, 16: 543-603.

Hollings, P. and Kerrich, R., 1999. Trace element systematics of ultramafic and mafic volcanic rocks from the 3 Ga North Caribou greenstone belt, northwestern Superior Province. Precambrian Research, 93(4): 257-279.

Hollings, P. and Wyman, D., 1999. Trace element and Sm-Nd systematics of volcanic and intrusive rocks from the 3 Ga Lumby Lake Greenstone belt, Superior Province: evidence for Archean plume-arc interaction. Lithos, 46(2): 189-213.

Hopkins, M., Harrison, T.M. and Manning, C.E., 2008. Low heat flow inferred from >4[thinsp]Gyr zircons suggests Hadean plate boundary interactions. Nature, 456(7221): 493-496.

Hoskin, P.W.O. and Schaltegger, U., 2003. The Composition of Zircon and Igneous and Metamorphic Petrogenesis. Reviews in Mineralogy and Geochemistry, 53(1): 27-62.

Irving, A.J., 1978. A review of experimental studies of crystal/liquid trace element partitioning. Geochimica et Cosmochimica Acta, 42(6): 743-770.

Jaffrés, J.B.D., Shields, G.A. and Wallmann, K., 2007. The oxygen isotope evolution of seawater: A critical review of a long-standing controversy and an improved geological water cycle model for the past 3.4 billion years. Earth-Science Reviews, 83(1–2): 83-122.

Jagoutz, O. and Kelemen, P.B., 2015. Role of Arc Processes in the Formation of Continental Crust. Annual Review of Earth and Planetary Sciences, 43(1): 363-404.

Jirsa, M.A., Boerboom, T.J., Chandler, V.W., Mossler, J.H., Runkel, A.C. and Setterholm, D.R., 2011. S-21 Bedrock Geologic Map of Minnesota. , Minnesota Geological Survey, State Map Series, S-21,.

Johnson, T.E., Brown, M., Gardiner, N.J., Kirkland, C.L. and Smithies, R.H., 2017. Earth's first stable continents did not form by subduction. Nature, 543(7644): 239-242.

Johnson, T.E., Brown, M., Kaus, B.J.P. and VanTongeren, J.A., 2014. Delamination and recycling of Archaean crust caused by gravitational instabilities. Nature Geosci, 7(1): 47-52.

Jull, M. and Kelemen, P.B., 2001. On the conditions for lower crustal convective instability. Journal of Geophysical Research: Solid Earth, 106(B4): 6423-6446.

Kamber, B.S., 2015. The evolving nature of terrestrial crust from the Hadean, through the Archaean, into the Proterozoic. Precambrian Research, 258: 48-82.

Kamber, B.S., Ewart, A., Collerson, K.D., Bruce, M.C. and McDonald, G.D., 2002. Fluid-mobile trace element constriants on the role of slab melting and implications for Archaean crustal growth models. Contributions to Mineralogy and Petrology, 144(1): 38-56.

Kay, R.W. and Mahlburg-Kay, S., 1991. Creation and destruction of lower continental crust. Geologische Rundschau, 80(2): 259-278.

Kelemen, P.B., 1995. Genesis of high Mg# andesites and the continental crust. Contributions to Mineralogy and Petrology, 120(1): 1-19.

Keller, C.B. and Schoene, B., 2012. Statistical geochemistry reveals disruption in secular lithospheric evolution about 2.5 Gyr ago. Nature, 485(7399): 490-U100.

Kemp, A. and Hawkesworth, C., 2013. Growth and differentiation of the continental crust from isotope studies of accessory minerals. In: R. Rudnick (Editor), Treatise on Geochemistry. The Crust. The Crust, vol. 12, second ed. Elsevier Science, Oxford.

Kemp, A.I.S., Hawkesworth, C.J., Collins, W.J., Gray, C.M. and Blevin, P.L., 2009. Isotopic evidence for rapid continental growth in an extensional accretionary orogen: The Tasmanides, eastern Australia. Earth and Planetary Science Letters, 284(3–4): 455-466.

Kemp, A.I.S., Hawkesworth, C.J., Foster, G.L., Paterson, B.A., Woodhead, J.D., Hergt, J.M., Gray, C.M. and Whitehouse, M.J., 2007. Magmatic and crustal differentiation history of granitic rocks from Hf-O isotopes in zircon. Science, 315(5814): 980-983.

Kemp, A.I.S., Wilde, S.A., Hawkesworth, C.J., Coath, C.D., Nemchin, A., Pidgeon, R.T., Vervoort, J.D. and DuFrane, S.A., 2010. Hadean crustal evolution revisited: New constraints from Pb–Hf isotope systematics of the Jack Hills zircons. Earth and Planetary Science Letters, 296(1–2): 45-56.

King, E.M., Valley, J.W., Davis, D.W. and Edwards, G.R., 1998. Oxygen isotope ratios of Archean plutonic zircons from granite-greenstone belts of the Superior Province: indicator of magmatic source. Precambrian Research, 92(4): 365-387.

Korenaga, J., 2008. Urey ratio and the structure and evolution of Earth's mantle. Reviews of Geophysics, 46(2): n/a-n/a.

Krogh, T.E., Harris, N.B.W. and Davis, G.L., 1976. Archean rocks from the eastern Lac Seul region of the English River gneiss belt, northwestern Ontario

Part 2, Geochronology. Canadian Journal of Earth Sciences, 13(9): 1212-1215.

Kump, L.R. and Barley, M.E., 2007. Increased subaerial volcanism and the rise of atmospheric oxygen 2.5[thinsp]billion years ago. Nature, 448(7157): 1033-1036.

Labrosse, S. and Jaupart, C., 2007. Thermal evolution of the Earth: Secular changes and fluctuations of plate characteristics. Earth and Planetary Science Letters, 260(3–4): 465-481.

Langford, F.F. and Morin, J.A., 1976. Development of the Superior Province of Northwestern Ontario by merging island arcs. American Journal of Science, 276(9): 1023-1034.

Langmuir, C.H., Vocke, R.D., Hanson, G.N. and Hart, S.R., 1978. A general mixing equation with applications to Icelandic basalts. Earth and Planetary Science Letters, 37(3): 380-392.

Laurent, O., Martin, H., Doucelance, R., Moyen, J.-F. and Paquette, J.-L., 2011. Geochemistry and petrogenesis of high-K "sanukitoids" from the Bulai pluton, Central Limpopo Belt, South Africa: Implications for geodynamic changes at the Archaean–Proterozoic boundary. Lithos, 123(1–4): 73-91.

Laurent, O., Martin, H., Moyen, J.F. and Doucelance, R., 2014. The diversity and evolution of late-Archean granitoids: Evidence for the onset of "modern-style" plate tectonics between 3.0 and 2.5 Ga. Lithos, 205: 208-235.

Loucks, R.R., 2014. Distinctive composition of copper-ore-forming arcmagmas. Australian Journal of Earth Sciences, 61(1): 5-16.
Lu, Y.-J., Loucks, R.R., Fiorentini, M.L., Yang, Z.-M. and Hou, Z.-Q., 2015. Fluid flux melting generated postcollisional high Sr/Y copper ore–forming water-rich magmas in Tibet. Geology, 43(7): 583-586.
Lu, Y.J., Loucks, R.R., Fiorentini, M.L., McCuaig, T.C., Evans, N.J., Yang, Z.-M., Hou, Z.-Q., Kirkland, C.L., Parra-Avila, L.A. and Kobussen, A., 2016. Zircon Compositions as a Pathfinder for Porphyry Cu±Mo±Au Deposits. Soc. Econ. Geol. Spec. Publ, 19: 329-347.
Lyons, T.W., Reinhard, C.T. and Planavsky, N.J., 2014. The rise of oxygen in Earth's early ocean and atmosphere. Nature, 506(7488): 307-315.
Martin, H., 1987. Petrogenesis of Archaean Trondhjemites, Tonalites, and Granodiorites from Eastern Finland: Major and Trace Element Geochemistry. Journal of Petrology, 28(5): 921-953.
Martin, H., Moyen, J.F. and Rapp, R., 2010. The sanukitoid series: magmatism at the Archaean-Proterozoic transition. Earth and Environmental Science Transactions of the Royal Society of Edinburgh, 100: 15-33.
Martin, H., Smithies, R.H., Rapp, R., Moyen, J.F. and Champion, D., 2005. An overview of adakite, tonalite–trondhjemite–granodiorite (TTG), and sanukitoid: relationships and some implications for crustal evolution. Lithos, 79(1–2): 1-24.
Maurice, C., David, J., Bédard, J.H. and Francis, D., 2009. Evidence for a widespread mafic cover sequence and its implications for continental growth in the Northeastern Superior Province. Precambrian Research, 168(1–2): 45-65.
McIntire, W.L., 1963. Trace element partition coefficients—a review of theory and applications to geology. Geochimica et Cosmochimica Acta, 27(12): 1209-1264.
Melnyk, M., Davis, D.W., Cruden, A.R. and Stern, R.A., 2006. U–Pb ages constraining structural development of an Archean terrane boundary in the Lake of the Woods area, western Superior Province, Canada. Canadian Journal of Earth Sciences, 43(7): 967-993.
Mole, D.R., Fiorentini, M.L., Thebaud, N., Cassidy, K.F., McCuaig, T.C., Kirkland, C.L., Romano, S.S., Doublier, M.P., Belousova, E.A., Barnes, S.J. and Miller, J., 2014. Archean komatiite volcanism controlled by the evolution of early continents. Proceedings of the National Academy of Sciences, 111(28): 10083-10088.
Moyen, J.-F., 2011. The composite Archaean grey gneisses: Petrological significance, and evidence for a non-unique tectonic setting for Archaean crustal growth. Lithos, 123(1–4): 21-36.
Moyen, J.-F. and Martin, H., 2012. Forty years of TTG research. Lithos, 148: 312-336.
MRN (Ministère des Ressources naturelles), 2002. Carte géologique du Québec. Édition 2002. . Ministère des Ressources naturelles; DV 2002-06.
Murphy, J.B. and Nance, R.D., 2002. Sm–Nd isotopic systematics as tectonic tracers: an example from West Avalonia in the Canadian Appalachians. Earth-Science Reviews, 59(1–4): 77-100.
Musacchio, G., White, D.J., Asudeh, I. and Thomson, C.J., 2004. Lithospheric structure and composition of the Archean western Superior Province from seismic refraction/wide-angle reflection and gravity modeling. Journal of Geophysical Research-Solid Earth, 109(B3).
Næraa, T., Scherstén, A., Rosing, M.T., Kemp, A.I.S., Hoffmann, J.E., Kokfelt, T.F. and Whitehouse, M.J., 2012. Hafnium isotope evidence for a transition in the dynamics of continental growth 3.2Gyr ago. Nature, 485(7400): 627-30.
Nash, W.P. and Crecraft, H.R., 1985. Partition coefficients for trace elements in silicic magmas. Geochimica et Cosmochimica Acta, 49(11): 2309-2322.
Nisbet, E.G., Cheadle, M.J., Arndt, N.T. and Bickle, M.J., 1993. Constraining the potential temperature of the Archaean mantle: A review of the evidence from komatiites. Lithos, 30(3): 291-307.
O'Neill, C., Lenardic, A., Moresi, L., Torsvik, T.H. and Lee, C.T.A., 2007. Episodic Precambrian subduction. Earth and Planetary Science Letters, 262(3–4): 552-562.
Ontario Geological Survey, 2003. 1: 250 000 Scale Bedrock Geology of Ontario, MRD 126. Ontario Geological Survey.
Parman, S.W., 2007. Helium isotopic evidence for episodic mantle melting and crustal growth. Nature, 446(7138): 900-3.
Parmenter, A.C., Lin, S.F. and Corkery, M.T., 2006. Structural evolution of the Cross Lake greenstone belt in the northwestern Superior Province, Manitoba: implications for relationship between vertical and horizontal tectonism. Canadian Journal of Earth Sciences, 43(7): 767-787.

Patchett, P.J., Kouvo, O., Hedge, C.E. and Tatsumoto, M., 1981. Evolution of continental crust and mantle heterogeneity - Evidence from Hf isotopes. Contributions to Mineralogy and Petrology, 78(3): 279-297.

Payne, J.L., McInerney, D.J., Barovich, K.M., Kirkland, C.L., Pearson, N.J. and Hand, M., 2016. Strengths and limitations of zircon Lu-Hf and O isotopes in modelling crustal growth. Lithos, 248–251: 175-192.

Pearson, D.G., Parman, S.W. and Nowell, G.M., 2007. A link between large mantle melting events and continent growth seen in osmium isotopes. Nature, 449(7159): 202-5.

Percival, J.A., Sanborn-Barrie, M., Skulski, T., Stott, G.M., Helmstaedt, H. and White, D.J., 2006. Tectonic evolution of the western Superior Province from NATMAP and Lithoprobe studies. Canadian Journal of Earth Sciences, 43(7): 1085-1117.

Percival, J.A., Skulski, T., Sanborn-Barrie, M., Stott, G.M., Leclair, A.D., Corkery, M.T. and Boily, M., 2012. Geology and tectonic evolution of the Superior Province, Canada. Tectonic Styles in Canada: The Lithoprobe Perspective, Special Paper, 49: 321-378.

Polat, A., 2012. Growth of Archean continental crust in oceanic island arcs. Geology, 40(4): 383-384.

Polat, A. and Kerrich, R., 2000. Archean greenstone belt magmatism and the continental growth–mantle evolution connection: constraints from Th–U–Nb–LREE systematics of the 2.7 Ga Wawa subprovince, Superior Province, Canada. Earth and Planetary Science Letters, 175(1–2): 41-54.

Rapp, R.P., Norman, M.D., Laporte, D., Yaxley, G.M., Martin, H. and Foley, S.F., 2010. Continent Formation in the Archean and Chemical Evolution of the Cratonic Lithosphere: Melt–Rock Reaction Experiments at 3–4 GPa and Petrogenesis of Archean Mg-Diorites (Sanukitoids). Journal of Petrology, 51(6): 1237-1266.

Rapp, R.P., Watson, E.B. and Miller, C.F., 1991. Partial melting of amphibolite/eclogite and the origin of Archean trondhjemites and tonalites. Precambrian Research, 51(1-4): 1-25.

Robert, F., Poulson, K.H., Cassidy, K., F. and Hodgeson, C.J., 2005. Gold Metallogeny of the Superior and Yilgarn Cratons. Economic Geology, 100th Anniversary Volume: 1001-1033.

Rudnick, R. and Gao, S., 2003. Composition of the continental crust. Treatise on geochemistry, 3: 1-64.

Rudnick, R.L., 1995. Making continental crust. Nature, 378(6557): 571-578.

Satkoski, A.M., Bickford, M.E., Samson, S.D., Bauer, R.L., Mueller, P.A. and Kamenov, G.D., 2013. Geochemical and Hf–Nd isotopic constraints on the crustal evolution of Archean rocks from the Minnesota River Valley, USA. Precambrian Research, 224: 36-50.

Scherer, E.E., Whitehouse, M.J. and Münker, C., 2007. Zircon as a Monitor of Crustal Growth. Elements, 3(1): 19-24.

Shields, G.A., 2007. A normalised seawater strontium isotope curve: possible implications for Neoproterozoic-Cambrian weathering rates and the further oxygenation of the Earth. eEarth, 2(2): 35-42.

Shirey, S.B. and Hanson, G.N., 1984. Mantle-derived Archaean monzodiorites and trachyandesites. Nature (310): 222-224.

Shirey, S.B. and Richardson, S.H., 2011. Start of the Wilson Cycle at 3 Ga Shown by Diamonds from Subcontinental Mantle. Science, 333(6041): 434-436.

Sizova, E., Gerya, T., Brown, M. and Perchuk, L.L., 2010. Subduction styles in the Precambrian: Insight from numerical experiments. Lithos, 116(3–4): 209-229.

Sizova, E., Gerya, T., Stüwe, K. and Brown, M., 2015. Generation of felsic crust in the Archean: A geodynamic modeling perspective. Precambrian Research, 271: 198-224.

Smart, K.A., Tappe, S., Stern, R.A., Webb, S.J. and Ashwal, L.D., 2016. Early Archaean tectonics and mantle redox recorded in Witwatersrand diamonds. Nature Geosci, 9(3): 255-259.

Smithies, R.H. and Champion, D.C., 2000. The Archaean High-Mg Diorite Suite: Links to Tonalite–Trondhjemite–Granodiorite Magmatism and Implications for Early Archaean Crustal Growth. Journal of Petrology, 41(12): 1653-1671.

Smithies, R.H., Champion, D.C. and Van Kranendonk, M.J., 2009. Formation of Paleoarchean continental crust through infracrustal melting of enriched basalt. Earth and Planetary Science Letters, 281(3–4): 298-306.

Smithies, R.H., Champion, D.C., Van Kranendonk, M.J., Howard, H.M. and Hickman, A.H., 2005. Modern-style subduction processes in the Mesoarchaean: Geochemical evidence from the 3.12 Ga Whundo intra-oceanic arc. Earth and Planetary Science Letters, 231(3–4): 221-237.

Söderlund, U., Patchett, P.J., Vervoort, J.D. and Isachsen, C.E., 2004. The 176Lu decay constant determined by Lu–Hf and U–Pb isotope systematics of Precambrian mafic intrusions. Earth and Planetary Science Letters, 219(3–4): 311-324.

Spencer, C.J., Cawood, P.A., Hawkesworth, C.J., Prave, A.R., Roberts, N.M.W., Horstwood, M.S.A. and Whitehouse, M.J., 2015. Generation and preservation of continental crust in the Grenville Orogeny. Geoscience Frontiers, 6(3): 357-372.

Stein, M. and Hofmann, A.W., 1994. Mantle plumes and episodic crustal growth. Nature, 372(6501): 63-68.

Stone, D., 2010. Precambrian geology of the central Wabigoon Subprovince area, northwestern Ontario. Ontario Geological Survey, Open File Report 5422: 130.

Stone, D. and Davis, D.W., 2006. Revised tectonic domains of the south-central Wabiggon Subprovince, Summary of Field Work and Other Activities 2006. Ontario Geological Survey, pp. 11-1 to 11-18.

Stott, G., 1997. The Superior Province, Canada. In: M.J.d. Wit and L.D. Ashwal (Editors), Greenstone Belts. Oxford Clarendon Press, Oxford Monograph on Geology and Geophysics 35, pp. 480-507.

Stott, G. and Corfu, F., 1991. Uchi subprovince. Geology of Ontario. Edited by PC Thurston, HR Williams, RH Sutcliffe, and GM Stott. Ontario Geological Survey, Special, 4(Part 1): 145-238.

Stott, G., Corkery, M.T., Percival, J.A., Simard, M. and Goutier, J., 2010. A Revised Terrane Subdivision of the Superior Province.

Stott, G.M., 2011. A Revised Terrane Subdivision of the Superior Province in Ontario; Ontario Geological Survey, Miscellaneous Release--Data 278.

Taylor, H.P., 1980. The effects of assimilation of country rocks by magmas on 18O/16O and 87Sr/86Sr systematics in igneous rocks. Earth and Planetary Science Letters, 47(2): 243-254.

Taylor, S.R. and McLennan, S.M., 1985. The continental crust: its composition and evolution. Blackwell, Oxford.

Thurston, P., Osmani, I. and Stone, D., 1991. Northwestern Superior Province: review and terrane analysis. Geology of Ontario. Edited by PC Thurston, HR Williams, RH Sutcliffe, and GM Stott. Ontario Geological Survey, Special, 4(Part 1): 81-144.

Thurston, P.C., 2002. Autochthonous development of Superior Province greenstone belts? Precambrian Research, 115(1–4): 11-36.

Thurston, P.C. and Chivers, K.M., 1990. Secular variation in greenstone sequence development emphasizing Superior Province, Canada. Precambrian Research, 46(1): 21-58.

Tomlinson, K., Davis, D., Stone, D. and Hart, T., 2003. U–Pb age and Nd isotopic evidence for Archean terrane development and crustal recycling in the south-central Wabigoon subprovince, Canada. Contributions to Mineralogy and Petrology, 144(6): 684-702.

Tomlinson, K.Y., Hughes, D.J., Thurston, P.C. and Hall, R.P., 1999. Plume magmatism and crustal growth at 2.9 to 3.0 Ga in the Steep Rock and Lumby Lake area, Western Superior Province. Lithos, 46(1): 103-136.

Tomlinson, K.Y., Stott, G.M., Percival, J.A. and Stone, D., 2004. Basement terrane correlations and crustal recycling in the western Superior Province: Nd isotopic character of granitoid and felsic volcanic rocks in the Wabigoon subprovince, N. Ontario, Canada. Precambrian Research, 132(3): 245-274.

Valley, J.W., Kinny, P.D., Schulze, D.J. and Spicuzza, M.J., 1998. Zircon megacrysts from kimberlite: Oxygen isotope variability among mantle melts. Contributions to Mineralogy and Petrology, 133(1-2): 1-11.

van Hunen, J. and Moyen, J.-F., 2012. Archean Subduction: Fact or Fiction? Annual Review of Earth and Planetary Sciences, 40(1): 195-219.

van Hunen, J. and van den Berg, A.P., 2008. Plate tectonics on the early Earth: Limitations imposed by strength and buoyancy of subducted lithosphere. Lithos, 103(1–2): 217-235.

Van Kranendonk, M.J., 2011. Onset of Plate Tectonics. Science, 333(6041): 413-414.

Vervoort, J.D. and Kemp, A.I.S., 2016. Clarifying the zircon Hf isotope record of crust–mantle evolution. Chemical Geology, 425: 65-75.

Vervoort, J.D. and Patchett, J.P., 1996. Behavior of hafnium and neodymium isotopes in the crust: Constraints from Precambrian crustally derived granites. Geochimica et Cosmochimica Acta, 60(19): 3717-3733.

Viljoen, D., Chackowsky, L., Lenton, P. and Broome, H.J., 1999. Geology, magnetic, and gravity maps of Manitoba: a digital perspective. . Geological Survey of Canada, Open File 3695.

Voice, P.J., Kowalewski, M. and Eriksson, K.A., 2011. Quantifying the Timing and Rate of Crustal Evolution: Global Compilation of Radiometrically Dated Detrital Zircon Grains. The Journal of Geology, 119(2): 109-126.

Wang, C., Bagas, L., Lu, Y., Santosh, M., Du, B. and McCuaig, T.C., 2016. Terrane boundary and spatio-temporal distribution of ore deposits in the Sanjiang Tethyan Orogen: Insights from zircon Hf-isotopic mapping. Earth-Science Reviews, 156: 39-65.

Watson, E.B. and Cherniak, D.J., 1997. Oxygen diffusion in zircon. Earth and Planetary Science Letters, 148(3): 527-544.

Watson, E.B. and Harrison, T.M., 2005. Zircon Thermometer Reveals Minimum Melting Conditions on Earliest Earth. Science, 308(5723): 841-844.

Weaver, B.L. and Tarney, J., 1984. Empirical approach to estimating the composition of the continental crust.

White, D.J., Musacchio, G., Helmstaedt, H.H., Harrap, R.M., Thurston, P.C., van der Velden, A. and Hall, K., 2003. Images of a lower-crustal oceanic slab: Direct evidence for tectonic accretion in the Archean western Superior province. Geology, 31(11): 997-1000.

Wilson, J.F., Orpen, J.L., Bickle, M.J., Hawkesworth, C.J., Martin, A. and Nisbet, E.G., 1978. Granite-greenstone terrains of the Rhodesian Archaean craton. Nature, 271(5640): 23-27.

Wyman, D. and Hollings, P., 1998. Long-lived mantle-plume influence on an Archean protocontinent: Geochemical evidence from the 3 Ga Lumby Lake greenstone belt, Ontario, Canada. Geology, 26(8): 719-722.

Wyman, D.A., 2013a. A critical assessment of Neoarchean "plume only" geodynamics: Evidence from the Superior Province. Precambrian Research, 229(0): 3-19.

Wyman, D.A., 2013b. A reply to "How many arcs can dance on the head of a plume?" by Jean Bédard, Precambrian Research, 2012. Precambrian Research, 229(0): 198-202.

Wyman, D.A., Ayer, J.A. and Devaney, J.R., 2000. Niobium-enriched basalts from the Wabigoon subprovince, Canada: evidence for adakitic metasomatism above an Archean subduction zone. Earth and Planetary Science Letters, 179(1): 21-30.

Yang, J.-H., Wu, F.-Y., Wilde, S.A., Xie, L.-W., Yang, Y.-H. and Liu, X.-M., 2007. Tracing magma mixing in granite genesis: in situ U–Pb dating and Hf-isotope analysis of zircons. Contributions to Mineralogy and Petrology, 153(2): 177-190.

Yogodzinski, G.M., Vervoort, J.D., Brown, S.T. and Gerseny, M., 2010. Subduction controls of Hf and Nd isotopes in lavas of the Aleutian island arc. Earth and Planetary Science Letters, 300(3–4): 226-238.

Chapter 2: Methods

2.1. FIELD INVESTIGATIONS

Sampling across the south-central Wabigoon Superterrane was undertaken over two field seasons in July-September 2013 and August-September 2014 with three objectives: (i) regional sampling of felsic to intermediate intrusive rocks (ii) targeted sampling of volcanic and sedimentary rocks within supracrustal assemblages, and (iii) sampling of mineralisation.

2.1.1. Regional sampling

The purpose of regional sampling was to provide a temporal and spatial crustal cross section of the study area collecting representative materials for the petrographic, geochemical and isotopic characterization. Figure 2-1 shows the distribution of samples collected during 2013 – 2014 fieldwork. Emphasis was placed on sampling lithological and textural variations of the late mantle-derived sanukitoid suite, compositional and textural representatives of the TTG suite intrusions and gneisses and the late granite-granodiorite intrusions. The topographic terrain and accessibility influenced sampling distribution, where access provided by provincial highways, logging access roads and lakeshore were natural foci of investigation. Rock cuts along highways, access roads and lakeshore outcrops provided superior exposure and opportunity for sampling (Figure 2-2). All samples were split into a portion for a polished thin section, a portion for whole rock geochemistry, a representative hand specimen, and where applicable, a portion for mineral separation.

2.1.2. Belt-scale study of greenstone belts & mineralisation

The purpose of the greenstone belt study was to compare the stratigraphic, structural and metamorphic variations with the isotopic variations. Specific areas within the greenstone belts were targeted based on inconsistencies in historical interpretations and observations determined by literature review. These targeted field investigations provide context to the mapping and observations of previous workers, thereby aiding in the interpretation of the tectonic history of the terrane. Detailed mapping and descriptions of the area are provided by Wilks and Nisbet (1988), Fenwick (1976), Jackson (1985), Fralick and King (1996), Stone et al. (1992), Hollings and Wyman (1999), Tomlinson et al. (1999), Fralick et al. (2008), Stone (2008); (Stone, 2010) and Buse et al. (2009).

Like the study of stratigraphy and structure, the study of mineralisation was designed to give context to previous work. Observations of structure and alteration assemblages were made of several gold deposits and occurrences in the area including Hammond Reef, Harold Lake, Fern Elizabeth and the Zephyr Zone. Exhalative Au-Zn occurrences in the Lumby Lake greenstone belt were sampled. Magmatic Ni-Cu-PGE occurrences within the Entwine Lake and Quetico intrusions were also sampled and described.

Figure 2-1: Geological map of the study area showing the sample locations. Samples with in-situ zircon analyses are indicated by yellow diamonds. Green triangles indicate samples analysed for geochemistry and petrography. Geology and shaded magnetic relief is from Ontario Geological Survey (2011). Solid and dashed lines indicate current and possible terrane designations.

2.1.3. Petrography of polished thin sections

Petrographic characterisation of thin sections was undertaken at the University of Western Australia using the polarising microscope. Petrography was used in conjunction with field observations, and in some cases geochemistry, to identify rocks using modal percentages of minerals present and textures, to determine igneous paragenetic crystallisation sequences using crystal morphology and textures.

Appendix A includes sample reports detailing petrography and field context, whole rock geochemistry, zircon morphology and microstructure and isotopic results with analytical conditions for each sample for which zircon isotopic work was undertaken by KEB for this study.

2.2. ANALYTICAL TECHNIQUES

2.2.1. Whole rock major and trace elements

2.2.1.1. Activation Laboratories Ltd. – Samples collected in 2011by KEB and in 2012 by Y-JL

Whole rock geochemical analyses for eighteen samples collected in August 2011 within the Entwine Intrusive Complex were analysed by Activation Laboratories Ltd. in September 2011. Samples were prepared in Thunder Bay (crushing and pulverising) and geochemical analyses were made in Ancaster, Ontario Canada. Precious metals were analysed by fire assay in Thunder Bay.

Major and trace elements were analysed by fusion – inductively coupled plasma mass spectrometry (ICP-MS). Each sample was mixed with a flux of lithium metaborate and lithium tetraborate and fused in an induction furnace in preparation for major and trace element analyses. The fused sample was poured into a solution of 5% nitric acid plus an internal standard while molten, and then mixed for 30 minutes until dissolved. A combination simultaneous/sequential Thermo Jarrell-Ash ENVIRO II ICP or a Varian Vista 735 ICP was used to measure major and select trace elements (Sc, Be, V, Ba, Sr, Y, Zr; Code 4LITHO (11+)). Seven USGS and CANMET calibration standards were used, one of which was measured every 10 samples. For the remainder of the trace elements, the fused sample was diluted and then analysed using a Perkin Elmer Sciex ELAN 6000, 6100 or 9000 ICP-MS (Code 4B2). One fused duplicate, three blanks and five controls were analysed. The instrument was calibrated with a standard every 40 samples measured.

Gold, Pt and Pd were analysed by fire assay in Thunder Bay (Method Code 1C-Exp ICPOES). About 30g of pulp was mixed with borax, soda ash, silica or litharge fluxes and Ag as a collector and placed in fire clay crucibles. Preheating started at 850°C, was sequentially raised to 950°C and 1060°C for a total of one hour. Molten slag was poured into a mould leaving a lead button at the

base. The lead button was placed in a preheated cupel to absorb the lead at 950°C in order to recover the Ag doré bead with Au, Pt and Pd. The Ag doré bead was digested in 95°C HNO 3 + HCl, cooled for 2 hours and then analysed by ICP/OES (Optical Emission Spectrometry) using a Varian 735 ICP-MS. Calibration was made every 45 samples. Two method blanks, three sample duplicates and two certified reference materials were analysed every 42 samples.

Samples collected by Yongjun Lu in 2012 were analysed by Activation Laboratories Ltd in Ancaster, Ontario, Canada in 2014. Fusion-ICP-MS was used to measure most elements including major and select trace elements (Sc, Be, V, Ba, Sr, Y, Zr) (Code 4LITHO (FeO)(11+) - ICP/MS (WRA4B2)) and a suite of trace elements (FUS-ICP: Sc, Be, V, Sr, Y, Zr, Ba; FUS-MS: Co, Ni, Cu, Zn, Ga, Ge, As, Rb, Nb, Mo, Ag, In, Sn, Sb, Cs, rare earth elements (REE: La, Ce, Pr, Nd, Sm, Eu, Gd, Tb, Dy, Ho, Er, Tm, Yb, Lu), Hf, Ta, W, Tl, Pb, Bi, Th, U) following the procedures outlined above. FUS-ICP Total digestion – ICP (method code 4B1 total digestion – ICP) using four acids (hydrofluoric, then a mixture of nitric and perchloric acids) was used to measure Cd, Cu, Ni, Zn, S, Ag, Pb and Cr . Following programmed heating cycles to dryness, digested samples were dissolved in hydrochloric acid and analysed using a Varian Vista 735 ICP. FeO was determined by titration (Code 4F-FeO Titration). Sample was digested in cold ammonium metavanadate and hydrofluoric acid. Ferrous ammonium sulphate was added prior to titration using potassium dichromate.

2.2.1.2. Geoscience Laboratories – Samples from 2013-2014 Fieldwork

Samples collected during the 2013 and 2014 field season by KEB were analysed for whole rock geochemistry by Geoscience Laboratories in Sudbury, Ontario following the procedures outlined below: Rock samples were crushed using a small jaw-crusher with steel plates, the sample was split using a rifle, and an agate mill pulverized the sample (method code SAM-AGM). Solution preparation was completed using closed-vessel multi-acid digest for inductively coupled plasma mass spectrometry (ICP-MS) and inductively coupled plasma atomic emission spectrometry (ICP-AES) (method codes SOL-CAIO; IMC-100/IAC-100). Rare earth elements (REE: La, Ce, Pr, Nd, Sm, Eu, Gd, Tb, Dy, Ho, Er, Tm, Yb, Lu) plus Y, Th, and U, high field strength elements (HFSE: Zr, Nb, Hf, Ta, Ti), large ion lithophile elements (LILE: Ba, Rb, Sr, Cs, Th, Pb), transition metals (Sc, V, Cr, Co, Ni, Cu, Zn), in addition to Be, Bi, Cd, Ce, Ga, In, Li, Mo, Sb, Sn, Tl, Tm and W were determined by ICP-MS. Al, Ba, Be, Ca Co,Cr, Cu, Fe, K, Li, Mg, Mn, Na, Ni, P, Pb, S, Sc, Sr, Ti, V, Y and Zn were determined by ICP-AES. Results for elements analysed by both ICP-MS and ICP-AES were generally in agreement unless near the detection limit of either method.

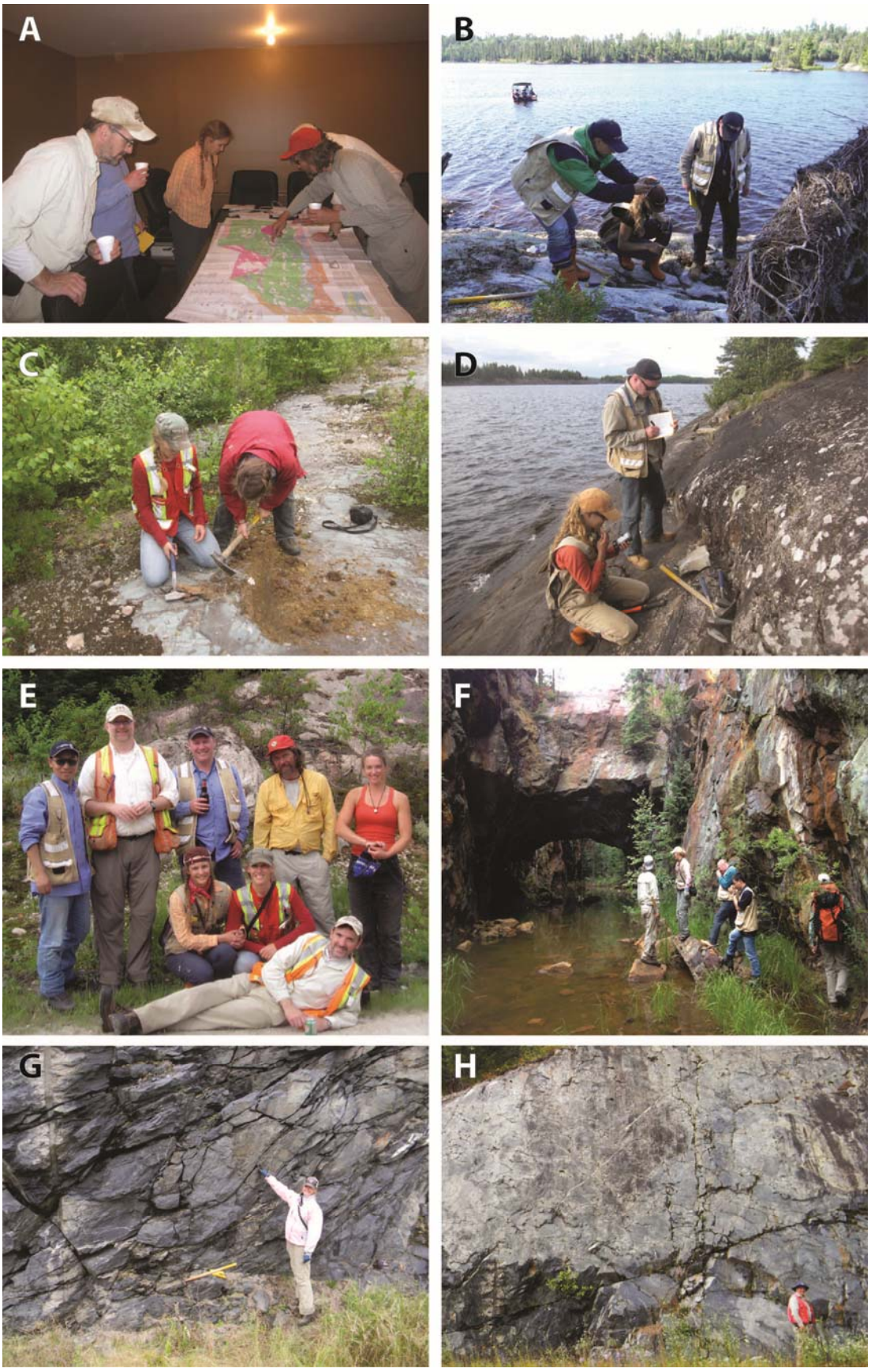
A
B
C
D
E
F
G
H

Figure 2-2: Fieldwork photos: A. Planning a field trip through the Lumby Lake greenstone belt in Bjorkman Prospecting office, from left to right: Mark Smyk (Ministry of Northern Development and Mines; MNDM), Cam McCuaig, KEB, Pete Hollings, Karl Bjorkman. B. Examining crosscutting quartz veins in the Marmion gneiss, Marmion Lake with Yongjun Lu and Cam McCuaig. C. Jessica and Ruth Bjorkman extracting a sample for geochemical analyses, Lumby Lake greenstone belt. D. Sampling a rhyolite lapilli tuff, Finlayson Lake greenstone belt, KEB and Cam McCuiag. E. Lumby Lake greenstone belt field trip, from left to right, Yongjun Lu, Pete Hollings, Cam McCuaig, Karl Bjorkman, Ruth Bjorkman, KEB, Jessica Bjorkman, Mark Smyk. F. Open cut and arch in the gabbro-hosted Atikokan Iron Mine, Karl and Katarina Bjorkman, Cam McCuaig, Yongjun Lu, Ruth Bjorkman. G. Karla Bjorkman pointing out large-scale 'S' cleavage with a reverse fault (demarked by hammer) within the Wapagesi volcanic group, Western Wabigoon terrane, near the contact with the Marmion terrane, Highway 622. H. Gary Beakhouse (Ontario Geological Survey) with a hill of pristine pillows in the Western Wabigoon terrane.

Wavelength dispersive X-ray fluorescence spectrometry (XRF; method code XRF-T02) was used to analyse for As, Ba, Co, Cr, Ga, Nb, Ni, Pb, Rb, Sr, Th, Y and Zr. Metals such as Ni show very good agreement with results of ICP-MS measurements after acid digest. XRF results for Zr have systematically lower values. Major elements were analysed by XRF (method code XRF-M01), and reported as oxides including SiO_2, TiO_2, Al_2O_3, CaO, Fe_2O_3 K_2O, MgO, MnO, Na_2O, P_2O_5 and LOI.

Precious metals including Au and PGE were analysed by fire assay (method code IMP-200). CO_2 and S were analysed by combustion in an oxygen rich environment to oxidize C and S which were then measured by infrared absorption (method code IRC-100). Specific gravity was obtained for all samples (method code SGT-R01).

Duplicates were analysed every ten samples. Duplicates were within uncertainty except for a felsic volcanic sample, KAT20130814-07, where several elements are in disagreement between sample and duplicate. One reference material and one blank were included every twenty samples.

Table B-1 in Appendix B lists geochemical results with associated detection limits for all samples.

2.2.2. Zircon grain mount construction and imaging

Zircons from rocks of the Sanukitoid suite were separated by Apatite to Zircon Inc. or Geotrack International Pty. Ltd. Rocks were first crushed to a size of <500µm. Heavy minerals were separated from lighter minerals using heavy liquid, tetrabromoethane (TBE; SG. 2.95) and Methylene Iodide (SG. 3.32), separation. Paramagnetic and ferromagnetic minerals such as titanite and composites were removed from the heavy (SG. > 2.95) concentrate with a horizontal Frantz Isodynamic separator.

Zircons were handpicked from amongst abundant apatite and occasionally sulphide minerals under a microscope to include representative zircons from all size and morphological populations with

emphasis on the clearest and largest grains. Selected zircons were placed on mounts with four natural zircon standards: (i) fragments of M257, a gem-quality 5.1412 g detrital zircon extracted from a placer deposit in the Sri Lankan Highland Complex (Kröner et al., 1994; Nasdala et al., 2008) (ii) OGC-1, from the Owens Gully Diorite within the Mount Edgar Granitic Complex, East Pilbara Terrane, Pilbara Craton, Western Australia (Stern et al., 2009) (iii) Temora 2, <500 μm clear zircons from high level Middledale Gabbroic Diorite stock within the Palaeozoic Lachlan Orogen of Eastern Australia (Black et al., 2003; Black et al., 2004) and (iv) fragments of Penglai, which occur as megacrysts within the 4.4 ± 0.1 Ma alkaline basalt at Penglai, northern Hainan Island, southern China (Li et al., 2010). NBS611 glass was also placed onto mounts for accurate location of the ^{204}Pb peak during U-Pb analysis by SHRIMP.

Mounts were then cast in epoxy resin using a 25 mm diameter mould and EpoFix epoxy. After curing for 12 hours at room temperature and six hours in a 40°C oven, mounts were polished to expose the near mid-point of grains. Sandpaper with P2000 grit was employed initially, and followed progressively using 6, 3 and 1 micron diamond compounds. The zircons of each sample were photographed in reflected and transmitted light on a polarizing microscope.

Mounts were then thoroughly cleaned using successive solutions of isopropanol, petroleum spirit, soap solution and deionised water. Each cleaning step included an ultrasonic bath and thorough wiping with a Kimwipe. The mounts were then dried with N_2 and put in a 50°C overn for at least one hour. They were then coated with 40 nm of gold and imaged using cathodoluminescence (CL) and back scattered electron (BSE) techniques on the TESCAN VEGA3 scanning electron microscope (SEM) at the Centre for Microscopy, Characterisation and Analysis (CMCA), University of Western Australia (UWA) to reveal internal microstructures. BSE images were collected for most samples using an accelerating voltage (HV) of ~15 kV, beam intensity of 12-15 (~5 nA), 150x – 200x magnification and scanning speed of 6-7. Zones in a zircon with higher atomic number appear brighter in BSE images so REE and U-Th rich zones are typically brighter than pure zircon. CL images were collected for all samples using a HV of ~15kV, beam intensity between 14-18 depending on luminescence of particular zircons, 150-200x magnification and scanning speed of 7-8. The CL technique capitalises on excess electron–hole pairs associated with the presence of Dy^{3+} and also Sm^{3+}, Eu^{2+}, Tb^{3+} and Y^{3+} in zircon (Hanchar and Miller, 1993). When excited by an electron beam the electrons emit visible light upon returning to the ground state and are the luminescent portions of zircons. High U-Th zones of zircon are subject to radiation damage which affects vacancies and typically results in low luminescent zones (Nelson et al., 2000). Zircon

microstructure imaged by CL techniques typically provided the most meaningful insight, and was useful in guiding analytical placements.

After each secondary ion mass spectrometry (SIMS) session (U-Pb and oxygen isotopes), mounts were recoated with gold and analysed zircons were imaged individually in reflected light and using secondary electron (15kV, beam intensity 10-13 (~5 nA), magnification dependent on zircon size but <1000x) and cathode-luminescence techniques (15kV, beam intensity 14-19, magnification dependent on zircon size, <1000x) in order to assess the quality of SIMS spots, confirm microbeam analyses in the same zircon domain and capture complexities encountered such as inclusions, cracks and core-rim interfaces. Gold coating was removed prior to zircon Lu-Hf isotopic and trace element analyses.

2.1.1.1 U-(Th)-Pb zircon geochronology by SIMS

Highest quality zircons of each population were selected for U-(Th)-Pb isotope analyses by ion microprobe at the Sensitive High Resolution Ion Microprobe II (SHRIMP II) at the John de Laeter Centre of Mass Spectrometry at Curtin University, Perth, Australia (Figure 2-3). A primary ion beam generated in the duoplasmatron was filtered to select O^{2-} ions using a Wein filter. The O^{2-} beam current intensity was then tuned using source steering, matching lens, matching lens steering and the Kohler lens. A Kohler aperture of 100 or 70 μm was set to maximise beam intensity and obtain an elliptical spot shape at a size small enough to accommodate the size and internal growth zones of zircons being analysed for each session. Primary beam intensity therefore varied between sessions depending on the size of zircons analysed, typically between 1.3 and 2.7 nA, producing a sputtering diameter of 18-30 μm.

The secondary beam was tuned on the primary U/Pb calibration zircon using quadrupole lenses to maximise intensity, typically between 40-60 pA. The primary U/Pb calibration and concentration was the 561.3 ± 0.3 Ma ($^{206}Pb/^{238}U$ age) M257 zircon, which has $^{206}Pb/^{238}U = 0.09100 \pm 0.00003$ and $^{207}Pb/^{235}U = 0.7392 \pm 0.0003$, ~840 ppm U, and Th/U ~0.27 (Nasdala et al., 2008). Mass calibration was made on M257 using the ^{254}UO peak. Collector positions were modified to maximise mass resolution for the ^{254}UO and $^{196}Zr_2O$ peaks. The $^{196}Zr_2O$ peak was used to estimate the ^{204}Pb peak, which was located using NBS glass; the ^{204}Pb peak was placed above centre to avoid interference. The background measurement was placed 0.045 AMU from the ^{204}Pb peak. Subsequent Pb peaks were located using the natural zircon standard OGC-1 and checked on a metamict grain whereas U^+, ThO^+ and UO^+ were centred using M257. Mass resolution ($M/\Delta M$) measured on M257 was >5000.

Methods

Peak count rates were measured sequentially over nine mass stations for Zr_2O^+, Pb^+ (204, 206, 207, 208), U^+, ThO^+ , UO^+ (+background) using an electron multiplier in pulse-counting mode and averaged over six scans after cycling the magnet. M257 was measured every 3-4 unknowns. Zircons from OGC-1 ($^{207}Pb^*/^{206}Pb^*$ = 10.29907 ± 0.00011, 3465.4 ± 0.6 Ma; Stern et al., 2009) were analysed every 8-10 unknowns to monitor $^{207}Pb/^{206}Pb$ accuracy and enable correction for $^{207}Pb/^{206}Pb$ fractionation. Fractionation occurred during two sessions. The affected samples (WS-37A,C and WS-49B,C) were corrected for fractionation using the true $^{207}Pb/^{206}Pb$ ratio for OGC-1 to calculate a fractionation factor which was then applied to the $^{207}Pb/^{206}Pb$ ratios of the unknowns. The calculated ages of samples corrected for fractionation differed by <0.009 Ga.

Data reduction of the results was accomplished using the SQUID 2.50 and Isoplot 3.71 add-ins in Microsoft Excel developed by Ludwig (2009). Table 2 in Appendix A lists all U-Pb isotope results. Measured ^{204}Pb was used to correct for common Pb using the Stacey and Kramers (1975) terrestrial Pb evolution model for all samples. Radiogenic lead is indicated by an asterisk. All SHRIMP results were screened for high common Pb, high U-Th contents, discordance, high background counts and poor instrument sensitivity, where sensitivity is defined as cps/nA/ppm Pb. Analyses typically in excess of five counts ^{204}Pb or background, 5% discordance (in a few cases with unimodal populations, <10% discordance were included), 1000 ppm U and with a sensitivity <15 were excluded. Post-analysis imaging was used to check for analysis within the desired zircon growth to exclude mixed ages, to discriminate between inherited, magmatic and metamorphic populations, and to check for irregularities such as cracks and inclusions.

2.1.1.2 Oxygen isotope measurement in zircons by SIMS

Mounts were imaged and then polished to remove SHRIMP pits (~2µm deep). Mounts were then coated with ~30nm of gold. This enabled O isotope analyses within the same growth domain as U-Pb age measurements were made, most commonly directly over previous SHRIMP pits, but shifted to exclude cracks or inclusions where present. Least discordant zircons with were prioritised.

Oxygen isotopes were measured on the Cameca IMS 1280 at the CMCA, UWA (Figure 2-3). A 10keV $^{133}Cs^+$ primary beam was used in combination with an incidence electron gun to offset charging with the secondary beam. The primary Gaussian beam (focussed) ranged from 1.2 –2.9 nA with an impact energy intensity of 20keV. The rastered beam was used over 20 µm during a 50 s pre-sputter and over 15µm during 160 s analysis. The analytical acquisition included field aperture and exit slit using the ^{16}O signal in multi-collection mode. Nuclear magnetic resonance (NMR) regulation was used to lock the axial mass at the beginning of each session. Simultaneous

measurement of ^{16}O and ^{18}O was made using dual faraday cups with a mass resolution of ~2500 during two sets of 10 cycles.

During the July-August 2015 session, the field aperture was 3000µm, corresponding to x100 field magnification, entrance slit was 170µm, exit slit 500 µm. The first analytical session of mount WS-36 was compromised by a problem with beam shift so the mount was repolished and analysed again. During the January 2016 session the field aperture was 4000µm, corresponding to x133 field magnification, entrance slit was 120µm and exit slit 500 µm. Typical count rates for the July-August 2015 session for ^{18}O were ~ $1.5*10^9$ cps and for ^{16}O ~$3*10^6$ cps, whereas for the January 2016 session, count rates for ^{18}O were ~ $2*10^9$ cps and for ^{16}O ~$4*10^6$ cps.

Standards were measured between every 4 (July-August 2015) or 5-6 (January 2016) unknowns. Outliers were excluded from the mean calculation. Spot-to-spot reproducibility for standards varied from 0.3 – 0.7 ‰ (2 s.d.) during a July-August 2015 session and 0.19 – 0.33 ‰ (2 s.d.) for the January 2016 session.

Measured $^{18}O/^{16}O$ of zircons was normalized to and corrected for instrumental mass fraction and time drift using one of either Penglai ($^{18}O/^{16}O$ = 2.015848*10-3±1.0026*10-7, or $\delta^{18}O$ =5.31 ± 5.31 ± 0.10‰ (2σ), Li et al., 2010) or Temora 2 ($^{18}O/^{16}O$ = 2.021643*10-3±2.0052*10-8, or $\delta^{18}O$=8.20 ‰, Black et al., 2004). An additional linear adjustment was made for mass fractionation using both standards (Penglai, Temora 2) for samples WS-36A and B, and WS-37A and C. Each unknown uncertainty contains propogated standard precision and in-run errors of each spot. Post O isotope measurement was followed by detailed imaging to access the veracity of the analyses. Analyses which encountered cracks, inclusions or altered portions of zircons, and analyses of zircons with greater than 5% U-Pb discordance were excluded from calculated sample averages.

Table C-2 in Appendix C lists all oxygen isotope results.

2.1.1.3 Lu-Hf isotopes in zircon by LA-MC-ICP-MS

Lutetium-hafnium isotope data were measured in zircons selected from samples previously analysed for U-Pb and O isotopes. Data were collected using a Coherent GeoLas 193 nm ArF laser connected to a Thermo-Scientific Neptune multi-collector inductively coupled plasma mass spectrometer (MC-ICP-MS) at the Advanced Analytical Centre, James Cook University (JCU), Townsville, Australia (Figure 2-3). Spots of 31, 42 or 58 µm diameter were ablated at a 4 Hz laser repetition rate using a laser energy of ~6 J/cm^2. Ablation diameter was modified to ensure analyses

Figure 2-3: Analytical instrumentation used for zircon analyses in this investigation. A. The SHRIMP II at Curtin University with Yongjun Lu, KEB and technician Hao Gao. B. The Cameca IMS 1280 at UWA with Dr. Heejin Jeon. C and D. The GeoLas laser and Neptune multi-collector mass spectrometer at JCU with Tony Kemp and Dr Yi Hu; and Linda Iaccheri and Tony Kemp.

within the same zircon growth zone from where age determinations were made, commonly directly over SIMS pits from prior O isotope analysis. Each analysis was preceded by 30s of baseline collection followed by 60 s of ablation and analyte signal acquisition, comprising 60 measurement cycles of 1s integration time. Time delays between analyses ensured that the ^{180}Hf signal returned to background levels. Helium (1-1.5 l/min, optimised daily) carrier gas transported the sample particles from the laser-ablation cell to a glass mixing chamber with Ar (0.8-0.9 l/min) and sequential addition of N_2 (5-6 ml/min) to improve sensitivity before entering the ICP torch.

Nine masses were simultaneously measured using faraday cups, these being 171 (Yb), 173 (Yb), 175 (Lu), 176 (Hf, Lu Yb), 177 (Hf, centre cup), 178 (Hf), 179 (Hf) and 180 (Hf ± W). Isobaric interferences from ^{176}Lu and ^{176}Yb on ^{176}Hf were corrected using the measured interference-free

isotopes of ^{175}Lu and ^{171}Yb in conjunction with canonical values for ^{176}Lu/^{175}Lu (0.02655; Vervoort et al., 2004) and ^{176}Yb/^{171}Yb=0.897145 (Segal et al., 2003) and their element-specific mass bias factor which is a measure of mass fractionation (β, where $\beta=\ln(R_{true}/R_{meas})/\ln(M_a/M_b)$ and R=isotope ratios and M=atomic mass) such that:

Equations 2-1: Isobaric interference correction calculations.

$$^{176}Lu = {}^{175}Lu_{meas} * \left({}^{176}Lu/{}^{175}Lu\right)_{true} / \left(M^{{}^{176}Lu}/M^{{}^{175}Lu}\right)^{\beta_{Lu}}$$

$$^{176}Yb = {}^{171}Yb_{meas} * \left({}^{176}Yb/{}^{171}Yb\right)_{true} / \left(M^{{}^{176}Yb}/M^{{}^{171}Yb}\right)^{\beta_{Yb}}$$

and,

$$^{176}Hf = {}^{176}(Hf + Yb + Lu)_{meas} - \left({}^{176}Lu + {}^{176}Yb\right)$$

Once corrected for interference, ^{176}Hf/^{177}Hf was also corrected for mass bias using ^{179}Hf/^{177}Hf$_{true}$ (0.7325; Patchett et al., 1981) to calculate β in the same manner as for Yb and Lu. Where Yb signal intensities permitted, β_{Yb} was calculated from the interference-free isotope pairs ^{173}Yb/^{171}Yb=1.130172 (Segal et al., 2003). The mass bias factor for Lu (β_{Lu}) cannot be accurately determined from measured fractionation of Lu isotopes because ^{176}Lu is compromised by interference of ^{176}Yb and ^{176}Hf. By convention β_{Lu} was assumed to approximate β_{Yb} as these elements are chemically similar (Kemp and Hawkesworth, 2013; Woodhead et al., 2004).

Session normalization was made using the low REE zircon Mud Tank (^{176}Hf/^{177}Hf$_{solution}$ =0.282507 ± 6; Woodhead and Hergt, 2005) reported relative to the Hf standard solution JMC, with ^{176}Hf/^{177}Hf=0.282160), measured throughout each analytical session. Reported analytical uncertainties in 176Hf/177Hf of sample zircons combine the reproducibility of Mud Tank zircon analysed in the same session and the in-run error of the analysis. The time-resolved signals were evaluated in order to exclude unstable signals and portions which ablated through zircons from selected signals before processing.

Reference zircons of variably elevated (Yb + Lu)/Hf were analysed to assess the effects of the ^{176}Yb interference correction on ^{176}Hf. Temora 2 with ^{176}Hf/^{177}Hf$_{solution}$ =0.282686 ± 8 and FC1from anorthosite of the Duluth Complex in Minnesota, USA with ^{176}Hf/^{177}Hf$_{solution}$ =0.282184 ± 16 (Woodhead and Hergt, 2005) were analysed throughout the November to December 2015 session and the April 2016 session. Mean^{176}Hf/^{177}Hf values within error of solution values indicate accurate correction of ^{176}Hf for ^{176}Yb and ^{176}Lu interferences (Table 4, Appendix A). For an additional check

on the accuracy of analyses, the measured $^{178}Hf/^{177}Hf$ and $^{180}Hf/^{177}Hf$ were compared with IUPAC values of $^{178}Hf/^{177}Hf$ ~1.46729 and $^{180}Hf/^{177}Hf$ ~1.8867.

Initial $^{176}Hf/^{177}Hf$ was calculated from measured $^{176}Hf/^{177}Hf$ and $^{176}Lu/^{177}Hf$, the Lu decay constant ($\lambda\ ^{176}Lu = 1.865\times10^{-11}\ yr^{-1}$; Scherer et al., 2001; $\lambda\ ^{176}Lu = 1.867\times10^{-11}\ yr^{-1}$;Söderlund et al., 2004) and U-Pb age (t) previously determined by SIMS, using the standard decay equation (Equation 2-2):

Equation 2-2: Decay equation for $^{176}Lu \rightarrow {}^{177}Hf$.

$$\left(^{176}Hf/^{177}Hf\right)_i = \left(^{176}Hf/^{177}Hf\right)_{meas} - \left(^{176}Lu/^{177}Hf\right)_{meas}\left(e^{\lambda t} - 1\right)$$

Calculation of ε_{Hf} ($\varepsilon_{Hf} = (^{176}Hf/^{177}Hf_{zrc(t)}/\ ^{176}Hf/^{177}Hf_{CHUR(t)}) - 1)*10000$) allows for easy comparison of initial $^{176}Hf/^{177}Hf$ by measuring the deviation from the reference CHUR (CHondritic Uniform Reservoir) in parts per ten thousand. We used the CHUR(t) values calculated from a present-day value of $^{176}Hf/^{177}Hf = 0.282785 \pm 11$ and $^{176}Lu/^{177}Hf = 0.0336 \pm 1$ (Bouvier et al., 2008).

2.1.1.4 Trace elements in zircon by LA-ICP-MS

Trace element data were measured at the Advanced Analytical Centre, JCU using a Coherent GeoLas 193 nm ArF laser connected to a Varian 820 quadrupole ICP-MS. The background was measured for 30 or 35 s depending on zircon thickness. Samples were ablated at a 10 Hz laser repetition rate using a laser beam energy of ~6 J/cm^2 for a total signal collection time of 75 s. Helium (1.5 l/min) flushed the sample cell and transported particles to the Ar plasma. Spots of 23, 31, 42 or 58 µm diameter were ablated over the clearest inclusion-free and crack-free portions of zircons. Ablation diameter was modified to maximise diameter within a particular growth domain while excluding portions of the zircon with imperfections such as cracks and inclusions. The particular isotope of each element and dwell time is indicated in Table 5, Appendix A. Less abundant odd isotopes of each element were measured to avoid elemental and molecular interference on the even isotopes.

A block of standards were measured between every 10-15 unknowns: Two analyses each of international glass standards NIST-610 and NIST-612, and one analysis each of natural zircon standard 91500 from a porphyroblastic syenite gneiss at Kuehl Lake, Renfrew County, Ontario, Canada (Wiedenbeck et al., 1995) and Temora 2 were measured. NIST-610 and Temora were measured with a 43 µm spot whereas NIST-612 and zircon 91500 were measured with a 58 µm

spot. Thirty-four elements were measured in 97 analysed spots (96 zircons) from eight samples on April 19, 2016 and 35 elements were measured in 74 zircons from eight samples on April 22, 2016.

The NIST-612 international glass standard was used to calculate elemental concentrations and correct for instrumental drift using the compositions determined by Norman et al. (1996). Elemental calibration was made by normalising to measured ^{29}Si assuming 33 wt % SiO_2 content for all zircons. The April 29 data were split into three sessions to account for (i) a change in count rates/sensitivity when mounts were exchanged, and (ii) bracketing sessions with similar count rates. The April 19 data were treated as one continuous session. The precision of NIST-612 analyses at 2σ are 2-10% for REE, Y, Sr, Nb, Hf, Ta, Th and U at the ppm concentration level, and from 3% to 11% for Sc, Ti, V and Pb. The precision and accuracy of NIST-610 analyses are 2σ are 4-14% for REE, Y, Sr, Nb, Hf, Ta, <19% for Th and U, and from 5% to 15% for Sc, Ti, V and Pb. The precision and accuracy of 91500 analyses are 2σ are 5-15% for REE, Y, Sr, Nb, Hf, Ta, Th and U, except where La was below detection limits and Pr which had <40% uncertainty, and from 2% to 15% for Ti and Pb. Measured element abundances for 91500 zircons are within the recommended ranges reported in Wiedenbeck et al. (2004).

Inclusions, especially apatite, were ubiquitous in many of the zircons analysed, and despite taking care to avoid them by consulting high resolution imaging, inclusions were commonly encountered. To mitigate the possibiliy of including mineral inclusions, the signal of each isotope of each analysis was reviewed. Where obvious spikes were encountered the signal was filtered. In the cases of the natural zircons, the best window was selected to exclude compromised portions of analyses (typically by mineral inclusions). Mineral inclusions were most often highlighted by anomalously high LREE, especially La and Pr, and elements such as Ca ± P ± W ± Sr ± Ti ± Nb ± V ± Sc and in some cases Mo ± Cu. Some analyses were completely compromised by inclusions. Potential inclusions were then investigated by evaluation of chondrite normalised REE patterns, and checking against Ca, Sr, Ti, and P. The following criteria were used to systematically exclude contaminated analyses: La >1 ppm is taken to reflect apatite contamination; Fe >5,000 ppm is taken to reflect contamination by Fe oxides; Ti >50 ppm is taken to reflect contamination by Ti-(Fe-) oxides; and Ba >8 ppm is taken to represent contamination by fluid inclusions and cracks (Lu et al., 2016).

Table C-4 in Appendix C lists all zircon trace element results.

2.3. CONTOUR MAPS OF ISOTOPE AND CHEMICAL DATA

Spatial contouring of isotopic and geochemical data (Chapters 3 and 4) was accomplished using the spatial analyst extension in ArcGIS. The natural neighbour interpolation method was employed, as suggested by Champion and Huston (2016). The kriging interpolation technique was also explored. Kriging uses statistical models to make predictions rather than deterministics interpolations that are based directly on surrounding points or resulting smoothness. Kriging allows for more control by the user, but tended to cause a strong linear warp to these data inconsistent with geology.

Natural neighbour interpolation produces a smooth approximation using a local subset of data around a query point. Therefore, it does not infer trends in the data. The algorithm works by using the Delaunay triangulation to assign edges between a subset of points for the point dataset (Sibson, 1981). These edges intersect at nodes, therefore, the nearest subset of data points are represented by polygons. Then the algorithm creates a polygon (called a Voroni cell) over the point to be interpreted, also based on the Delaunay triangulation (see Figure __ for explanatory diagram) to create edges between data points. Weights are then assigned to the underlying polygons (created by the Delaunay triangulation and corresponding to the points of the surrounding data) that the Veroni cell overlaps. The weights reflect the area of overlap. This is described by Equation 2-3 (Sibson, 1981).

Equation 2-3: Natural neighbour interpolation.

$$G(x,y) = \sum_{i=1}^{n} w_i f(x_i, y_i)$$

$$G(x,y) - estimate\ at\ (x,y)$$
$$w_i - weights$$
$$f(x_i, y_i) - known\ data\ at\ (x_i, y_i)$$

Natural neighbour interpolation produced an interpolation more consistent with geology than Inverse Distance Weighted (IDW) interpolation. The IDW method is also deterministic. It finds a subset of the closest points and simply assigns weight by distance to the query point.

Bins were constructed for whole rock geochemical data using Jenks Natural Breaks (Jenks, 1967). Bins were manually constructed for U-Pb and Lu-Hf isotopic data. This was done to highlight natural meaningful geological breaks. Jenks natural breaks did not yield meaningful breaks in the study area for isotopic data. This is because the maps were constructed using data from the whole of

the Superior Craton. As breaks are determined by area, areas poorly represented by sampling (far north in Ontario, including North Caribou, Hudson Bay, and much of Quebec) skewed the distribution. For overlapping data points, the mean was used.

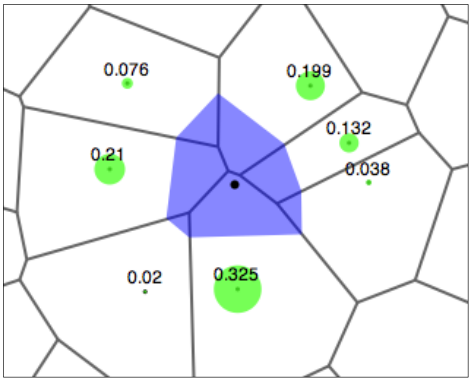

Figure 2-4: A schematic diagram (https://en.wikipedia.org/wiki/Natural_neighbor_interpolation) to illustrate the principles of the natural neighbor interpolation. A voroni cell is created around each data point. The point to be interpreted, here the black dot, is also given a Voroni cell, here the purple region. The amount of overlap with surrounding points provides the basis for assigning the weights, here represented by the size of the green circles.

A caveat for interpolation of geological data using automated methods is that the contours produce untrue geological pictures. The areas between data points are naturally represented as a transition by the contouring, but this is seldom a reflection of geology. For example, consider two rock bodies that are separated by an igneous contact, where the respective units are 10 km apart. Measured ages return 3.0 Ga for Unit 1 and 2.7 Ga for Unit 2. The only geological meaningful ages are 3.0 and 2.7 Ga. However, the interpolation will suggest that rocks between these samples range gradationally between 3.0 – 2.7 Ga. This is geologically false. Only measured points are real. Therefore, interpolation of geological data is limited to the purpose of illuminating broad patterns in dataset. It has the benefit of excluding direct human bias during the interpretation. Nevertheless, bias is introduced by the method chosen and the parameters used. Moreover, bias is inherent in datasets. Some bias is geological, whereas some directly reflects sampling distribution that is influenced by, for example, accessibility.

REFERENCES

Black, L.P., Kamo, S.L., Allen, C.M., Aleinikoff, J.N., Davis, D.W., Korsch, R.J. and Foudoulis, C., 2003. TEMORA 1: a new zircon standard for Phanerozoic U–Pb geochronology. Chemical Geology, 200(1–2): 155-170.

Black, L.P., Kamo, S.L., Allen, C.M., Davis, D.W., Aleinikoff, J.N., Valley, J.W., Mundil, R., Campbell, I.H., Korsch, R.J., Williams, I.S. and Foudoulis, C., 2004. Improved 206Pb/238U microprobe

geochronology by the monitoring of a trace-element-related matrix effect; SHRIMP, ID–TIMS, ELA–ICP–MS and oxygen isotope documentation for a series of zircon standards. Chemical Geology, 205(1–2): 115-140.

Bouvier, A., Vervoort, J.D. and Patchett, P.J., 2008. The Lu–Hf and Sm–Nd isotopic composition of CHUR: Constraints from unequilibrated chondrites and implications for the bulk composition of terrestrial planets. Earth and Planetary Science Letters, 273(1–2): 48-57.

Buse, S., Lewis, D. and Magnus, S., 2009. Field investigations in the Lumby Lake greenstone belt, northwestern Ontario: new insights into the geology, structure and economic potential.

Champion, D.C. and Huston, D.L., 2016. Radiogenic isotopes, ore deposits and metallogenic terranes: Novel approaches based on regional isotopic maps and the mineral systems concept. Ore Geology Reviews, 76: 229-256.

Fenwick, K.G., 1976. M2297 Finlayson Lake, Rainy River District, Map, 2000 Series. Ontario Ministry of Northern Development and Mines, Ontario Geological Survey, pp. 52B13, Finlayson Lake, Freeborn, Ontario, Canada, Schwenger, Steeprock Lake.

Fralick, P., Hollings, P. and King, D., 2008. Stratigraphy, geochemistry, and depositional environments of Mesoarchean sedimentary units in western Superior Province: Implications for generation of early crust. In: K.C. Condie and V. Pease (Editors), When Did Plate Tectonics Begin on Planet Earth. Geological Society of America Special Papers, pp. 77-96.

Fralick, P. and King, D., 1996. Mesoarchean evolution of western Superior Province: evidence from metasedimentary sequences near Atikokan, Western Superior Transect, Second Annual Workshop, Lithoprobe Secretariat, University of British Columbia, Vancouver, British Columbia, pp. 29-35.

Hanchar, J.M. and Miller, C.F., 1993. Geochemistry of Accessory Minerals Zircon zonation patterns as revealed by cathodoluminescence and backscattered electron images: Implications for interpretation of complex crustal histories. Chemical Geology, 110(1): 1-13.

Hollings, P. and Wyman, D., 1999. Trace element and Sm-Nd systematics of volcanic and intrusive rocks from the 3 Ga Lumby Lake Greenstone belt, Superior Province: evidence for Archean plume-arc interaction. Lithos, 46(2): 189-213.

Jackson, M.C., 1985. Geology of the Lumby Lake area, western part, districts of Kenora and Rainy River. Ontario Geological Survey, Open File Report 5534. 151p.

Jenks, G.F., 1967. The data model concept in statistical mapping. International yearbook of cartography, 7(1): 186-190.

Kemp, A. and Hawkesworth, C., 2013. Growth and differentiation of the continental crust from isotope studies of accessory minerals. In: R. Rudnick (Editor), Treatise on Geochemistry. The Crust. The Crust, vol. 12, second ed. Elsevier Science, Oxford.

Kröner, A., Kehelpannala, K. and Kriegsman, L.M., 1994. Origin of compositional layering and mechanism of crustal thickening in the high-grade gneiss terrain of Sri Lanka. Precambrian Research, 66(1): 21-37.

Li, X.-H., Long, W.-G., Li, Q.-L., Liu, Y., Zheng, Y.-F., Yang, Y.-H., Chamberlain, K.R., Wan, D.-F., Guo, C.-H., Wang, X.-C. and Tao, H., 2010. Penglai Zircon Megacrysts: A Potential New Working Reference Material for Microbeam Determination of Hf–O Isotopes and U–Pb Age. Geostandards and Geoanalytical Research, 34(2): 117-134.

Ludwig, K., 2009. SQUID 2: A User's Manual, rev. 12 Apr, 2009. Berkeley Geochron. Ctr. Spec. Pub. 5 110 p.

Nasdala, L., Hofmeister, W., Norberg, N., Martinson, J.M., Corfu, F., Dörr, W., Kamo, S.L., Kennedy, A.K., Kronz, A. and Reiners, P.W., 2008. Zircon M257-a Homogeneous Natural Reference Material for the Ion Microprobe U-Pb Analysis of Zircon. Geostandards and Geoanalytical Research, 32(3): 247-265.

Nelson, D.R., Robinson, B.W. and Myers, J.S., 2000. Complex geological histories extending for ≥4.0 Ga deciphered from xenocryst zircon microstructures. Earth and Planetary Science Letters, 181(1–2): 89-102.

Norman, M., Pearson, N., Sharma, A. and Griffin, W., 1996. Quantitative analysis of trace elements in geological materials by laser ablation ICPMS: instrumental operating conditions and calibration values of NIST glasses. Geostandards Newsletter, 20(2): 247-261.

Ontario Geological Survey, 2011. 1: 250 000 Scale Bedrock Geology of Ontario-Revision 1, MRD 126-REV-1. Ontario Geological Survey.

Patchett, P.J., Kouvo, O., Hedge, C.E. and Tatsumoto, M., 1981. Evolution of continental crust and mantle heterogeneity - Evidence from Hf isotopes. Contributions to Mineralogy and Petrology, 78(3): 279-297.

Scherer, E., Munker, C. and Mezger, K., 2001. Calibration of the Lutetium-Hafnium clock. Science, 293(5530): 683-7.

Segal, I., Halicz, L. and Platzner, I.T., 2003. Accurate isotope ratio measurements of ytterbium by multiple collection inductively coupled plasma mass spectrometry applying erbium and hafnium in an improved double external normalization procedure. Journal of Analytical Atomic Spectrometry, 18(10): 1217-1223.

Sibson, R., 1981. A brief description of natural neighbour interpolation. Interpreting multivariate data, 21, 21-36 pp.

Söderlund, U., Patchett, P.J., Vervoort, J.D. and Isachsen, C.E., 2004. The 176Lu decay constant determined by Lu–Hf and U–Pb isotope systematics of Precambrian mafic intrusions. Earth and Planetary Science Letters, 219(3–4): 311-324.

Stacey, J.S. and Kramers, J.D., 1975. Approximation of terrestrial lead isotope evolition by a two-stage model. . Earth and Planetary Science Letters, 26.

Stern, R.A., Bodorkos, S., Kamo, S.L., Hickman, A.H. and Corfu, F., 2009. Measurement of SIMS Instrumental Mass Fractionation of Pb Isotopes During Zircon Dating. Geostandards and Geoanalytical Research, 33(2): 145-168.

Stone, D., 2008. Precambrian geology, Atikokan area; Ontario Geological Survey, Preliminary Map P.3349–Revised, scale 1:50 000.

Stone, D., 2010. Precambrian geology of the central Wabigoon Subprovince area, northwestern Ontario. Ontario Geological Survey, Open File Report 5422: 130.

Stone, D., Kamineni, D.C. and Jackson, M.C., 1992. Precambrian geology of the Atikokan area, northwestern Ontario; . Geological Survey of Canada, Bulletin 405: 106p.

Tomlinson, K.Y., Hughes, D.J., Thurston, P.C. and Hall, R.P., 1999. Plume magmatism and crustal growth at 2.9 to 3.0 Ga in the Steep Rock and Lumby Lake area, Western Superior Province. Lithos, 46(1): 103-136.

Vervoort, J.D., Patchett, P.J., Söderlund, U. and Baker, M., 2004. Isotopic composition of Yb and the determination of Lu concentrations and Lu/Hf ratios by isotope dilution using MC-ICPMS. Geochemistry, Geophysics, Geosystems, 5(11): n/a-n/a.

Wiedenbeck, M., AllÉ, P., Corfu, F., Griffin, W.L., Meier, M., Oberli, F., Quadt, A.V., Roddick, J.C. and Spiegel, W., 1995. THREE NATURAL ZIRCON STANDARDS FOR U-TH-PB, LU-HF, TRACE ELEMENT AND REE ANALYSES. Geostandards Newsletter, 19(1): 1-23.

Wiedenbeck, M., Hanchar, J.M., Peck, W.H., Sylvester, P., Valley, J., Whitehouse, M., Kronz, A., Morishita, Y., Nasdala, L., Fiebig, J., Franchi, I., Girard, J.P., Greenwood, R.C., Hinton, R., Kita, N., Mason, P.R.D., Norman, M., Ogasawara, M., Piccoli, P.M., Rhede, D., Satoh, H., Schulz-Dobrick, B., Skår, O., Spicuzza, M.J., Terada, K., Tindle, A., Togashi, S., Vennemann, T., Xie, Q. and Zheng, Y.F., 2004. Further Characterisation of the 91500 Zircon Crystal. Geostandards and Geoanalytical Research, 28(1): 9-39.

Wilks, M.E. and Nisbet, E.G., 1988. Stratigraphy of the Steep Rock Group, northwest Ontario: A major Archaean unconformity and Archaean stromatolites. Canadian Journal of Earth Sciences, 25: 370–391.

Woodhead, J., Hergt, J., Shelley, M., Eggins, S. and Kemp, R., 2004. Zircon Hf-isotope analysis with an excimer laser, depth profiling, ablation of complex geometries, and concomitant age estimation. Chemical Geology, 209(1–2): 121-135.

Woodhead, J.D. and Hergt, J.M., 2005. A preliminary appraisal of seven natural zircon reference materials for in situ Hf isotope determination. Geostandards and Geoanalytical Research, 29(2): 183-195.

Chapter 3: Late Archaean geodynamic changes in the Southwestern Superior Craton implied from secular geochemistry of felsic intrusions

ABSTRACT

The late Archaean (3.0-2.7 Ga) was a time of magmatic diversification globally, but the magnitude and timing of changes are only partially constrained, and the petrogenetic processes and tectonic triggers behind the secular variations remain unclear. This study integrates geochemical and geochronological data in a spatial reference frame for 3.0– 2.7 Ga felsic intrusive rocks from the Marmion terrane in the Western Superior Craton of Canada. Secular and special variations illuminate evolving magma petrogenesis and help unravel the nature and placement of terrane margins.

The Marmion terrane records a series of peaks in U-Pb ages and inheritance at 3.0, 2.93, 2.9, 2.82, 2.78, 2.73, and 2.69 Ga superimposed on near-continuous magmatism. Hiatuses occur from 2.89 – 2.82 Ga and 2.78 – 2.75 Ga. Felsic intrusions are tightly coupled in time and space with greenstone belt development, requiring a tectonic mechanism able to simultaneously produce the tholeiitic basalt – komatiitic basalt sequences and calc-alkalic felsic magmatism. Inheritance <3.0 Ga measured within a granodiorite emplaced in the Irene-Eltrut Lakes gneisses demonstrates that Marmion basement extends west of the current designation. Inheritance measured to 2.8 Ga within a 2.72 Ga phase of the Atikwa batholith within the Western Wabigoon terrane suggests accretion of the Western Wabigoon terrane to the composite Marmion – Winnipeg River terrane before 2.72 Ga. Alternatively the Western Wabigoon is an autochthonous back arc rift with respect to the Marmion – Winnipeg River terrane.

The data highlight two stepwise changes in chemistry within felsic intrusive rocks: at 2.75 Ga and 2.69 Ga, the latter with the appearance of sanukitoids. At 2.75 Ga, variability in major oxides increases, and some LILE, LREE, MREE, Sr/Y and La/Lu increase. These changes can be attributed to a greater melting depth and imply a thicker crust and lithosphere and/or may reflect a change in subduction angle or onset of subduction. With the intrusion of a sanukitoid suite at ~2.69 Ga, there is an increase in Mg#, MgO, FeO, P_2O_5, Ni, Co, Cr, Sc, LREE and MREE, and steeper HREE. The high abundances of both compatible and incompatible elements suggest a contribution from a metasomatised mantle.

3.1. INTRODUCTION

The Superior Craton is the largest contiguous block of Archaean crust in the world. As such, geologic, geochemical, isotopic and structural characterisation of this craton holds promise for painting a coherent picture from its inception to growth, assembly and cratonisation. Perhaps the greatest constraint on the cratonic evolution has been provided by the advent and ongoing application of U-Pb geochronology, which provides the fundamental temporal context for stratigraphic, structural, metamorphic and isotopic studies. Geochronological and isotopic studies in the Superior Craton have highlighted crustal domains ('terranes') with distinct magmatic histories and basement signatures (e.g., Stott, 2011; Tomlinson et al., 2004). However, many isotopically defined terrane boundaries are geologically cryptic. For example, the Wabigoon superterrane of the Western Superior Craton comprises four isotopically distinct terranes with internal margins that have been overprinted by younger magmatism and/or deformation. The nature of these terrane boundaries therefore remains enigmatic. Clarifying terrane relationships bears much on geodynamic models of the Wabigoon superterrane and the Superior Craton.

The present study investigates the crustal evolution and nature of the margins of the Marmion terrane in the south-central Wabigoon superterrane using the secular chemistry of granite-gneiss complexes. Despite its relatively small size (13900 km^2), the Marmion terrane records a protracted and near-continuous history of magmatism and greenstone belt formation from 3.0 Ga across the Meso-Neoarchaean boundary to cratonisation at <2.7 Ga. Consequently, it is an ideal place to evaluate the temporal evolution of igneous geochemistry, to test models for granite-greenstone associations, and to consider correlations in lithosphere ages between and within terranes.

Previous work in the Western Superior Craton alluded to a change in the chemistry of granitic rocks with time and in space. Ermanovics et al. (1979) noted a secular evolution from sodic to potassic magmatism in Neoarchaean felsic intrusive rocks of the Western Wabigoon – Winnipeg River area, whereas Ayres and Cerny (1982) stressed a spatial control on chemistry of intrusive rocks by the crust into which the granites were emplaced. Beakhouse and McNutt (1991) interpreted the observed secular and spatial changes as petrogenetic shifts from earlier melting of basalt at depth to later infracrustal melting in a subduction-accretionary setting. Corfu and Stone (1998) also interpreted a progressive shift within the Berens River area of the north-western Superior craton from early tonalite to granodiorite and then to granite, culminating in late granite and monzodiorite, in the framework of convergent margin tectonics. Only one Mesoarchaean rock was represented by these studies, and secular changes across the Mesoarchaean remain unclear.

This contribution presents a spatially constrained, geochemical – chronological picture of felsic intrusive rocks of the southwestern Superior Craton in order to provide a window into the tectonic processes and differentiation mechanisms that generated them. Unravelling the local geochronology and geochemistry of the granites in the study area sheds light on some of the questions at the heart of Archaean geology such as the conundrum of bimodal chemistry of granite-greenstone belts, the significance of the punctuated magmatic record, and the timing and tectonic significance of geochemical shifts. Specific aims include compiling a comprehensive timeframe of magmatism, identification of temporal and spatial periods of reworking preserved in inherited zircons, and elucidating relationships to the lower crust and mantle lithosphere. Proximal areas of neighbouring crust, including the Winnipeg River, Eastern Wabigoon, Western Wabigoon and Wawa terranes as well as the Quetico basin, were also sampled to better understand the nature of the designated terrane margins. Data from a parallel study of the Wabigoon superterrane (Lu et al., unpublished data) is integrated in order to afford comparisons to surrounding terranes. The U-Pb geochronology for this study provides time constraints for subsequent Hf and O isotopic studies presented in Chapter 4. In this chapter, geochemical data is applied in a general sense to evaluate broad comparisons between lithological groups and over time, but is incorporated as part of detailed petrogenetic investigations in Chapters 5 and 6.

3.2. GEOLOGICAL SETTING

In the Western Superior Craton, subparallel and east-west trending 100-400 km-wide volcano-plutonic terranes and superterranes (comprised of previously amalgamated terranes) are separated by linear, highly metamorphosed sedimentary basins stretching >1000 km (Figure 3-1). The prominent alternating pattern led Langford and Morin (1976) to develop a model of cratonisation through amalgamation of magmatic arcs with intervening accretionary prisms. A plate tectonic understanding has since become the reigning paradigm for the Superior Craton (Card, 1990; Percival and Williams, 1989; Stott, 1997). Non-plate tectonic models involving mantle plumes and/or mantle convection without subduction have also been proposed (Bedard et al., 2003; Hamilton, 1998). Irrespective of the mechanism, structural and geophysical evidence support horizontal assembly during the Kenoran Orogeny (Bédard and Harris, 2014; Percival et al., 2006; Percival and Williams, 1989; White et al., 2003). Tectono-thermal chronology indicates that the broader Kenoran Orogeny occurred as several accretion events from north to south, where Paleo- to Mesoarchean fragments – the Hudson Bay terrane, North Caribou superterrane, composite Winnipeg River-Marmion terrane, and the Minnesota River Valley terrane – were progressively assembled over ~10 m.y periods (Percival et al., 2006 and references therein). The following

paragraphs summarise the significant magmatic-metamorphic features of the Western Superior Craton.

3.2.1. Hudson Bay terrane

The Hudson Bay terrane to the far north (Figure 3-1) comprises 3.2-3.1 Ga and 2.85-2.81 Ga felsic magmatism with sparse greenstone belts (Böhm et al., 2003; Skulski et al., 2000). Evidence for an Eo - Paleoarchaean history is provided by detrital zircons <3.9 Ga in paragneiss with Nd model ages to 4.2 Ga (Böhm et al., 2003) together with a 3.54 Ga orthogneiss, <3.8 Ga Nd model ages in orthogneiss (Böhm et al., 2000) and >3.5 Ga inherited zircons (Skulski et al., 2000). Metamorphism

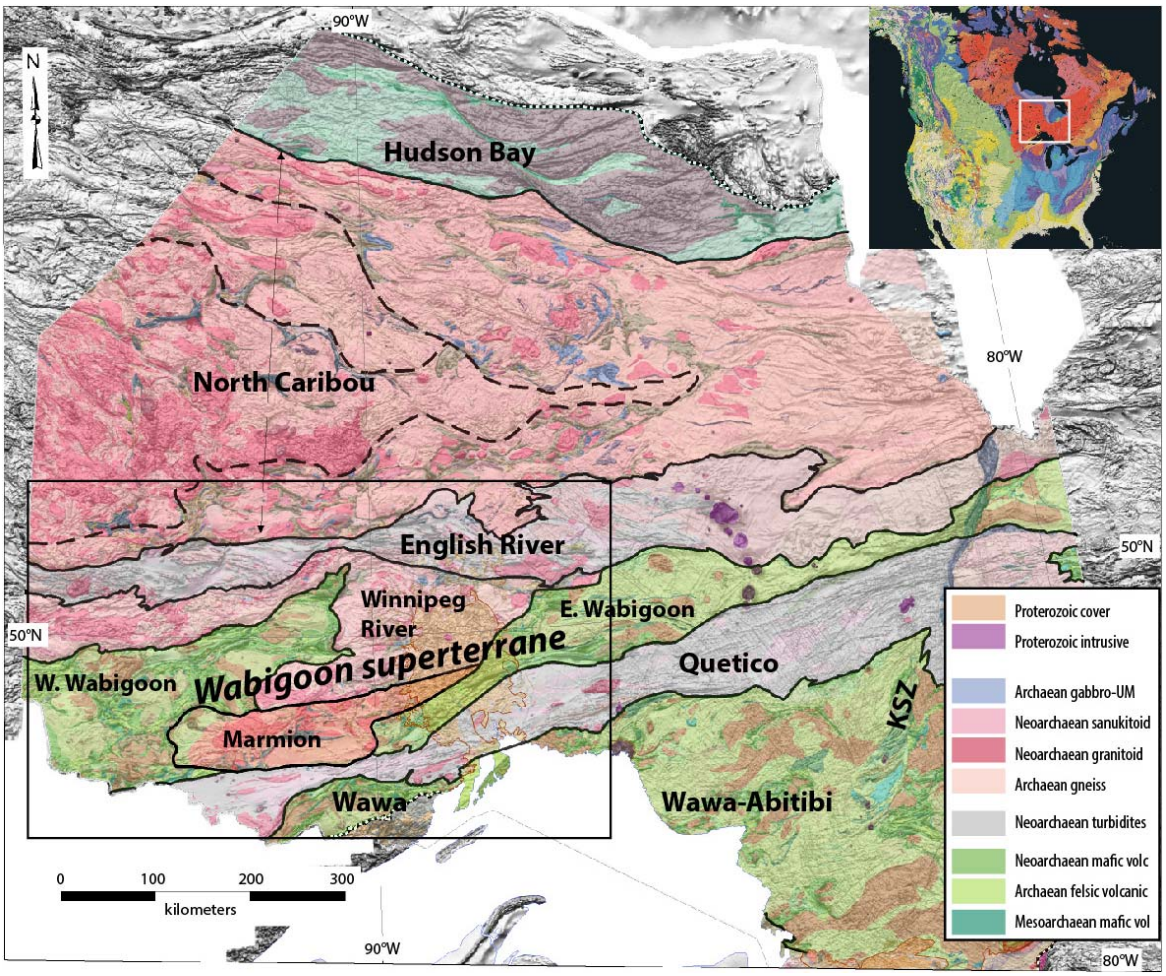

Figure 3-1: Geological map of the Superior Craton in Ontario with shaded magnetic relief. Black outline indicates extent of Figure 3-2. Geology and shaded magnetic relief from Ontario Geological Survey (2011), terrane divisions from Stott (2011). The Wabigoon superterrane is indicated between the English R. and Quetico basins. Abbreviations: KSZ – Kapuskasing structural zone, W-A – Wawa-Abitibi. Inset shows the simplified geology map of the North American continent with the location of the study area highlighted by the white square. Tectonic and map of North America from (Barton et al., 2003).

at 2.74 Ga (Skulski et al., 2000) is postulated to record an early deformation event, followed by amphibolite grade metamorphism at 2.68 and 2.61 Ga (Böhm et al., 2003), an interpreted result of accretion with the North Caribou superterrane.

3.2.2. North Caribou terrane

In an accretionary model, the North Caribou terrane is considered to be the nucleus against which the Hudson Bay terrane from the north, and the remaining fragments to the south were accreted (Thurston et al., 1991). The North Caribou terrane records felsic to intermediate intrusive magmatism and komatiitic-basaltic greenstone belt activity from 3.0 to 2.7 Ga. It has been subdivided into domains and terranes which have been variably correlated with each other, and which retain Nd and Hf isotopic signatures indicative of reworking 3.0 Ga material (Corfu and Stott, 1996; Henry et al., 2000; Hollings et al., 1999; Stevenson et al., 2009; Wyman et al., 2011). Both the northern (Island Lake and Oxford-Stull domains) and southern (Uchi domain/terrane) margins have a greater ratio of greenstone belts to granitic plutons compared with the core, formerly the Berens River and Sachigo subprovinces. Seismic lines image north dipping reflectors in the south and south dipping reflectors in the north (White et al., 2003). These reflectors have been interpreted as a doubly verging orogen with the North Caribou in an upper plate setting during collision with the Hudson Bay Terrane and with the composite Winnipeg River – Marmion terrane (Percival et al., 2006). An alternative interpretation involves a crustal scale synclinorium, which is supported in the south (over the north-dipping reflectors) by southward increases in paleopressures (Hynes and Song, 2006).

3.2.3. English River basin

The southern margin of the North Caribou terrane is in fault contact with the turbiditic English River basin. English River greywackes contain detrital zircons from 3.25 to 2.70 Ga (Corfu et al., 1995; Stott et al., 2002) and are intruded by 2.70 Ga plutons (Corfu et al., 1995). The 2.713 to 2.701 Ga North Caribou – Wabigoon collision (Stott and Corfu, 1991) is thought to be ~ contemporaneous with sedimentation within the English River basin. Basin margins grade from greenschist facies inward to high T and low P migmatitic amphibolite and to central granulite facies at ~750°C and 0.6 kbar (Harris, 1976; Perkins and Chipera, 1985). Consequent peraluminous granites abound in amphibolite and granulite facies portions of the belt. Granulite metamorphism and concomitant peraluminous granite emplacement are dated at 2.69 Ga, followed by later metamorphism and pegmatite intrusion at 2.68 and 2.67 Ga (Corfu et al., 1995). The southern margin is in faulted contact with the Wabigoon superterrane (Card, 1990).

3.2.4. Wabigoon superterrane

The Wabigoon superterrane comprises four isotopically distinct terranes: the Paleoarchaean Winnipeg River, Mesoarchaean Marmion, and Neoarchaean Western and Eastern Wabigoon terranes (see Figure 3-1). Whereas sharp geological contrasts mark external boundaries of the Wabigoon superterrane, much of the internal boundaries (defined by Nd isotopes) are cryptic in geology and geophysics and are overprinted by post-tectonic emplacement of large, multiphase granitic batholiths (Figure 3-2). The Wabigoon superterrane was initially subdivided into a central diapiric axis (Edwards and Sutcliffe, 1980) flanked by lower metamorphic grades and with volcanic-dominated geology to the east and west. Neodymium isotopic work by Henry et al. (2000) and Tomlinson et al. (2004) was instrumental in establishing the distinct histories within the Wabigoon superterrane that U-Pb geochronology and metamorphism hinted at, and provided a means to place terrane divisions on a map.

Some uncertainty remains as to the placement and nature of internal terrane margins, but the current understanding suggests that the plutonic 3.4 Ga Winnipeg River terrane (Beakhouse, 1991) stretches across the northern margin, and consists largely of Mesoarchaean crust reworked by Neoarchaean granitic plutonism, typically <2.73 Ga (Tomlinson et al., 2004). The oldest rocks of the Wabigoon superterrane are located within the 3.32 to 3.05 Ga Tannis Lake (Davis et al., 1988; Melnyk et al., 2006) and 3.26 to 3.17 Ga Cedar Lake (Corfu, 1988; Melnyk et al., 2006) and 3.08 Ga Caribou Lake (Davis et al., 1988) tonalite gneisses in the northwest, in an area with a paucity of greenstone belts thought to represent the middle crust (Beakhouse and McNutt, 1991). Hafnium isotopic signatures in zircons from the Tannis Lake and Caribou Lake gneisses indicate reworking of Paleoarchaean crust (Davis et al., 2005). Nd model ages of up to 3.4 Ga distinguish the Winnipeg River terrane from the Marmion terrane, which yields Nd model ages <3.02 Ga (Davis and Jackson, 1988; Tomlinson et al., 2004).

The <2.8 Ga greenstone-dominated Western Wabigoon terrane (Henry et al., 1998; Henry et al., 2000) contains mostly 2.74 – 2.72 Ga tholeiitic to calc-alkaline volcanism (Corfu and Davis, 1992; Davis et al., 1985; Davis and Trowell, 1982; Stone et al., 2010) interspersed with approximately contemporaneous large TTG batholiths (Blackburn et al., 1985; Tomlinson et al., 2004). Several plutonic rocks are dated at ~2.71 Ga (Beakhouse et al., 1988; Corfu, 1988; Davis and Smith, 1991). The Western Wabigoon terrane is thought to have developed either as an ensialic rift (Blackburn et al., 1991), or oceanic crust formed separately from the Marmion and Winnipeg River terranes (Davis and Smith, 1991; Melnyk et al., 2006; Percival and Helmstaedt, 2004; Percival et al., 2004; Tomlinson et al., 2004). Sanborn-Barrie and Skulski (2006) interpret collision with the Winnipeg

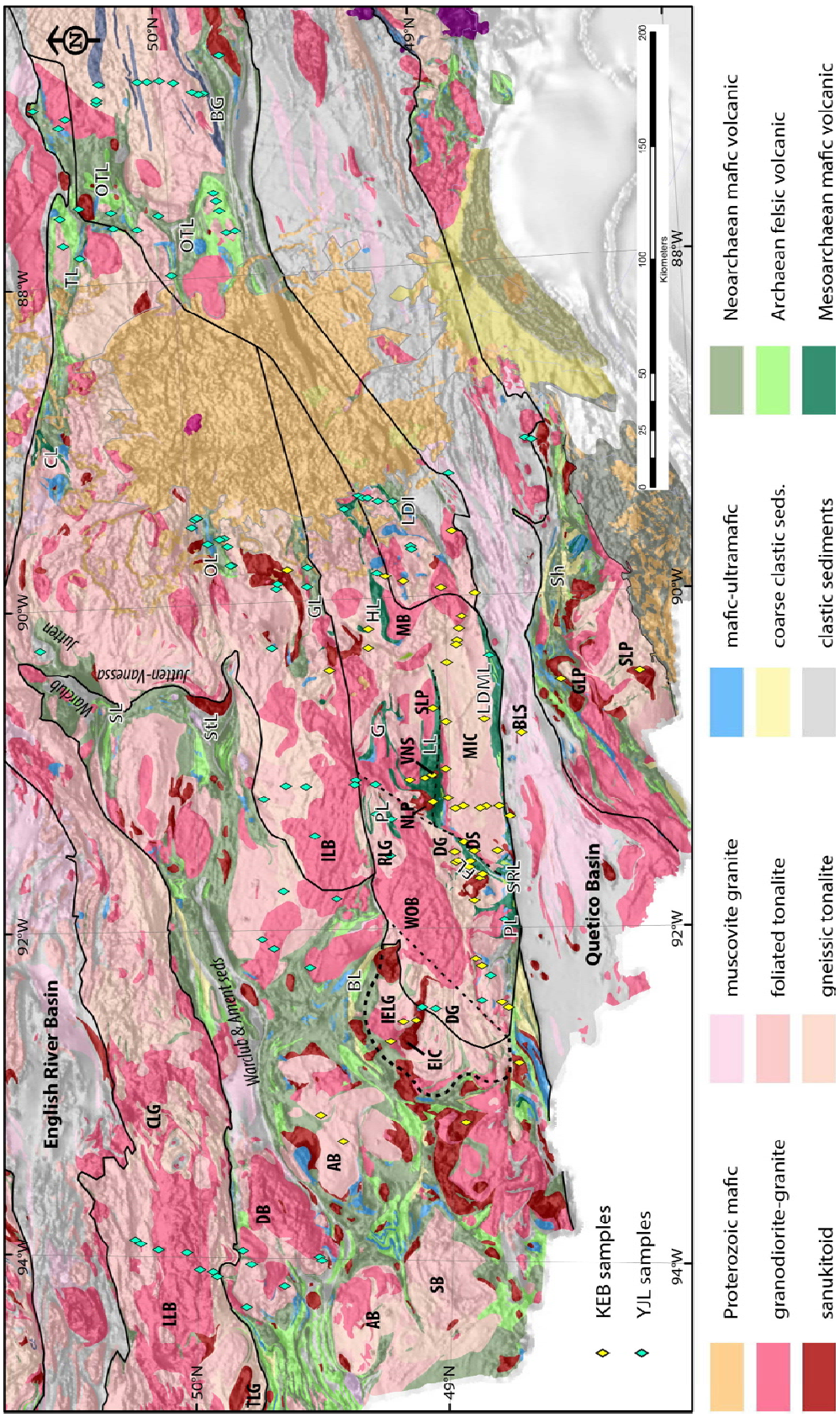
English River Basin
Quetico Basin
Warclub & Amment seds
Jutten-Vanessa
Warclub
Jutten
KEB samples
YJL samples
Proterozoic mafic
granodiorite-granite
sanukitoid
muscovite granite
foliated tonalite
gneissic tonalite
mafic-ultramafic
coarse clastic seds.
clastic sediments
Neoarchaean mafic volcanic
Archaean felsic volcanic
Mesoarchaean mafic volcanic
Kilometers
94°W
92°W
90°W
88°W
50°N
49°N
CLG
LLB
TLG
DB
AB
SB
ILB
BL
IELG
EIC
DG
WOB
RLG
PL
NLP
VNS
LL
SLP
G
DS
SRL
MIC
LDML
BLS
GLP
SLP
Sh
LDI
HL
MB
GL
OL
StL
SL
CL
TL
OTL
BG

Figure 3-2: Wabigoon superterrane showing sample locations. Terrane boundaries are from Stott (2011), shown in solid black lines. Thick dashed line to the west indicates proposed placement of the Marmion – Western Wabigoon terrane boundary. Thinner dashed lines indicate the cryptic structure internal to the Marmion terrane imaged by whole rock chemistry just west of the Hillyer domain and the WOB, the Marmion shear zone (MSZ) and Lumby Lake fault. Abbreviations for intrusions in black lettering from west to east: TLG – Tannis Lake gneiss, LLB – Lount Lake batholith, DB – Dryberry batholith, AB – Atikwa batholith, CLG – Cedar Lake gneiss, IELG – Irene-Eltrut Lakes gneisses EIC – Entwine intrusive complex, WOB – White Otter batholith, DG – Dashwa gneisses, RLG – Raven Lake Gneiss, ILB – Indian Lake batholith, DS – Diversion stock, NLP – Norway Lake pluton, VNS – Van Nostrand stock, MIC – Marmion intrusive complex, SLP – Scotch Lake pluton, BLS – Brule Lake stock, GLP – Greenwater Lake pluton, SLS – Sunbow Lake pluton and MB – Muskeg batholith; Abbreviations for greenstone belts in white lettering from west to east: BL – Bending Lake, PL – Perch Lake, SR – Steep Rock, FL – Finlayson Lake, PL – Phyllis Lake, G – Graham, LL – Lumby Lake, StL – Sturgeon Lake, SL – Savant Lake, LDML – Lac Des Milles Lacs, Sh – Shebandewan, HL – Heaven Lake, GL – Garden Lake, OL – Obonga Lake, LDI – Lac Des Illes, CL – Caribou Lake (also location of Caribou Lake gneiss), TL – Toronto Lake, OTL – Onaman - Tashota, BG – Beardmore - Geraldton. The location of the Jutten and Vanessa assemblages are indicated. Yellow and green diamonds indicate samples analysed for U-Pb during this study and by Lu et al. (unpublished) respectively.

River terrane at 2.703 – 2.696 Ga during the deposition of the Warclub and Ament Bay sediments (Figures 3-2, 3-3). However, inherited <2.8 Ga zircons within the 2.71 Ga Snowshoe batholith (west of Figure 3-2) in the northwest and Mesoarchaean zircons in <2.71 Ga sedimentary rocks (Davis and Smith, 1991) support amalgamation before a 2.713 +0.013/-0.002 Ga tonalite dike lacking D1 deformation and concomitant with deformation events recorded in the Winnipeg River terrane as proposed by Percival et al. (2004). The proposed cryptic suture lies between the <2.88 to >2.75 Ga basalt-dominated Jutten and 2.93 Ga Vanessa assemblages and 2.78-2.72 Ga oceanic crust to the west within the eastern Savant and Sturgeon Lakes greenstone belts respectively (Sanborn-Barrie and Skulski, 2006). Within the Jutten assemblage, basal conglomerate sits unconformably on Winnipeg River basement. Overlying quartzite contains 3.6 – 2.9 Ga detrital zircons interpreted to be sourced from the Winnipeg River terrane (Davis and Moore, 1991), and the succession is interpreted as a continental margin sequence (Sanborn-Barrie and Skulski, 2006).

The greenstone-dominated Eastern Wabigoon terrane in the southeast records <2.9 Ga magmatism, inheritance and Nd model ages, and may have reworked Marmion crust (Tomlinson et al., 2004) or developed separately . The current designation (Stott, 2011) places the 3.0-2.92 Ga stratigraphy of the Toronto and Tashota assemblages within the Winnipeg River terrane, and the remainder of the Onaman-Tashota greenstone belt within the Eastern Wabigoon terrane. Central volcanism occurred at 2.78-2.769, 2.738 and 2.734-2.722 Ga within the respective Onaman, Willet, Elmherst-Rickaby and Metcalfe-Venus assemblages (Stott et al., 2002; Tomlinson et al., 2004).

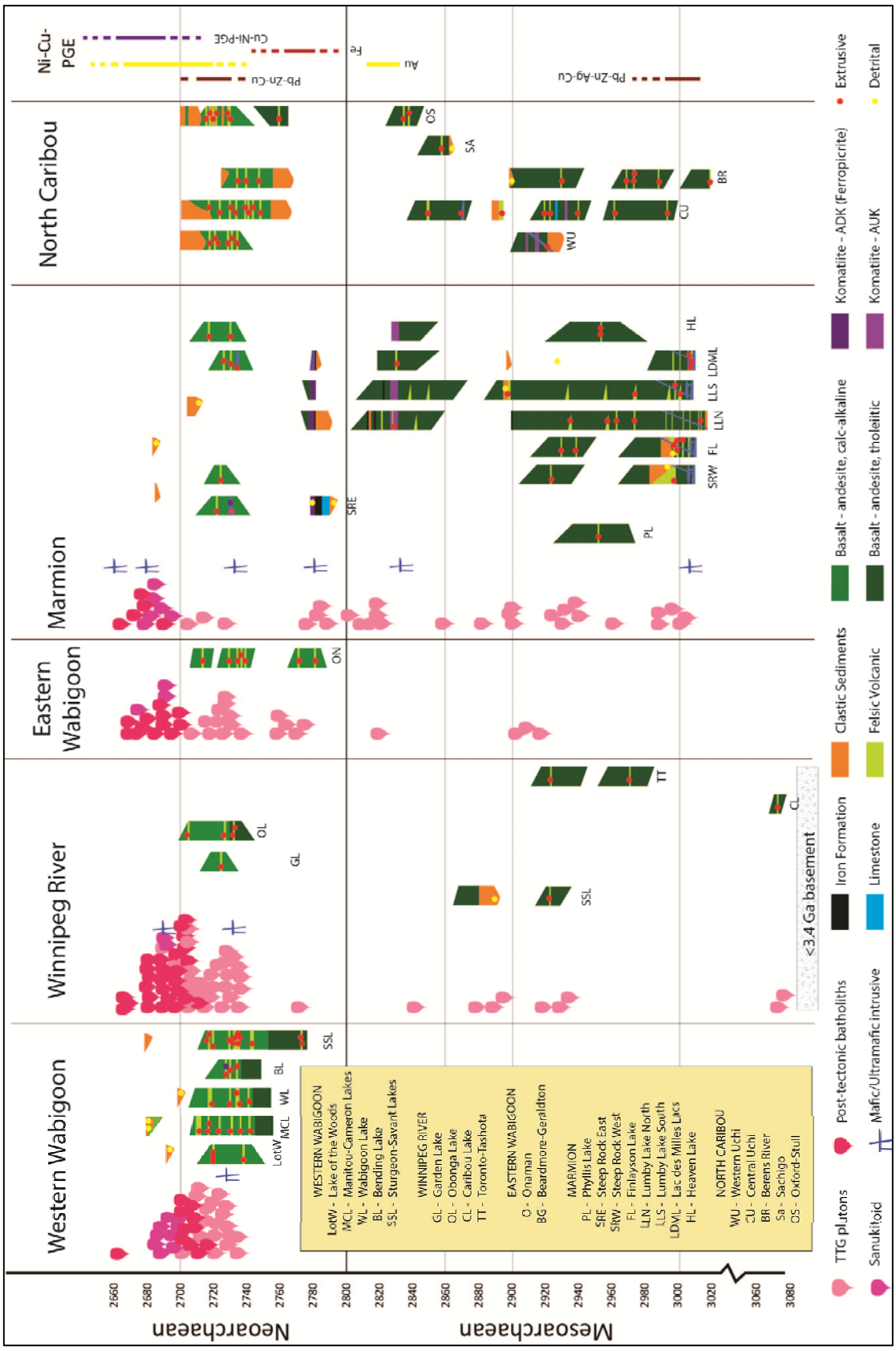
Western Wabigoon
Winnipeg River
Eastern Wabigoon
Marmion
North Caribou
Ni-Cu-PGE
Cu-Ni-PGE
Pb-Zn-Cu
Fe
Au
Pb-Zn-Ag-Cu
Neoarchaean
Mesoarchaean
2660
2680
2700
2720
2740
2760
2780
2800
2820
2840
2860
2880
2900
2920
2940
2960
2980
3000
3020
3060
3080
LotW
MCL
WL
BL
SSL
OL
GL
ON
SRE
PL
SRW
FL
LLN
LLS
LDWL
HL
TT
CL
SSL
OS
SA
WU
CU
BR
<3.4 Ga basement
WESTERN WABIGOON
LotW - Lake of the Woods
MCL - Manitou-Cameron Lakes
WL - Wabigoon Lake
BL - Bending Lake
SSL - Sturgeon-Savant Lakes
WINNIPEG RIVER
GL - Garden Lake
OL - Oboga Lake
CL - Caribou Lake
TT - Toronto-Tashota
EASTERN WABIGOON
O - Onaman
BG - Beardmore-Geraldton
MARMION
PL - Phyllis Lake
SRE - Steep Rock East
SRW - Steep Rock West
FL - Finlayson Lake
LLN - Lumby Lake North
LLS - Lumby Lake South
LDWL - Lac des Milles Lacs
HL - Heaven Lake
NORTH CARIBOU
WU - Western Uchi
CU - Central Uchi
BR - Berens River
Sa - Sachigo
OS - Oxford-Stull
TTG plutons
Post-tectonic batholiths
Sanukitoid
Mafic/Ultramafic intrusive
Iron Formation
Limestone
Clastic Sediments
Felsic Volcanic
Basalt - andesite, calc-alkaline
Basalt - andesite, tholeiitic
Komatiite - ADK (Ferropicrite)
Komatiite - AUK
Extrusive
Detrital

Figure 3-3: Stratigraphic columns for the greenstone belts of the Wabigoon superterrane, organised by terrane. Greenstone belts of the North Caribou terrane are included for comparison by domain rather than greenstone belt. Age references for the Wabigoon superterrane are included with Supplementary Table 3-4. Age compilation for greenstone belts of the North Caribou terrane was not exhaustive (Beakhouse et al., 1999; Corfu and Stone, 1998; Corfu and Stott, 1993; Corfu et al., 1998; Corfu and Wallace, 1986; Sanborn-Barrie et al., 2001; Tomlinson et al., 1998)

Post tectonic 2.698 – 2.685 Ga sanukitoid (Buse et al., 2010; Davis et al., 1990; Davis et al., 1989; Stern and Hanson, 1991; Stone, 2010a and references therein) and 2.69 – 2.67 Ga monzogranite-granodiorite (Stone, 2010a and references therein; Stone et al., 2010; Whalen et al., 2004b) intrude across the Wabigoon superterrane. Synchronous late pull-apart basins with 2.69 to >2.85 Ga synorogenic coarse clastic sediments were developed in the central axes of greenstone belts and along major faults (Davis et al., 1989; Stone, 2010a) during collision with the Wawa terrane during the 2.695 – 2.680 Ga Shebandowan orogeny (Corfu and Stott, 1998; Lodge et al., 2013). Alternatively, late Timiskaming-type sediments were deposited in late subsiding basins concurrent with vertical tectonism (Lin et al., 2013; Parmenter et al., 2006).

3.2.5. Quetico basin

The steep dextral Quetico fault marks the boundary between the Marmion – Western Wabigoon greenstone belts and the Quetico basin turbidites, with a strike length >300 km (Poulsen et al., 1980). Farther east, southward-dipping volcanic rocks of the Eastern Wabigoon terrane are interpreted to be tectonically interleaved with sediments of the Quetico basin (Devaney and Williams, 1989; Lafrance et al., 2004).

A local provenance from the north is postulated for the Quetico basin turbidites based on sub-angular zircons, bimodal quartzofeldspathic and komatiitic basalt detritus (Valli et al., 2004) and prominent age peaks at 3.0 and 2.7 Ga (Davis et al., 1990). Deposition is constrained by zircon ages from 2.698 – 2.689 Ga (Fralick et al., 2006) and the 2.688 Ga Sapawe Stock (Davis et al., 1990). Locally preserved channels, graded beds and dewatering structures in the Quetico basin face northwards (Percival, 1989), but imbricated panels young southward (Davis et al., 1990). Like the English River terrane, high T and low- to medium-P metamorphism of the Quetico basin is symmetrical with greenschist facies at the margins and up to granulite facies in the centre (Pan et al., 1998; Percival, 1989; Percival and Williams, 1989). Metamorphism reached amphibolite conditions soon after deposition, at ~2.69 –2.67 Ga (Pan et al., 1998; Valli et al., 2004) synchronous with 2.67 Ga S-type granitic intrusions (Pan et al., 1998), and granulite metamorphism at 2.65 Ga (Pan et al., 1998). Although an accretionary prism interpretation is favoured for the Quetico basin (Fralick et al., 2006; Pan et al., 1998; Percival, 1989; Williams, 1991), the low P metamorphism remains puzzling. However, local relict kyanite and staurolite provide evidence for an earlier

medium P, low T event (670-730 MPa, 500-560°C), thought to be related to Barrovian-type metamorphism prior to the late high T event (Pan and Fleet, 1993; Pan and Fleet, 1999).

3.2.6. Wawa terrane

To the south, the contact with the Wawa-Abitibi terrane has been interpreted as an unconformity (Fralick et al., 2006) or a thrust fault (Williams, 1991). Herein the Wawa terrane refers to rocks west of the Kapuskasing structural zone, a crustal section tectonically exhumed in the early Proterozoic (Percival and West, 1994). Although thought to be continuous with the Abitibi terrane, the Wawa terrane contains older rocks and evidence for interaction with an older basement. In contrast, the Abitibi is largely isotopically juvenile with rare inheritance to 2.93 Ga and no evidence for interaction with older substrate (Corfu and Noble, 1992). The Wawa terrane contains an early 2.92 Ga plutonic event (Moser, 1994), followed by paired 2.89-2.88, 2.75-2.745, 2.73-2.72, 2.701, 2.690 Ga intrusive and extrusive magmatism (Corfu and Stott, 1986; Corfu and Stott, 1998; Lodge et al., 2013; Turek et al., 1992). Sedimentary rocks of the Quetico basin locally extend into the Wawa terrane along the boundary (Fralick et al., 2006). Intrusions of sanukitoid plutons in the Wawa terrane are younger than those of the Wabigoon by ~5 m.y.

3.2.7. Minnesota River Valley terrane

The Minnesota River Valley terrane (<3.6 Ga; Card, 1990; Goldich and Fischer, 1986; Satkoski et al., 2013) is separated from the Wawa terrane by the enigmatic Great Lakes Tectonic Zone, a surmised thrust fault (Percival et al., 2006). At 3.524 – 2.604 Ga (Bickford et al., 2006), some of the oldest rocks of the Superior Craton are located here and themselves record an earlier history with Hf isotopes in zircons ranging from $\varepsilon_{Hf(3.5\ Ga)}$ = 1.9 to -2.6 (Satkoski et al., 2013).

3.2.8. Geology of the Marmion terrane

The Marmion terrane records the most complete spectrum of Meso- to Neoarchaean ages across its greenstone assemblages and plutonic rocks. Segmented, arcuate, bifurcating and tapered greenstone belts of the Marmion are largely 3.02 – 2.82 Ga (Buse et al., 2010; Davis and Jackson, 1988; Fralick and King, 1996; Stone et al., 1992; Tomlinson et al., 1999). Mesoarchaean basalt-komatiite sequences contain minor intercalated felsic to intermediate volcanic horizons, and clastic and chemical sedimentary rocks. Greenstone belts are concentrated along the margins of the 3.0 Ga Marmion intrusive complex (Davis and Jackson, 1988), a large multiphase TTG batholith stretching over 100km from Atikokan to east of Lac Des Milles Lacs (Figure 3-2). Greenstone belts also wrap around the 2.96 – 2.89 Ga Dashwa gneisses (Davis, 2009; reported in Stone, 2010b), in a dome-like structure, and are concentrated along the southern margin of the terrane in contact with mylonite of the Quetico Fault. The Neoarchaean volcanism that dominates other terranes of the Wabigoon is

restricted to the southern margin of the Marmion terrane within the Perch Lake, Steep Rock and Lac Des Milles Lacs greenstone belts (Figure 3-2; Stone, 2010a and references therein).

The relationships of greenstone belts to the surrounding TTG and to each other remain unclear. Recent models, based on lithofacies relationships of the Lumby Lake, Finlayson Lake and Steep Rock Lake greenstone belts surrounding the Marmion intrusive complex, include (i) unconformable deposition of various assemblages on TTG basement of lithofacies with distinct prehistories, which were subsequently tectonically amalgamated (Buse et al., 2009; Stone, 2007; Tomlinson et al., 1999), (ii) plume-arc interaction to account for the plateau-like basaltic komatiite and calc-alkaline TTG magmatism (Hollings and Wyman, 1999), and (iii) growth of an oceanic plateau where TTG resulted from the melting at the base (Fralick et al., 2008). The latter two models call for subsequent deformation resulting in fault-dissected synclinal geometry of previously-continuous assemblages.

Multiple generations of mafic dikes and sills intrude all lithologies, but are most conspicuous where they intrude TTG complexes (Figure 3-4A). Within the Marmion intrusive complex, many of the mafic dikes are cut by younger TTG phases. There is a particularly high abundance of dikes proximal to contacts with greenstone belts, and where observed, with the exception of the Steep Rock belt, all contacts are intruded by a mafic or TTG dike or stock, insomuch that the nature of the original contact is no longer observable. The base of the Steep Rock greenstone belt is an exception, where spectacularly-preserved conglomerate channels eroded into weathered TTG basement (Wilks and Nisbet, 1988). Here, a large number of mafic dikes are truncated at the erosive unconformity, constraining their age to at least >2.78 Ga. Baddeleyite from gabbro cutting Marmion tonalite gneiss was dated at 3.00 Ga (Davis, 2008; reported in Stone, 2010a) and a gabbro dike near the Lac Des Milles Lac greenstone belt was dated at 3.01 Ga (Hamilton et al., 2007; reported in Stone, 2010).

The Marmion terrane records greenschist to upper amphibolite facies metamorphism. Greenstone belts grade to amphibolite at margins, but narrow belts and slivers such as the Graham and Phyllis Lake belts in the north, are completely at amphibolite facies (Stone, 2010a). The Irene-Eltrut Lakes gneisses in the west contain ~100 – 1000 m wide mafic amphibolite slivers thought to be supracrustal remnants (Stone, 2010a).

Major faults of the area include the east-west striking Quetico Fault and central Lumby Lake Fault, and several north-easterly striking structures, the most prominent of which is the Marmion Shear Zone in the central Marmion terrane. The Marmion shear zone is long-lived, having been active

before the intrusion of the Diversion Stock, which intruded along its length, and then reactivated during the Kenoran orogeny (Backeberg et al., 2014).

3.3. METHODS

Detailed analytical methods for whole rock geochemical and in-situ U-Pb geochronological analyses are presented in Chapter 2. The following is an abbreviated description. Collected samples were trimmed and prepared for polished thin sections, whole rock geochemistry and zircon separation. Whole rock geochemical analyses were carried out by either (i) Activation Laboratories in Canada using ICP-MS of fused disks except for FeO which was analysed by wet chemistry, or (ii) Geoscience Laboratories in Sudbury, Ontario, Canada using ICP-MS of a multi-acid digest or XRF, except for Au and PGE which were analysed by fire assay.

Mineral separation was done by Apatite to Zircon Inc. or Geotrack International Pty. Ltd. Zircons picked from the non-magnetic fraction were cast in epoxy resin with standards before polishing to expose their near mid-point. Cleaned mounts were gold-coated (40 nm) and imaged on a polarizing microscope, and using cathodoluminescence and back scattered electron techniques on the TESCAN scanning electron microscope at the Centre for Microscopy, Characterisation and Analysis (CMCA), University of Western Australia (UWA). Representative high quality grains were analysed for in-situ (U-Th)-Pb isotopes using the SHRIMP II at the John de Laeter Centre of Mass Spectrometry, UWA. SQUID 2.50 and Isoplot 3.71 Microsoft Excel add-ins (Ludwig, 2009) were employed in data reduction. Table 3-1 summarises analytical conditions and reproducibility of standard reference materials.

3.4. RESULTS

3.4.1. Field, petrographic and geochemical context of samples

Samples taken for zircon geochronology covered a range of rock types in the study area. In broad terms, intrusive samples include TTG to granite, and post-tectonic granodiorite-granite and diorite-monzonite of the sanukitoid suite. Two felsic to intermediate volcanic rocks were also sampled for geochronology.

3.4.1.1. TTG

This study follows the convention of previous workers in the Western Superior Craton (e.g. Beakhouse, 2007; Corfu and Stone, 1998; Stone, 2010a) by including granitoid rocks across a continuum of compositions that overlaps partly with the strict geochemical definition of TTGs (e.g. Moyen and Martin, 2012). Accordingly, TTG-type rocks underlie ~40% of the study area

Table 3-1: Analytical conditions and precision of standards for U-Pb SHRIMP data. Natural zircon M257 was used for U-Pb calibration, and OGC (3.4654 ± 0.0006 Ga; Stern et al., 2009) to monitor accuracy of $^{207}Pb/^{206}Pb$ ages. Samples corrected for mass fractionation by OGC indicated by *.

						M257			OGC-1 (3465.4 ± 0.6 Ma)				
Date	Mount	Samples	Beam intensity (nA)	Spot size (μm)	Typical sensitivity (cps/nA/ ppm Pb)	n	spot-to-spot consistency (%; 1σ)	$^{238}U/^{206}Pb$ calibration uncertainty (%; 1σ)	n	Age	2σ	MSWD	Additional Notes
4/29/2014	WS-32	A,B,C	-2.1	25	20	13	0.68	0.25	5	3463	5	0.63	
4/28/2014	WS-33	A,B,C	-1.5	28	18	15	1.03	0.38	6	3463	5	2.00	M257-6, 14 and 12 excluded (low sensitivity)
2/14/2014	WS-34	A,B	-2.1	28	21	9	0.84	0.39	3	3464	4	2.50	session terminated partway
3/3/2014	WS-34	B,C	-2.1	20	20	12	1.04	0.37	4	3462	4	1.04	
7/2/2015	WS-35	A*	-2.4	28	23	14	0.80	0.25	6	3454	4	1.13	fractionation correction using OGC
6/24/2014	WS-35	A,B	-1.8	28	14	11	1.30	0.47	4	3464	7	0.56	
7/3/2014	WS-35	C	-1.6	28	16	12	0.00	0.17	2	3467	10	0.49	
5/23/2014	WS-36	A,B,C	-2.2	25	20	14	0.00	0.22	5	3467	5	0.43	
5/12/2014	WS-37	A,C*	-2.0	28	20	13	1.11	0.36	6	3459	6	0.94	fractionation correction using OGC
7/11/2014	WS-37	B	-2.1	27	23	14	0.00	0.12	7	3471	4	0.12	
4/14/2014	WS-38	A,B	-1.5	25	18	11	0.71	0.30	5	3460	6	0.10	M257-3,4,5 excluded
5/5/2014	WS-38	C	-1.9	21	19	10	0.50	0.23	4	3461	7	1.15	
4/29/2014	WS-39	A,B	-1.4	19	20	11	1.17	0.40	5	3470	20	2.00	poor OGC; OGC used from WS-33
5/5/2014	WS-39	C	-1.6	20	20	11	0.99	0.34	4	3465	9	0.70	poor OGC; OGC used from WS-38
12/4/2014	WS-43	A	-2.0	28	25	6	0.48	0.26	3	3467	65	3.00	session terminated partway
12/5/2014	WS-43	B,C	-1.7	30	23	10	0.56	0.25	4	3470	5	0.44	
12/12/2014	WS-44	C	-1.9	20	23	11	0.81	0.29	5	3461	4	1.91	
12/12/2014	WS-45	A,B	-2.6	30	22	15	1.11	0.36	2	3467	4	0.84	small aberration on spot
1/23/2015	WS-49	B,C*	-1.7	22	22	30	2.20	0.43	11	3474	4	1.25	fractionation correction using OGC
2/16/2015	WS-53	A,B,C	-1.2	18	22	22	0.00	0.15	8	3466	5	0.43	
6/15/2015	WS-54	A,B,C	-2.0	18	16	13	1.29	0.39	5	3470	4	1.43	
1/11/2016	WS-54	C	-2.1	30	16	11	0.78	0.30	4	3466	6	1.39	
5/16/2015	WS-55	A,B	-1.6	25	23	16	1.05	0.30	5	3464	3	1.19	
10/1/2015	WS-55	C	-2.1	18	16	17	2.01	0.63	8	3463	4	0.41	
10/10/2015	WS-56	A,B,C,D	-1.7	17	16	22	0.76	0.25	8	3467	5	1.25	Variable primary signal
11/21/2015	WS-57	A,B,C,D	-1.9	17	14	25	1.52	0.37	12	3468	3	0.46	High background counts
1/9/2016	WS-58	A,B,C,D,E	-1.9	20	16	27	1.33	0.29	11	3468	4	0.37	Variable primary signal/sensitivity

(Beakhouse, 2007; Stone, 2010a), occurring as discrete plutons and in large batholitic complexes such as the Marmion intrusive complex, and Dashwa, Raven Lake, and Irene-Eltrut Lakes gneisses. The rocks are grey to white, medium-grained and commonly foliated to gneissic and gradational to migmatite (Figure 3-4C,D, 5A,B). Modal mineralogy of plagioclase-quartz-K feldspar forms a continuum between tonalite through granodiorite to granite where biotite tonalite is more common than (biotite-) hornblende tonalite and granodiorite. Gneissic varieties can range to quartz diorite or diorite and some retain inclusions of mafic rocks (Figure 3-4B). There is between 5-20% mafic minerals in foliated varieties, whereas the heterogeneous gneiss and migmatite display a larger range in modal composition, but on average extend to higher contents of mafic minerals (~20%). Accessory phases include magmatic epidote, titanite, apatite, Fe-Ti oxides and zircon. A few samples have local alteration of biotite to epidote ± chlorite and alteration of feldspars to sericite-epidote-carbonate.

Rocks sampled from the TTG suite are siliceous (64-75 wt % SiO_2), calc-alkaline to calcic, metaluminous to weakly peraluminous (A/CNK ~ 0.9 to1.15), magnesian (Mg# 0.3 – 0.53) and sodic. Contents of Al_2O_3 vary between 13.5 – 16.7 wt % (Figure 3-6). Compared to the other felsic to intermediate intrusive rocks of the study area, TTGs have moderate rare earth element (REE) contents, with variably steep light REE (LREE: La to Sm; La/Sm = 2.3 - 12) and a large range in heavy REE pattern (HREE: Gd to Lu; Dy/Yb = 0.9 – 2.7) from steep to concave to flat (Figure 3-7). Europium anomalies (Eu/Eu*) are variable between weakly negative and distinctly positive (<2.5 but mostly <1.5). Large ion lithophile element (LILE) abundances are lower than post-tectonic suites. High field strength elements (HFSE) are variable, but negative Nb-Ta and Ti anomalies persist through all samples. Pre-tectonic granites form a continuum with TTG, but they also share a few of the geochemical characteristics of the post-tectonic granite-granodiorite (GG) suite such as higher Rb/Sr and lower Eu/Eu*.

3.4.1.2. Post-tectonic Granite-Granodiorite

Foliated to massive to K-feldspar porphyritic granite, monzogranite to monzodiorite and granodiorite underlies ~30% of the study area (Figures 3-4E, 5F). These rocks occur as large syn (2.70 – 2.69) to post-tectonic (<2.69 Ga) batholiths such as the White Otter, Indian and Muskeg batholiths. They are medium to coarse-grained, pink to white, and generally more leucocratic than TTG. Early-formed, distinctly zoned plagioclase is common, occasionally with orthoclase phenocrysts. More commonly, late microcline is the dominant K-feldspar, and infills spaces as well as forms large oikocrysts enclosing a variety of minerals. Mafic minerals are dominated by biotite, with lesser hornblende. Epidote, apatite, titanite, Fe-Ti oxides, zircon and allanite are common

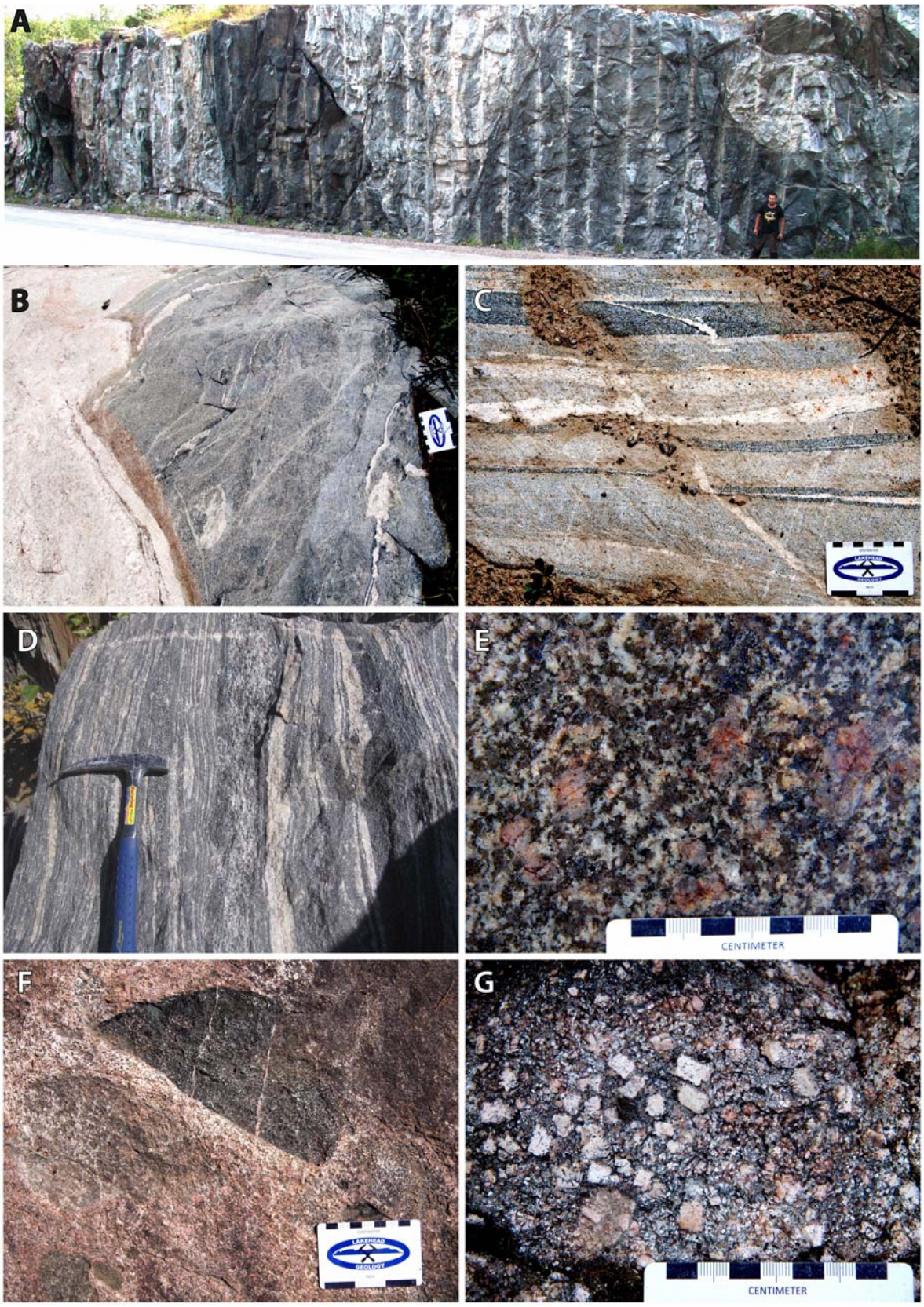
A
B
C
D
E
CENTIMETER
F
G
CENTIMETER

Figure 3-4: Field photos from the Marmion terrane. A. mafic dikes cutting tonalite gneiss exposed in a road cut north of the eastern Steep Rock greenstone belt on Highway 622. B. Mafic raft in foliated tonalite south of the Lumby Lake greenstone belt near the Sapawe Road. C. Marmion tonalite gneiss with derived leucosome from amphibolitic bands. D. Dashwa tonalite gneiss west of the Finlayson Lake greenstone belt on Highway 622. E. K-feldspar porphyritic hornblende granodiorite of the Scotch Lake pluton. F. Diorite inclusions in monzodiorite of the Van Nostrand Lake sanukitoid stock along the East Pinecone Road. G. Late microcline-porphyritic phase of the Van Nostrand Lake stock, East Pinecone Road.

accessory phases. Where occurring as post-tectonic intrusions, plutonic and supracrustal xenoliths are common.

Granite – granodiorite (GG) suites are alkali-calcic, magnesian (Mg# 0.15 to 0.5) and more peraluminous than TTG and sanukitoids (A/CNK <1.2). A combination of high SiO_2, K_2O, Th, U, Rb and LREE and low CaO, MgO, P_2O_3 and compatible transition elements distinguishes the granite – granodiorite suite. These rocks also extend to higher Rb/Sr and Nb/Nb*, and lower Eu/Eu* than the TTG and sanukitoids. Also, unlike the sanukitoid suite, but like the TTG suite, GG rocks do not form a coherent trend of increasing La/Sm with SiO_2 but rather scatter in an opposite trend, suggesting they are not directly related to the sanukitoid suite by differentiation as proposed by Whalen et al. (2004b).

3.4.1.3. Post-tectonic Sanukitoid

The sanukitoid suite is post to syn-tectonic, forming intrusive complexes <30x10 km characterised by a wide compositional range in phases, and a distinctive mineralogy reflecting the abundance of both compatible and incompatible trace elements. Sanukitoid rocks range from diorite to monzogranite within a single complex, although not all phases are present in all complexes. Endmembers can be linked by fractional crystallisation (Stern and Hanson, 1991). Compared to TTG, there is a distinctly higher ratio of K-feldspar – most often microcline – to plagioclase, most evident in primitive varieties. Pyroxene is an early crystallised phase, followed by Fe-Ti oxides, plagioclase and apatite (e.g. Figure 3-5H). Hornblende commonly occurs as coronas around corroded pyroxene cores, which may be mantled in turn by biotite with increasing silica. Monzonite to monzodiorite phases may contain rounded to angular ultramafic to dioritic enclaves (e.g. Figure 3-4F). Titanite is a ubiquitous accessory phase, along with epidote and zircon. Late-crystallised microcline in evolved endmembers is typically poikilitic and megacrystic, containing euhedral crystals of plagioclase, titanite and zircon (Figures 3-4G, 3-5G). Coeval igneous-textured mafic to ultramafic inclusions are abundant, and contemporaneous pyroxenite and gabbro are found within and nearby. Intrusion margins also contain country rock xenoliths.

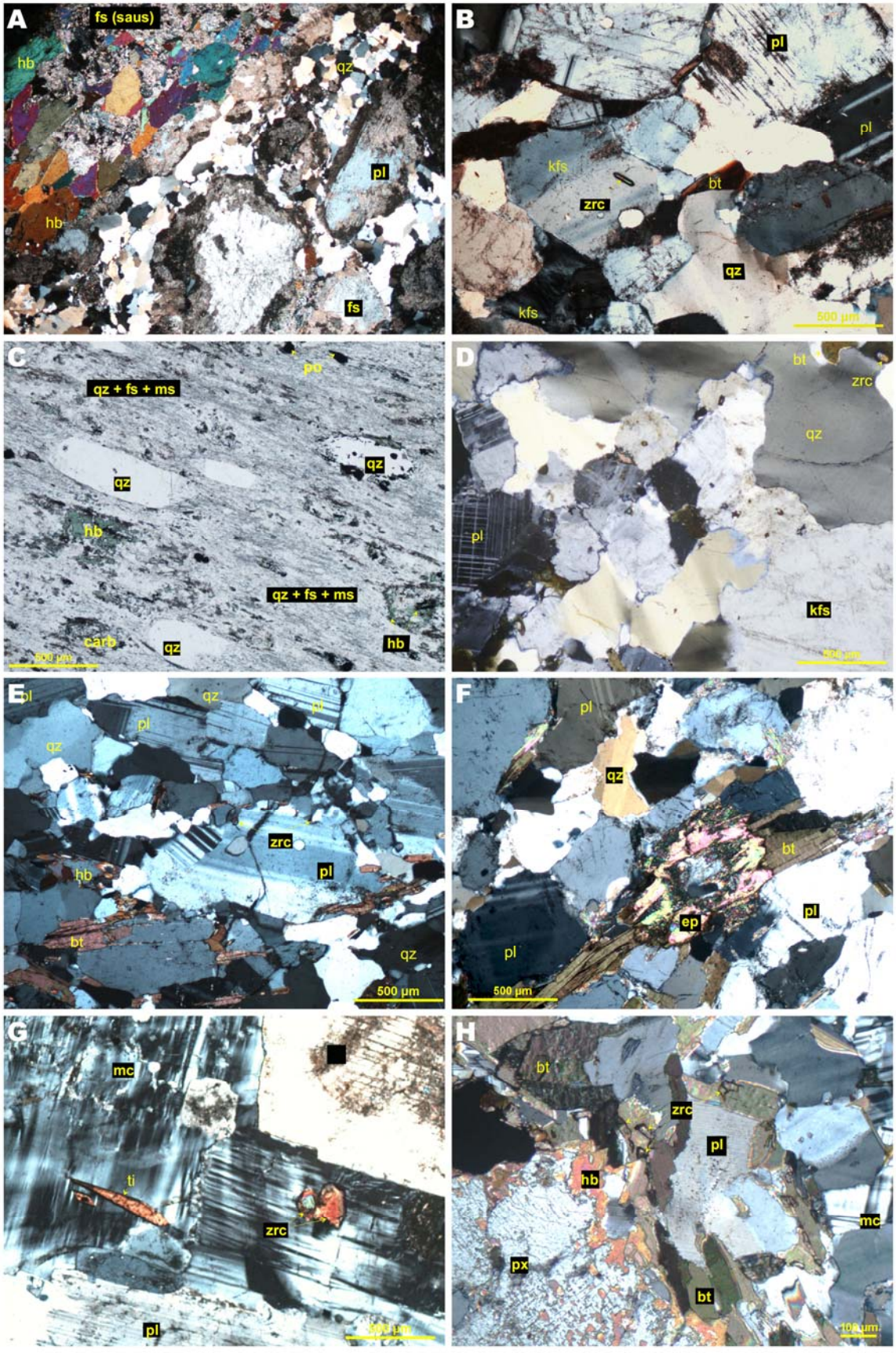
A
fs (saus)
hb
qz
pl
hb
fs
B
pl
pl
kfs
bt
zrc
qz
kfs
500 µm
C
po
qz + fs + ms
qz
qz
hb
qz + fs + ms
carb
qz
hb
500 µm
D
bt
zrc
qz
pl
kfs
500 µm
E
pl
qz
pl
qz
zrc
hb
pl
bt
qz
500 µm
F
pl
qz
bt
ep
pl
pl
500 µm
G
mc
ti
zrc
pl
500 µm
H
bt
zrc
pl
hb
mc
px
bt
100 µm

Figure 3-5: Petrographic images of representative samples. A. 3.015 Ga amphibolite facies banded tonalite gneiss from the Marmion intrusive complex (WS-36A). B. 2.999 Ga granodiorite from the Marmion intrusive complex with elongate zircons typically within feldspars (WS-37B). C. 2.974 Ga quartz porphyritic rhyolite tuff from the northern Lumby Lake belt (WS-56D). D. 2.931 Ga biotite feldspar-porphyritic granodiorite from the Dashwa gneisses west of the Finlayson Lake greenstone belt (WS-38C) with equant zircons in feldspars. E. 2.785 Ga biotite tonalite gneiss from the eastern Marmion intrusive complex. F. 2.691 Ga biotite-epidote foliated tonalite from the Hillyer domain of Stone (2010a), zircons in biotite (WS-44C). G. 2.688 Ga monzogranite from the Eye-Dashwa sanukitoid stock with zircon and titanite within microcline. H. 2.685 Ga pyroxene-hornblende-biotite monzodiorite of the Entwine sanukitoid intrusive complex with interstitial zircons (WS-49B). Mineral abbreviations: qz – quartz, pl – plagioclase, kfs – K feldspar, fs – feldspar, mc – microcline, px – pyroxene, hb – hornblende, bt – biotite, ms – muscovite, ep – epidote, carb – carbonate, zrc – zircon, ti – titanite, po - pyrrhotite.

Sanukitoids are metaluminous (A/CNK = 0.6 to 1.08) and alkali-calcic, with a calc-alkalic differentiation trend and high Mg#'s (<0.72) (Figure 3-6). The hallmark chemistry of sanukitoid magmatism in the study includes a large range in SiO_2 (55 – 71 wt%), and high compatible trace elements Ni, Cr and V, elevated P_2O_3, LILE (Ba, Sr, K, Rb) and LREE with steep REE and HREE. Consequently, sanukitoids have very high Sr/Y for a given Y or SiO_2 compared to the TTG and GG of the study area. Eu anomalies are typically ~1 or weakly negative but are positive in related anorthositic phases. In spite of the large range in rock composition, the incompatible element patterns of sanukitoid intrusions studied are tightly grouped, with deep troughs for Ta-Nb and Ti and variable relative depletions in Zr-Hf. Their coherence on multi-element diagrams contrasts with comparative scatter in TTG and GG suites. Compared to TTG and GG, sanukitoids also have much higher Be, W, PGE, Au, Tl and distinctly lower Zr/Zr* and Nb/Nb*.

3.4.1.4. Felsic to intermediate volcanic rocks

Rhyolite to dacite horizons are scattered throughout greenstone belts in the Marmion terrane, but are most common in the Lumby Lake and Lac Des Milles Lacs belts north and south of the Marmion intrusive complex (Figure 3-2). Felsic to intermediate volcanic horizons tend to be deformed and carbonate-sericite altered, and may be intercalated with exhalative sulphides, but commonly retain primary volcanic textures characteristic of ash, crystal and lapilli tuffs (Figure 3-5C). Rocks along the south margin have been extremely tectonised during 2.7 Ga transpression concentrated along the Quetico fault, but retain pyroclastic textures. A quartz crystal dacite tuff along Gargoyle Lake in the Lumby Lake belt and a rhyolitic tuff within the western Finlayson belt were sampled for geochronology. Both samples were metamorphosed to amphibolite facies and retain a pervasive foliation overprinted by a spaced cleavage.

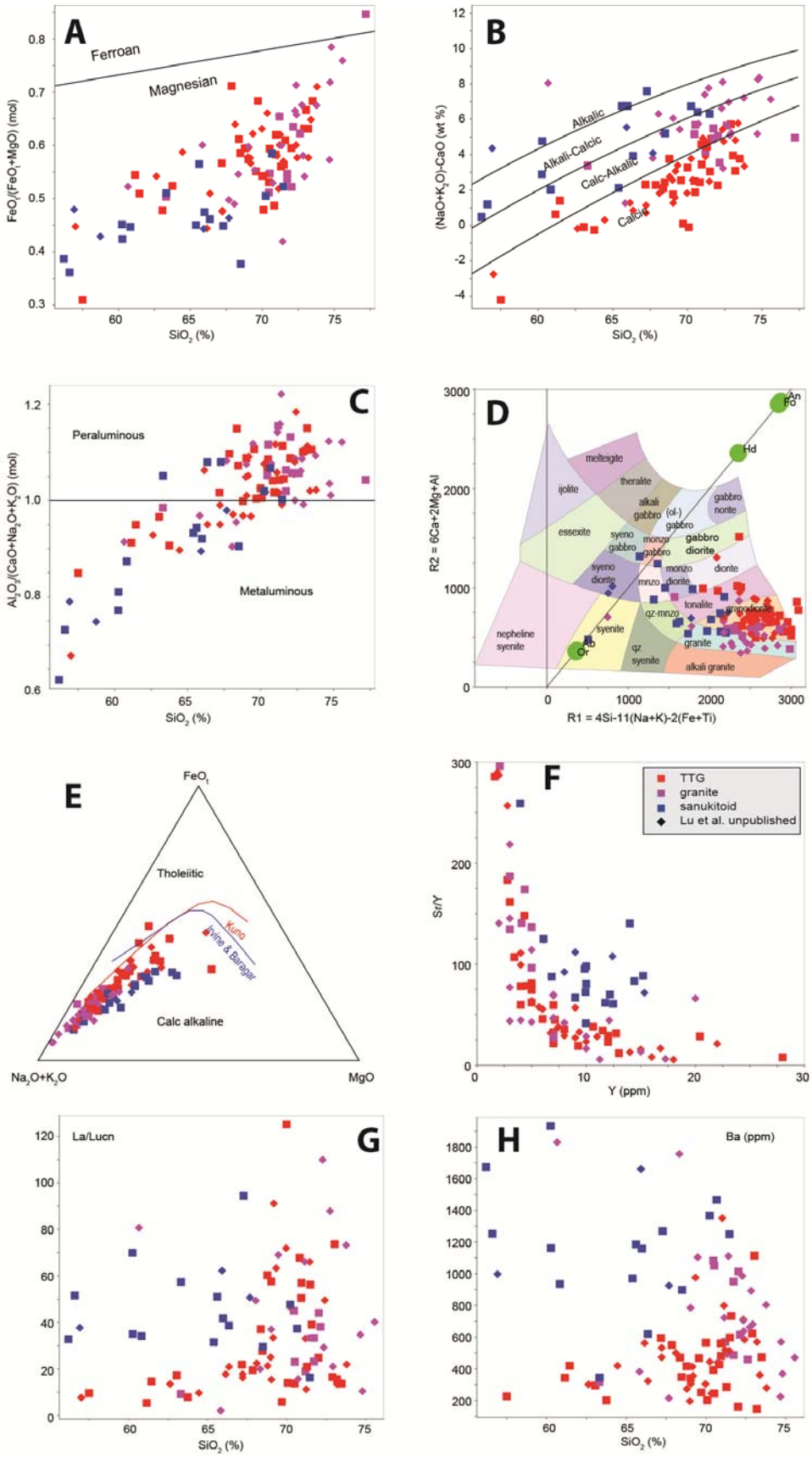
A
Ferroan
Magnesian
FeO_t/(FeO_t+MgO) (mol)
SiO2 (%)
B
Alkalic
Alkali-Calcic
Calc-Alkalic
Calcic
(NaO+K2O)-CaO (wt %)
SiO2 (%)
C
Peraluminous
Metaluminous
Al2O3/(CaO+Na2O+K2O) (mol)
SiO2 (%)
D
An
Fo
Hd
melteigite
ijolite
theralite
alkali gabbro
(ol-) gabbro
gabbro norite
essexite
syeno gabbro
monzo gabbro
gabbro diorite
syeno diorite
monzo diorite
mnzo diorite
tonalite
granodiorite
qz-mnzo
syenite
granite
nepheline syenite
Ab
Or
qz syenite
alkali granite
R2 = 6Ca+2Mg+Al
R1 = 4Si-11(Na+K)-2(Fe+Ti)
E
FeOt
Tholeiitic
Kuno
Irvine & Baragar
Calc alkaline
Na2O+K2O
MgO
F
TTG
granite
sanukitoid
Lu et al. unpublished
Sr/Y
Y (ppm)
G
La/Lucn
SiO2 (%)
H
Ba (ppm)
SiO2 (%)

Figure 3-6: Select plots of whole-rock geochemistry of samples that also have reported geochronology. Plots A, B and C from Frost et al. (2001) classification scheme for granitic rocks. A. Plot of $FeO_t/(MgO+FeO_t)$ versus SiO_2 showing all samples are magnesian. B. Diagram of the modified alkali lime index. C. Aluminum saturation index. D. R1-R2 plutonic classification diagram from De la Roche et al. (1980). E. AFM diagram showing that all sampled suites follow a calc-alkaline differentiation trend. Curves from Irvine and Baragar (1971) and Kuno (1966). F. Sr/Y versus Y, showing that sanukitoid rocks have distinctly higher Sr/Y for a given Y than TTG and GG. Red – TTG (tonalite – trondjhemite - granodiorite), pink – pre-tectonic granite, purple – post-tectonic granite – granodiorite, blue – sanukitoid.

Felsic volcanic rocks have similar geochemistry to TTG intrusions, with high SiO_2 (>70 wt %), and are metaluminous to weakly peraluminous, calc-alkaline, magnesian, with low Mg # (~0.4). They show enrichments in LREE, and steep REE patterns with steep to shallow HREE, pronounced negative Nb-Ta and Ti anomalies, distinctly positive Zr-Hf anomalies and weakly positive Eu anomalies.

3.4.2. Zircon microstructure and in-situ U-Pb ages

3.4.2.1. U-Pb interpretation

Table 3-2 presents U-Pb ages, zircon morphology and zircon saturation temperatures calculated from whole rock analyses (Watson and Harrison, 1983) for the 54 samples dated by this study. Unless specified, all reported ages are attributed to magmatic crystallisation ages calculated from the weighted mean of $^{207}Pb/^{206}Pb$ ages. Magmatic crystallisation ages were interpreted and differentiated from inherited and metamorphic populations using morphological and internal microstructure of zircons such as pristine oscillatory or sector zoning (e.g. Corfu et al., 2003) in combination with U-Th-Pb characteristics, the statistical distribution of populations, and in some cases, field evidence. Magmatic zircons of the study have a large variation in morphology and internal structure, which varies with composition and not necessarily age. In some samples, internal morphology of magmatic zircons also varies widely. Accordingly, morphological characteristics of magmatic populations were evaluated sample-by-sample. Table 3-2 gives a brief overview of each sample with the main zircon microstructure and U-Pb characteristics. Detailed descriptions including concordia plots, weighted mean and probability density plots for each sample analysed can be found in Appendix A.

Inheritance is distinguished in some samples by cores that have a distinct interface, often characterized by a resorption texture, between the core and rimming zircon domains. However, many inherited zircons do not exhibit core-rim interfaces and may just be partially resorbed xenocrysts that are slightly rounded and/or more equant compared to magmatic grains (Figure 3-8). Inherited grains commonly have distinct Th/U or U + Th contents from magmatic zircons.

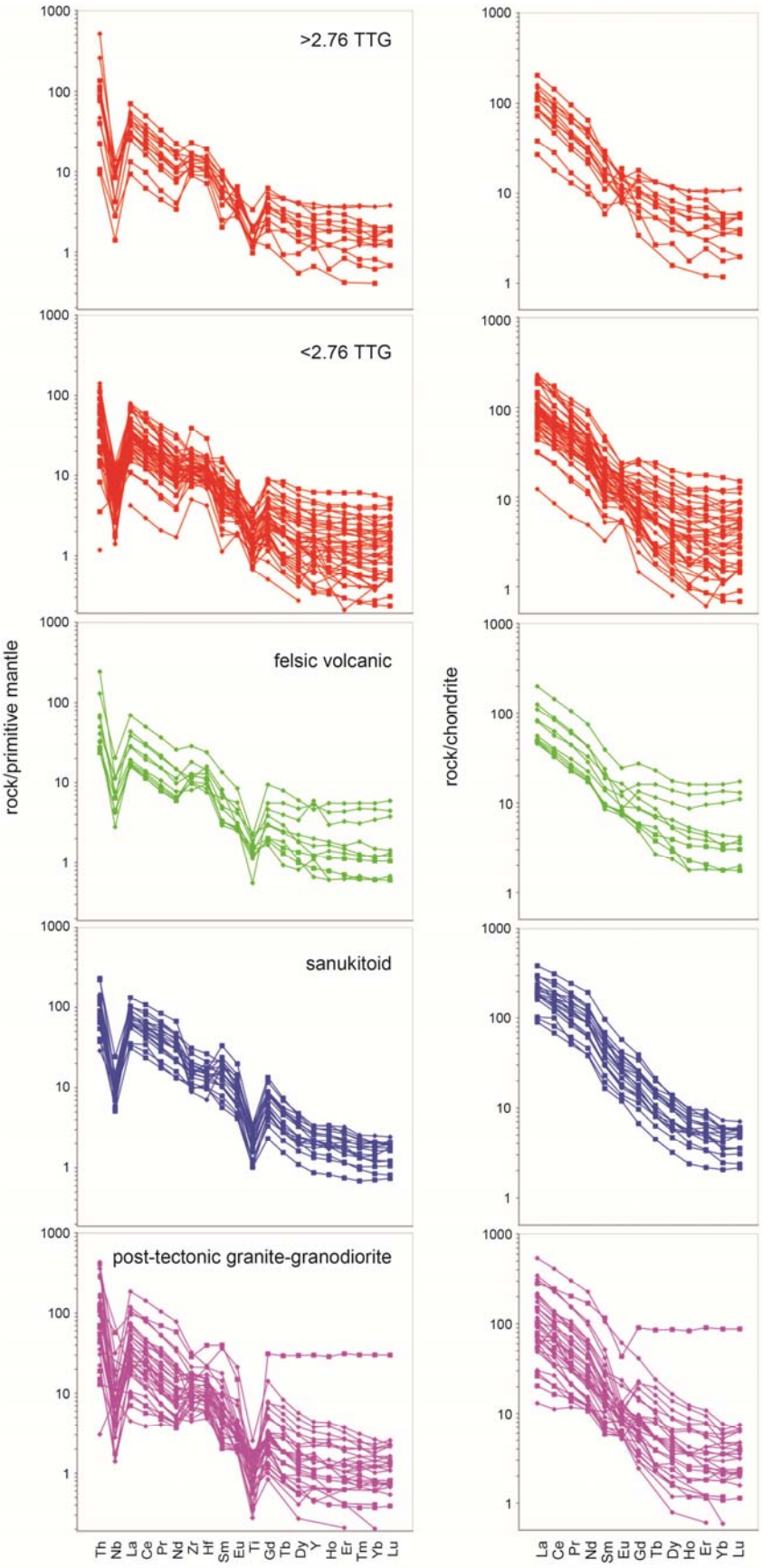
>2.76 TTG
<2.76 TTG
felsic volcanic
sanukitoid
post-tectonic granite-granodiorite
rock/primitive mantle
rock/chondrite
1000
100
10
1
Th Nb La Ce Pr Nd Zr Hf Sm Eu Ti Gd Tb Dy Y Ho Er Tm Yb Lu
La Ce Pr Nd Sm Eu Gd Tb Dy Ho Er Yb Lu

Figure 3-7: Multiple whole-rock trace element diagrams for samples dated by this study. The left panel shows patterns for trace elements normalized to primitive mantle. The right panel shows chondrite normalised REE. Normalisation values from Sun and McDonough (1989). Sanukitoids have the steepest REE and HREE whereas post-tectonic granite - granodiorite have shallower HREE. TTG and felsic volcanic rocks show similar patterns, with many overlapping values.

Interpreted inherited zircons in one sample may share characteristics with magmatic populations of another. For example, many of the 3.0 Ga inherited zircons from this study are equant luminescent fragments with either sector zoning or planar banding typical of 3.0 Ga tonalite (Figure 3-8). In many samples, zircons have thin unzoned and highly luminescent rims that are considered to represent metamorphic growth. These metamorphic rims are commonly too thin to date. Where identified, they tend to have low Th/U (<0.05). Figure 3-9 illustrates age subdivision for a complex sample, where the inferred magmatic and inherited components are of similar age.

The highest quality zircons were targeted for analyses, but some of these zircons were compromised by Pb redistribution due to hydrothermal alteration, thermal resetting or recrystallisation. Pb mobility was inferred from disturbed microstructures, high amounts of U + Th, high common Pb and/or discordance. High U + Th zircons are prone to Pb mobility due to radiation damage. Zircons with high U + Th or ^{204}Pb were therefore treated with caution, with a typical cut-off of 1000 ppm U and six counts of ^{204}Pb per scan. Exceptions include a few samples with unusually high U, but concordant analyses and low ^{204}Pb. Modern Pb loss was differentiated from ancient Pb loss by distribution on concordia diagrams. Analyses which form a discordia plotting as a horizontal trend on Tera-Wasserburg plots (i.e. with the same ^{207}Pb/^{206}Pb ages but different ^{238}U/^{208}Pb ages) are interpreted as recording recent Pb loss. Analyses which form a discordia that intercepts the concordia at an earlier time, or which are displaced to younger ages along the concordia, were interpreted as displaying ancient Pb loss (Figure 3-10). High resolution imaging following in-situ analysis showed that many discordant analyses encountered cracks or similar disturbances.

3.4.2.1.1. Using Lu-Hf isotopes to aid in age interpretation

In a few ambiguous cases where analyses plot along the concordia as one or more populations, ^{177}Hf/^{176}Hf measured within the same zircon domains was used to better understand the nature of populations and the role of ancient Pb loss. Presuming sufficient age distinction exists between populations within a sample, a plot of ^{176}Hf/^{177}Hf$_{(t)}$ versus age can distinguish between ancient Pb loss and true crystallisation ages (see Figure 5 of Kemp and Hawkesworth, 2013; and Figure 1 of Vervoort and Kemp, 2016). Zircons affected by ancient Pb loss will plot on a near-horizontal trend in ^{176}Hf/^{177}Hf$_{(t)}$ – time space because zircon ^{176}Lu/^{177}Hf is very low (0.001). In contrast, distinct

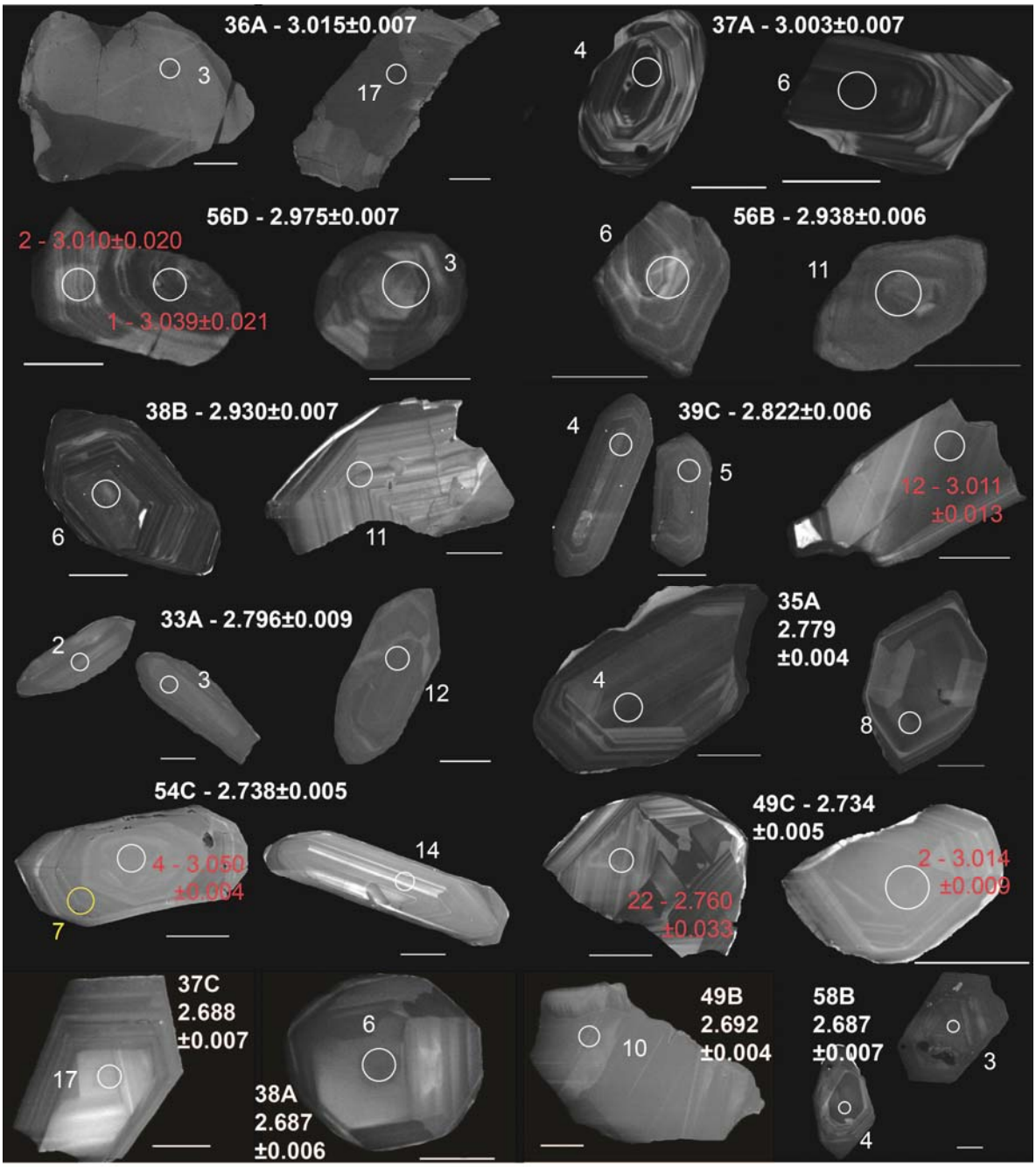

Figure 3-8: Cathodoluminescence images for selected zircons representing the morphological and geological age ranges of samples. White bars indicate 50 µm. Figure is organised with the oldest magmatic ages in the top and youngest ages at the bottom. Sample mount numbers are indicated in white bold with the interpreted magmatic age in Ga (e.g. 36A – 3.015±0.007) and SHRIMP spots are indicated by a white circle with a corresponding spot number. Red spot numbers and ages represent analyses interpreted as reflecting inherited ages. Discordant analyses are indicated in yellow. Note the differing morphologies from 3.0 Ga mafic tonalite gneiss (top left) and 3.0 Ga granodiorite (top right), through younger tonalite, granodiorite and granite, and zircons from four different sanukitoid intrusions (bottom row). Examples of zircon morphologies for each sample are shown in Appendix A.

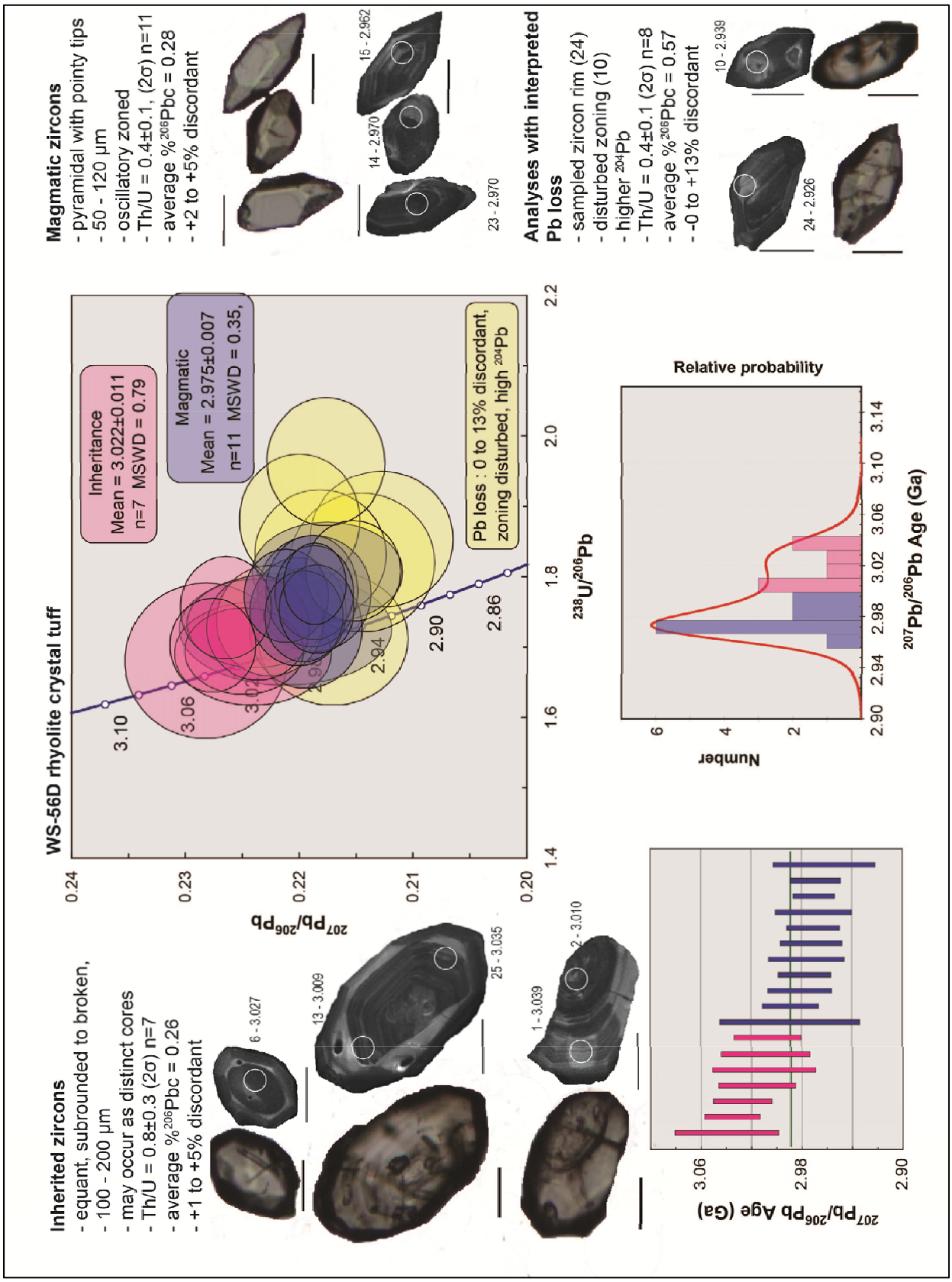
Inherited zircons
- equant, subrounded to broken,
- 100 - 200 µm
- may occur as distinct cores
- Th/U = 0.8±0.3 (2σ) n=7
- average %206Pbc = 0.26
- +1 to +5% discordant
6 - 3.027
13 - 3.009
25 - 3.035
1 - 3.039
2 - 3.010
WS-56D rhyolite crystal tuff
Inheritance
Mean = 3.022±0.011
n=7 MSWD = 0.79
Magmatic
Mean = 2.975±0.007
n=11 MSWD = 0.35,
Pb loss : 0 to 13% discordant,
zoning disturbed, high 204Pb
207Pb/206Pb
238U/206Pb
Relative probability
Number
207Pb/206Pb Age (Ga)
Magmatic zircons
- pyramidal with pointy tips
- 50 - 120 µm
- oscillatory zoned
- Th/U = 0.4±0.1, (2σ) n=11
- average %206Pbc = 0.28
- +2 to +5% discordant
14 - 2.970
15 - 2.962
23 - 2.970
Analyses with interpreted Pb loss
- sampled zircon rim (24)
- disturbed zoning (10)
- higher 204Pb
- Th/U = 0.4±0.1 (2σ) n=8
- average %206Pbc = 0.57
- -0 to +13% discordant
10 - 2.939
24 - 2.926

Figure 3-9: Illustration of age divisions based on zircon morphology and microstructure using WS-56D as an example. Zircon images are shown of zircon cross sections in transmitted light and cathodoluminescence (50μ scale bars are indicated). The inherited population has a distinct morphology from the zircons crystallised during emplacement of the rhyolite crystal tuff, with inherited populations typically exhibiting much larger, sub-rounded grains with more mineral inclusions and a higher luminescence. These grains may be broken or show discordant core-rim interfaces. Inherited zircons have higher Th/U. Magmatic zircons are typically clear with well-developed pyramidal faces and pointed tips. They mostly show oscillatory zoning. Zircons interpreted to have experienced Pb loss are not as clear, commonly contain cracks, and show evidence of disturbed zoning. All of the youngest excluded ages have elevated common Pb.

crystallisation populations will form a negative trend reflecting the $^{176}Lu/^{177}Hf$ of their source, around 0.015 for the bulk crust (Griffin et al., 2002) and higher (~0.019) for mafic crust. Figure 3-11 schematically illustrates Pb loss versus true crystallisation populations. Figure 3-12 shows $^{176}Hf/^{177}Hf_{(t)}$ – time plots for four samples for which Hf isotope compositions aided in age assignment.

Many of the inferred magmatic ages reported here are in agreement with previous geochronology by TIMS within the same intrusions (Table 3-3). The present study has also identified additional intrusive phases in some igneous complexes and identified inherited zircon cores, particularly in the Winnipeg River terrane, but also within the Marmion and Western Wabigoon terranes. Table 3-3 illustrates that this study has identified more inheritance than previous TIMS age determinations within the same intrusions, highlighting an advantage of in-situ measurements. The zircon morphology of the major rock divisions is summarised below. These descriptions are generalisations to which there are many exceptions.

3.4.2.2. TTG

Tonalitic compositions are found in rocks of all ages of the study area from 3.02 Ga to 2.69 Ga. The tonalites typically yielded homogenous zircon populations with large, clear to translucent honey-brown and equant crystals. They tend to have low U, and are moderately luminescent with sector zonation and occasional planar banding (Figure 3-8). Zircons from more mafic compositions are commonly round and may be broken. Zircons from relatively felsic tonalites are euhedral, pyramidal and multifaceted, and mantled by oscillatory zoning. Some populations have recrystallised rims and internal domains. The oldest magmatic zircons are also some of the lowest U and best preserved zircons, despite coming from tonalitic gneiss to migmatite. They tend to be concordant, or to have undergone recent Pb loss, although some samples show ancient Pb loss (Figure 3-10). Examples include a 3.015±7 Ga (WS-36A) amphibolite band within tonalite gneiss and a 3.003±7 Ga (WS-37A) tonalite - granodiorite gneiss from the mid-west and northwest Marmion intrusive complex respectively, a 2.930±0.007 (WS-38B) biotite

Table 3-2: *In-situ* U-Pb results, Zr saturation temperature and zircon morphology and microstructure for samples dated by this study.

Mount ID	Sample	NAD83, Zone 15N		Rock Suite	Terrane	$^{207}Pb^*/^{206}Pb^*$ determination by SHRIMP			
		x	y			Age (Ga ± 2σ)	n	MSWD	xenocrysts
WS-32A	12-8-16-1A	720855	5418359	SAN	M	2.684 ± 0.004	13	0.8	
WS-32B	12-8-16-2	710474	5424162	GG	M	*2.685*	*minimum age*		
WS-32C	12-8-16-3A	705139	5425371	SAN	M	2.686 ± 0.008	9	1.03	
WS-33A	12-8-16-4A	699616	5426252	TTG	M	2.796 ± 0.009	9	2.5	
WS-33B	12-8-16-4B	699616	5426252	GG	M	2.689 ± 0.005	3	0.003	2.727±0.009 n=3; 2.70±0.016 n=3
WS-33C	12-8-16-5	697887	5426530	TTG	M	2.785 ± 0.005	8	0.33	
WS-34A	12-8-16-6	689921	5430767	TTG	M	*2.793*	*minimum age*		
WS-34B	12-8-16-8	669925	5436744	GG	M	2.702 ± 0.004	11	0.75	2.812±0.006, 2.766±0.017
WS-34C	12-8-16-10	663801	5430975	TTG	M	2.788 ± 0.005	11	1.6	
WS-35A	12-8-16-12	643096	5431180	TTG	M	2.793 ± 0.005	31	1.13	
WS-35B	12-8-28-5b	626867	5407542	TTG	M	2.787 ± 0.010	6	0.24	2.825±0.009 n=9
WS-35C	12-8-28-6	626771	5413291	TTG	M	2.928 ± 0.007	12	1.4	2.962±0.007, n=5
WS-36A	12-8-28-7	625965	5415901	TTG	M	3.015 ± 0.007	14	0.7	
WS-36B	12-8-28-8	626954	5423288	TTG	M	2.845 ± 0.008	5	1.9	2.893±0.0011, n=5
WS-36C	*12-8-28-9*	*625930*	*5426965*	*GG*	M	*Age not determined. Discordant, high U grains*			
WS-37A	12-8-28-10	630473	5430217	TTG	M	3.003 ± 0.007	13	0.94	
WS-37B	12-8-17-1	585366	5418458	TTG	M	2.999 ± 0.002	25	1.17	
WS-37C	12-8-17-2B	595231	5416234	SAN	M	2.688 ± 0.007	14	1.4	
WS-38A	12-8-17-3	596932	5415043	SAN	M	2.687 ± 0.006	16	0.87	
WS-38B	12-8-17-4	602055	5426615	TTG	M	2.930 ± 0.007	17	1.6	
WS-38C	12-8-17-5	606661	5427130	TTG	M	2.931 ± 0.005	12	1.4	
WS-39A	12-8-17-6	602819	5425692	TTG	M	2.928 ± 0.005	11	0.57	
WS-39B	12-8-17-8	600093	5420833	TTG	M	2.939 ± 0.005	10	0.61	
WS-39C	12-8-17-10	607258	5408437	TTG	M	2.822 ± 0.006	12	1.6	3.011±0.013
WS-43A	KAT20130711-01	723061	5433394	GG	M	*2.691*	*minimum age*		2.906±0.005 n=3
WS-43B	KAT20130711-03	725864	5449722	GG	M	2.700 ± 0.007	12	0.85	
WS-43C	KAT20130711-04	727926	5457689	TTG	M	2.687 ± 0.006	5	1.8	
WS-45A	KAT20130712-09	559697	5418062	SAN	M	2.682 ± 0.003	15	1.15	

Table 3-2: *In-situ* U-Pb results, Zr saturation temperature and zircon morphology and microstructure for samples dated by this study.

Mount ID	Sample	NAD83, Zone 15N		Rock	Terrane	$^{207}Pb^{*}/^{206}Pb^{*}$ determination by SHRIMP			
		x	y	Suite		Age (Ga ± 2σ)	n	MSWD	xenocrysts
WS-45B	KAT20130713-01	538162	5403610	GG	M	2.723 ± 0.002	12	0.83	
WS-45C	*KAT20130713-02*	*540480*	*5406389*	*GG*	M	*Age not determined, strongly altered grains*			
WS-49B	KAT20130822-04	532477	5443956	SAN	M	2.692 ± 0.004	26	1.5	
WS-49C	KAT20130822-07	531831	5449613	GG	M	2.734 ± 0.005	8	0.87	3.014, 2.985, 2.954; 2.827±8 n=5, 2.785
WS-53A	KAT20130728-07	607118	5418511	GG	M	2.898 ± 0.008	9	0.85	3.015±0.020; 2.941±0.014; 2.938±0.018
WS-53B	KAT20130823-04	479144	5476127	TTG	WW	2.723 ± 0.008	10	1.07	2.868±0.014; 2784-2767
WS-53C	KAT20130920-04	704608	5465081	GG	M	2.701 ± 0.009	20	1.4	2.902±0.011; 2.899±0.014
WS-54A	KAT20130830-02	611021	5423216	TTG	M	2.893 ± 0.004	11	0.65	
WS-54B	KAT20130920-05	665163	5414196	GG	M	2.789 ± 0.006	17	1	
WS-54C	KAT20130913-06	730599	5500664	TTG	WR	2.738 ± 0.003	22	0.97	2.764±0.007 n=7; 3.050±0.008; 2.826, 2.792
WS-55A	KAT20130823-07	487433	5422153	SAN	WW	2.690 ± 0.004	10	1.05	
WS-55B	KAT20130911-01	748105	5428569	GG	EW	2.724 ± 0.003	21	0.81	
WS-55C	KAT20130920-02	696317	5465081	SAN	M	2.690 ± 0.005	28	1.4	
WS-56A	KAT20140821-01	682835	5380696	SAN	WA	2.693 ± 0.007	12	1.08	
WS-56B	KAT20140814-01	602503	5420512	FV	M	2.938 ± 0.006	15	0.27	
WS-56C	KAT20140820-02	659430	5397987	SAN	Q	2.696 ± 0.008	9	0.68	
WS-56D	KAT20140911-02	639098	5440211	FV	M	2.974 ± 0.007	14	0.34	3.019±0.010 n=8
WS-57A	KAT20140825-01	686978	5346123	SAN	WA	2.710 ± 0.008	11	1.6	
WS-57B	KAT20130919-02	523228	5455211	GG	M	*2.694*	*minimum age*		
WS-57C	KAT20130822-11	686517	5482083	GG	WR	2.688 ± 0.003	11	0.69	3.010±0.019 n=5
WS-57D	KAT20130823-03	490752	5485888	TTG	WW	2.698 ± 0.006	12	1.16	
WS-58A	KAT20140815-02	638202	5446906	GG	M	2.813 ± 0.005	12	1.4	
WS-58B	KAT20130730-11	628580	5436666	SAN	M	2.687 ± 0.007	14	1.5	
WS-58C	KAT20130815-01	622697	5403009	SAN	M	2.686 ± 0.005	14	0.84	
WS-58D	KAT20130806-06	640655	5436978	SAN	M	2.692 ± 0.008	12	1.4	
WS-58E	KAT20130823-11	513838	5398865	SAN	WW	2.687 ± 0.004	15	0.71	

Table 3-2: *In-situ* U-Pb results, Zr saturation temperature and zircon morphology and microstructure for samples dated by this study.

Mount ID	Rock description	Whole rock Zr (ppm)	Whole rock SiO_2 (%)	M	T (°C)	Zircon Size (µm)	Aspect ratio
WS-32A	Hornblende tonalite gneiss	167	66.4	1.50	782	40x80 to 120x250	1:2
WS-32B	Biotite K-feldspar porphyritic granodiorite	102	71.7	1.40	748	60x100 to 130x400	1:2.5
WS-32C	Biotite tonalite	172	65.4	1.76	766	60x150 to 200x200	1:1.5
WS-33A	Amphibolite tonalite to granodiorite gneiss	213	61.2	1.88	775	20x150 to 100x300	1:4
WS-33B	Granite	177	72.1	1.37	796	30x250 to 60x400	1:6
WS-33C	Biotite - hornblende tonalite gneiss	166	70.1	1.50	781	20x120 to 120x400	1:3
WS-34A	Garnet biotite - muscovite granodiorite	116	72.0	1.35	762	20x150 to 50x250	1:5
WS-34B	Garnet staurolite biotite Kfeldspar-MX granodiorite	77	72.6	1.40	726	30x100 to 120x250	1:2
WS-34C	Biotite K-feldspar porphyritic granodiorite	140	70.5	1.43	772	100x120 to 200x500	1:1, 1:4
WS-35A	Hornblende tonalite	437	69.7	1.49	873	30x50 to 60x120	1:2
WS-35B	Biotite granodiorite	124	73.5	1.28	772	30x70 to 80x180	1:1.5
WS-35C	Banded granodiorite gneiss	100	69.6	1.37	748	100x150 to 150x300	1:3
WS-36A	Banded hornblende tonalite (amphibolite facies)	31	49.4	3.08	572	140x140 to 300x300	1:1
WS-36B	Biotite feldspar-porphyritic granodiorite	190	69.0	1.42	799	50x100 to 100x500	1:3
WS-36C	*Biotite granodiorite*	*141*	*72.8*	*1.27*	*784*	*40x100 to 70x300*	*1:3*
WS-37A	Quartz granodiorite gneiss	101	76.1	1.36	750	100x120 to 250x260	1:1.2
WS-37B	Biotite granodiorite Dashwa gneiss	258	67.9	1.40	829	50x100 to 250x350	1:2
WS-37C	Monzogranite	150	70.7	1.44	777	70x100 to 200x250	1:1
WS-38A	Hornblende syenodiorite	218	60.3	2.30	748	150x150 to 250x250	1:1
WS-38B	Biotite tonalite gneiss	137	70.5	1.38	773	40x70 to 200x400	1:2
WS-38C	Biotite feldspar-porphyritic granodiorite	159	68.5	1.45	781	20x120 to 120x350	1:2
WS-39A	Biotite granodiorite	136	68.4	1.33	777	30x100 to 150x250	1:2
WS-39B	Epidote granite	129	73.2	1.26	777	30x100 to 120x300	1:2
WS-39C	Amphibolite tonalite to granodiorite gneiss	244	63.8	1.22	838	20x100 to 90x250	1:4
WS-43A	Post-tectonic	123	70.5	1.44	760	50x100 to 120x270	1:2
WS-43B	Biotite-hornblende quartz diorite	81	57.5	2.20	679	60x60 to 250x250	1:1
WS-43C	Biotite tonalite gneiss	125	71.3	1.45	761	40x90 to 70x250	1:3
WS-45A	Monzodiorite, Hillyer	299	56.6	2.60	752	70x70 to 200x300	1:1

Table 3-2: *In-situ* U-Pb results, Zr saturation temperature and zircon morphology and microstructure for samples dated by this study.

Mount ID	Rock description	Whole rock Zr (ppm)	Whole rock SiO_2 (%)	M	T (°C)	Zircon Size (µm)	Aspect ratio
WS-45B	Granite gneiss, Hillyer	320	77.2	1.32	856	60x120 to 160x250	1:1.5
WS-45C	*Hillyer*	*67*	*71.8*	*1.46*	*711*	*40x80 to 60x90*	*1:2*
WS-49B	Biotite-pyroxene monzodiorite, Entwine L.	213	56.2	3.07	695	80x100 to 180x400	1:2
WS-49C	Biotite-epidote monzodiorite, north of Entwine L.	90	63.3	1.76	714	20x50 to 40x120	1:2
WS-53A	Granodiorite - Diversion Stock	112	72.9	1.33	760	40x120 to 90x250	1:2.5
WS-53B	Tonalite - Atikwa batholith	87	71.7	1.49	729	40x100 to 70x200	1:2.5
WS-53C	Biotite granite	105	70.0	1.49	744	40x100 to 80x200	1:2
WS-54A	Granodiorite - Diversion Stock	103	67.2	1.53	740	50x100 to 100x250	1:2.5
WS-54B	Chlorite granite - Marmion intrusive complex	118	63.1	1.72	737	40x120 to 70x300	1:3
WS-54C	Biotite granodiorite	147	70.9	1.47	773	50x150 to 120x300	1:3
WS-55A	Quartz syenite - Weller Lake	127	70.2	1.52	758	80x140 to 140x220	1:1.5
WS-55B	Monzodiorite					40x130 to 100x250	1:2
WS-55C	Quatrz syenite	232	60.8	1.99	774	60x120 to 200x300	1:1.5
WS-56A	Greenwater feldspar porphyritic monzogranite	114	68.5	1.74	734	40x70 to 75x120	1:1.5
WS-56B	Finlayson L. felsic volcanic tuff	136	71.9	1.58	759	40x100	1:3
WS-56C	Brule L. monzogranite	107	63.3	1.64	735	30x70 to 50x200	1:3
WS-56D	Lumby L. felsic volanic crystal tuff	139	70.2	1.42	772	25x70 to 50x100	1:2
WS-57A	Sunbow Lake Monzogranite	234	60.3	2.18	762	80x200 to 160x500	1:3
WS-57B	Granodiorite, north of Entwine	201	61.5	1.83	773	70x180 to 200x400	1:2
WS-57C	Biotite granite	145	68.8	1.58	764	40x200 to 150x600	1:4
WS-57D	Tonalite - Atikwa batholith	146	70.9	1.49	771	80x80 to 150x300	1:1
WS-58A	Upper Scotch biotite granite	164	71.6	1.42	786	40x100 to 100x250	1:3
WS-58B	Norway monzogranite	349	65.6	1.73	831	80x120 to 200x250	1:1.2
WS-58C	Sapawe megacrystic monzonite	194	66.0	1.76	775	80x100 to 130x300	1:1.5
WS-58D	Van Nostrand megacrystic monzonite	49	48.4	3.18	594	40x100 to 200x200	1:1.5
WS-58E	Ottertail megacrystic monzogranite	112	71.5	1.51	748	70x120 to 200x300	1:2

Table 3-2: *In-situ* U-Pb results, Zr saturation temperature and zircon morphology and microstructure for samples dated by this study.

Mount	Zircon morphology and internal microstructure
WS-32A	euhedral, prismatic, flat, multifaceted; mostly clear; cracked zircons are red-brown; occasional apatite inclusions; luminescent; sector and oscillatory zoning; some resorbed cores; thin white rim
WS-32B	subhedral, prismatic to equant; translucent yellow brown to dark copper-brown; apatite common inclusions; dark; fine oscillatory zoning
WS-32C	euhedral multifaceted equant zircons; sub-rounded prismatic zircons; mostly clear; a few cracked and dark brown; few apatite inclusions; luminescent; sector zoned cores mantled by oscillatory zoning; some resorbed cores
WS-33A	subhedral, prismatic to acicular and equant; translucent to brown; commonly cracked; inclusions; luminescent; oscillatory zoning, few cores with sector zoning or banding
WS-33B	subhedral, acicular to prismatic; translucent honey brown to dark brown; many tiny (apatite) inclusions; dark; fine oscillatory zoning
WS-33C	subhedral prismatic; many broken; few equant; translucent honey brown to dark with cracks; inclusions; luminescent; oscillatory zoning, few sector zoned cores; local recrystallised zones
WS-34A	subhedral, acicular to prismatic, mostly flat faced; translucent honey and dark brown and cracked; few inclusions; dark; fine oscillatory zoning
WS-34B	subhedral, prismatic; translucent honey and dark brown and cracked; few inclusions; dark; oscillatory and banding, occasional white rims; xenocrysts: large equant fragments and cores, clear, bright, planar banding
WS-34C	equant and multifaceted to pyramidal, few prismatic; clear to coppery brown with cracks; inclusions; luminescent; unzoned to sector zoned, resorption textures and bright rims common
WS-35A	equant and multifaceted to pyramidal, few prismatic; clear; inclusions; luminescent; sector zoning, banding, oscillatory mantles; xenocrysts: dark, subhedral, oscillatory zoned
WS-35B	pyramidal with pointed tips, few prismatic; clear to honey, few dark brown and cracked; apatite inclusions; luminescent; sector zoning, banded, few oscillatory
WS-35C	euhedral to subhedral, prismatic; dark brown, cracked; apatite inclusions; dark; anhedral oscillatory zoning, commonly altered; xenocrysts: rounded, brown, equant to pyramidal
WS-36A	equant, rounded fragments; clear to coppery; inclusions; bright; sector zoning, banded
WS-36B	euhedral to subhedral, flat, prismatic; dark brown, few clear; inclusions; dark; oscillatory zoning is commonly disturbed
WS-36C	anhedral to subhedral, prismatic, flat; many broken; copper-brown; few inclusions; dark; banding and oscillatory zoning
WS-37A	euhedral pyramidal, rounded equant fragments; clear, few dark brown and cracked; inclusions; luminescent; sector zoning, banding, oscillatoy mantles, bright rims
WS-37B	subhedral, prismatic and pyramidal; clear and dark brown (large); apatite inclusions; dark; unzoned with few banded cores, oscillatory mantles
WS-37C	euhedral, equant to pyramidal, multifaceted; clear to coppery, dark brown with cracks; inclusions; weakly luminescent; sector zoning, oscillatory mantles
WS-38A	euhedral, equant to pyramidal, multifaceted; few prismatic and flat; clear; inclusions; weakly luminescent; planar banding/sector zoning mantled by unzoned or oscillatory zoning
WS-38B	subhedral, pyramidal to equant; mostly clear; many apatite inclusions; weakly luminescent; unzoned/sector zoned, with oscillatory mantles, white rims
WS-38C	subhedral to euhedral, prismatic and equant; clear and dark brown (large); many inclusions; dark; oscillatory zoning is commonly truncated by white rims giving a resorbed texture

Table 3-2: *In-situ* U-Pb results, Zr saturation temperature and zircon morphology and microstructure for samples dated by this study.

Mount	Zircon morphology and internal microstructure
WS-39A	euhedral to subhedral, pyramidal to prismatic; copper-brown, few clear; few inclusions; weakly luminescent; oscillatory zoned cored with dark unzoned rims
WS-39B	euhedral to subhedral, pyramidal to prismatic; mostly dark brown; few inclusions; luminescent; oscillatory; some unzoned recrystallisation
WS-39C	euhedral to subhedral, acicular to flat prisms, commonly broken; clear and dark brown (large); few inclusions; luminescent; oscillatory; some unzoned recrystallisation; xenocrysts: luminescent, sector-zoned angular fragment
WS-43A	euhedral to subhedral, pyramidal to prismatic; brown and cracked; inclusions; dark; oscillatory zoning
WS-43B	equant, euhedral to broken fragments; clear; inclusions; luminescent; sector zoning and planar banding
WS-43C	euhedral to subhedral, prismatic, flat sides; translucent to dark brown; few inclusions; dark; oscillatory zoning, cores marked by white band
WS-44C	euhedral prismatic, flat to acicular, commonly broken; clear to copper-brown; inclusions; dark; dark oscillatory to planar banded cores with bright rims
WS-45A	euhedral to rounded, prismatic to equant; translucent steel-brown; inclusions; weakly luminescent; sector-oscillatory zoned +banded cores, unzoned dark rims
WS-45B	mostly euhedral, equant; dark brown, few honey; inclusions; dark; unzoned, a few oscillatory zoned crystals
WS-45C	subhedral, prismatic; clear to brown; inclusions; dark; poor separate
WS-49B	anhedral equant fragments; clear to translucent brown, cracks; many inclusions; luminescent; sector and oscillatory zoning
WS-49C	flat, prismatic; equant and multifaceted; clear to dark brown; inclusions; weakly luminescent; oscillatory zoning, many recrystallised portions; xenocrysts: rounded and equant, dark to luminescent
WS-49C	flat, prismatic; equant and multifaceted; clear to dark brown; inclusions; weakly luminescent; oscillatory zoning, many recrystallised portionsrounded and equant, dark to luminescent
WS-53A	flat euhedral prisms, sub-rounded pyramidal ; very dark brown, many cracks; many inclusions; dark; oscillatory zoning; xenocrysts: dark, prismatic, corroded and broken
WS-53B	flat, prismatic; equant and multifaceted; clear to dark brown; inclusions; dark and luminescent; oscillatory zoning; xenocrysts: distinctly luminescent cores, mostly unzoned
WS-53C	anhedral pyramidal, euhedral prismatic; clear to honey brown; inclusions; dark; oscillatory zoning; xenocrysts: larger, distinct cores with planar banding truncated by rims
WS-54A	subhedral prismatic; very dark brown, many cracks; many inclusions; dark; oscillatory zoning
WS-54B	flat, prismatic to pyramidal; clear; apatite inclusions; luminescent; planar banding mantled by oscillatory zoning
WS-54C	flat, prismatic euhedral to rounded pyramidal; translucent to dark brown; many inclusions; dark; oscillatory zoning; xenocrysts: dark to luminescent cores with truncated oscillatory zoning, rounded
WS-55A	eu-subhedral equant, multifaceted; translucent copper brown with cracks; many inclusions; dark; sector zoned cores mantled by oscillatory zoning
WS-55B	subhedral, prismatic to pyramidal; translucent honey brown; many inclusions; dark; oscillatory mantles on oscillatory to sector zoned cores

Table 3-2: *In-situ* U-Pb results, Zr saturation temperature and zircon morphology and microstructure for samples dated by this study.

Mount	Zircon morphology and internal microstructure
WS-55C	subhedral, equant; translucent brown with cracks; many inclusions; weakly luminescent; cores mantled by oscillatory zoning; xenocrysts: luminescent cores with oscillatory zoning or banding
WS-56A	euhedral, multifaceted, pyramidal equant; clear; few inclusions; dark; oscillatory mantles on oscillatory to sector zoned cores; xenocrysts: several luminescent cores
WS-56B	euhedral, pyramidal to prismatic, pointed tips; clear to honey brown. ; inclusions; weakly luminescent; oscillatory zoning with rare sector zoned cores
WS-56C	subhedral, prismatic with flat edges; clear to translucent coppery brown; many inclusions; dark; oscillatory zoning with thin white metamorphic rims
WS-56D	euhedral, pyramidal with pointed tips; clear; apatite inclusions; dark; oscillatory zoning; xenocrysts: large, rounded, luminescent sector to oscillatory zonation
WS-57A	subhedral, prismatic; clear to reddish brown; inclusions; weakly luminescent; oscillatory zoning; xenocrysts: luminescent unzoned to sector zoned cores
WS-57B	an-subhedral, prismatic to pyramidal; translucent red-brown to dark brown; inclusions; dark; oscillatory zoning; xenocrysts: luminescent sector and oscillatory zoned cores
WS-57C	sub-anhedral, prismatic to equant; clear to dark copper brown ; inclusions; dark; oscillatory zoning; xenocrysts: luminescent oscillatory zoned cores
WS-57D	eu-subhedral, equant and multifaceted; clear to light brown; inclusions; dark; oscillatory zoning
WS-58A	subhedral, pyramidal; translucent brown to dark brown; inclusions; dark; oscillatory zoning
WS-58B	euhedral, prismatic flat to equant; translucent red-brown to dark brown; inclusions; dark; oscillatory zoning
WS-58C	euhedral, prismatic flat to equant; clear to reddish brown; inclusions; dark; oscillatory zoning
WS-58D	euhedral, prismatic flat to equant; clear; inclusions; weakly luminescent; oscillatory zoning
WS-58E	euhedral, pyramidal to prismatic; translucent to dark copper brown; apatite inclusions; weakly luminescent; oscillatory zoning

All ages are calculated from the $^{207}Pb/^{206}Pb$ weighted means except those in italics, which are minimum ages reflecting the oldest concordant zircon analysis. Zircon saturation temperatures are calculated from whole rock Zr and 'M-value', where M=(Na + K + 2Ca)/(Al·Si) following Watson and Harrison (1983).

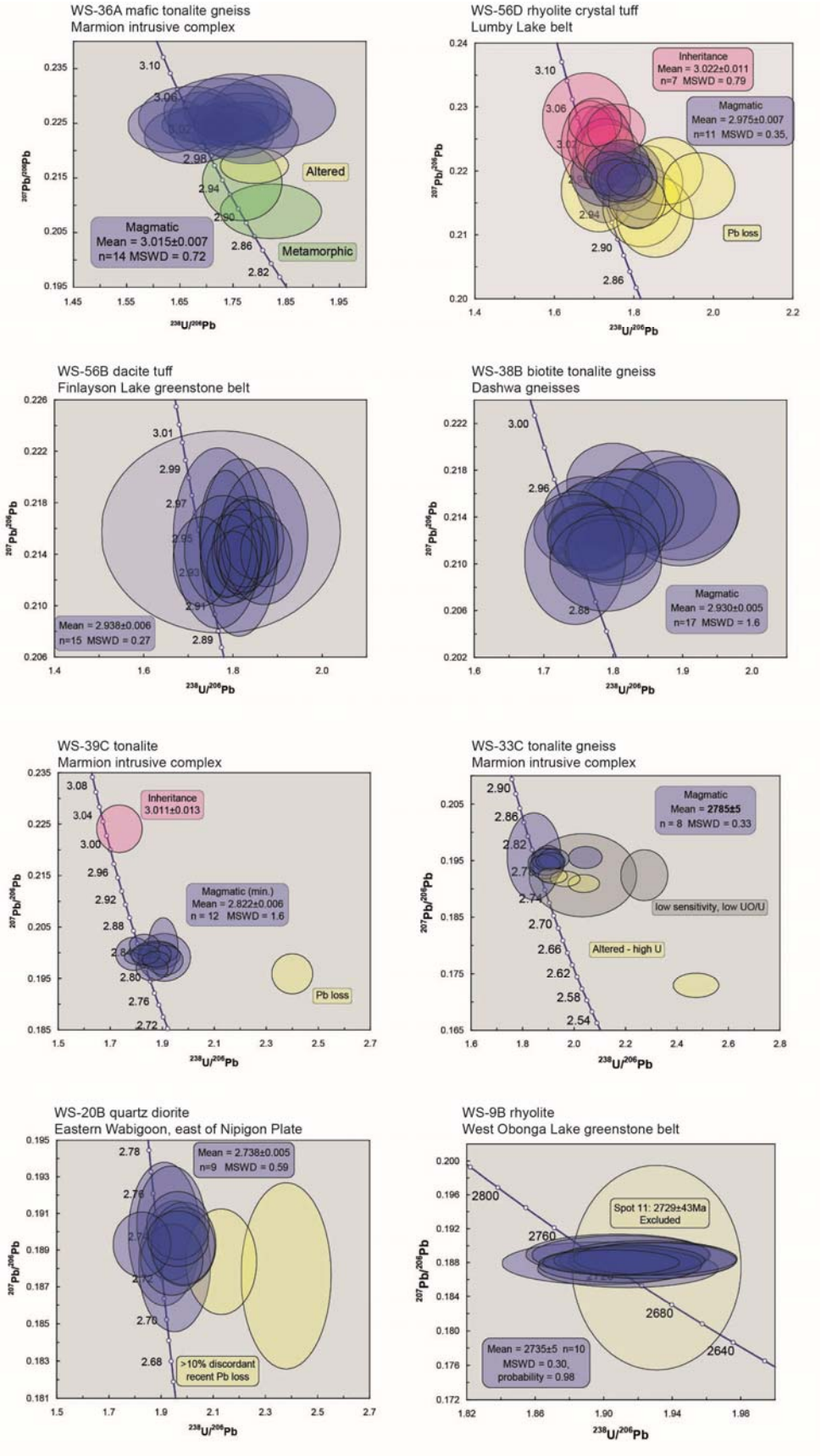
WS-36A mafic tonalite gneiss
Marmion intrusive complex
Altered
Metamorphic
Magmatic
Mean = 3.015±0.007
n=14 MSWD = 0.72
WS-56D rhyolite crystal tuff
Lumby Lake belt
Inheritance
Mean = 3.022±0.011
n=7 MSWD = 0.79
Magmatic
Mean = 2.975±0.007
n=11 MSWD = 0.35,
Pb loss
WS-56B dacite tuff
Finlayson Lake greenstone belt
Mean = 2.938±0.006
n=15 MSWD = 0.27
WS-38B biotite tonalite gneiss
Dashwa gneisses
Magmatic
Mean = 2.930±0.005
n=17 MSWD = 1.6
WS-39C tonalite
Marmion intrusive complex
Inheritance
3.011±0.013
Magmatic (min.)
Mean = 2.822±0.006
n = 12 MSWD = 1.6
Pb loss
WS-33C tonalite gneiss
Marmion intrusive complex
Magmatic
Mean = 2785±5
n = 8 MSWD = 0.33
low sensitivity, low UO/U
Altered - high U
WS-20B quartz diorite
Eastern Wabigoon, east of Nipigon Plate
Mean = 2.738±0.005
n=9 MSWD = 0.59
>10% discordant
recent Pb loss
WS-9B rhyolite
West Obonga Lake greenstone belt
Spot 11: 2729±43Ma
Excluded
Mean = 2735±5 n=10
MSWD = 0.30,
probability = 0.98
207Pb/206Pb
238U/206Pb

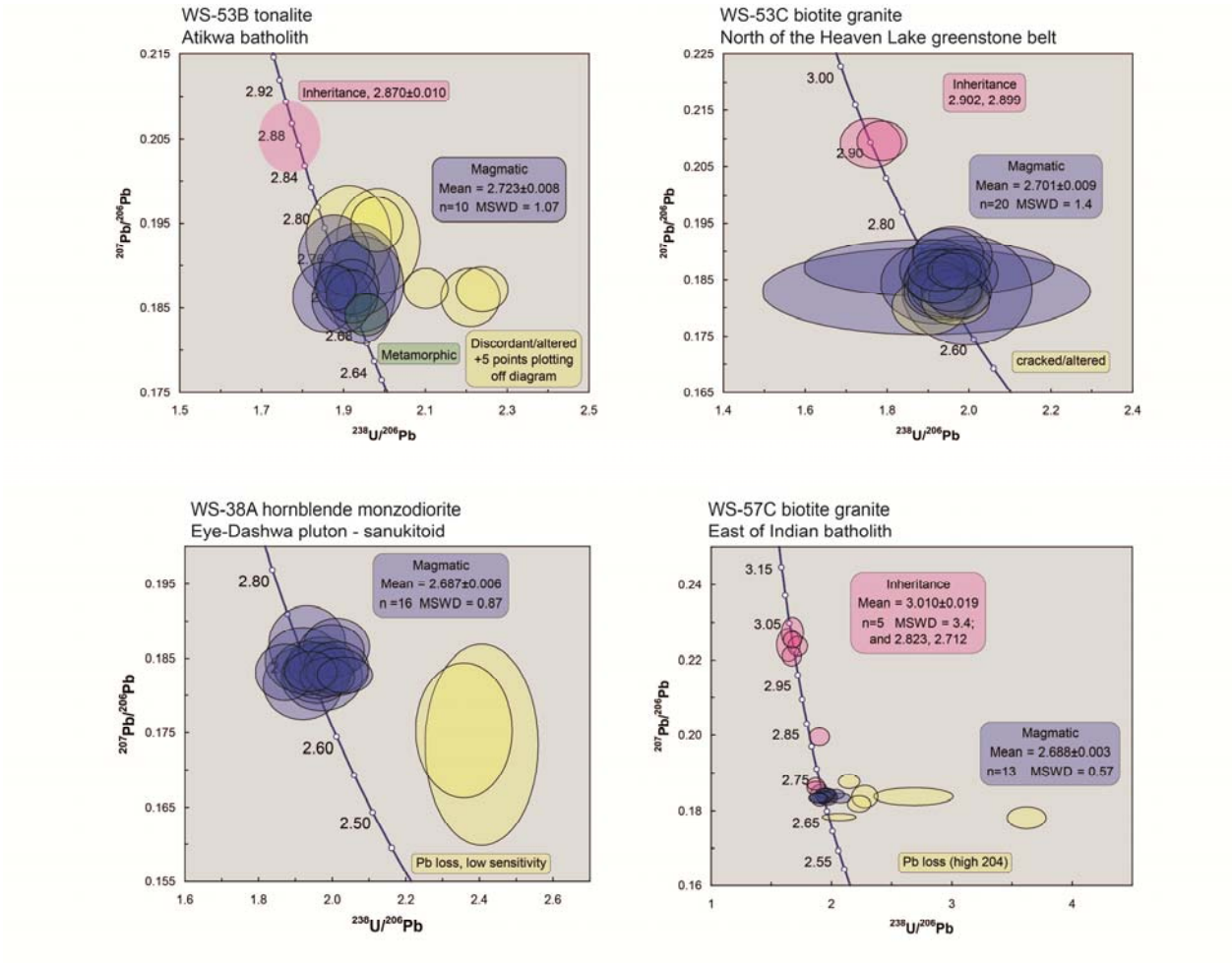

Figure 3-10: Tera-Wasserburg concordia plots for selected samples spanning a range in ages from 3.0 to 2.7 Ga, arranged from oldest to youngest. All ages are reported as weighted means of $^{207}Pb^{*}/^{206}Pb^{*}$ ages with uncertainty at the 2σ level. All data point error ellipses are plotted at 2σ. Magmatic populations are indicated by blue ellipses, inheritance by pink ellipses and metamorphism by green ellipses. Analyses with interpreted Pb loss, disturbed or altered grains are indicated by yellow ellipses which were excluded from calculated populations. Where discordance appears to reflect recent Pb loss for a unimodal age (e.g. WS-38B), discordant analyses were included in the weighted mean. If inheritance was identified in addition to a magmatic population, analyses with >10% discordance were excluded. Many samples record both recent and ancient Pb loss (e.g. WS-53C, WS-57C).

tonalite gneiss from the Dashwa gneisses west of the Finlayson Lake greenstone belt, and a 2.785±0.005 (WS-33C) biotite-hornblende tonalite in the eastern Marmion intrusive complex.

Granodiorite to granitic compositions host progressively smaller zircons, with greater variability in morphology and internal microstructure. A 2.999±0.002 Ga (WS-37B) amphibolite band within granodiorite gneiss to migmatite was dated from within the Dashwa gneiss immediately east of the Nevison arm of the western Steep Rock greenstone belt. This is the first 3.0 Ga age measured in the

Dashwa gneisses (Figure 3-2). Many of the 2.93 to 2.9 Ga rocks of the Marmion intrusive complex and Dashwa gneisses are granodioritic, for example, samples WS-38C (2.931±0.005 Ga) and WS-39A (2.928±0.005 Ga). Colour ranges from clear to dark brown with many inclusions. In some cases, the large dark grains with cracks and inclusions have the most euhedral internal structure and yield the most concordant ages. Prismatic forms with oscillatory zoning are dominant, but can range from equant to acicular, and planar banding is not uncommon. Zircons from granodiorite tend to be less luminescent and higher in U with more radiation damage and higher amounts of common Pb than zircons from tonalite. They are concordant to strongly discordant, with both recent and ancient Pb loss (e.g. WS-53A, 2.898±0.008 Ga; Figure 3-10). Inheritance in granodiorite and granite is more common than in tonalite, and may form one or more coherent populations or several grains falling along the concordia. In the latter case, it is difficult to discriminate zircons formed by magmatic crystallisation from those that have undergone ancient Pb loss based on U-Pb data alone. For example, a phase from the Marmion intrusive complex (WS-35C; 2.928±0.007) contains three distinct populations with concordant zircons in each population. Another sample within the Marmion intrusive complex (WS-35B; 2.787±0.010) contains populations at 2.79 Ga and 2.83 Ga. In these cases, $^{176}Hf/^{177}Hf$ aided in veracity of interpreted populations, where identical Lu-Hf compositions indicated that younger analyses experienced Pb loss during later thermal events rather than representing distinct crystallisation events (Figure 3-12).

Granitic samples tend to yield particularly poor quality high U zircons. Zircons are generally reddish brown to dark brown and are smaller than zircons from tonalite and granodiorite, with longer aspect ratios. These zircons tend to have low luminescence, and where preserved, zircons show oscillatory zonation that is commonly disturbed. These samples have lower average zircon saturation temperatures than tonalite (Table 3-2). Ages from pretectonic granites tend to be complex (e.g. WS-53B, 2.723±8 Ga), with inherited populations and both recent and ancient Pb loss. These characteristics in many cases translated into a minimum magmatic age or unresolved ages. Accordingly the ages of such granitic rocks are underrepresented by this study.

3.4.2.3. Syn to post-tectonic alkali granite – granodiorite

Zircons from samples from the GG suite show a wide range in morphology, but tend to be small to medium, subhedral, translucent reddish or honey brown to dark brown, with low luminescence and oscillatory zonation. They commonly retain variably resorbed inherited zircons. Like pre-tectonic alkali granites, post-tectonic granites have poor quality zircons that have experienced Pb loss (e.g. WS-33B, 2.689±0.005 Ga; Figure 3-10). Post-tectonic granodiorites on the other hand generally

host clearer, more luminescent zircons with a moderately concordant magmatic population but may also have complexities from inheritance and later thermal disturbance (e.g. WS-32B).

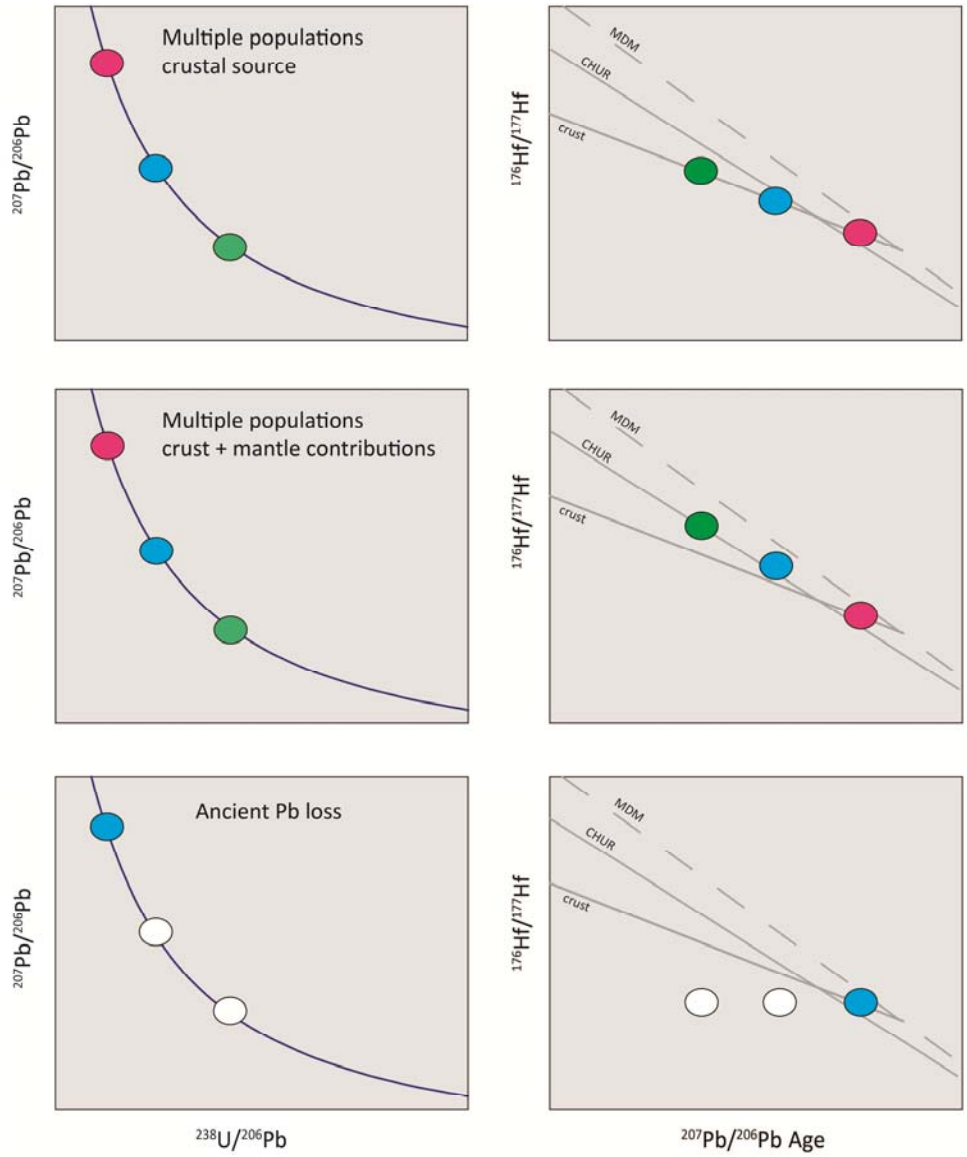

Figure 3-11: $^{176}Hf/^{177}Hf$ – time cartoons illustrating the use of Hf isotope compositions to aid in verifying age interpretations. In the case of multiple crystallisation ages from a one-component source, successively younger populations will plot along a crustal evolution line defined by the $^{176}Lu/^{177}Hf$ of the crustal source (~0.015). If magmas have a mantle-derived contribution in younger populations, they will plot between the crustal and mantle evolution lines (above the crustal line because the mantle has higher $^{176}Lu/^{177}Hf$). If the zircons have experienced ancient Pb loss, their young ages are only apparent. If the Hf has not been disturbed, these zircons will plot along a near horizontal trend because $^{176}Lu/^{177}Hf$ of zircons is low (~0.001).

Table 3-3: Comparison of $^{207}Pb/^{206}Pb$ ages determined by this study with age previously determined by TIMS methods for samples from the same intrusions/complexes. References for TIMS ages follow.

SHRIMP - this study				*TIMS*				
Mount	**Rock type**	**Age (2σ)**	**Inheritance**	**Sample**	**Rock type**	**Age (2σ)**	**Inheritance**	**Ref**
Hillyer				**Hillyer**				
WS-44C	biotite granodiorite	2.693±0.003		07DS43	leuco tonalite gneiss	2.88	~3.000	7
WS-45B	granite gneiss	2.723±0.002		00KYT11	hornblende tonalite	2.869±0.004		5
				06DS52	biotite tonalite	2.866±0.008		12
				06DS50	biotite granodiorite	2.686±0.006		12
Atikwa batholith				**Atikwa batholith**				
WS-53B	tonalite	2.723±0.008	2.868±14; 2.784-2.767	DD78-6	trondhjemite	2.7318±0.0016		8
WS-57D	tonalite	2.698±0.006		DD78-4	trondhjemite	2.7322±0.0029		8
Muskeg batholith				**Muskeg batholith**				
WS-32B	biotite FP granodiorite	2.685		05DS48	Kfs megacrystic granite	2.686±0.002	2.69	5
WS-43A	granodiorite	2.691±0.009	2.906±0.005					
Shelby				**Shelby**				
WS-55B	monzodiorite	2.724±0.003		DD85-3	tonalite gneiss	2.775±0.008		3
				05DS85	tonalite gneiss	2.7736±0.0012		5
Wawang				**Wawang**				
WS-57C	biotite granite	2.688±0.003	3.010±0.019	00KYT34	tonalite gneiss	2.712±0.002		15
Sanukitoid				**Sanukitoid**				
WS-49B	bt-px monzodiorite - Entwine	2.692±0.004		06DS23	monzodiorite	2.685±0.008		12
WS-37C	monzogranite - Eye-Dashwa	2.688±0.007			biotite-hornblende granite	2.684±0.025		16
WS-38A	hb syenodiorite - Eye-Dashwa	2.686±0.006						
WS-58B	granite - Norway	2.687±0.007		09SB278	quartz monzonite	2.6859±0.0007		1
WS-58E	mx monzogranite - Ottertail	2.687±0.004		13	quartz monzodiorite	2.6861±0.0015		10
WS-58C	mx monzogranite - Sapawe	2.686±0.005		ON+200	quartz monzonite	2.688±0.004		9
WS-57A	monzogranite - Sunbow	2.71±0.008		C-92-31	monzodiorite	2.684±0.001		2
WS-58D	mx monzogranite - Van Nostrand	2.692±0.008		09SB254	monzonite	2.6845±0.0009		1

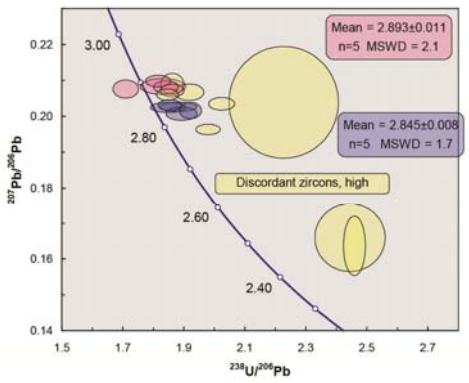
Mean = 2.893±0.011
n=5 MSWD = 2.1
Mean = 2.845±0.008
n=5 MSWD = 1.7
Discordant zircons, high
3.00
2.80
2.60
2.40
$^{207}Pb/^{206}Pb$
$^{238}U/^{206}Pb$

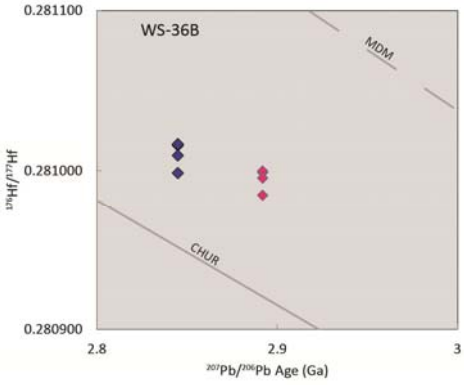
WS-36B
MDM
CHUR
$^{176}Hf/^{177}Hf$
$^{207}Pb/^{206}Pb$ Age (Ga)

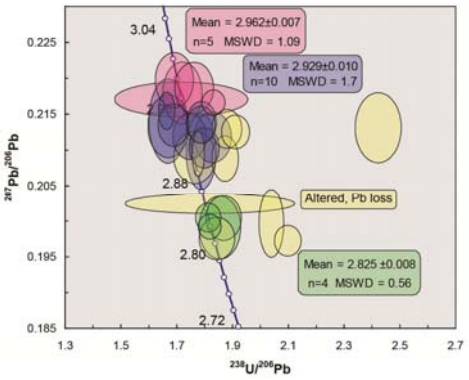
Mean = 2.962±0.007
n=5 MSWD = 1.09
Mean = 2.929±0.010
n=10 MSWD = 1.7
Altered, Pb loss
Mean = 2.825 ±0.008
n=4 MSWD = 0.56
3.04
2.88
2.80
2.72
$^{207}Pb/^{206}Pb$
$^{238}U/^{206}Pb$

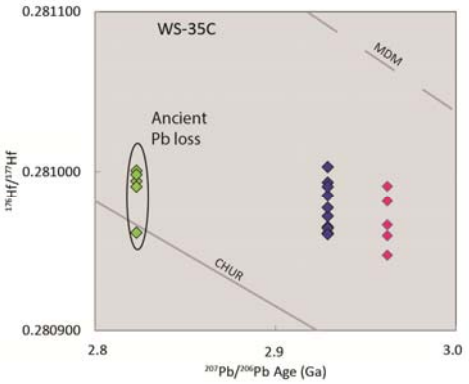
WS-35C
MDM
Ancient
Pb loss
CHUR
$^{176}Hf/^{177}Hf$
$^{207}Pb/^{206}Pb$ Age (Ga)

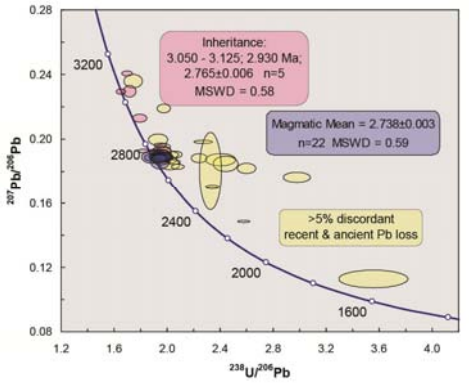
Inheritance:
3.050 - 3.125; 2.930 Ma;
2.765±0.006 n=5
MSWD = 0.58
Magmatic Mean = 2.738±0.003
n=22 MSWD = 0.59
>5% discordant
recent & ancient Pb loss
3200
2800
2400
2000
1600
$^{207}Pb/^{206}Pb$
$^{238}U/^{206}Pb$

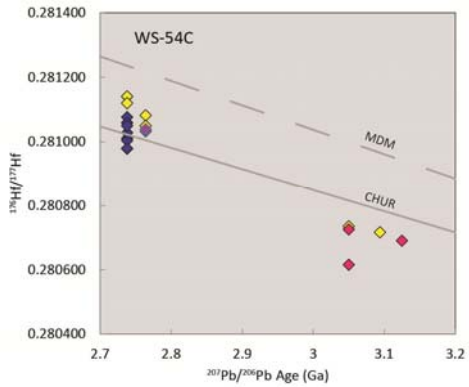
WS-54C
MDM
CHUR
$^{176}Hf/^{177}Hf$
$^{207}Pb/^{206}Pb$ Age (Ga)

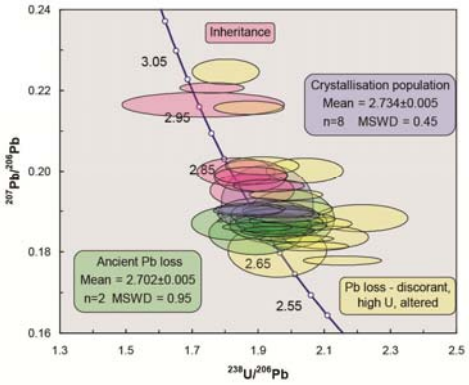
Inheritance
Crystallisation population
Mean = 2.734±0.005
n=8 MSWD = 0.45
Ancient Pb loss
Mean = 2.702±0.005
n=2 MSWD = 0.95
Pb loss - discorant,
high U, altered
3.05
2.95
2.85
2.65
2.55
$^{207}Pb/^{206}Pb$
$^{238}U/^{206}Pb$

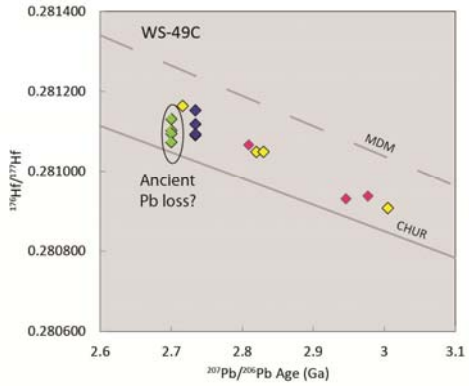
WS-49C
MDM
Ancient
Pb loss?
CHUR
$^{176}Hf/^{177}Hf$
$^{207}Pb/^{206}Pb$ Age (Ga)

Figure 3-12: Examples of complex samples where $^{176}Hf/^{177}Hf$ compositions measured in the same zircon domain as ages aided in age assignment. WS-36B contains two populations close in age, but their different $^{176}Hf/^{177}Hf$ corroborates different age populations. WS-35C contains three statistically distinct populations. The two oldest ages are interpreted as inherited and magmatic respectively. The youngest population is interpreted as reflecting ancient Pb loss. However, if the low $^{176}Hf/^{177}Hf$ outlier is excluded, this interpretation is inconclusive. WS-54C has an inherited component that was reworked during younger magmatism with a juvenile contribution because younger magmatism plots distinctly above a crustal evolution line. The two younger populations have nearly identical and overlapping $^{176}Hf/^{177}Hf$ suggesting they are one population, but it is possible that the youngest population reflects multiple contributions from the ancient component and a younger component. WS-49C also shows evidence for multiply aged inheritance, and the successively increasing $^{176}Hf/^{177}Hf$ with each population suggests they represent true crystallisation ages. As with WS-54C, the case for the youngest population is ambiguous because it reflects a mixed source.

3.4.2.4. Sanukitoid

Zircons from the sanukitoid suite (2.69 – 2.68 Ga) have variable morphology and microstructure, reflecting the large geochemical compositional range (Figure 3-8). More primitive varieties, such as diorite and monzodiorite, have large, equant to pyramidal, clear zircons with high luminescence and both sector and oscillatory zoning, such as the 2.692±0.004 Ga monzodiorite phase of the Entwine intrusion (WS-49B). Evolved compositions are bimodal in character, with dominantly prismatic elongate forms and oscillatory zoning, for example, the 2.686±0.005 Ga megacrystic monzonite phase of the Sapawe stock (WS-58C). The sanukitoid suite has the highest zircon saturation temperatures associated with mafic compositions (Table 3-2). The zircons tend to be concordant and unimodal in measured U-Pb age, with the exception of inheritance measured in the Brule, Sunbow and Greenwater Lakes plutons.

3.4.2.5. Felsic volcanic

Zircons of the two volcanic samples analysed differ from plutonic zircons of the study area in having distinct pyramidal faces with pointed tips. They are relatively small (~35x70µm) equant to elongate with aspect ratios ranging from 1:1.5 to 1:3, clear to light reddish brown, euhedral, with low luminescence and oscillatory zonation. Unzoned or sector zoned luminescent centres characterise several igneous zircons from both samples (Figure 3-8). Sample WS-56B from the western Finlayson greenstone belt has a unimodal population at 2.938± 0.006 Ga. Sample WS-56D from Gargoyle Lake was dated at 2.974± 0.007 Ga and contains a 3.019±0.010 Ga inherited population of cores and xenocrysts, which are larger and luminescent, with oscillatory zonation (Figures 3-8, 3-9).

3.4.3. Age distribution of the Marmion terrane

Within the Wabigoon superterrane as a whole, the largest and broadest age peak extends from 2.745 – 2.67 Ga (Figure 3-13). Other prominent peaks occur at 2.78, 2.82, 2.88, 2.93, 3.00, 3.05 and ~3.25

Ga (Figure 3-13). Although all terranes within the Wabigoon superterrane record the peak in magmatism at ~2.7 Ga, the Marmion and Eastern Wabigoon terranes record two distinct pulses at 2.73 and 2.69 Ga whereas the Western Wabigoon and Winnipeg River terranes also record substantial intervening magmatism.

The Marmion terrane records a spectrum of ages from 3.0 to 2.7 Ga, with extensive Mesoarchaean crystallisation ages (Figure 3-14). The data define eight peaks of semi-regular intervals: 3.0, 2.96, 2.93, 2.89, 2.82, 2.78, 2.72, and 2.69 Ga. Notable hiatuses occur from 2.865 – 2.83 Ga and 2.78 – 2.75 Ga (Figures 3-14). Quiescent periods are not as sustained in the Marmion terrane as in the neighbouring Winnipeg River and Eastern Wabigoon terranes (Figure 3-14).

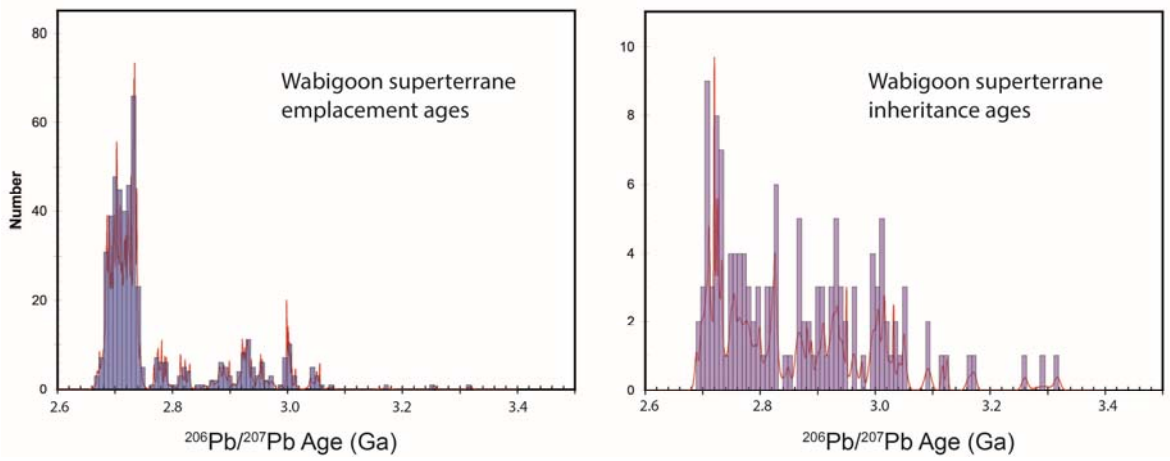

Figure 3-13: Cumulative probability distribution (curve) and a histogram (bins) of geochronology compiled from this and previous studies for the Wabigoon superterrane. Each age reflects a distinct sample rather than a single zircon age. Age distribution is separated into interpreted emplacement ages (left) and inheritance ages (right). There is a major peak in emplacement ages centred over 2.7 Ga. Several smaller peaks in emplacement ages also emerge, notably at 3.2, 3.0, 2.96, 2.93, 2.89, 2.82, and 2.75. Inheritance age distribution also peaks at 2.7 Ga, but does not show the distinct peaks of the emplacement ages. Data within the Wabigoon superterrane was compiled by KEB and includes previous geochronology by TIMS (references listed in Supplementary Table 3-4) and unpublished data from Lu et al.

The Marmion intrusive complex was thought to have a nearly uni-modal age distribution at 3.003 Ga (Tomlinson et al., 1999; Tomlinson et al., 2004) but locally extending to 2.957 Ga (Davis et al., 2005). This study has highlighted magmatism at 3.02, 2.93, ~2.90, 2.825, 2.78, and 2.68 Ga with a general eastward younging (Figure 3-15). The ages recorded by the various phases of the Marmion Intrusive Complex closely mirror the timing of volcanism in the greenstone belts that surround it. In contrast, the 2.94 – 2.93 Ga Dashwa gneisses immediately west of the Finlayson Lake greenstone belt are nearly unimodal in age, despite analysis of multiple chemically distinct phases (samples WS-38B,C and WS-39A,B, this study; two samples dated by Davis (Jack Satterly Geochronology

Laboratory), 1986, reported in Stone et al., 1992). A 2.938±0.006 Ga felsic volcanic tuff (sample WS-56B) and a 2.931±0.002 Ga felsic volcanic horizon (Tomlinson et al., 2003) from the western Finlayson Lake belt bracket mafic volcanic rocks, highlighting corresponding ages to the Dashwa gneisses they are in contact with. The contact between the Dashwa gneisses and the Finlayson Lake belt is highly deformed, making interpretation of its nature complex. Nevertheless, the contact is free from a younger intervening intrusion. The 2.999 Ga granodiorite gneiss – migmatite within the Dashwa gneisses to the west is nearby 2.9985±0.0008 Ga Nevison felsic volcanic rocks (D.W. Davis (Jack Satterly Geochronology Laboratory, unpublished data, 1986), reported in Stone et al., 2002).

In contrast to the contact between the Dashwa gneiss and Finlayson Lake greenstone belt, feldspar porphyry stocks intrude along the length of the contacts between the Marmion intrusive complex and surrounding greenstone belts, with the exception of the erosive basal conglomerates of the Steep Rock belt. Two ages obtained from porphyritic tonalite-granodiorite immediately south of the Lumby Lake greenstone belt yielded ages of 2.788±0.005 Ga and 2.793±0.005 Ga (WS-34C, WS-35A), consistent with the 2.78 Ga age (Buse et al., 2010) for a tonalite stock along the south margin of the Lumby Lake belt (in dark pink, Figure 3-2). These new ages confirm that this intrusion continues west beyond the mapped extent but consistent with the magnetic signature. Two samples from the petrographically similar granodiorite of the Diversion Stock, between the Finlayson Lake belt and the Marmion intrusive complex, showed that the Diversion Stock was emplaced at 2.89 Ga.

3.4.4. Age distribution of surrounding terranes

The Winnipeg River terrane contains the oldest inherited grains. The oldest inheritance measured in this study was >3.05 Ga within a 2.738±0.005 Ga granodiorite just north of the boundary between the Marmion and Winnipeg River terranes. The xenocrysts of Lu et al. (unpublished data) range up to 3.17 Ga. Despite recording signatures of the oldest crust for the area, there is a prominence of Neoarchaean ages in the Winnipeg River terrane. Distinct gaps in magmatic ages occur from 3.20 – 2.98 Ga and 2.84 – 2.78 Ga.

The Western Wabigoon terrane as defined by Stott (2011) contains a major peak in magmatism from 2.745 to 2.680 Ga. Within that, there are also peaks at 2.739, 2.720 and 2.701 Ga, and a few samples aged 2.775 Ga. The Eastern Wabigoon terrane records magmatism at ~2.92, 2.9 and 2.82 Ga, with peaks at 2.78, 2.74 – 2.72, and 2.69 Ga (Figure 3-14). The peaks of the Eastern Wabigoon terrane correspond to magmatic pulses in the Marmion terrane but with a restricted record >2.8 Ga.

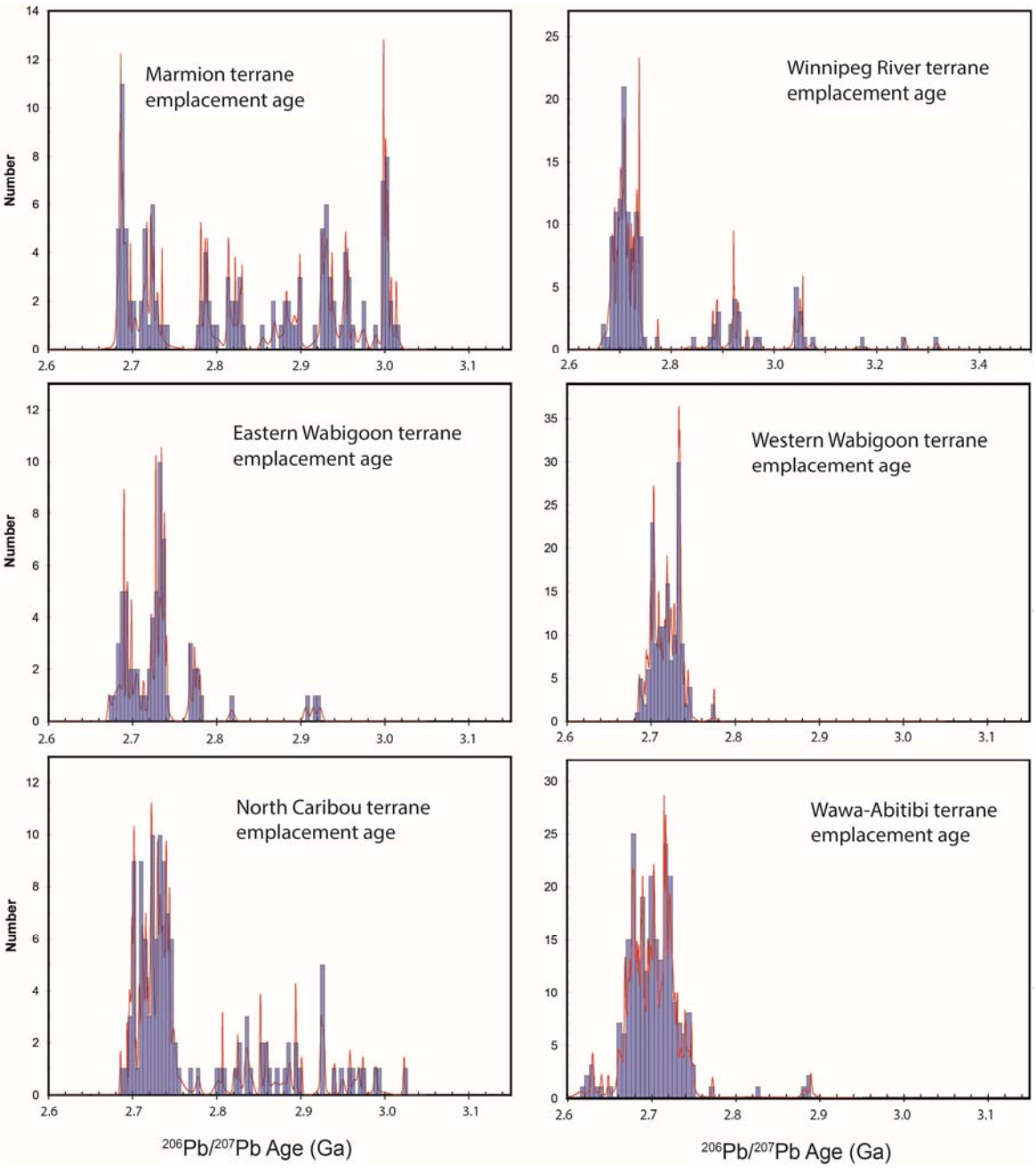

Figure 3-14: Cumulative probability distribution (curve) and a histogram (bins) of magmatic emplacement ages compiled from this and previous studies for terranes of the Western Superior Craton. Each age reflects a distinct sample rather than a single zircon age. Inheritance is not included. Like the Wabigoon superterrane (Figure 3-13), all terranes record a peak in magmatism centred over 2.7 Ga, but this peak is comprised of two distinct peaks in the Marmion and Eastern Wabigoon terranes. Although the Winnipeg River terrane contains the oldest ages, the Marmion terrane has a much more continuous record of Mesoarchaean magmatism, with a distinct peak at 3.0 Ga. Data within the Wabigoon superterrane includes previous geochronology by TIMS (references listed in Supplementary Table 3-4) and unpublished data from Lu et al. Data for the Wawa-Abitibi and North Caribou terranes were obtained from the Canadian Geochronology Knowledgebase (Geological Survey of Canada, 2013) for comparison.

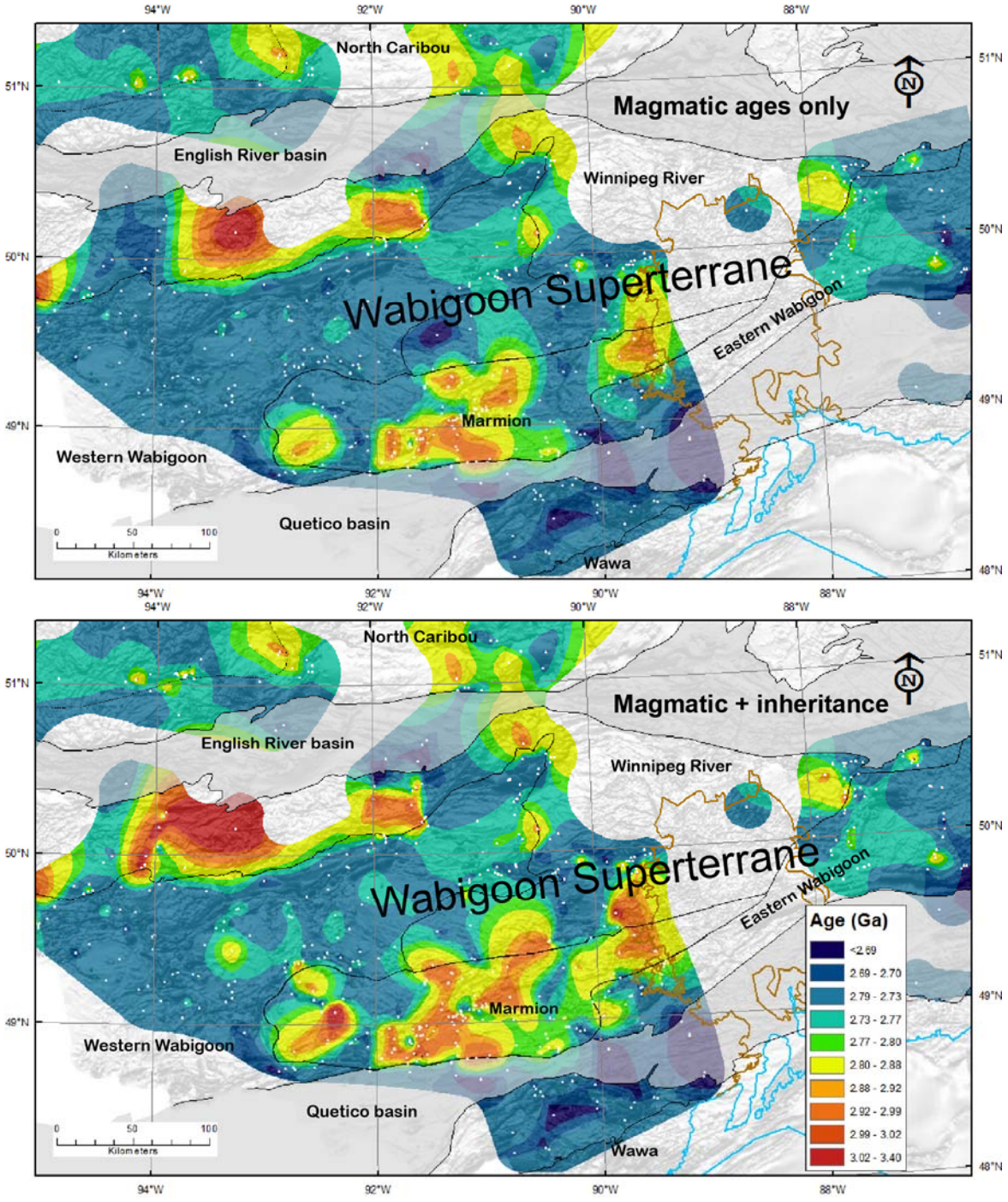

Figure 3-15: Contoured maps portraying spatial distribution of zircon ages. Legend indicates age ranges, with warmest colours (reds and orange) representing older ages and cooler colours (greens and blue) representing younger ages. Upper map includes only magmatic ages and the lower map includes the oldest inherited age population of each sample. Age determinations are indicated by white dots. Data within the Wabigoon superterrane was compiled by the author. The Canadian Geochronology Knowledgebase (Geological Survey of Canada, 2013) was used for data outside of the Wabigoon superterrane. Contouring was accomplished using the spatial analyst extension in ArcGIS, with the natural neighbour interpolation method as suggested by Champion and Huston (2016). Areas with low data density are not

contoured, and shaded magnetic relief is plotted for reference. Terrane boundaries from Stott (2011, Marmion - Western Wabigoon boundary modified by this study) are shown by black outlines. The Proterozoic Nipigon diabase extent is indicated by brown outline, extending to Lake Superior.

A <2.9 Ga a granodiorite (WS-43A) is just east of margin of the Marmion terrane within the Eastern Wabigoon terrane.

The North Caribou superterrane records a similar protracted history to the Marmion terrane, of crustal recycling to 3.0 Ga. Its record is less punctuated than the Marmion terrane. Like the Winnipeg River and Western Wabigoon terranes but slightly older, the North Caribou superterrane records a large peak from 2.75 – 2.68 Ga. The Wawa terrane records a very large peak centred over 2.7 Ga from 2.75 – 2.66 Ga with a few scattered ages to 2.62 Ga and at 2.77, 2.83 and 2.89 Ga.

3.4.5. Inheritance

Inheritance is preserved in magmatism within the Marmion at 2.97, 2.93, 2.9, 2.82, 2.78 and 2.72-2.70 Ga, indicating periods of crustal reworking where older zircon-bearing crust was sampled (Figure 3-16). A key implication is that TTG magmas had multiple sources rather than a single basaltic parent, which is commonly assumed for geochemical and experimental models (e.g. Drummond et al., 1996; Foley et al., 2002). These times of crustal reworking correspond to peaks in magmatism, and their significance is further explored in Chapter 4 using Hf isotopes. Inherited zircons in the Marmion terrane range in age as far back as the earliest measured crystallisation ages at 3.02 Ga. As with magmatic emplacement ages, there is a prominent 3.0 Ga peak in inherited age populations of the Marmion terrane. Felsic to intermediate volcanic horizons of the Lumby Lake greenstone belt, such as the 2.974±0.007 Ga crystal tuff from Gargoyle Lake, commonly contain large 3.0 Ga xenocrysts and cores (Figure 3-8). Consequently, early TIMS ages for some horizons in the Lumby Lake belt were overestimated, as noted by Buse et al. (2010). Inherited ages to 3.0 Ga were also measured in a granodiorite intruding the Irene-Eltrut Lakes gneisses, west of the proposed location for the terrane boundary between the Marmion terrane and the Western Wabigoon terrane (Stott, 2011; Tomlinson et al., 2004).

Inherited ages in the Eastern Wabigoon terrane range up to 2.93 Ga and are localised within 2.73 – 2.69 Ga magmatism (Figure 3-16). Inheritance in the Western Wabigoon is also recorded in 2.73 magmatism and has not been noted to exceed 2.78 Ga (Blackburn et al., 1991; Tomlinson et al., 2004), but inheritance measured within the north-central Western Wabigoon terrane includes a 2.868 Ga xenocryst and several 2.78 Ga inherited zircons within a 2.72 Ga phase of the Atikwa batholith (WS-53B). Inheritance in the Winnipeg River terrane was measured in a 2.9 Ga pluton and is common in magmatic rocks ranging in crystallisation ages from 2.73 to 2.68 Ga.

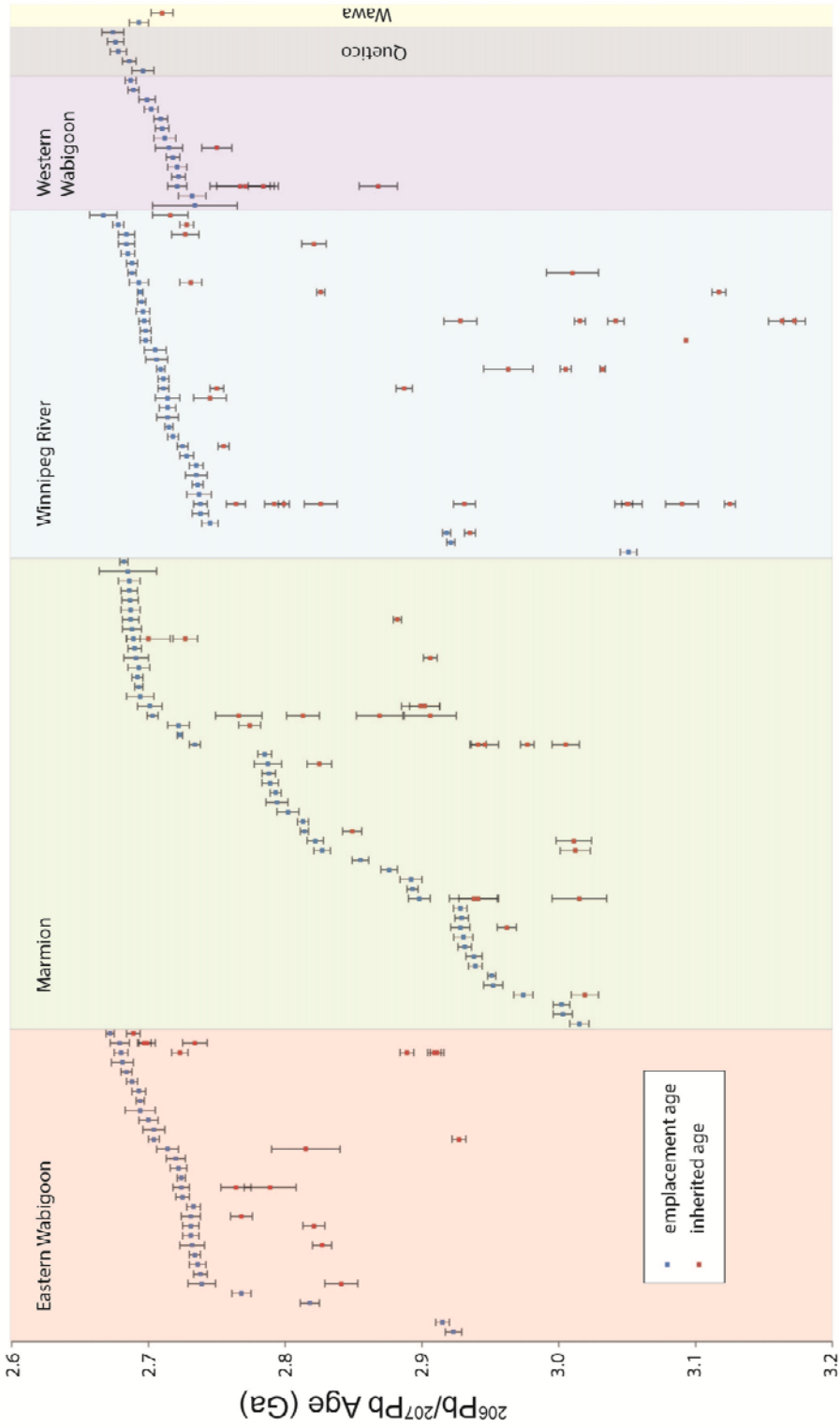

Figure 3-16: Space-time plot of results from this study and Lu et al. (unpublished data) showing periods of reworking older zircon-bearing rocks across various terranes. Analytical error bars indicate 2 standard deviations of the weighted mean. Inheritance is particularly abundant in Neoarchaean magmatism within the Winnipeg River and Eastern Wabigoon terranes, but is also localised in several phases through time in the Marmion terrane.

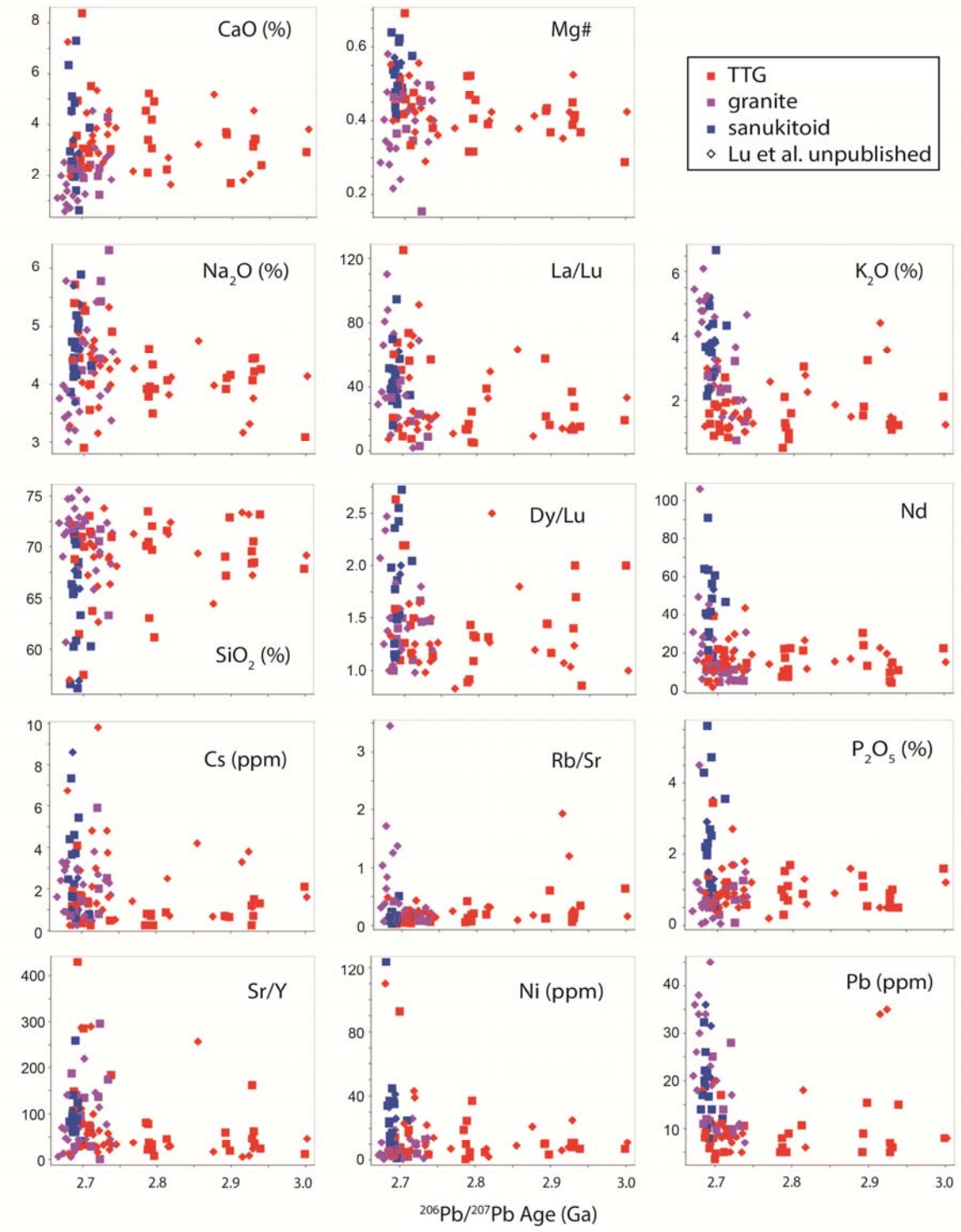

Figure 3-17: Geochemistry – age plots. Data from this study are indicated as filled squares and unpublished data from Lu et al. as filled diamonds. Symbols are colour-coded as follows: TTG – red, alkali granites – purple and sanukitoid suite – blue. These plots illustrate the stepwise changes in geochemistry at: (i) 2.75 Ga, where variability in major oxides and Mg# increase, and LILE, Sr/Y and La/Yb increase. (ii) <2.70 Ga , where late granite-granodiorite (GG) rocks are marked by higher Rb/Sr, LILE, K2O and sanukitoids with high Mg#, P2O5, Ni, LILE, Sr/Y and wide ranges in CaO and Na2O

3.4.6. Geochemistry through time

A main feature of this dataset is an abrupt increase in the geochemical variability of magmatic rocks at 2.75 Ga (Figure 3-17). Before 2.75 Ga, TTGs form a broad band with approximately consistent compositional ranges and averages between 3.0 to 2.8 Ga. After 2.75 Ga, magmatism shows increased variability in most major elements. Although contrast is most evident in the GG and sanukitoid rocks, modest changes also specifically affect TTG. Contents of CaO, FeO, MgO, MnO and Na_2O/K_2O range to higher values in TTG whereas Na_2O contents vary to large ranges but are skewed toward higher values. Some LILE, such as Cs, and ratios of La/Lu and Sr/Y also increase in a few TTG post-2.75 Ga.

Samples from the GG suite show opposite trends in most major elements to the TTG suite, thus together producing expansion in variability. For example, CaO, FeO, MgO, MnO and Na_2O/K_2O decrease in GG. However, GG have a large range in Na_2O similar to post-2.75 Ga TTG. Rocks of the GG suite are enriched in K_2O and other LILE including Rb, Cs and Ba compared to TTG, and show marked decreases in CaO/Na_2O+K_2O. Trends to higher Rb/Sr and Nb/Nb*, with lower Eu/Eu* are restricted to the GG suite. A very striking shift in chemistry accompanies sanukitoid emplacement <2.70 Ga, contemporaneous with GG. High Mg#, MgO, FeO, P_2O_5, Ni, Co, Cr, Sc, LILE, LREE and MREE, and low SiO_2 and Na_2O/K_2O marks this transition.

3.4.7. Geochemistry across space

Contour maps in Figure 3-18 illustrate the spatial variations in whole rock geochemistry of the igneous rocks for several representative elements and ratios. The characteristic features of the various rocks types are visible in these maps. For example, the large post-tectonic granite-granodiorites such as the White Otter batholith stand out as LILE-enriched patches (e.g. K_2O, Th) with low MgO, CaO, Na_2O, Mg#, and sanukitoid intrusions plot as positive anomalies for LILE, CaO, MgO, Mg# and transition metals. While these variations reflect the rock type, not all variations are intuitive from the geology maps. Lower LILE (Pb, Th, K, Rb) characterises the southern half of Marmion terrane and the western margin, with steep gradients to higher LILE along northern margin and external to the Marmion terrane.

The Marmion terrane contains a central corridor of low Na_2O along the Marmion Shear Zone, which includes the Dashwa gneisses west of the Finlayson Lake greenstone belt. The western margin of this corridor aligns with a cryptic structure stretching between the western margin of the Hillyer domain of Stone and Davis (2006) and west of the White Otter batholith (Figures 3-2, 3-18). High LILE (except Sr), low MgO, CaO, Mg #, Na2O, transition metals and Dy/Yb highlight this structure. West of this structure, especially within the Western Wabigoon terrane, HREE patterns

are distinctly steeper (higher Dy/Yb ratios). This structure also corresponds to younger emplacement ages, and samples that contain inherited zircons.

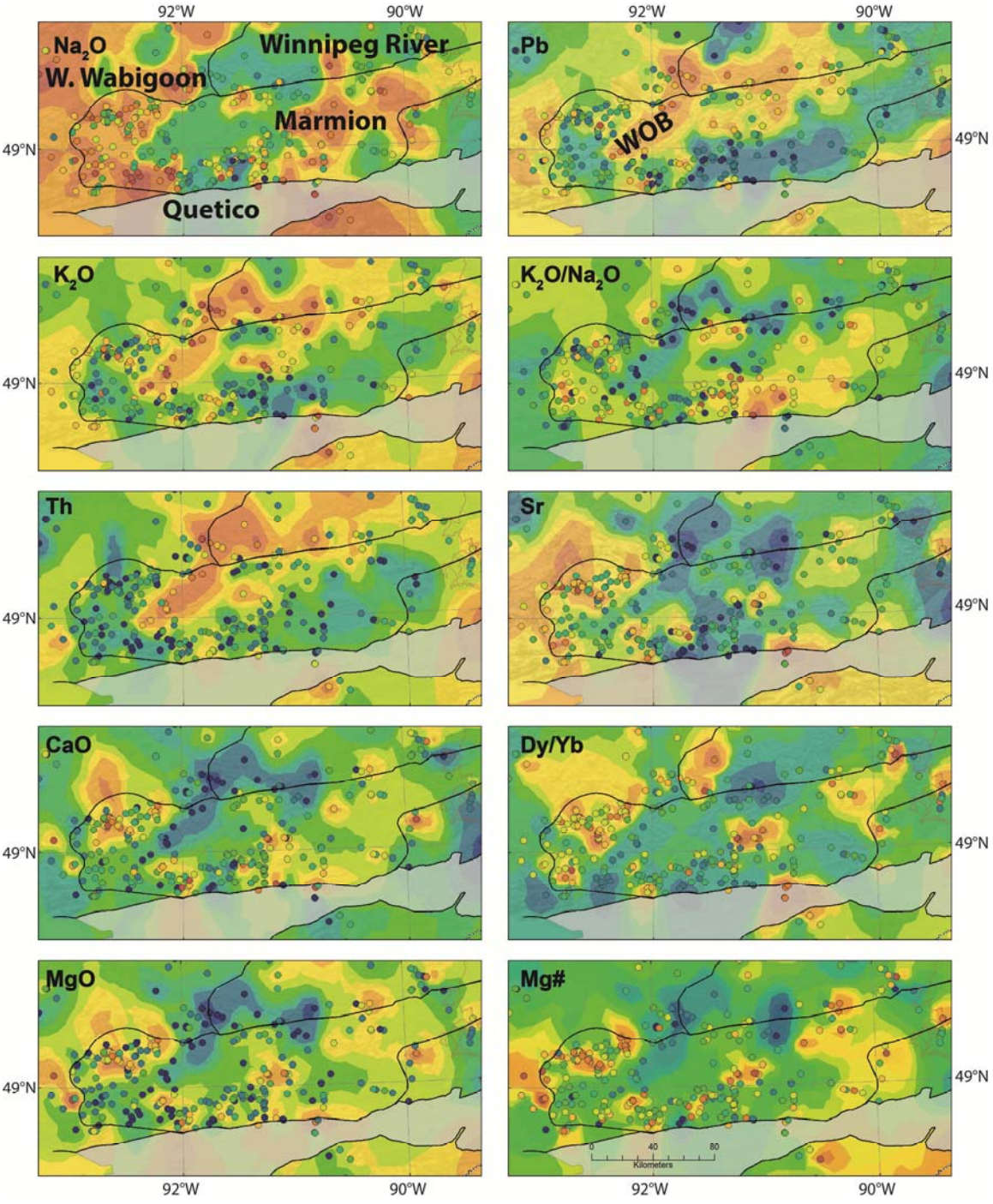

Figure 3-18: Contoured geochemistry maps. Colours indicate increasing abundances from blue to red and for the purpose of broad comparison. The natural neighbour interpolation method using natural breaks (Jenks) was used within the spatial analyst extension in ArcGIS to create the images. Terranes are indicated on the top left map, and the location of the White Otter Batholith (WOB) is indicated on the top right map.

High CaO, Na_2O, MgO, with low Sr, K_2O and Dy/Yb characterise the western Marmion intrusive complex relative to other TTG such as the Dashwa and Irene-Eltrut Lakes gneisses.

3.5. DISCUSSION

3.5.1. Extent of Marmion basement and terrane correlations

Constraining the spatial extent and nature of the Marmion terrane is important for understanding the crustal growth of the Western Superior Craton, and illuminating Meso- to Neoarchaean crustal growth. The distribution of crystallisation ages and inherited zircons measured by this study agree with previous conclusions for a 3.0 Ga basement to the Marmion Terrane (Davis and Jackson, 1988; Tomlinson et al., 2003), as inheritance within the Marmion terrane reaches, but never exceeds the distinct peak at 3.02 Ga. However, the geochronology results shed new light on the placement and nature of terrane margins, and by extension, their tectonic environment.

3.5.1.1. Placement and nature of the Marmion – Western Wabigoon boundary redefined

The Marmion – Western Wabigoon terrane boundary is thought to mark the location of a <2.71 Ga collision (Sanborn-Barrie and Skulski, 2006). The boundary placement was based on isotopic investigations of Tomlinson et al. (2004) and modified according to geophysical image interpretation by Stott (2011). Inheritance <3.0 Ga within the granodiorite intruding the Irene-Eltrut Lakes gneisses shows that Marmion aged basement extends ~30 km west of the designation. The Marmion – Western Wabigoon terrane boundary likely sits where the greenstone belts meet the Dashwa and Irene-Eltrut Lakes gneisses, which coincides with a change in magnetic signature (Figure 3-2).

The Western Wabigoon terrane has been interpreted as allochthonous with respect to the Marmion and Winnipeg River terranes (Percival et al., 2006; Sanborn-Barrie and Skulski, 2006; Tomlinson et al., 2004). However, inheritance measured in the 2.82 Ga Atikwa batholith (see Table 3-2, mount WS-53B, also Figure 3-2) supports either autochthonous growth of the Western Wabigoon terrane, or an earlier accretion with respect to the composite Winnipeg River-Marmion terrane. The measured inheritance in the Atikwa batholith is similar in age to intrusions in the Marmion and Winnipeg River terranes. It is therefore likely that the Atikwa magmatism sampled material or detritus typical of Winnipeg River – Marmion basement by 2.72 Ga. The Atikwa magmatism predates the postulated collision of the Western Wabigoon with the Winnipeg River-Marmion composite terrane at 2.703 – 2.696 Ga (Sanborn-Barrie and Skulski, 2006) but does coincided with deformation events from 2.73 – 2.71 Ga within the central Western Wabigoon terrane (Edwards and Stauffer, 1999) and the Winnipeg River terrane (Brown, 2002). As the Atikwa magmatism preceded

intrusion of 2.71 Ga plutons in the north and south with Mesoarchaean Nd isotopic signatures (Tomlinson et al., 2004), the Atikwa batholith inheritance is new isotopic evidence for earlier accretion or autochthonous development.

At the newly proposed Marmion – Western Wabigoon boundary location, greenstone belts of the Western Wabigoon appear contiguous with the amphibolite slivers within the Marmion gneisses (see Figure 2). Greenstone belt continuity across terrane boundaries favours autochthonous growth of the Western Wabigoon terrane. However, at the Western Wabigoon – Winnipeg River margin, the Jutten assemblage (Figure 2, and Figure 3, base of SSL greenstone belt) is interpreted as a continental margin sequence next to a possible discontinuous fore arc-accretionary wedge (Sanborn-Barrie and Skulski, 2006) within the Western Wabigoon terrane (Warclub sediments, Figure 3-2; youngest clastic sediments in Western Wabigoon greenstone belts, Figure 3-3). The postulated fore arc is 0 to <20 km across strike, and there is continuity in the ages across the proposed suture. Alternatively, greenstone belt stratigraphy records the development of the Western Wabigoon terrane on the margin of the Winnipeg River – Marmion terrane, with tectonic imbrication occurring during the Kenoran Orogeny. In this model, the Jutten assemblage recorded uplift of the Winnipeg River terrane, and deformed Warclub sediments record thrust imbrication in response to ongoing orogeny in the north and south (see Figure 3-19).

In detail, similar depositional settings, recorded in greenstone stratigraphic assemblages in the Marmion and Western Wabigoon terranes, favours a shared evolution. The Jutten assemblage along the Western Wabigoon – Winnipeg River margin contains >2.88 Ga detrital zircons (Sanborn-Barrie and Skulski, 2006 and references therein). It may have appeared contemporaneously with the basal conglomerates of the Steep Rock greenstone belt in the southern Marmion terrane (Figure 3-3), which contains >2.78 Ga zircons in the Wagita Formation (Davis, 2008; reported in Stone, 2010). Conglomerate and sandstone of the Wagita Formation give way to shallow water stromatolitic carbonates, then iron formation and pyroclastic komatiite before ~2.735 Ga pillowed basalt and andesite, initially recording uplift followed by subsidence in the Steep Rock greenstone belt (Fralick et al., 2008; Fralick and King, 1996; Schaefer and Morton, 1991; Stone, 2007; Wilks and Nisbet, 1988). The timing and nature of the preserved Neoarchaean stratigraphic record in the Marmion terrane is similar to that of the Jutten-Surgeon-Savant Lakes succession along the Western Wabigoon – Winnipeg River terrane margin (Figure 3-3). The collective stratigraphy may therefore record contemporaneous emergence in both localities followed by a transition to a deeper water depositional environment (see schematic representation in Figure 3-19). Collectively, inheritance in the Atikwa batholith as measured in this investigation, greenstone belt continuity across the

Marmion-Western Wabigoon terranes, and comparable Neoarchaean stratigraphy are consistent with autochthonous growth of the Western Wabigoon terrane.

3.5.1.2. Eastern Wabigoon relationship to the Marmion terrane

The <2.9 Ga magmatic pulses and 2.93 Ga inheritance characterising the Eastern Wabigoon terrane coincide with thermal pulses recorded in the Marmion terrane. Although a 3.0 Ga signature is lacking, these data raise the possibility that Marmion basement extends eastward as postulated by Tomlinson et al. (2004), or that, rather than an inferred exotic oceanic origin (Percival et al., 2006), the Eastern Wabigoon developed on the margin of the Marmion ± Winnipeg River terrane, as interpreted by Percival et al. (2012).

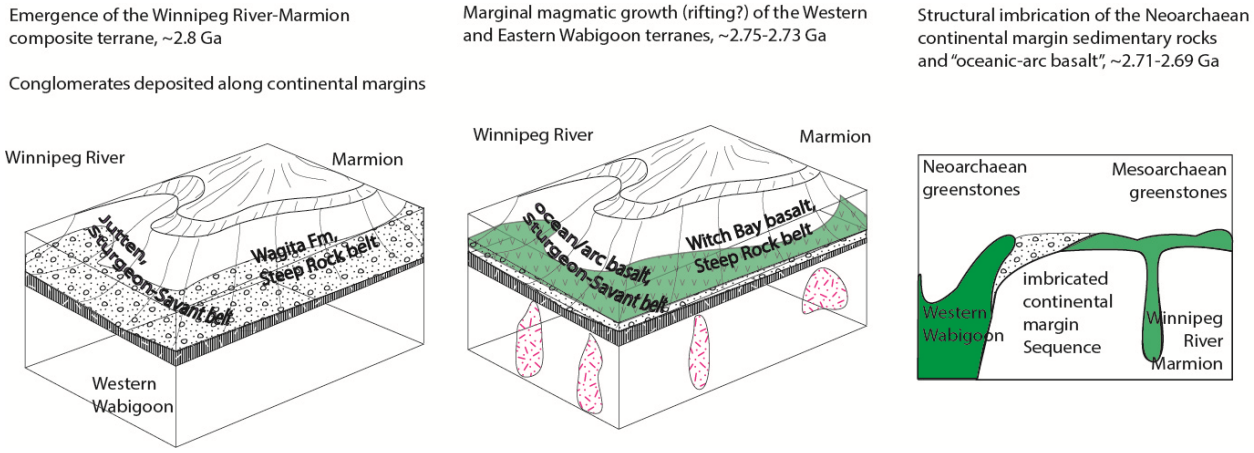

Figure 3-19: Schematic illustration of the Neoarchaean evolution of the Western Wabigoon, Winnipeg River and Marmion terranes. Emergence or rifting of the composite Winnipeg River – Marmion terranes at ~2.8 Ga is recorded in the Jutten assemblage and Wagita Formation. The Western Wabigoon grew by magmatic addition in a marginal or internal rift setting <2.8 Ga, and was structurally imbricated <2.8 Ga.

3.5.1.3. Timing and nature of the Marmion – Winnipeg River consolidation

The results of this study support the Marmion – Winnipeg River boundary location of Tomlinson et al. (2004) because samples north of the presently defined Marmion terrane boundary contain ≥3.05 Ga inheritance. Although the Marmion and Winnipeg River basements are isotopically distinct (Davis et al., 2005; Henry et al., 1998; Tomlinson et al., 2004), it is unclear whether the Marmion terrane was a marginal magmatic addition or was accreted to the Winnipeg River terrane. Tomlinson et al. (2004) postulated that shared 2.92-2.89 Ga plutonism of the Winnipeg River and Marmion terrane indicated their amalgamation by 2.92 Ga. Beakhouse (1991) argued that the north-western portion of the Winnipeg River terrane lacks 2.75 to 2.71 Ga magmatic activity that characterises the rest of the Wabigoon superterrane and may have remained separate until then. However, extensive Neoarchaean magmatism which characterises the Winnipeg River and Western

Wabigoon terranes is also restricted to the southern margin of the Marmion terrane (Figure 3-3), resulting in conflicting models based on contemporaneous magmatism alone. If the ~2.8 Ga Jutten assemblage of the Winnipeg River terrane and the Wagita formation of the eastern Steep Rock belt in the Marmion terrane are contemporaneous, their similar stratigraphic record supports a >2.8 Ga shared history. A lack of Neoarchaean supracrustal belts between the Marmion and Winnipeg River terranes also supports pre-2.8 Ga amalgamation. Volcanism at ~2.73 Ga in (i) the Obonga Lake greenstone belt, which was deposited unconformably on Winnipeg River crust (Tomlinson et al., 2002), (ii) the Witch Bay volcanism in the southern Marmion terrane, and (iii) the greenstone belts of the Western Wabigoon terrane, also favours a shared Neoarchaean history.

3.5.1.4. Comparison to the North Caribou superterrane

Like the Marmion terrane, the North Caribou terrane experienced protracted magmatism from 3.0 – 2.7 Ga (Figure 3-14). Moreover, greenstone belts from the North Caribou terrane record a similar sequence of events and timing (Figure 3-3). Comparisons between the isotopic signatures of magmatic events at 3.0 Ga suggest an early shared history (Davis et al., 2005). Stratigraphic correlations between the Wallace Lake greenstone belt of the North Caribou terrane and those of the central Marmion were made by Fralick et al. (2008). Recent structural work in the Marmion Terrane by Backeberg et al. (2014) suggests that two deformation events predate the intrusion of the 2.89 Ga Diversion Stock. The 3.0 Ga North Caribou greenstone belt within the North Caribou terrane is also interpreted to record an early deformation event prior to the intrusion of the 2.9 Ga North Caribou pluton (Thurston et al., 1991). Evidence for early deformation events in both terranes provides additional evidence for the speculative correlation, but explaining the presence of the ancient intervening Winnipeg River terrane remains a difficulty. A model that can reconcile the current geometric arrangement of terranes is presented in Chapter 4.

If the history of the Marmion and North Caribou terranes are linked, and the Marmion and Eastern and Western Wabigoon terranes developed marginally with respect to the Winnipeg River terrane, the current paradigm for the Kenoran Orogeny - accretion of exotic Mesoarchaean fragments – needs to be reassessed. The nature of these terrane boundaries and implications for the development of the Superior Craton are further explored using Lu-Hf isotopes in Chapter 4.

3.5.2. Granite-greenstone correlations

The compositional bimodality of granite-greenstone terranes is a global feature of Archaean cratons. Bimodal chemistry characterises Phanerozoic intraplate settings, for example, flood basalt-rhyolite provinces such as the Parana and Karoo igneous provinces (Duncan et al., 1984; Peate, 1997), but is typically absent in modern subduction zone settings. Much debate centres on how to

reconcile the seemingly incongruent geochemistry of TTG, some of which is analogous to adakites of modern subduction zones, to that of komatiite-basalt successions retaining the chemical fingerprint similar to that of oceanic plateaus (e.g. Barnes and Van Kranendonk, 2014; Bédard et al., 2013; Wyman and Kerrich, 2010). Explanations either (i) call for temporally or spatially disparate origins for TTG's and komatiitic basalt (Tomlinson et al., 2002), (ii) invoke combinations of geodynamic settings such as interaction between a plume or mid-ocean ridge and subduction (Hollings et al., 1999), (iii) favour either an ocean plateau (Bedard et al., 2003; Johnson et al., 2017), (iv) mantle upwelling (Herzberg, 2014; Herzberg and Rudnick, 2012) or (iv) subduction model (Martin et al., 2014).

The geochronology of the greenstone belts and TTG of the Marmion terrane place some constraints, at least locally, on this debate. Marmion terrane greenstone belt events are nearly synchronous with intrusive events in adjacent gneiss and intrusive complexes. For example, measured ca. 2.94 – 2.93 Ga ages in the Finlayson Lake greenstone belt appear contemporaneously with intrusive events in the surrounding Dashwa Gneisses. Likewise, ca 3.0 to 2.7 Ga age peaks in greenstones surrounding the Marmion intrusive complex coincide with age peaks in the Marmion intrusive complex.

Voluminous, extensive and multi-generational mafic dikes cutting the Marmion intrusive complex corroborate an intimate coupling of granite-greenstone events. Many of these dikes are truncated at the base of the <2.8 Ga East Steep Rock belt, and some have been dated at 3.00 Ga (Davis, 2008; Hamilton et al., 2007; reported in Stone, 2010), indicating overlapping ages with greenstone volcanism. Furthermore, Tomlinson et al. (1999) and Fralick et al. (2008) noted that mafic dikes and komatiitic volcanism have similar geochemistry and were likely co-genetic, with dikes feeding an overlying volcanic pile. The contemporaneity of felsic and mafic-ultramafic magmatism, together with spatial relationships, suggests a petrogenetic linkage. This may be explained by a tectonic model involving crustal and mantle melts that had limited interaction in order to preserve a bimodal association so prominent in Archaean cratons globally.

3.5.2.1. Finlayson Lake greenstone belt interpretation

Time-constrained stratigraphy can help illuminate the structure of the volcanic units, which bears upon relationships to the underlying basement and permissible geodynamic reconstructions. Geochronological results from the western Finlayson Lake felsic volcanic sample, with previous geochronology, indicate that the volcanic rocks young eastward. This is consistent with pillow facing directions, excluding local structural reversals (Fenwick, 1976; Stone et al., 1992; this study). Way-up features in sedimentary and volcanic rocks, together with geochronology, indicate

that the eastern Finlayson Lake greenstone belt becomes younger to the west (Fenwick, 1976; Fralick et al., 2008; Stone et al., 1992; this study). Thus, the synclinal interpretation of Fenwick (1976), Stone et al. (1992) and Fralick et al. (2008) is supported by the geochronology, whereas the antiformal interpretation of Backeberg et al. (2014) is not. However, if a syncline, the belt is distinctly asymmetric and at least partly dismembered.

Stone (2010a) noted a similarity between the central Finlayson volcanic rocks and the ~2.73 Ga Witch Bay volcanic rocks of the eastern Steep Rock greenstone belt and suggested a structural emplacement as a klippe from the south. Another possibility is that the central Finlayson greenstone belt correlates with the Witch Bay assemblage, and was deposited unconformably on Mesoarchaean basalt.

The Lumby Lake greenstone belt to the northeast is also asymmetric. However, it has many more datable felsic volcanic horizons throughout, which indicate similarly aged rocks in both the north and south portions with inward younging. Thus, the evidence for synclinal structure within the Lumby Lake belt is compelling. A broad synclinorium presents a challenge to interpretations of allochthonous origin for structurally divided portions of greenstone belts of the Marmion terrane (Buse et al., 2009; Stone, 2010a; Tomlinson et al., 1999). The synclinal geometry and the coupling of greenstone – granite events support an autochthonous origin for greenstones of the Marmion terrane. Autochthonous greenstone growth emphasises the need for Mesoarchaean tectonic models capable of generating and preserving bimodal crust.

3.5.3. Secular shifts in TTG geochemistry

As the volumetrically and temporally dominant rocks of the study area, the TTG suite has the greatest potential to reveal geochemical changes through time and, by inference, changes in their source and/or genesis. Although somewhat coherent in major element distribution, TTGs of this investigation display a wide range in HREE, Sr/Y and Eu/Eu* through time (Figures 3-6, 3-7 and 3-17). The geochemical examination of six petrographic granitic suites of Stone (2010a) within the southwestern Wabigoon superterrane similarly show great variation in incompatible elements from 3.0 – 2.7 Ga. In comparison, Neoarchaean felsic intrusive rocks in the Berens River area exhibit coherent secular geochemical trends (Corfu and Stone, 1998).

Many of the TTG of the Marmion terrane have moderate Sr/Y, flat to shallow HREE and low compatible and transition elements (Figures 3-6, 3-7), indicative of low P melting. Notwithstanding the general scatter in the data presented herein, increases in Na_2O, Al_2O_3, La/Lu and some LILE in felsic to intermediate intrusive rocks of the Marmion terrane (see Figure 3-17) are synchronous with

greater chemical variation in magmatism <2.75 Ga. These chemical changes are consistent with a transition from to melting/magmatic fractionation in the presence of plagioclase, which fractionates Na and Al, to melting/magmatic fractionation in the presence of garnet, which fractionates REE (e.g. Halla et al., 2009; Moyen, 2011). The change to greater variations in melting depths follows the subaerial emergence of the Marmion terrane <2.8 Ga as recorded in the basal conglomerates of the Steep Rock group. Thus, the depositional environment, as recorded in greenstone belt stratigraphy, supports a thicker lithosphere and greater melting depths inferred from geochemistry.

A secular change from low P to high P melting depths as recorded by TTG geochemistry is a global phenomenon in Archaean Cratons (Martin and Moyen, 2002), but the timing of the transition, and explanations for the cause, vary. In fact, there is little agreement of the genesis of high and low P TTG. For example, a predominance of low pressure TTG in the Pilbara was argued to be derived from infracrustal melting/fractionation rather than slab melting, which they argued would tend to be at higher pressures (Smithies et al., 2009). Gardiner et al. (2017) argued both low and high P TTG's were generated in a plateau-like setting based on isotopic evidence for crustal reworking. In contrast, Halla et al. (2009) attribute high pressure TTG petrogenesis to melting beneath a thickened plateau and low pressure TTGs from shallow slab melting. Therefore, depth of melting alone does not define petrogenesis.

In a study by Martin and Moyen (2002) a global secular change from low to high pressure TTG is accompanied by increases in Mg#, Ni and Cr, where pre-3.5 Ga TTG's show no interaction with peridotite. They interpret these coupled changes to reflect the effects of cooling geotherms of the Earth through time on subduction magmatism where a change occurs from shallow slab melting in the presence of plagioclase in hot subduction zones with little interaction with the mantle wedge, to deeper slab melting in cooler subduction zones and increased interaction with the mantle wedge. The present dataset does not record increases in Mg#, Ni and Cr until post-tectonic sanukitoid magmatism. Thus, the 2.75 Ga change recorded by Marmion TTGs indicates a change to larger variation in melting depths, i.e., from low P TTG to both low P and high P TTG, but the relatively constant Mg# across this transition at ca. 2.75 Ga argues against a changing mantle contribution. Therefore, a thickened lithosphere is a better fit to the geochemical evidence, rather than a change from flat to steeper subduction.

3.5.4. Post-tectonic high-K sanukitoid and granite-granodiorite

Many authors have observed a major shift in igneous geochemistry coincident with intrusion of post-tectonic sanukitoids (Beakhouse, 2007; Halla et al., 2009; Laurent et al., 2014; Martin et al., 2010; Whalen et al., 2004b) and their contemporaneous to slightly younger high-K crustal melts.

The present dataset records this shift within sanukitoid chemistry <2.69 Ga. The extension to lower SiO_2, and much higher MgO, FeO, Mg#, and elevated compatible transition metals has been used to infer contribution from the mantle (Shirey and Hanson, 1986; Stern et al., 1989). Steeper REE, and especially HREE, has been shown to reflect melting at high pressures in the presence of garnet (Rapp et al., 2010).

The GG suite corresponds to the biotite granite suite of Stone (2010a), the I-type crustal suite of Beakhouse (2007), and is included in the granodiorite-granite-monzonite suite of Whalen et al. (2004b). This suite is most often interpreted as being derived from infracrustal melting of (largely) tonalites with some supracrustal material (e.g. Beakhouse and McNutt, 1991), although Whalen et al. (2004b) argue for a significant mantle contribution and a continuum with the sanukitoid suite. GG and sanukitoids overlap in time and commonly space, and show similarities in texture and geochemistry, however, the GG are distinct from sanukitoid in many ways. GG have distinctly lower compatible elements (Ti, Ca, Fe, Mg, Mn, Ni, Cr etc.) than sanukitoids. Where the sanukitoid rocks follow a distinct fractionation trend for La/Lu (Figure 3-6) and La/Sm, the TTG and GG are scattered and if anything the GG shows an opposite trend. Also, whereas TTG and GG show decreasing trends on an Al_2O_3 versus SiO_2 diagram, sanukitoid has constant Al_2O_3, with the two suites showing distinct trends which cross each other. Other distinctions include high Rb/Sr and Th and U and the low CaO, MgO, Eu/Eu* and TiO_2 of GG compared to sanukitoid (Figure 3-17). Thus, although there may be a continuum between the suites, and their temporal link implies a relationship, they do appear to have distinct origins. Higher SiO_2 and TTG inclusions within GG rocks suggest that crustal melting was important in the genesis of GG. Low Ca compared to K+Na may be related to plagioclase retention in the source (Moyen, 2011), which is supported by negative Eu/Eu* anomalies of GG. Melting experiments of TTG at varying low to mid pressures (4 and 10 kbars) yield compositions analogous to GG rocks (e.g. Patiño Douce, 1997; Skjerlie and Johnston, 1993). This relationship is further evaluated using Hf isotopes in Chapter 5.

Sanukitoids and GG intrusions tend to occur along, or proximal to, terrane boundaries. This is illustrated by the geochemical contour maps, which provide a proxy for rock type. For example, LILE (such as K_2O, Pb, and Th) and Mg# are elevated in intrusive rocks around the Marmion terrane (Figure 3-18). In addition to mapping out some of the terrane boundaries, they also outline northeast structures, some of which cross terrane boundaries, notably, the continuation of the Winnipeg River – Western Wabigoon boundary southwest into the Marmion terrane along the White Otter batholith (Figure 3-18). Late northeast trending structures such as the Entwine Lake Fault are located across the Western Superior Craton, and stand out in magnetic signatures.

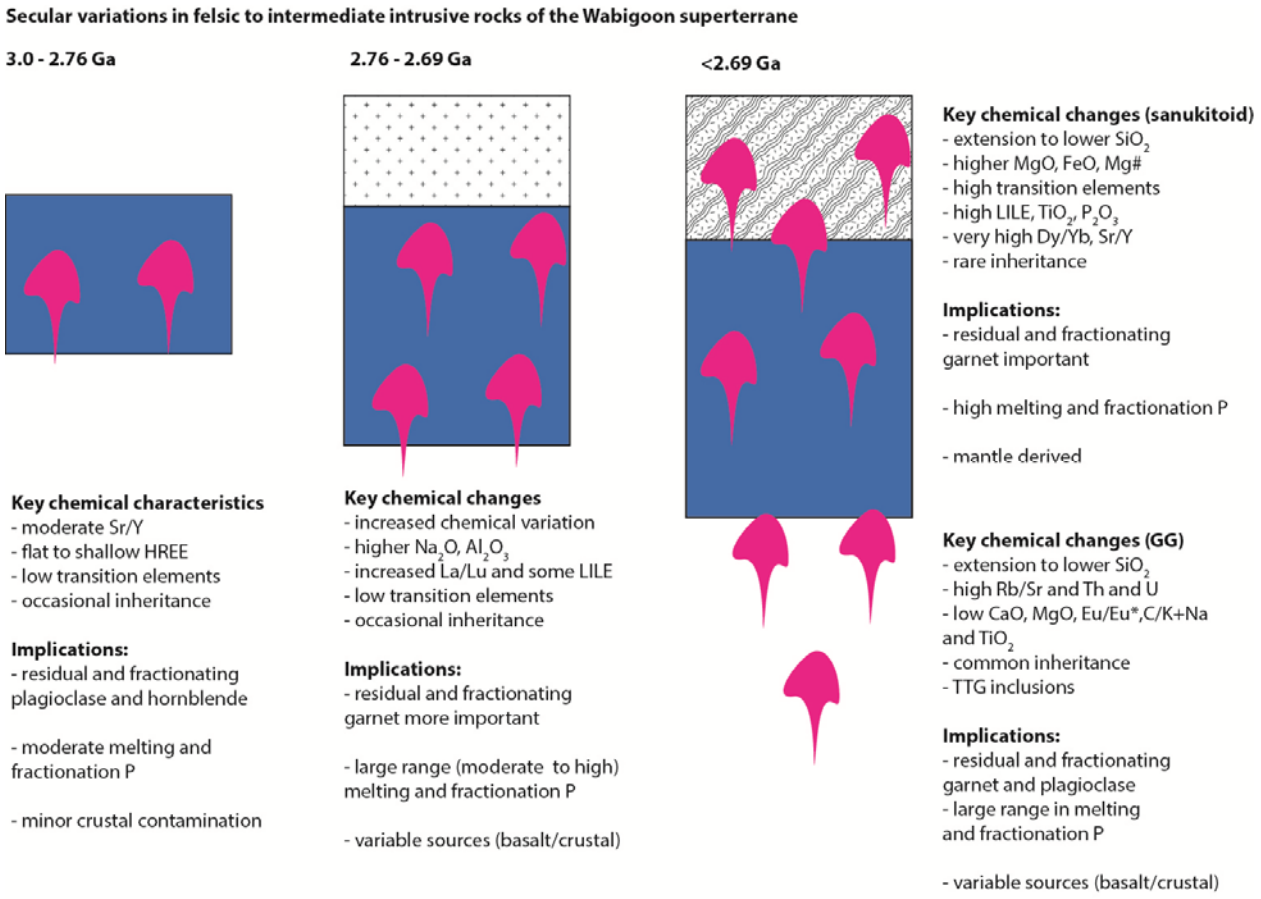

Figure 3-20: Schematic diagram illustrating secular chemical variations in felsic to intermediate intrusive rocks of the Wabigoon superterrane, and related implications for melting and/or fractionation depth and magma sources.

It is possible that some of these late northeast features are fundamental structures reflecting an earlier history (Bédard and Harris, 2014), a concept that is supported by microstructural work on the northeast-trending Marmion Shear Zone which was active before 2.9 Ga (Backeberg and Rowe, 2012) and reactivated during the Kenoran Orogeny. Thus, the northeast-trend in the geochemistry is likely mapping a fundamental Mesoarchaean structure reactivated in the Neoarchaean to control the emplacement of intrusive rocks. A spatial change in geochemistry across the structure parallel to the White Otter Batholith corroborates a fundamental lithospheric structure. There is higher Dy/Yb in the Irene-Eltrut Lakes gneisses than the Dashwa gneisses and the Marmion intrusive complex (Figure 3-18). Higher Dy/Lu relates to more fractionated HREE, which in turn, points to fractionation or melting in the presence of garnet. Garnet is a high P mineral. A greater depth of melting may indicate a thicker lithosphere.

3.6. CONCLUSIONS

The geochronological findings of this study help to extend the geological understanding of the central Wabigoon superterrane and provide additional insight into Mesoarchaean – Neoarchaean evolution of the Superior Craton, and the architecture of the western part of the craton.

Inherited zircons within the Irene-Eltrut Lakes area establishes placement of the Marmion-Western Wabigoon boundary westward 30 km from its current designation. Inheritance within the 2.72 Ga Atikwa batholith suggests sampling of Winnipeg River – Marmion aged basement by 2.72 Ga, and favours an autochthonous development of the Western Wabigoon terrane, or an earlier accretion. The Jutten assemblage of the Western Wabigoon, built on the margin of the Winnipeg River terrane, possibly correlates to the Steep Rock basal conglomerates of the Marmion terrane. If so, contemporaneous uplift and emergence occurred in both localities, strengthening the case for a composite terrane by 2.8 Ga. Similar magmatism across the Marmion - Eastern Wabigoon terranes suggests that the Eastern Wabigoon terrane may not be exotic with respect to the Marmion terrane. These results indicate that the distinct isotopic signatures of the Wabigoon superterrane are not necessarily indicative of allochthonous origins. This suggests that models that envision in-situ growth for the Superior Craton are permissible by this data, and models that are in part upheld by isotopically distinct basement signatures, such as accretion of exotic fragments, may need revision.

Zircon inheritance records several periods of crustal reworking within the Wabigoon superterrane. The Winnipeg River terrane, with the oldest preserved crust records the most inheritance in its magmatism. Maps of geochronological data and igneous geochemistry image structures that developed early (terrane margins, Marmion shear zone, Hillyer – White Otter structure) and were exploited by later magmatism. These structures tend to also host plutons with older zircon inheritance. Hence, late melts appear to have exploited an early architecture, and accordingly, these late magmas map out fundamental lithospheric structures.

The protracted history of the Marmion terrane demonstrates that the greenstone and TTG emplacement are intimately spatially and temporally linked. Accordingly, a tectonic process able to produce synchronous bimodal geochemistry is required. The geochronology, combined with stratigraphic correlations, supports disrupted and asymmetrical synclinal greenstone belt geometry rather than exotic tectonostratigraphic assemblages. Consequently, geodynamic models that can generate and preserve contemporaneous bimodal magmatism best account for the Mesoarchaean crustal growth.

The geochemistry of felsic intrusions changed at ~2.75 and ~2.69 Ga. The shift at 2.75 Ga records evidence for deeper melting in addition to melting in the plagioclase stability field. This may reflect a change in character of the crust/lithosphere such as structural thickening caused by compression and/or a change in tectonic regime within the Wabigoon superterrane such as the onset of subduction. Chemistry of TTG in the Marmion terrane indicates that melting and/or crystal fractionation was occurring at both high (garnet stable) and low (plagioclase stable) pressures. The shift associated with the onset of sanukitoid intrusion at 2.69 Ga has been noted across most Archaean cratons and records a distinct mantle contribution as well as the greatest enrichments in incompatible elements, most often attributed to melting of a TTG-metasomatised mantle triggered by slab break-off (Laurent et al., 2014; Shirey and Hanson, 1986; Smithies and Champion, 2000). The genesis of TTG and sanukitoid magmatism is examined in greater detail using insights from Lu-Hf and O isotopes in Chapters 5 and 6.

Supplementary Table 3-4: U-Pb age compilation used for probability density plots and stratigraphic columns.

Sample ID[1]	Sample ID[2]	UTM Zone 15N		Rock code[3]	$^{207}Pb/^{206}Pb$ age[4] (Ga)	Int.[5]	Inh.[6]	Min.[7]	Ref.[8]	Ref.[9]	Terr-ane[10]
		Easting	Northing								
12-8-24-1	WS-17A	940281	5537547	ttg	2.923 ± 0.005	C			56		EW
12-8-24-2	WS-17B	939743	5539675	ttg	2.915 ± 0.005	C			56		EW
KAT20130711-01	WS-43A	723061	5433394	gran	2.906 ± 0.005	C			76		EW
12-8-15-7	WS-23C	760925	5460846	gran	2.818 ± 0.006	C			56		EW
	40	882981	5547920	fvt	2.781 ± 0.002	C			38		EW
05DS73		723380	5445360	ton	2.777 ± 0.003	C			18	64	EW
	43	884884	5545790	grdr	2.777 ± 0.003	C			39		EW
DD85-3				tgn	2.775 ± 0.008	C			16	64	EW
05DS85		736906	5440760	tgn	2.774 ± 0.001	C			18	64	EW
	34	882738	5554860	iv	2.769 ± 0.006	C			1		EW
96GRS4060G	WS-4B	886348	5557286	gran	2.768 ± 0.007	C			56		EW
	33	886416	5557300	f	2.768 ± 0.001	C			38		EW
	48	871946	5524460	iv	2.741 ± 0.001	C			53		EW
12-8-15-5	WS-23B	762171	5465367	gran	2.739 ± 0.01	C	2.841		56		EW
	53	887114	5582471	fvct	2.739 ± 0.001	C			40		EW
12-8-24-11	WS-20B	879877	5523592	ttg	2.738 ± 0.005	C			56		EW
12-8-23-3	WS-21B	888817	5530520	fv	2.738 ± 0.008	C			56		EW
	52	890698	5583690	fv	2.738 ± 0.001	C			40		EW
	47	873120	5530770	qp	2.738 ± 0.001	C			53		EW
	49	879311	5527090	grdr	2.736 ± 0.002	C			53		EW
	29	901269	5582550	iv	2.735 ± 0.001	C			38		EW
	44	871631	5542230	gab	2.734 ± 0.001	C			53		EW
	50	893425	5531850	ton	2.734 ± 0.001	C			53		EW
99GRS5009A	WS-5B	893055	5531962	ttg	2.734 ± 0.004	C			56		EW
12-8-23-1A	WS-21A	896427	5533172	ttg	2.733 ± 0.006	C			56		EW
	45	872076	5539450	gab	2.732 ± 0.001	C			51		EW
TH001-149	WS-10B	760831	5454426	fv	2.732 ± 0.009	C	2.827		56		EW
99GRS5010A	WS-3A	879234	5527474	ttg	2.731 ± 0.007	C			56		EW
DD85-3	WS-8C	739981	5446184	ttg	2.731 ± 0.007	C	2.768		56		EW
12-8-15-1	WS-22C	763304	5469505	fv	2.731 ± 0.006	C	2.821		56		EW
97KYT-75		763285	5469530	fvt	2.729 ± 0.002	C	2.813		70		EW
DD86-25A		745093	5452405	ton	2.728 ± 0.002	C			16	64	EW
TH01-149		760980	5454350	ivt	2.728 ± 0.001	C			70		EW
DD95-4		762323	5467740	qfp	2.728 ± 0.002	C	2.758		70		EW
	28	893559	5577690	iv	2.728 ± 0.001	C			53		EW
DD86-25A	WS-8B	741304	5446661	ttg	2.725 ± 0.005	C			56		EW
12-8-15-4	WS-23A	762305	5467576	fv	2.723 ± 0.006	C	2.789		56		EW
	31	881095	5568810	iv	2.722 ± 0.001	C			38		EW
12-8-24-10	WS-20A	944158	5583535	ttg	2.722 ± 0.006	C			56		EW
KAT20130911-01	WS-55B	748105	5428569	gran	2.721 ± 0.003	C			76		EW
12-8-24-9	WS-19C	937148	5584440	ttg	2.72 ± 0.007	C			56		EW
	38	860217	5551700	iv	2.713 ± 0.002	C			38		EW
12-8-24-7	WS-19A	945244	5566599	ttg	2.709 ± 0.01	C	2.815		56		EW
	36	874889	5549150	qp	2.706 ± 0.004	C			37		EW
96GRS4127G	WS-2A	860056	5551603	fv	2.704 ± 0.004	C	2.927		56		EW
12-8-24-8	WS-19B	935846	5584684	gran	2.703 ± 0.008	C			56		EW
KAT20130711-03	WS-43B	725864	5449722	ttg	2.7 ± 0.007	C			76		EW

Supplementary Table 3-4: U-Pb age compilation used for probability density plots and stratigraphic columns.

Sample ID[1]	Sample ID[2]	UTM Zone 15N		Rock code[3]	$^{207}Pb/^{206}Pb$ age[4] (Ga)	Int.[5]	Inh.[6]	Min.[7]	Ref.[8]	Ref.[9]	Terr-ane[10]
		Easting	Northing								
C-84-41	54	935000	5530000	gran	2.699 ± 0.001	C			12		EW
	27	887030	5577740	mnzo	2.698 ± 0.001	C			37		EW
96GRS0338C	WS-4C	887582	5578132	gran	2.694 ± 0.011	C			56		EW
98GRS1280D	WS-5A	889490	5592178	san	2.694 ± 0.003	C			56		EW
	24	889554	5592080	mnzo	2.694 ± 0.001	C			38		EW
Murphy 1		747853	5452420	gab	2.693 ± 0.001	C			49		EW
03DS91		747519	5447943	dior	2.69 ± 0.001	C		ti	50	64	EW
C-84-40	54	960392	5532326	dior	2.69 ± 0.001	C			12		EW
C-84-42	54	959000	5532300	ton	2.69 ± 0.001	C			12		EW
DD85-2		746668	5451861	gab	2.689 ± 0.001	C			16	64	EW
12-8-23-5	WS-20C	957060	5530800	san	2.689 ± 0.004	C			56		EW
12-8-24-6	WS-18C	945387	5562372	ttg	2.686 ± 0.015	C			56		EW
12-8-16-1A	WS-32A	720855	5418359	san	2.685 ± 0.004	C			76		EW
96GRS004G	WS-3B	880263	5566632	ttg	2.681 ± 0.008	C			56		EW
12-8-24-3	WS-17C	940923	5542629	ttg	2.681 ± 0.007	C	2.734		56		EW
12-8-24-4	WS-18A	945006	5550807	gran	2.678 ± 0.007	C	2.911		56		EW
12-8-24-5	WS-18B	945798	5557007	gran	2.672 ± 0.003	C	2.689		56		EW
	35	880728	5550710	sst	2.782 ± 0.001	C			39		EW
	42	882414	5547670	id	2.774 ± 0.004	I	2.774		37		EW
DD95-4		762323	5467740	qfp	2.728 ± 0.002	C	2.779		70		EW
12-8-15-4	WS-23A	762305	5467576	fv	2.723 ± 0.006	C	2.764		56		EW
	37	874592	5549700	sst	2.709 ± 0.006	D			39		EW
	46	872734	5532930	ivt	2.709 ± 0.006	D			53		EW
	41	883052	5544810	sst	2.707 ± 0.003	D			37		EW
	32	889481	5570720	sst	2.707 ± 0.01	D			53		EW
		765886	5452545	cng	2.696	D			19	64	EW
12-8-24-3	WS-17C	940923	5542629	ttg	2.681 ± 0.007	C	2.699		56		EW
12-8-24-3	WS-17C	940923	5542629	ttg	2.681 ± 0.007	C	2.697		56		EW
12-8-24-4	WS-18A	945006	5550807	gran	2.678 ± 0.007	C	2.909		56		EW
12-8-24-4	WS-18A	945006	5550807	gran	2.678 ± 0.007	C	2.889		56		EW
12-8-24-4	WS-18A	945006	5550807	gran	2.678 ± 0.007	C	2.723		56		EW
12-8-28-7	WS-36A	625965	5415901	ttg	3.015 ± 0.007	C			76		M
DD97-5		645328	5441694	fv	3.014 ± 0.001	C			70		M
DD84-10		624430	5427561	ton	3.009 ± 0.008	C			70		M
07DS39		647759	5407779	fvct	3.008 ± 0.001	C			20		M
06DS80		639112	5406190	lgab	3.005 ± 0.001	C			48	64	M
06DS81		601160	5413760	fvct	3.003 ± 0.001	C			48	64	M
12-8-28-10	WS-37A	630473	5430217	ttg	3.003 ± 0.007	C			76		M
	24	624404	5427832	gns	3.003 ± 0.003	C			67		M
07DS46		598541	5409158	gab	3.002 ± 0.001	C			20		M
DD85-10		598425	5409110	ton	3.002 ± 0.003	C			70		M
09SB037		624048	5432575	fvct	3.001 ± 0.001	C			33	78	M
DD97-4		624030	5432510	fv	3.001 ± 0.001	C			70		M
05DS126		593700	5406040	qfp	2.999 ± 0.001	C			18	64	M
Sample 1		621029	5432763	fvt	2.999 ± 0.003	C			27		M
Sample 2		632109	5432335	qp	2.999 ± 0.002	C			27		M
12-8-20-6	WS-26C	623228	5461504	ttg	2.999 ± 0.007	C			56		M

Supplementary Table 3-4: U-Pb age compilation used for probability density plots and stratigraphic columns.

Sample ID[1]	Sample ID[2]	UTM Zone 15N		Rock code[3]	$^{207}Pb/^{206}Pb$ age[4] (Ga)	Int.[5]	Inh.[6]	Min.[7]	Ref.[8]	Ref.[9]	Terr-ane[10]
		Easting	Northing								
07DS47		623608	5429579	ton	2.999 ± 0.001	C			21		M
07DS04		583601	5409319	fv	2.999 ± 0.001	C			20		M
07DS36		606516	5457250	tgn	2.998 ± 0.001	C			20		M
00KYT-25		622735	5461789	tgn	2.989 ± 0.005	C			69		M
09SB125		625878	5433323	fvct	2.974 ± 0.007	C			33	78	M
KAT20140911-02	WS-56D	639098	5440211	fv	2.974 ± 0.007	C	3.019		76		M
96KYT-50		643036	5440069	fvt	2.963 ± 0.005	C	3.016		70		M
09SB311		638271	5440385	fvt	2.959 ± 0.009	C			33	78	M
08DS20		582280	5425092	tgn	2.957 ± 0.001	C			21		M
00KYT-24		620809	5454850	fvt	2.956 ± 0.001	C			70		M
96KYT-252		757844	5475642	fvt	2.954 ± 0.001	C			70		M
96KYT-249		756394	5476046	fd	2.953 ± 0.002	C			70		M
07DS35		661214	5445587	ton	2.952 ± 0.004	C	2.993		20		M
96KYT-252	WS-1B	757503	5475729	fv	2.951 ± 0.003	C			56		M
00KYT-24	WS-13C	620971	5454920	fv	2.948 ± 0.007	C			56		M
12-8-17-8	WS-39B	600093	5420833	ttg	2.939 ± 0.005	C			76		M
KAT20140814-01	WS-56B	602503	5420512	fv	2.938 ± 0.006	C			76		M
03DS93		733130	5474740	tgn	2.937 ± 0.001	C			17	64	M
09SB253		643231	5439393	fvt	2.936 ± 0.016	C			33	78	M
		602020	5424440	ton	2.936 ± 0.01	C			43		M
DD88-15		604450	5420873	fvt	2.931 ± 0.002	C			70		M
12-8-17-5	WS-38C	606661	5427130	ttg	2.931 ± 0.005	C			76		M
12-8-17-4	WS-38B	602055	5426615	ttg	2.93 ± 0.007	C			76		M
05DS56		659562	5465150	ton	2.929 ± 0.004	C			18	64	M
12-8-28-6	WS-35C	626771	5413291	ttg	2.929 ± 0.007	C			76		M
00KYT-14	WS-12C	577022	5405448	fv	2.929 ± 0.005	C			56		M
		597830	5424500	tgn	2.928 ± 0.01	C			43		M
12-8-17-6	WS-39A	602819	5425692	ttg	2.928 ± 0.005	C			76		M
00KYT14		577155	5405380	fvlt	2.926 ± 0.001	C			70		M
03DS92		742745	5486637	ton	2.924 ± 0.009	C		ti	50	64	M
00KYT16		519920	5409812	tgn	2.924 ± 0.002	C			69		M
06DS73		727850	5457880	ton	2.917 ± 0.012	C			48	64	M
09SB024		626910	5434739	fvct	2.899 ± 0.001	C			33	78	M
KAT20130728-07	WS-53A	607118	5418511	gran	2.898 ± 0.008	C	3.015		76		M
PT1		629412	5434560	fvt	2.898 ± 0.002	C	2.903		70		M
KAT20130830-02	WS-54A	611021	5423216	ttg	2.893 ± 0.004	C			76		M
12-8-28-8	WS-36B	626954	5423288	ttg	2.892 ± 0.008	C			76		M
08DS27		585400	5411544	tgn	2.886 ± 0.007	C	2.875		21		M
08DS27		585400	5411544	tgn	2.886 ± 0.007	C	2.965		21		M
00KYT15		577300	5405566	ton	2.883 ± 0.002	C			71		M
07DS43		541762	5417697	tgn	2.88 ± 0.01	C	3.000		21		M
00KYT-11	WS-12A	541331	5415111	ttg	2.876 ± 0.01	C			56		M
00KYT11		541452	5415004	ton	2.869 ± 0.004	C			69		M
06DS52		557750	5415800	ton	2.866 ± 0.008	C			64		M
00KYT-19	WS-11A	537649	5435526	ttg	2.855 ± 0.006	C			56		M
DD98-4		693300	5412160	fvlt	2.83 ± 0.001	C			70		M
00KYT02		637385	5437460	fvt	2.828 ± 0.002	C			70		M

Supplementary Table 3-4: U-Pb age compilation used for probability density plots and stratigraphic columns.

Sample ID[1]	Sample ID[2]	UTM Zone 15N		Rock code[3]	$^{207}Pb/^{206}Pb$ age[4] (Ga)	Int.[5]	Inh.[6]	Min.[7]	Ref.[8]	Ref.[9]	Terr-ane[10]
		Easting	Northing								
09DS221		687000	5413000	ivbx	2.828 ± 0.007	C			33	78	M
DD98-7	WS-16B	693250	5411950	ttg	2.827 ± 0.006	C	3.012		56		M
09SB342		646156	5439511	fvt	2.822 ± 0.001	C			33	78	M
12-8-17-10	WS-39C	607258	5408437	ttg	2.822 ± 0.006	C	3.011		76		M
05DS60		630017	5457740	ton	2.817 ± 0.004	C		ti	18	64	M
09DS222		681500	5409500	ivbx	2.817 ± 0.008	C			33	78	M
05DS57		650020	5462475	ton	2.814 ± 0.001	C			18	64	M
12-8-20-1	WS-25A	636160	5461930	ttg	2.814 ± 0.003	C	2.849		56		M
KAT20140815-02	WS-58A	638202	5446906	gran	2.813 ± 0.004	C			76		M
12-8-16-4A	WS-33A	699616	5426252	gran	2.802 ± 0.008	C			76		M
12-8-16-6	WS-34A	689921	5430767	gran	2.794 ± 0.008	C			76		M
09DS220		684500	5422000	ton	2.789 ± 0.001	C			33	78	M
KAT20130920-05	WS-54B	665163	5414196	ttg	2.789 ± 0.006	C			76		M
12-8-16-10	WS-34C	663801	5430975	gran	2.788 ± 0.005	C			76		M
12-8-28-5b	WS-35B	626867	5407542	gran	2.787 ± 0.01	C	2.825		76		M
09SB408		636422	5432072	ton	2.786 ± 0.001	C			33	78	M
12-8-16-5	WS-33C	697887	5426530	ttg	2.785 ± 0.005	C			76		M
09DS223		681000	5413000	gran	2.781 ± 0.001	C			33	78	M
DD98-6		685620	5418565	ton	2.781 ± 0.002	C			70		M
12-8-16-12	WS-35A	643096	5431180	gran	2.779 ± 0.004	C			76		M
12-8-16-4B	WS-33B	699616	5426252	gran	2.742 ± 0.021	C			76		M
05DS154		600330	5403550	lgab	2.735 ± 0.001	C			18	64	M
00KYT19		537761	5436468	tgn	2.732 ± 0.01	C			71		M
05DS133		594058	5402278	ton	2.73 ± 0.002	C	2.865		18	64	M
06DS74		715177	5442745	tgn	2.729 ± 0.012	C	2.796		48	64	M
05DS87		692750	5409820	ivbx	2.725 ± 0.001	C			18	64	M
06DS75		696700	5431600	ton	2.725 ± 0.006	C	2.811	ti	48	64	M
KAT20130713-01	WS-45B	538162	5403610	gran	2.723 ± 0.002	C			76		M
11		569210	5399360	fv	2.722 ± 0.001	C			41		M
06DS77		616997	5441522	ton	2.722 ± 0.008	C	2.932		48	64	M
DD86-23	WS-9C	729239	5461372	ttg	2.722 ± 0.008	C	2.774		56		M
00KYT23		605622	5454407	ton	2.721 ± 0.001	C			69		M
03DS94		687712	5432346	ton	2.717 ± 0.001	C		ti	17	64	M
09SB020		629138	5436475	mdst	2.716 ± 0.006	C			33	78	M
KAT20130822-07	WS-49C	531831	5449613	gran	2.716 ± 0.004	C	3.005		76		M
06DS22		518247	5448150	ton	2.716 ± 0.006	C			64		M
07DS78		616363	5437305	ton	2.713 ± 0.004	C	2.950		48	64	M
06DS76		680430	5445957	ton	2.712 ± 0.006	C			48	64	M
DD07-3		552086	5444622	ton	2.709 ± 0.009	C			20		M
12-8-16-8	WS-34B	669925	5436744	gran	2.703 ± 0.004	C	2.869		76		M
KAT20130920-04	WS-53C	704608	5465081	ttg	2.701 ± 0.009	C	2.902		76		M
07DS42b		567573	5422363	ton	2.697 ± 0.001	C			20		M
12-8-16-2	WS-32B	710474	5424162	gran	2.696 ± 0.021	C			76		M
09SB409		634318	5437549	gab	2.693 ± 0.002	C			33	78	M
KAT20130806-06	WS-58D	640655	5436978	san	2.693 ± 0.007	C			76		M
KAT20130822-04	WS-49B	532477	5443956	san	2.692 ± 0.004	C			76		M
KAT20130712-07	WS-44C	556496	5415193	ttg	2.691 ± 0.003	C			76		M

Supplementary Table 3-4: U-Pb age compilation used for probability density plots and stratigraphic columns.

Sample ID[1]	Sample ID[2]	UTM Zone 15N		Rock code[3]	$^{207}Pb/^{206}Pb$ age[4] (Ga)	Int.[5]	Inh.[6]	Min.[7]	Ref.[8]	Ref.[9]	Terr-ane[10]
		Easting	Northing								
KAT20130920-02	WS-55C	696317	5465081	san	2.69 ± 0.005	C			76		M
09SB215		630185	5433427	gab	2.688 ± 0.001	C			33	78	M
12-8-17-2B	WS-37C	595231	5416234	san	2.688 ± 0.007	C			76		M
KAT20130711-04	WS-43C	727926	5457689	ttg	2.687 ± 0.006	C	2.882		76		M
KAT20130730-11	WS-58B	628580	5436666	san	2.687 ± 0.007	C			76		M
12-8-17-3	WS-38A	596932	5415043	san	2.687 ± 0.006	C			76		M
05DS48		707560	5423735	granmx	2.686 ± 0.002	C	2.690		18	64	M
12-8-16-3A	WS-32C	705139	5425371	san	2.686 ± 0.008	C			76		M
00KYT-20	WS-11B	538166	5441544	san	2.686 ± 0.006	C			56		M
06DS50		568130	5413120	grdr	2.686 ± 0.006	C			64		M
DD86-22		733478	5458252	gab	2.686 ± 0.002	C			16	64	M
09SB278		628506	5436958	mnzo	2.686 ± 0.001	C			33	78	M
WOB86		587900	5432889	gran	2.685 ± 0.002	C		ti	15		M
06DS23		532330	5443920	mnzo	2.685 ± 0.008	C			64		M
09SB254		640650	5436988	mnzo	2.685 ± 0.001	C			33	78	M
		595442	5417355	gran	2.684 ± 0.025	C		ti	75		M
KAT20130712-09	WS-45A	559697	5418062	san	2.682 ± 0.003	C			76		M
		599320	5406790	sst	3.003 ± 0.001	D			14	79	M
Z1		601040	5414724	sst	3.002	D			46		M
Z1		601040	5414724	sst	3.001	D			46		M
Z1		601040	5414724	sst	3.001	D			46		M
Z1		601040	5414724	sst	2.999	D			46		M
Z1		601040	5414724	sst	2.999	D			46		M
		596880	5409971	sst	2.997 ± 0.001	D			46		M
09SB038		626465	5434759	sst	2.997 ± 0.002	D			33	78	M
		599316	5409238	cgn	2.994	D			43		M
12-8-28-6	WS-35C	626771	5413291	ttg	2.962 ± 0.007	I	2.962		76		M
DD07-8		598554	5409164	mdst	2.939 ± 0.02	D			64		M
DD07-8		598554	5409164	mdst	2.939 ± 0.02	D			64		M
04DS57		653680	5410603	cng	2.927	D			17	64	M
04DS57		653680	5410603	cng	2.927	D			17	64	M
04DS57		653680	5410603	cng	2.927	D			17	64	M
04DS57		653680	5410603	cng	2.927	D			17	64	M
04DS57		653680	5410603	cng	2.927	D			17	64	M
04DS57		653680	5410603	cng	2.927	D			17	64	M
KAT20130728-07	WS-53A	607118	5418511	gran	2.898 ± 0.008	C	2.941		76		M
KAT20130728-07	WS-53A	607118	5418511	gran	2.898 ± 0.008	C	2.938		76		M
KAT20130919-02	WS-57B	523228	5455211	gran	2.864 ± 0.001	C			76		M
12-8-28-6	WS-35C	626771	5413291	ttg	2.823 ± 0.009	I	2.823		76		M
DD07-7		603490	5406575	uvlt	2.782 ± 0.015	D	2.782		64		M
DD07-7		603490	5406575	uvlt	2.782 ± 0.015	D	2.995		64		M
97KYT-60		599320	5407880	uvlt	2.78	I	2.780		70		M
97KYT-60		599320	5407880	uvlt	2.78	I	2.995		70		M
97KYT-60		599320	5407880	uvlt	2.78	I	2.997		70		M
DD07-5		604023	5406559	sst	2.779 ± 0.022	D			20		M
DD07-5		604023	5406559	sst	2.779 ± 0.022	D			20		M
KAT20130822-07	WS-49C	531831	5449613	gran	2.716 ± 0.004	C	2.977		76		M

Supplementary Table 3-4: U-Pb age compilation used for probability density plots and stratigraphic columns.

Sample ID[1]	Sample ID[2]	UTM Zone 15N		Rock code[3]	$^{207}Pb/^{206}Pb$ age[4] (Ga)	Int.[5]	Inh.[6]	Min.[7]	Ref.[8]	Ref.[9]	Terr-ane[10]
		Easting	Northing								
KAT20130822-07	WS-49C	531831	5449613	gran	2.716 ± 0.004	C	2.946		76		M
KAT20130822-07	WS-49C	531831	5449613	gran	2.716 ± 0.004	C	2.941		76		M
00KYT-22	WS-16C	605094	5455534	sed	2.709 ± 0.005	D			56		M
12-8-16-8	WS-34B	669925	5436744	gran	2.703 ± 0.004	C	2.906		76		M
KAT20130920-04	WS-53C	704608	5465081	ttg	2.701 ± 0.009	C	2.899		76		M
00KYT22		604990	5455570	cng	2.7	D			69		M
00KYT22		604990	5455570	cng	2.7	D			69		M
00KYT22		604990	5455570	cng	2.7	D			69		M
00KYT22		604990	5455570	cng	2.7	D			69		M
09DS251		606110	5421654	mdst	2.678	D			22		M
09DS251		606110	5421654	mdst	2.678	D			22		M
00KYT-12	WS-12B	552281	5411288	sed	2.665 ± 0.006	D			56		M
	15	595496	5417384	gran	2.665	T		ti	75		M
07DS40		633232	5405360	fvlt	3.006 ± 0.001	C			20		Q
C-93-24	54	311000	5381000	gab	2.725 ± 0.017	C			12		Q
ON+200		622784	5402685	qmnzo	2.688 ± 0.004	C			42		Q
KAT20130815-01	WS-58C	622697	5403009	san	2.686 ± 0.005	C			76		Q
12-8-15-11	WS-24B	788965	5396512	gran	2.676 ± 0.006	C			56		Q
12-8-15-10	WS-24A	773410	5430020	gran	2.674 ± 0.008	C			56		Q
04DS80		726017	5411947	ton	2.673 ± 0.001	C		ti	17	64	Q
15CZ		599510	5398130	mdst	2.796	D			42		Q
35BZ		588187	5398384	mdst	2.792	D			42		Q
103BZ		565867	5398206	mdst	2.788	D			42		Q
11AZ		602064	5398020	mdst	2.739	D			42		Q
33AZ		592060	5398600	mdst	2.709	D			42		Q
33AZ		592060	5398600	mdst	2.709	D			42		Q
KAT20140820-02	WS-56C	659430	5397987	san	2.709 ± 0.009	I	2.709		76		Q
3AZ		602950	5398943	mdst	2.707	D			42		Q
27BZ		594866	5399500	mdst	2.706	D			42		Q
27BZ		594866	5399500	mdst	2.706	D			42		Q
8BZ		602610	5397940	mdst	2.704	D			42		Q
45CZ		573300	5397680	mdst	2.704	D			42		Q
45CZ		573300	5397680	mdst	2.704	D			42		Q
101DZ		567275	5397826	mdst	2.704	D			42		Q
101DZ		567275	5397826	mdst	2.704	D			42		Q
101DZ		567275	5397826	mdst	2.704	D			42		Q
DD86-10		600812	5398020	mdst	2.701	D			42		Q
DD86-10		600812	5398020	mdst	2.701	D			42		Q
101EZ		566962	5397558	mdst	2.7	D			42		Q
101EZ		566962	5397558	mdst	2.7	D			42		Q
101EZ		566962	5397558	mdst	2.7	D			42		Q
DD86-11		604211	5397904	mdst	2.698	D			42		Q
DD86-11		604211	5397904	mdst	2.698	D			42		Q
DD86-11		604211	5397904	mdst	2.698	D			42		Q
DD86-11		604211	5397904	mdst	2.698	D			42		Q
DD86-11		604211	5397904	mdst	2.698	D			42		Q
C-93-33	54	609000	5316000	gab	2.725 ± 0.017	C			12		WA

Supplementary Table 3-4: U-Pb age compilation used for probability density plots and stratigraphic columns.

Sample ID[1]	Sample ID[2]	UTM Zone 15N		Rock code[3]	$^{207}Pb/^{206}Pb$ age[4] (Ga)	Int.[5]	Inh.[6]	Min.[7]	Ref.[8]	Ref.[9]	Terr-ane[10]
		Easting	Northing								
KAT20140821-01	WS-56A	682835	5380696	san	2.693 ± 0.007	C			76		WA
12-8-15-14	WS-24C	788296	5393691	gran	2.678 ± 0.006	C			56		WA
KAT20140825-01	WS-57A	686978	5346123	san	2.71 ± 0.008	I	2.710		76		WA
789-30		349370	5514789	tgn	3.317 ± 0.009	C?	3.317		58		WR
97-108		481400	5556100	ton	3.255 ± 0.005	C			58		WR
C-83-32		481400	5556100	ton	3.17 ± 0.02	C			10		WR
C-86-34	66	599721	5583520	ton	3.04 ± 0.01	C			13		WR
	18	774269	5599320	tgn	3.075 ± 0.01	C		ti	44		WR
	26	880948	5576990	fp	3.056 ± 0.001	C			37		WR
789-30		349370	5514789	tgn	3.055 ± 0.004	C			58		WR
1		349780	5515080	ton	3.051 ± 0.002	C			44		WR
96GRS4001G	WS-3C	880824	5577113	fv	3.051 ± 0.006	C			56		WR
BIB-98-B024h		604228	5560696	gran	3.046 ± 0.011	I?			7		WR
	56	603720	5561140	gns	3.046 ± 0.01	C			57		WR
C-87-31	58	596375	5572080	ton	3.04 ± 0.003	C		ti	52		WR
	59	571518	5575800	ton	3.04 ± 0.04	C			52		WR
	4	670231	5612360	tgn	2.97 ± 0.01	C			62		WR
	19	774241	5599150	ton	2.965 ± 0.01	C		ti	44		WR
	7	687978	5603120	qtz	2.948 ± 0.003	C			28		WR
	4	744392	5528430	grdr	2.931 ± 0.003	C			68		WR
OGS88-2	WS-7B	744392	5528430	ttg	2.93 ± 0.003	C			56		WR
	3	735080	5532950	cng	2.928 ± 0.01	C			57		WR
	24	679472	5556370	ivt	2.927 ± 0.01	C			62		WR
	1	867921	5591900	iv	2.923 ± 0.001	C			37		WR
	51	881285	5581010	fv	2.921 ± 0.001	C			40		WR
97GRS0701Z	WS-2B	867502	5591827	fv	2.921 ± 0.003	C			56		WR
97JRP1253	WS-6A	924906	5601280	ttg	2.918 ± 0.003	C	2.935		56		WR
	25	676753	5541860	qtz	2.912 ± 0.01	C			62		WR
	11	706615	5534680	tgn	2.89 ± 0.008	C		ti	60		WR
C-87-27	54	578463	5552230	gran	2.889 ± 0.003	C		ti	11		WR
C87-27		578750	5552220	gran	2.889 ± 0.003	C			11		WR
520-48		382000	5513800	tgn	2.881 ± 0.002	C	3.051		58		WR
	8	690251	5603540	fvt	2.881 ± 0.01	C			62		WR
C-83-28		384500	5515650	ton	2.875 ± 0.02	C			10		WR
C-83-33		448300	5531000	ton	2.84 ± 0.02	C			10		WR
C87-26		578750	5552220	ton	2822-2866	C	2.866		11		WR
	17	705442	5531670	tgn	2.774 ± 0.002	C			34		WR
00KYT-10	WS-15C	724448	5504890	ttg	2.745 ± 0.006	C			56		WR
	8	887947	5600710	ivt	2.739 ± 0.001	C			37		WR
	22	880422	5589190	ivt	2.738 ± 0.004	C			38		WR
KAT20130913-06	WS-54C	730599	5500664	ttg	2.738 ± 0.005	C	2.764		76		WR
95KYT-27	WS-16A	743932	5530379	fv	2.738 ± 0.006	C			56		WR
	5	879564	5599150	fi	2.738 ± 0.001	C			51		WR
	7	881373	5599270	iv	2.738 ± 0.001	C			53		WR
	21	879961	5597750	qp	2.738 ± 0.001	C			53		WR
	6	880345	5599490	fi	2.738 ± 0.001	C			51		WR
00KYT-07	WS-15B	723157	5491952	ttg	2.737 ± 0.009	C			56		WR

Supplementary Table 3-4: U-Pb age compilation used for probability density plots and stratigraphic columns.

Sample ID[1]	Sample ID[2]	UTM Zone 15N		Rock code[3]	$^{207}Pb/^{206}Pb$ age[4] (Ga)	Int.[5]	Inh.[6]	Min.[7]	Ref.[8]	Ref.[9]	Terr-ane[10]
		Easting	Northing								
	4	872849	5598740	tron	2.736 ± 0.001	C			53		WR
99GRS0066C	WS-2C	872909	5599060	gran	2.735 ± 0.008	C			56		WR
DD85-29	WS-9B	732465	5525628	fv	2.735 ± 0.005	C			56		WR
	16	918487	5603970	fd	2.734 ± 0.001	C			37		WR
	5	739479	5535130	gab	2.733 ± 0.007	C			28		WR
	15	919538	5607410	ivt	2.733 ± 0.001	C			37		WR
	18	924711	5599270	fd	2.733 ± 0.002	C			37		WR
12-8-20-5	WS-26B	635433	5501223	ttg	2.733 ± 0.005	C			56		WR
	7	743998	5530420	iv	2.732 ± 0.002	C			68		WR
12-8-20-4	WS-26A	635117	5492498	gran	2.729 ± 0.008	C	2.745		56		WR
99GRS0248A	WS-6B	928650	5598290	ttg	2.728 ± 0.005	C			56		WR
	23	884987	5590170	ivt	2.728 ± 0.001	C			38		WR
	8	732893	5525310	fv	2.727 ± 0.002	C			68		WR
00KYT06		714296	5484615	fv	2.726 ± 0.001	C			70		WR
DD85-28	WS-9A	732655	5525009	fv	2.725 ± 0.004	C	2.755		56		WR
	6	737550	5535100	sst	2.724 ± 0.003	C			28		WR
	37	681032	5517780	ton	2.723 ± 0.003	C			72		WR
	39	862615	5564120	tgn	2.723 ± 0.001	C			39		WR
	10	687409	5599900	mdst	2.72 ± 0.01	C			62		WR
07DS37		610464	5466497	ton	2.719 ± 0.01	I	2.923		21		WR
12-8-21-5	WS-29A	421782	5533144	ttg	2.719 ± 0.01	C	2.933		56		WR
J-551	33	691030	5528030	tgn	2.718 ± 0.007	C			9		WR
520-46A		382000	5513800	ton	2.717 ± 0.003	C			58		WR
	22	816180	5570570	tgn	2.716 ± 0.002	C			30		WR
00KYT-33	WS-14C	696103	5507461	gran	2.716 ± 0.006	C			56		WR
PBA98-521	WS-7C	741897	5535548	gab	2.715 ± 0.003	C			56		WR
	15	698159	5534680	ton	2.715 ± 0.013	C		ti	60		WR
98KYT-37	WS-10A	753083	5540215		2.714 ± 0.008	C			56		WR
00KYT-35	WS-15A	722297	5505601	ttg	2.714 ± 0.006	C			56		WR
00KYT34		687280	5482630	tgn	2.712 ± 0.002	C			71		WR
00KYT-27	WS-14A	629665	5510940	ttg	2.711 ± 0.004	C	2.887		56		WR
12-8-21-8	WS-30A	433994	5564925	gran	2.711 ± 0.004	C			56		WR
	6	684738	5605720	fvt	2.711 ± 0.004	C			61		WR
	21	780356	5598610	ton	2.709 ± 0.002	C			44		WR
12-8-21-9	WS-30B	435729	5567372	ttg	2.709 ± 0.003	C	3.032		56		WR
AC97-053		385000	5520400	grdr	2.709 ± 0.002	C			58		WR
	30	692863	5553370	grdr	2.709 ± 0.004	C		ti	72		WR
	20	773399	5593210	ton	2.708 ± 0.002	C			44		WR
AC97-043A		387400	5515850	gran	2.708 ± 0.002	C			58		WR
AC97-043B		387400	5515850	gran	2.708 ± 0.003	C			58		WR
520-49		382000	5513800	peg	2.708 ± 0.009	C			58		WR
	11	892245	5600120	qfp	2.706 ± 0.001	C			53		WR
12-8-30-5	WS-22A	753217	5540303	fv	2.706 ± 0.008	C			56		WR
	31	687676	5550100	mdst	2.706 ± 0.01	C		ti	60		WR
C87-25		578750	5552220	md	2.705 ± 0.005	C	2.876	ti, zrc	11		WR
C-87-25	54	578463	5552230	dior	2.705 ± 0.005	C			11		WR
12-8-30-7	WS-22B	749124	5542725	ttg	2.705 ± 0.008	C			56		WR

Supplementary Table 3-4: U-Pb age compilation used for probability density plots and stratigraphic columns.

Sample ID[1]	Sample ID[2]	UTM Zone 15N		Rock code[3]	$^{207}Pb/^{206}Pb$ age[4] (Ga)	Int.[5]	Inh.[6]	Min.[7]	Ref.[8]	Ref.[9]	Terr-ane[10]
		Easting	Northing								
C87-26		578750	5552220	ton	2.704 ± 0.002	C	2.866	ti, zrc	11		WR
C-87-26	54	578463	5552230	ton	2.704 ± 0.002	C		ti	11		WR
C-87-32	63	596938	5581270	mig	2.704 ± 0.01	C			13		WR
	2	740569	5537350	mdst	2.704 ± 0.01	C			57		WR
	9	753157	5540280	fv	2.703 ± 0.001	C			28		WR
	1	749905	5539060	mdst	2.702 ± 0.01	C			57		WR
	34	629470	5510844	gns	2.702 ± 0.001	C			69		WR
79-50		400430	5538750	grdr	2.702 ± 0.004	C			6		WR
	25	880763	5580030	qp	2.701 ± 0.001	C			38		WR
79-55		375540	5519100	qdior	2.700 ± 0.002	C			6		WR
12-8-21-4	WS-28D	419753	5531402	ttg	2.700 ± 0.004	C	3.093		56		WR
12-8-30-3	WS-21D	740816	5526952	ttg	2.699 ± 0.004	C			56		WR
C88-34	69	603900	5586000	ton	2.698 ± 0.002	C			13		WR
	20	932311	5612410	gran	2.698 ± 0.003	C			37		WR
12-8-21-10	WS-30C	431391	5557211	gran	2.698 ± 0.004	C	3.172		56		WR
J-446b	32	692945	5530300	id	2.697 ± 0.01	C		ti	9		WR
	9	887980	5601170	gab	2.695 ± 0.003	C			51		WR
97GRS0536B	WS-6C	932309	5612404	san	2.695 ± 0.003	C			56		WR
12-8-21-6	WS-29B	422602	5538895	gran	2.694 ± 0.002	C	3.117		56		WR
96KYT-144	WS-1A	731724	5491840	gran	2.693 ± 0.007	C	2.731		56		WR
12-8-20-3	WS-25C	636079	5471080	gran	2.693 ± 0.008	C			56		WR
79-51		394840	5534280	gran	2.690 ± 0.015	C	2.755		6		WR
	10	742755	5538170	gab	2.690 ± 0.001	C			28		WR
	36	697069	5523510	qdior	2.690 ± 0.002	C			34		WR
KAT20130822-11	WS-57C	686517	5482083	gran	2.688 ± 0.003	C	3.010		76		WR
12-8-21-7	WS-29C	430265	5544742	gran	2.688 ± 0.004	C			56		WR
	12	708482	5541720	grdr	2.688 ± 0.004	C		ti	73		WR
99GRS1040A	WS-4A	884842	5600584	fv	2.685 ± 0.005	C			56		WR
	26	676836	5541720	id	2.685 ± 0.003	C			61		WR
	33	696031	5507360	gran	2.685 ± 0.002	C			69		WR
00KYT-32	WS-14B	696103	5507461	gran	2.684 ± 0.006	C	2.821		56		WR
	14	705238	5531650	fd	2.684 ± 0.004	C			60		WR
BIB-98-B003d		605483	5563660	fd	2.681 ± 0.004	C			7		WR
	62	572147	5584270	gns	2.681 ± 0.02	C			52		WR
	57	605680	5564180	gran	2.681 ± 0.01	C			57		WR
	13	724615	5534510	gran	2.680 ± 0.01	C			57		WR
12-8-20-2	WS-25B	638039	5470596	gran	2.678 ± 0.004	C			56		WR
00KYT28		613745	5488309	gran	2.671 ± 0.01	C			71		WR
00KYT-28	WS-13B	613548	5488442	gran	2.667 ± 0.01	C	2.716		56		WR
OGS88-1	WS-7A	694613	5609126	sed	3.25 ± 0.008	D			56		WR
KAT20130913-06i	WS-54C	730599	5500664		3.125 ± 0.004	C	2.799		76		WR
KAT20130913-06i	WS-54C	730599	5500664		3.125 ± 0.004	C	3.125		76		WR
KAT20130913-06i	WS-54C	730599	5500664		3.09 ± 0.012	C	2.931		76		WR
KAT20130913-06i	WS-54C	730599	5500664		3.09 ± 0.012	C	3.090		76		WR
	30	878412	5571610	ivt	2.968 ± 0.002	D			53		WR
	2	871151	5591130	cng	2.924 ± 0.001	D			38		WR
	17	925988	5601700	grdr	2.922 ± 0.001		2.922		37		WR

Supplementary Table 3-4: U-Pb age compilation used for probability density plots and stratigraphic columns.

Sample ID[1]	Sample ID[2]	UTM Zone 15N		Rock code[3]	$^{207}Pb/^{206}Pb$ age[4] (Ga)	Int.[5]	Inh.[6]	Min.[7]	Ref.[8]	Ref.[9]	Terr-ane[10]
		Easting	Northing								
	3	871702	5590870	cng	2.784 ± 0.002	D			53		WR
	9	692322	5602510	peg	2.752	T		ti	62		WR
KAT20130913-06	WS-54C	730599	5500664	ttg	2.738 ± 0.005	C	3.051		76		WR
KAT20130913-06	WS-54C	730599	5500664	ttg	2.738 ± 0.005	C	3.050		76		WR
KAT20130913-06	WS-54C	730599	5500664	ttg	2.738 ± 0.005	C	2.826		76		WR
KAT20130913-06	WS-54C	730599	5500664	ttg	2.738 ± 0.005	C	2.792		76		WR
	19	928420	5597820	grdr	2.729 ± 0.001		2.729		53		WR
00KYT-27	WS-14A	629665	5510940	ttg	2.711 ± 0.004	C	2.750		56		WR
	10	889854	5600990	cgn	2.71	D			53		WR
12-8-21-9	WS-30B	435729	5567372	ttg	2.709	C	3.005		56		WR
12-8-21-9	WS-30B	435729	5567372	ttg	2.709	C	2.963		56		WR
C87-25		578750	5552220	md	2.705 ± 0.005	C	2.826	ti, zrc	11		WR
2		349780	5515080	md	2.701 ± 0.003	M		ti	44		WR
95KYT-09	WS-8A	752505	5541350	sed	2.700	D			56		WR
95KYT-09	WS-8A	752505	5541350	sed	2.917	D			56		WR
95KYT-09	WS-8A	752505	5541350	sed	2.865	D			56		WR
12-8-21-10	WS-30C	431391	5557211	gran	2.698 ± 0.004	C	3.163		56		WR
12-8-21-10	WS-30C	431391	5557211	gran	2.698 ± 0.004	C	3.042		56		WR
12-8-21-10	WS-30C	431391	5557211	gran	2.698 ± 0.004	C	3.015		56		WR
12-8-21-10	WS-30C	431391	5557211	gran	2.698 ± 0.004	C	2.928		56		WR
12-8-21-6	WS-29B	422602	5538895	gran	2.694 ± 0.002	C	2.826		56		WR
C-87-33	64	597064	5581150	gran	2.692 ± 0.002	M			13		WR
C-86-35	65	599748	5583670	amph	2.679 ± 0.002	M			13		WR
p864b	16	703110	5531580	myl	2.677	T		ti	8		WR
00KYT-28	WS-13B	613548	5488442	gran	2.667 ± 0.01	C	2.728		56		WR
79-50		400430	5538750	grdr	2.635 ± 0.056	C		fs	6		WR
79-51		394840	5534280	gran	2.43 ± 0.09	C		wr	6		WR
	21	652448	5546790	ivlt	2.775 ± 0.001	C			44		WW
	22	666861	5552900	ivlt	2.774 ± 0.01	C			62		WW
	17	663791	5574520	ivt	2.745 ± 0.002	C			31		WW
	20	643410	5541030	fvt	2.745 ± 0.01	C			62		WW
	23	669203	5549750	fvm	2.745 ± 0.01	C			62		WW
11GPB0388		513815	5469656	grdr	2.744 ± 0.001	C			5	77	WW
DD78-7		483230	5503660	ivct	2.743 ± 0.001	C			36		WW
09GPB0232		548072	5484585	fvlt	2.74 ± 0.001	C			5	77	WW
DD90-28		397010	5502170	mvm	2.738 ± 0.002	C			2		WW
	38	655352	5525760	fv	2.736 ± 0.009	C			32		WW
	44	647014	5529500	fv	2.736 ± 0.002	C			32		WW
	41	652862	5526690	fv	2.736 ± 0.003	C			32		WW
	39	653518	5526820	fv	2.735 ± 0.007	C			32		WW
BIB-98-B028d		607238	5557800	grdr	2.735 ± 0.002	C			7		WW
	42	651229	5527930	fv	2.735 ± 0.002	C			32		WW
	55	607544	5558470	grdr	2.735 ± 0.01	C			57		WW
	18	664008	5565490	ton	2.735 ± 0.003	C			74		WW
	40	653314	5527030	fv	2.735 ± 0.003	C			32		WW
DD78-43		515619	5507152	fvct	2.735 ± 0.004	C			36		WW
	45	641596	5526320	fv	2.735 ± 0.002	C			32		WW

Supplementary Table 3-4: U-Pb age compilation used for probability density plots and stratigraphic columns.

Sample ID[1]	Sample ID[2]	UTM Zone 15N		Rock code[3]	$^{207}Pb/^{206}Pb$ age[4] (Ga)	Int.[5]	Inh.[6]	Min.[7]	Ref.[8]	Ref.[9]	Terr-ane[10]
		Easting	Northing								
10DL302A		599790	5546925	fv	2.735 ± 0.003	C			54	77	WW
09DS206		558460	5468820	ivbx	2.735 ± 0.001	C			33	66	WW
05GPB7220		546416	5499170	qdior	2.734 ± 0.001	C			5	77	WW
09DS204		562000	5467190	ton	2.734 ± 0.001	C			33	66	WW
00KYT-29	WS-13A	589230	5502347	ttg	2.734 ± 0.031	C			56		WW
09DS209		556750	5464360	ivbx	2.734 ± 0.001	C			33	66	WW
Quartz Diorite		473030	5489420	qdior	2.734 ± 0.01	C			25		WW
	47	634372	5521160	ton	2.734 ± 0.001	C			31		WW
09GPB7747		517898	5498131	qdior	2.733 ± 0.001	C			5	77	WW
Katamiagamak gabbro		448900	5442100	gab	2.733 ± 0.01	C		baddel	26		WW
Mulcahy		473550	5494900	p	2.733 ± 0.001	C			59		WW
Blue Qtz' granodiorite		468600	5491080	grdr	2.733 ± 0.01	C			25		WW
	14	667810	5578920	i	2.733 ± 0.001	C			35		WW
10DL153		589135	5550237	fv	2.733 ± 0.001	C			54	77	WW
12-8-20-8	WS-27A	585855	5479001	gran	2.733 ± 0.008	C			56		WW
	50	572328	5543430	fvt	2.733 ± 0.001	C			31		WW
DD78-35		568291	5542046	fvt	2.733 ± 0.001	C			31		WW
	48	628374	5520050	gab	2.733 ± 0.002	C			31		WW
Bluffpoint Quartz Diorite		478950	5449120	qdior	2.732 ± 0.002	C			25		WW
09DS205		561620	5469460	ton	2.732 ± 0.001	C			33	66	WW
DD78-4		516372	5498817	ton	2.732 ± 0.003	C			36		WW
11DL428B		453442	5460858	fv	2.732 ± 0.002	C			54	77	WW
DD-78-6		481930	5503000	ton	2.732 ± 0.002	C			36		WW
Katamiagamak gabbro		448900	5442100	gab	2.732 ± 0.004	C			24		WW
Contact Zone Tonalite		478900	5445180	ton	2.732 ± 0.002	C			25		WW
10GPB0247		554080	5532007	fvct	2.731 ± 0.001	C			3	77	WW
	27	664744	5532770	mdst	2.731 ± 0.01	C			62		WW
06DS10		574950	5471340	ivbx	2.73 ± 0.007	C			64		WW
	19	639802	5561740	grdr	2.73 ± 0.008	C			74		WW
11GPB0348		514222	5462499	fvt	2.729 ± 0.002	C			5	77	WW
9		520420	5398310	ton	2.728 ± 0.002	C			41		WW
8		519320	5399550	fv	2.728 ± 0.004	C			41		WW
DD78-24		457700	5438700	ivt	2.728 ± 0.001	C			24		WW
8		346724	5508640	grdr	2.727 ± 0.002	C			29		WW
10		533350	5399380	fv	2.727 ± 0.001	C			41		WW
09DS210		556390	5463740	gab	2.727 ± 0.005	C			33	66	WW
12-8-20-14	WS-27D	555601	5490625	gran	2.726 ± 0.01	C			56		WW
DD78-19		434600	5455760	gab	2.725 ± 0.003	C			24		WW
DD78-26		446650	5432350	ton	2.724 ± 0.002	C			23		WW
6		352180	5491170	qdior	2.724 ± 0.002	C			29		WW
7		352720	5494120	ivt	2.723 ± 0.002	C			29		WW
Sabaskong gneiss		421026	5436612	tgn	2.723 ± 0.002	C			26		WW
2		531280	5480000	gab	2.722 ± 0.005	C			34		WW
12-8-20-11	WS-27B	563917	5506368	gran	2.722 ± 0.005	C			56		WW
KAT20130823-04	WS-53B	479144	5476127	ttg	2.721 ± 0.007	C	2.868		76		WW
12-8-21-13	WS-31C	426749	5485332	gran	2.721 ± 0.007	C			56		WW
	46	634451	5522900	fd	2.721 ± 0.004	C			47		WW

Supplementary Table 3-4: U-Pb age compilation used for probability density plots and stratigraphic columns.

Sample ID[1]	Sample ID[2]	UTM Zone 15N		Rock code[3]	$^{207}Pb/^{206}Pb$ age[4] (Ga)	Int.[5]	Inh.[6]	Min.[7]	Ref.[8]	Ref.[9]	Terr-ane[10]
		Easting	Northing								
Lawerence Lake Trondhjemite		476790	5453600	ton	2.72 ± 0.01	C			25		WW
1		352250	5492700	fd	2.72 ± 0.002	C			29		WW
	28	665623	5531530	d	2.72 ± 0.01	C			62		WW
DD90-42		362480	5505060	v	2.72 ± 0.003	C			2		WW
10GPB0246		542302	5539205	fvct	2.719 ± 0.001	C			3	77	WW
DD90-33		385130	5480520	fvt	2.719 ± 0.001	C			2		WW
10GPB0246		542302	5539205	fvct	2.719 ± 0.008	C			3	77	WW
1		526420	5479250	fvlt	2.719 ± 0.01	C	2.728		34		WW
10DS62		541500	5474600	lgab	2.718 ± 0.001	C			65		WW
Central Trondhjemite		461050	5480060	grdr	2.718 ± 0.01	C			25		WW
Chuck Lake pluton		481020	5455950	grdr	2.718 ± 0.01	C			25		WW
12-8-21-3	WS-28C	406072	5518392	ttg	2.718 ± 0.005	C			56		WW
	43	652551	5531540	fvt	2.718 ± 0.003	C			31		WW
Aulneau tonalite		396600	5456750	ton	2.717 ± 0.005	C			26		WW
2		352250	5492700	fd	2.716 ± 0.002	C	2.722		29		WW
Straw Lake Porphyry		475200	5442500	p	2.716 ± 0.01	C			25		WW
7		441300	5517400	qp	2.716 ± 0.002	C			34		WW
LOW892-129		405600	5503500	ton	2.716 ± 0.01	C			58		WW
	29	660943	5528960	mdst	2.716 ± 0.012	C			61		WW
	31	589009	5502215	ton	2.716 ± 0.002	C			69		WW
12-8-20-13	WS-27C	567978	5511669	gran	2.715 ± 0.01	C	2.750		56		WW
	13	667446	5585470	gran	2.714 ± 0.01	C		ti	61		WW
DD78-28		427420	5477190	fvm	2.714 ± 0.006	C			24		WW
	49	586720	5539730	cng	2.713 ± 0.002	C			44		WW
PW201		570500	5546800	cng	2.703 ± 0.002	D			45		WW
12-8-21-12	WS-31B	428332	5486411	gran	2.712 ± 0.008	C			56		WW
DD78-49		443540	5461820	fvt	2.712 ± 0.001	C			24		WW
9		346481	5506976	p	2.711 ± 0.002	C	2.733	tit-zir	29		WW
12-8-21-2	WS-28B	424862	5516245	gran	2.71 ± 0.005	C			56		WW
Aulneau granodiorite		405300	5470900	grdr	2.71 ± 0.004	C			26		WW
12-8-21-11	WS-31A	415422	5501695	gran	2.709 ± 0.005	C			56		WW
LOW892-129		405600	5503500	ton	2.709 ± 0.001	C			58		WW
4		357700	5496880	qdior	2.709 ± 0.001	C			29		WW
3		352250	5492700	dior	2.709 ± 0.002	C		tit-zir	29		WW
5		350263	5493641	p	2.708 ± 0.007	C	2.802	tit-zir	29		WW
4		537400	5532500	grdr	2.708 ± 0.003	C		ti	34		WW
J-737	34	689108	5527290	fd	2.707 ± 0.01	C			9		WW
8		462200	5515400	ton	2.706 ± 0.003	C	2.711		34		WW
	53	579615	5550270	sst	2.706 ± 0.002	C			45		WW
11SW657		457155	5459825	gran	2.705 ± 0.004	C			55		WW
	11	679961	5595840	ivt	2.705 ± 0.003	C			61		WW
1		555530	5531300	fv	2.704 ± 0.003	C			34		WW
	15	666157	5576010	fv	2.704 ± 0.002	C			35		WW
	12	679449	5592470	mdst	2.704 ± 0.01	C			35		WW
	2	660177	5588040	cng	2.704 ± 0.001	C			44		WW
05GPB1457		527906	5511721	fvct	2.703 ± 0.002	C			5	77	WW
8		539770	5471784	fvt	2.703 ± 0.003	C	2.710		34		WW

Supplementary Table 3-4: U-Pb age compilation used for probability density plots and stratigraphic columns.

Sample ID[1]	Sample ID[2]	UTM Zone 15N		Rock code[3]	$^{207}Pb/^{206}Pb$ age[4] (Ga)	Int.[5]	Inh.[6]	Min.[7]	Ref.[8]	Ref.[9]	Terr-ane[10]
		Easting	Northing								
	16	665178	5576260	mdst	2.703 ± 0.001	C			35		WW
6		553900	5540110	qp	2.703 ± 0.002	C			44		WW
	52	579714	5547710	fvt	2.703 ± 0.002	C			44		WW
DD78-50		526000	5479000	gran	2.703 ± 0.015	C	2.731		36		WW
11GPB0488		535312	5471437	fvct	2.703 ± 0.001	C	2.727		5	77	WW
11GPB0488		535312	5471437	fvct	2.703 ± 0.001	C	2.724		5	77	WW
11GPB0488		535312	5471437	fvct	2.703 ± 0.001	C	2.720		5	77	WW
7		579900	5548040	fvct	2.702 ± 0.01	C			44		WW
12-8-21-1	WS-28A	431073	5520149	gran	2.702 ± 0.005	C			56		WW
p865	35	690788	5527740	mdst	2.701 ± 0.01	C			9		WW
Herony Lake pluton		432534	5443537	qdior	2.701 ± 0.001	C			26		WW
	3	661204	5588670	ton	2.700 ± 0.01	C			44		WW
	5	669362	5602470	ton	2.700 ± 0.003	C		ti	61		WW
09GPB185B		417992	5450578	id	2.700 ± 0.001	C	2.720		5	77	WW
Stephen Lake pluton		439901	5460947	qdior	2.699 ± 0.002	C			26		WW
11GPB0399		513437	5464597	ivlt	2.699 ± 0.001	C	2.720		5	77	WW
5A and 5B		522730	5467660	qp	2.699 ± 0.003	C	2.705		34		WW
6		520000	5468200	fvct	2.699 ± 0.004	C	2.745		34		WW
KAT20130823-03	WS-57D	490752	5485888	ttg	2.699 ± 0.006	C			76		WW
09GPB7722		423950	5452927	grdrmx	2.699 ± 0.002	C			5	77	WW
9, K76-30		525880	5469280	mnzo	2.696 ± 0.002	C			34		WW
2		542450	5526100	grdr	2.696 ± 0.003	C		ti	34		WW
DD90-34		376280	5474450	mnzo	2.695 ± 0.003	C		ti	2		WW
3		542000	5516700	qdior	2.695 ± 0.002	C	2.710	ti, zrc	34		WW
LOW296-12		409200	5490200	grdrmx	2.695 ± 0.004	C		ti	58		WW
09DS202		562860	5475240	grdrmx	2.694 ± 0.001	C			33	66	WW
11GPB0505		549964	5471878	grdr	2.692 ± 0.001	C			5	77	WW
KAT20130823-07	WS-55A	487433	5422153	san	2.689 ± 0.004	C			76		WW
07DS44		546722	5435910	ton	2.688 ± 0.005	C	2.740		20		WW
07DS44		546722	5435910	ton	2.688 ± 0.005	C	3.293		20		WW
KAT20130823-11	WS-58E	513838	5398865	san	2.687 ± 0.004	C			76		WW
13		509600	5397240	qmnzo	2.686 ± 0.002	C			41		WW
6		499700	5522750	gran	2.685 ± 0.002	C			34		WW
92DF-5		523870	5518010	peg	2.665 ± 0.008	C		columl	63		WW
9		447900	5502400	gran	2.663 ± 0.005	C		monz,	34		WW
09DS179		580200	5479680	dia	1.887 ± 0.013	C		baddel	33	66	WW
	1	659035	5587870	fv	3.26 ± 0.01		3.260		62		WW
9		578730	5546810	cgn	2.903 ± 0.016	D			44		WW
	51	578803	5546620	cng	2.903 ± 0.016	D			44		WW
4		519200	5470000	cng	2.834	D			34		WW
DD90-40		352370	5504700	v	2.794	D			2		WW
DD90-30		400460	5489400	v	2.778 ± 0.005	D			2		WW
10		578730	5546810	cgn	2.758	D	2.919		44		WW
7, DD78-8		535940	5469070	qp	2.752	D	2.752		34		WW
7, DD78-8		535940	5469070	qp	2.752	D	2.761		34		WW
5		505800	5513350	mdst	2.729	D			34		WW
02GPB0934		528703	5520635	mdst	2.725 ± 0.005	D			4	77	WW

Supplementary Table 3-4: U-Pb age compilation used for probability density plots and stratigraphic columns.

Sample ID[1]	Sample ID[2]	UTM Zone 15N Easting	UTM Zone 15N Northing	Rock code[3]	$^{207}Pb/^{206}Pb$ age[4] (Ga)	Int.[5]	Inh.[6]	Min.[7]	Ref.[8]	Ref.[9]	Terr-ane[10]
02GPB0934		528703	5520635	mdst	2.725 ± 0.005	D			4	77	WW
02GPB0934		528703	5520635	mdst	2.725 ± 0.005	D			4	77	WW
02GPB0934		528703	5520635	mdst	2.725 ± 0.005	D			4	77	WW
02GPB0934		528703	5520635	mdst	2.725 ± 0.005	D			4	77	WW
2		542450	5526100	grdr	2.725	I	2.725		34		WW
05GPB1457		527906	5511721	fvct	2.722 ± 0.002	D			5	77	WW
KAT20130823-04	WS-53B	479144	5476127	ttg	2.721 ± 0.007	I	2.784		76		WW
KAT20130823-04	WS-53B	479144	5476127	ttg	2.721 ± 0.007	I	2.771		76		WW
KAT20130823-04	WS-53B	479144	5476127	ttg	2.721 ± 0.007	I	2.767		76		WW
Sample 5		501770	5395540	fi	2.717	D	2.717		41		WW
Sample 5		501770	5395540	fi	2.717	D	2.825		41		WW
8		556520	5538930	fvct	2.713	I	2.719		44		WW
11		586500	5539750	cgn	2.713 ± 0.002	D			44		WW
05GPB1457		527906	5511721	fvct	2.711 ± 0.002	D			5	77	WW
02GPB0933		526975	5521827	mdst	2.711 ± 0.004	D			4	77	WW
02GPB0933		526975	5521827	mdst	2.711 ± 0.004	D			4	77	WW
02GPB0933		526975	5521827	mdst	2.711 ± 0.004	D			4	77	WW
02GPB0936		532835	5509979	mdst	2.71 ± 0.007	D			4	77	WW
02GPB0936		532835	5509979	mdst	2.71 ± 0.007	D			4	77	WW
02GPB0936		532835	5509979	mdst	2.71 ± 0.007	D			4	77	WW
02GPB0936		532835	5509979	mdst	2.71 ± 0.007	D			4	77	WW
02GPB0936		532835	5509979	mdst	2.71 ± 0.007	D			4	77	WW
DD90-39		383030	5506530	fvat	2.709 ± 0.002	D			2		WW
3		521180	5470650	sst	2.706	D			34		WW
3		521180	5470650	sst	2.706	D			34		WW
3		521180	5470650	sst	2.706	D			34		WW
3		521180	5470650	sst	2.706	D			34		WW
3		521180	5470650	sst	2.706	D			34		WW
PW202		578900	5550400	sst	2.706	D			45		WW
PW202		578900	5550400	sst	2.706	D			45		WW
PW202		578900	5550400	sst	2.706	D			45		WW
PW202		578900	5550400	sst	2.706	D			45		WW
PW202		578900	5550400	sst	2.706	D			45		WW
09GPB7722		423950	5452927	grdrmx	2.705 ± 0.003	I	2.705		5	77	WW
6 and 7		504500	5395650	mdst	2.704	D			41		WW
6 and 7		504500	5395650	mdst	2.704	D			41		WW
6 and 7		504500	5395650	mdst	2.704	D			41		WW
6 and 7		504500	5395650	mdst	2.704	D			41		WW
6 and 7		504500	5395650	mdst	2.704	D			41		WW
6 and 7		504500	5395650	mdst	2.704	D			41		WW
6 and 7		504500	5395650	mdst	2.704	D			41		WW
6 and 7		504500	5395650	mdst	2.704	D			41		WW
6 and 7		504500	5395650	mdst	2.704	D			41		WW
6 and 7		504500	5395650	mdst	2.704	D			41		WW
6 and 7		504500	5395650	mdst	2.704	D			41		WW
11GPB7755		515831	5466571	grdr	2.703 ± 0.001	I	2.703		5	77	WW
PW201		570500	5546800	cng	2.703 ± 0.002	D			45		WW

Supplementary Table 3-4: U-Pb age compilation used for probability density plots and stratigraphic columns.

Sample ID[1]	Sample ID[2]	UTM Zone 15N Easting	UTM Zone 15N Northing	Rock code[3]	$^{207}Pb/^{206}Pb$ age[4] (Ga)	Int.[5]	Inh.[6]	Min.[7]	Ref.[8]	Ref.[9]	Terr-ane[10]
10DS63		545600	5472700	sst	2.702 ± 0.002	D			65		WW
02GPB0935		528927	5513207	mdst	2.7 ± 0.002	D			4	77	WW
10		578730	5546810	cgn	2.7	D	2.708	ti	44		WW
Herony Lake pluton		432534	5443537	qdior	2.699	M		ti	26		WW
5A and 5B		522730	5467660	qp	2.699 ± 0.003	C	2.709		34		WW
5A and 5B		522730	5467660	qp	2.699 ± 0.003	C	3.028		34		WW
5A and 5B		522730	5467660	qp	2.699 ± 0.003	C	3.032		34		WW
10		578730	5546810	cgn	2.698 ± 0.004	D		ti	44		WW
	51	578810	5546610	grdr	2.698 ± 0.004	M		ti	44		WW
10DS63		545600	5472700	sst	2.698 ± 0.006	D			65		WW
09GPB0214		521228	5469892	sst	2.697 ± 0.002	D			4	77	WW
09GPB0214		521228	5469892	sst	2.697 ± 0.002	D			4	77	WW
09GPB0214		521228	5469892	sst	2.697 ± 0.002	D			4	77	WW
Aulneau granodiorite		405300	5470900	grdr	2.696	M		ti	26		WW
12		538409	5399392	cgn	2.696 ± 0.005	D			41		WW
Aulneau tonalite		396600	5456750	ton	2.693	C		ti	26		WW
05GPB7220		546416	5499170	qdior	2.692 ± 0.023	M		ti	5	77	WW
09GPB7722		423950	5452927	grdrmx	2.69 ± 0.031	T		ti	5	77	WW
09DS207		557330	5467820	sst	2.68	D			33	66	WW
09DS207		557330	5467820	sst	2.68	D			33	66	WW
09DS208		556560	5466450	sst	2.68	D			33	66	WW
09DS208		556560	5466450	sst	2.68	D			33	66	WW
Sabaskong gneiss		421026	5436612	tgn	0	T		ti	26		WW

[1] Original sample ID

[2] Secondary sample ID, typically assigned during analysis

[3] Rock abbreviations as follows: amph – amphibolite, cgn – conglomerate, d – dike, dia – diabase, dior – diorite, f – felsic, fd – felsic dike, fi – felsic intrusive, fp – feldspar porphyry, fv – felsic volcanic, fvat – fv ash tuff, fvct – felsic volcanic crystal tuff, fvm – felsic volcanic massive flow, fvt – felsic volcanic tuff, gab – gabbro, gns – gneiss, gran – granite (mx=megacrystic), grdr – granodiorite, i – intermediate, id – intermediate dike, iv – intermediate volcanic, ivbx – iv breccia, ivct – iv crystal tuff, ivlt – iv lapilli tuff, ivt – iv tuff, lgab – leucogabbro, md – mafic dike, mdst – mudstone, mnzo – monzonite, mvm – mafic volcanic massive flow, myl – mylonite, p – porphyry, peg – pegmatite, qdior – quartz diorite, qfp – quartz-feldspar porphyry, qmnzo – quartz monzonite, qp – quartz porphyry, qtz – quartz, san – sanukitoid, sed – sediment, sst – sandstone, tgn – tonalite gneiss, ton – tonalite, tron – trondhjemite, ttg – TTG, uvlt – ultramafic volcanic lapilli tuff, v – volcanic.

[4] Sample age

[5] Age interpretation: C-crystallisation age of emplacement, D-detrital, I-inheritance

[6] Inherited $^{206}Pb/^{207}Pb$ age

[7] Mineral if not zircon: ti - titanite

[8] Age reference

[9] Age reported by.

[10] Tectonic terrane abbreviations as follows: EW – Eastern Wabigoon, M – Marmion, Q – Quetico, WA – Wawa, WR – Winnipeg River, WW – Western Wabigoon.

Table references as follows: 1.Anglin et al. (1988), 2. Ayer and Davis (1997), 3. Beakhouse and Davis, unpublished data, 4. Beakhouse and Heaman, unpublished data, 5. Beakhouse and Kamo, unpublished data, 6. Beakhouse et al. (1988), 7.

Bethune et al. (2006), 8.Brown et al. (2000), 9. Brown (2002), 10. Corfu (1988), 11. Corfu (1996), 12. Corfu (2000), 13. Corfu et al. (1995), 14. D. Davis (unpublished report), 15. Davis (1993), 16. Davis (2003), 17.(Davis, 2005), 18.(Davis, 2006), 19. Davis (2007), 20.Davis (2008), 21. Davis (2009), 22. Davis (2010, written communication), 23-24. Davis and Edwards (1982), 25. Davis and Edwards (1985), 26. Davis and Edwards (1986), 27. Davis and Jackson (1988), 28. Davis and Moore (1991), 29. Davis and Smith (1991), 30. Davis et al. (1988), 31. Davis and Trowell (1982), 32. Davis et al. (1985), 33. Davis and Hamilton (2010), 34. Davis (1989), 35. Davis (1996), 36. Davis et al. (1982), 37. Davis (1998), 38. Davis (1999a), 39. Davis (1999b), 40. Davis (2002), 41Davis et al. (1989), 42. Davis et al. (1990), 43. Davis (unpublished), 44. Davis et al. (1988), 45. Fralick and Davis (1999), 46. Fralick and King (1996), 47. Galley et al. (2000), 48. Hamilton et al. (2007), 49. Heaman and Easton (2006), 50. Kamo (2004), 51. Ketchum and Davis (2001), 52. Krogh et al. (1976), 53. Kwok et al. (2000), 54. Lewis and Kamo (unpublished), 55. Lewis et al. (2012),56. Lu et al. (unpublished data), 57. McNicoll and Percival, 59. Morrison et al. (1985), 60. Percival and Helmstaedt (2004), 61. Sanborn-Barrie and Skulski (2006), 62. T. Skulski, 64. Stone (2010a), 65. D. Stone and D. Davis, 67. K.Y. Tomlinson (1999, report), 68. K.Y. Tomlinson (1999, report), 69. Tomlinson et al. (2001), 70. Tomlinson et al. (2003), 71. Tomlinson et al. (2004), 72. Whalen et al. (2002), 73. Whalen et al. (2004a), 74. Whalen et al. (2004b), 75. Zartman and Kwak (1990).

REFERENCES

Anglin, C., Franklin, J., Loveridge, W., Hunt, P. and Osterberg, S., 1988. Use of zircon U–Pb ages of felsic intrusive and extrusive rocks in eastern Wabigoon Subprovince, Ontario, to place constraints on base metal and gold mineralization. Radiogenic age and isotopic studies: report, 2: 88-2.

Ayer, J.A. and Davis, D.W., 1997. Neoarchean evolution of differing convergent margin assemblages in the Wabigoon Subprovince: geochemical and geochronological evidence from the Lake of the Woods greenstone belt, Superior Province, Northwestern Ontario. Precambrian Research, 81(3–4): 155-178.

Ayres, L.D. and Cerny, P., 1982. Metallogeny of granitoid rocks in the Canadian Shield. The Canadian Mineralogist, 20(4): 439-536.

Backeberg, N.R. and Rowe, C.D., 2012. The Marmion Shear Zone, Atikoman, Ontario: Kinematic Study of an Archean Terrane Boundary, McGill University, Montreal, Canada.

Backeberg, N.R., Rowe, C.D., van Hinsberg, V.J. and Bellefroid, E.J., 2014. Structural and metamorphic evidence for Mesoarchaean subduction in the Finlayson Lake greenstone belt, Superior Province, Ontario. Precambrian Research, 249(0): 100-114.

Barnes, S.J. and Van Kranendonk, M.J., 2014. Archean andesites in the east Yilgarn craton, Australia: Products of plume-crust interaction? Lithosphere, 6(2): 80-92.

Barton, K.E., Howell, D.G. and Vigil, J.F., 2003. The North America tapestry of time and terrain. US Geological Survey.

Beakhouse, G.P., 1991. Winnipeg River subprovince. In: H.R.W. P.C. Thurston, R.H. Sutcliffe and G.M Stott (Editor), Geology of Ontario. Ontario Geological Survey, Special Volume 4, Part 1, pp. 279-301.

Beakhouse, G.P., 2007. Structurally controlled, magmatic hydrothermal model for Archean lode gold deposits: a working hypothesis, Open File Report 6193. Ontario Geological Survey, 133 pp.

Beakhouse, G.P., Heaman, L.M. and Creaser, R.A., 1999. Geochemical and U–Pb zircon geochronological constraints on the development of a Late Archean greenstone belt at Birch Lake, Superior Province, Canada. Precambrian Research, 97(1–2): 77-97.

Beakhouse, G.P. and McNutt, R.H., 1991. Contrasting types of Late Archean plutonic rocks in Northwestern Ontario - Implications for crustal evolution in the Superior Province. Precambrian Research, 49(1-2): 141-165.

Beakhouse, G.P., McNutt, R.H. and Krogh, T.E., 1988. Comparative Rb-Sr and U-Pb zircon geochronology of late- to post-tectonic plutons in the Winnipeg River belt, Northwestern Ontario, Canada. Chemical Geology: Isotope Geoscience section, 72(4): 337-351.

Bedard, J.H., Brouillette, P., Madore, L. and Berclaz, A., 2003. Archaean cratonization and deformation in the northern Superior Province, Canada: an evaluation of plate tectonic versus vertical tectonic models. Precambrian Research, 127(1-3): 61-87.

Bédard, J.H. and Harris, L.B., 2014. Neoarchean disaggregation and reassembly of the Superior craton. Geology, 42(11): 951-954.

Bédard, J.H., Harris, L.B. and Thurston, P.C., 2013. The hunting of the snArc. Precambrian Research, 229(0): 20-48.

Bethune, K.M., Helmstaedt, H.H. and McNicoll, V.J., 2006. Structural analysis of the Miniss River and related faults, western Superior Province: post-collisional displacement initiated at terrane boundaries. Canadian Journal of Earth Sciences, 43(7): 1031-1054.

Bickford, M.E., Wooden, J.L. and Bauer, R.L., 2006. SHRIMP study of zircons from Early Archean rocks in the Minnesota River Valley: Implications for the tectonic history of the superior province. Geological Society of America Bulletin, 118(1-2): 94-108.

Blackburn, C., Bond, W., Breaks, F., Davis, D., Edwards, G., Poulsen, K., Trowell, N. and Wood, J., 1985. Evolution of Archean volcanic-sedimentary sequences of the western Wabigoon Subprovince and its margins: a review. Evolution of Archean Supracrustal Sequences, Geol. Assoc. Can. Spec. Pap, 28: 89-116.

Blackburn, C.E., John, G.W., Ayer, J. and Davis, D.W., 1991. Wabigoon subprovince. In: Thurston, P.C., Williams, H.R., Sutcliffe, R.H., Stott, G.M. (Eds.), Geology of Ontario, Ontario Geological Survey Special, vol. 4, Pt. 1. pp. 303–381.

Böhm, C.O., Heaman, L.M., Creaser, R.A. and Corkery, M.T., 2000. Discovery of pre-3.5 Ga exotic crust at the northwestern Superior Province margin, Manitoba. Geology, 28(1): 75-78.

Böhm, C.O., Heaman, L.M., Stern, R.A., Corkery, M.T. and Creaser, R.A., 2003. Nature of Assean Lake ancient crust, Manitoba: a combined SHRIMP–ID-TIMS U–Pb geochronology and Sm–Nd isotope study. Precambrian Research, 126(1–2): 55-94.

Brown, J.L., 2002. Neoarchean evolution of the western-central Wabigoon boundary zone, Brightsand Forest Area, Ontario. University of Ottawa (Canada).

Brown, J.L., Percival, J.A., White, D. and McNicoll, V., 2000. Structure and evolution of the western-central Wabigoon subprovince boundary zone at the southeastern Sturgeon belt margin, Brightsand Forest Ontario; in: Harrap, R.M., Helmstaedt, H.H. (eds) Western Superior Lithoprobe Transect 5th Annual Workshop; Lithoprobe Report #70. Lithoprobe Secretariat, University of British Columbia, pp. 19-24.

Buse, S., Lewis, D., Davis, D.W. and Hamilton, M.A., 2010. U/Pb Geochronological Results from the Lumby Lake Greenstone Belt, Wabigoon Subprovince, Northwestern Ontario.

Buse, S., Lewis, D. and Magnus, S., 2009. Field investigations in the Lumby Lake greenstone belt, northwestern Ontario: new insights into the geology, structure and economic potential.

Card, K.D., 1990. A review of the Superior Province of the Canadian Shield, a product of Archean accretion. Precambrian Research, 48(1): 99-156.

Champion, D.C. and Huston, D.L., 2016. Radiogenic isotopes, ore deposits and metallogenic terranes: Novel approaches based on regional isotopic maps and the mineral systems concept. Ore Geology Reviews, 76: 229-256.

Corfu, F., 1988. Differential response of U-Pb systems in coexisting accessory minerals, Winnipeg River Subprovince, Canadian Shield: implications for Archean crustal growth and stabilization. Contributions to Mineralogy and Petrology, 98(3): 312-325.

Corfu, F., 1996. Multistage zircon and titanite growth and inheritance in an Archean gneiss complex, Winnipeg River Subprovince, Ontario. Earth and Planetary Science Letters, 141(1): 175-186.

Corfu, F., 2000. Extraction of Pb with artificially too-old ages during stepwise dissolution experiments on Archean zircon. Lithos, 53(3–4): 279-291.

Corfu, F. and Davis, D.W., 1992. A U–Pb geochronological framework for the western Superior Province, Ontario. In: P.C. Thurston, H.R. Williams, R.H. Sutcliffe and G.M. Stott (Editors), Geology of Ontario. Ontario Geological Survey, pp. 1335–1346.

Corfu, F., Hanchar, J.M., Hoskin, P.W.O. and Kinny, P., 2003. Atlas of Zircon Textures. Reviews in Mineralogy and Geochemistry, 53(1): 469-500.

Corfu, F. and Noble, S.R., 1992. Genesis of the southern Abitibi greenstone belt, Superior Province, Canada: Evidence from zircon Hf isotope analyses using a single filament technique. Geochimica et Cosmochimica Acta, 56(5): 2081-2097.

Corfu, F. and Stone, D., 1998. Age structure and orogenic significance of the Berens River composite batholiths, western Superior Province. Canadian Journal of Earth Sciences, 35(10): 1089-1109.

Corfu, F. and Stott, G., 1986. U-Pb ages for late magmatism and regional deformation in the Shebandowan Belt, Superior Province, Canada. Canadian Journal of Earth Sciences, 23(8): 1075-1082.
Corfu, F., Stott, G. and Breaks, F., 1995. U-Pb geochronology and evolution of the English River Subprovince, an Archean low P-high T metasedimentary belt in the Superior Province. Tectonics, 14(5): 1220-1233.
Corfu, F. and Stott, G.M., 1993. U–Pb geochronology of the central Uchi Subprovince, Superior Province. Canadian Journal of Earth Sciences, 30(6): 1179-1196.
Corfu, F. and Stott, G.M., 1996. The Oldest Rock on EarthHf isotopic composition and age constraints on the evolution of the Archean central Uchi Subprovince, Ontario, Canada. Precambrian Research, 78(1): 53-63.
Corfu, F. and Stott, G.M., 1998. Shebandowan greenstone belt, western Superior Province: U-Pb ages, tectonic implications, and correlations. GSA Bulletin, 110(11): 1467-1484.
Corfu, F., W. Davis, D., Stone, D. and Moore, M.L., 1998. Chronostratigraphic constraints on the genesis of Archean greenstone belts, northwestern Superior Province, Ontario, Canada. Precambrian Research, 92(3): 277-295.
Corfu, F. and Wallace, H., 1986. U–Pb zircon ages for magmatism in the Red Lake greenstone belt, northwestern Ontario. Canadian Journal of Earth Sciences, 23(1): 27-42.
Davis, D.W., 1989. Precise U-Pb age constraints on the tectonic evolution of the western Wabigoon subprovince, Superior Province, Ontario. Unpublished report, Energy, Mines and Resources Canada, 30p. .
Davis, D.W., 1993. Report on U-Pb Geochronology in the Atikokan Area, Wabigoon Subprovince, Toronto. Royal Ontario Museum Report, Ontario, Canada. 9p.
Davis, D.W., 1996. Provenance and depositional age constraints on sedimentation in the western Superior transect area from U–Pb ages of zircons, Western Superior Lithoprobe Transect 2nd Annual Workshop. Lithoprobe Secretariat, The University of British Columbia, Vancouver, BC, Lithoprobe Report, pp. 18-23.
Davis, D.W., 1998. Report on U-Pb geochronology of rocks from the Onaman Lake belt. Unpublished report to the Ontario Geological Survey, 1998, 19p. .
Davis, D.W., 1999a. Report on U-Pb geochronology of rocks from the Onaman Lake belt. Unpublished report to the Ontario Geological Survey, 21p. .
Davis, D.W., 1999b. U-Pb geochronology of zircons from the western Superior region. Unpublished report to P. Fralick, Lakehead University, 1999.
Davis, D.W., 2002. Report on U-Pb geochronology of rocks from the Onaman greenstone belt. Unpublished report to the Ontario Geological Survey, 12p.
Davis, D.W., 2003. U-Pb geochronology of rocks from the Lac Des Illes area, northwest Ontario; unpublished report of the Earth Sciences Department, Royal Ontario Museum, 100 Queen's Park, Toronto, Ontario.
Davis, D.W., 2005. Geochronology of granitoid rocks in the western Superior Province: applications of abrasion, anneal-leach and garnet-armour techniques to extraction of precise U-Pb ages from altered mineral populations; unpublished report to the Ontario Geological Survey by the Jack Satterly Geochronology Laboratory, Department of Geology, University of Toronto, Earth Sciences Centre, 22 Russell Street, Toronto, Ontario.
Davis, D.W., 2006. Geochronology of rocks from the Marmion terrane and Hudson Bay Lowland basement, western Superior Province; unpublished report to the Ontario Geological Survey by the Jack Satterly Geochronology Laboratory, Department of Geology, University of Toronto, Earth Sciences Centre, 22 Russell Street, Toronto, Ontario.
Davis, D.W., 2008. OGS geochronology report—Central Wabigoon project; unpublished report to the Ontario Geological Survey by the Jack Satterly Geochronology Laboratory, Department of Geology, University of Toronto, Earth Sciences Centre, 22 Russell Street, Toronto, Ontario.
Davis, D.W., 2009. OGS geochronology report - Central Wabigoon project; unpublished report to the Ontario Geological Survey by the Jack Satterly Geochronology Laboratory, Department of Geology, University of Toronto, Earth Sciences Centre, 22 Russell Street, Toronto, Ontario.
Davis, D.W., Amelin, Y., Nowell, G.M. and Parrish, R.R., 2005. Hf isotopes in zircon from the western Superior province, Canada: Implications for Archean crustal development and evolution of the depleted mantle reservoir. Precambrian Research, 140(3–4): 132-156.

Davis, D.W., Blackburn, C.E. and Krogh, T.E., 1982. Zircon U–Pb ages from the Wabigoon–Manitou Lakes region, Wabigoon Subprovince, northwest Ontario. Canadian Journal of Earth Sciences, 19(2): 254-266.

Davis, D.W. and Edwards, G.R., 1982. Zircon U–Pb ages from the Kakagi Lake area, Wabigoon Subprovince, northwest Ontario. Canadian Journal of Earth Sciences, 19(6): 1235-1245.

Davis, D.W. and Edwards, G.R., 1985. The petrogenesis and melallogenesis of the Atikwa-Lawerence volcanic-plutonic terrane. Ontario Geological Survey, Miscellaneous Paper 127, 101-111.

Davis, D.W. and Edwards, G.R., 1986. Crustal evolution of Archean rocks in the Kakagi Lake area, Wabigoon Subprovince, Ontario, as interpreted from high-precision U-Pb geochronology. Canadian Journal of Earth Sciences, 23(2): 182-192.

Davis, D.W. and Hamilton, M.A., 2010. OGS Geochronology Report Atikokan Region. Report to the Ontario Geological Survey. 55p.

Davis, D.W. and Jackson, M.C., 1988. Geochronology of the Lumby Lake greenstone belt: A 3 Ga complex within the Wabigoon subprovince, northwest Ontario. GSA Bulletin, 100(6): 818-824.

Davis, D.W., Krogh, T.E., Hinzer, J. and Nakamura, E., 1985. Zircon dating of polycyclic volcanism at Sturgeon Lake and implications for base metal mineralization. Economic Geology, 80(7): 1942-1952.

Davis, D.W. and Moore, M., 1991. Geochronology in the western Superior Province. Unpublished report, Royal Ontario Museum.

Davis, D.W., Pezzutto, F. and Ojakangas, R.W., 1990. The age and provenance of metasedimentary rocks in the Quetico Subprovince, Ontario, from single zircon analyses: implications for Archean sedimentation and tectonics in the Superior Province. Earth and Planetary Science Letters, 99(3): 195-205.

Davis, D.W., Poulsen, K.H. and Kamo, S.L., 1989. New Insights into Archean Crustal Development from Geochronology in the Rainy Lake Area, Superior Province, Canada. Journal of Geology, 97(4): 379-398.

Davis, D.W. and Smith, P.M., 1991. Archean gold mineralization in the Wabigoon Subprovince, a product of crustal accretion: evidence from U-Pb geochronology in the Lake of the Woods area, Superior Province, Canada. The Journal of Geology: 337-353.

Davis, D.W., Sutcliffe, R.H. and Trowell, N.F., 1988. Geochronological constraints on the tectonic evolution of a late Archaean greenstone belt, Wabigoon Subprovince, Northwest Ontario, Canada. Precambrian Research, 39(3): 171-191.

Davis, D.W. and Trowell, N.F., 1982. U-Pb zircon ages from the eastern Savant Lake-Crow Lake metavolcanic-metasedimentary belt, northwest Ontario. Canadian Journal of Earth Sciences, 19(4): 868-877.

De la Roche, H., Leterrier, J., Grandclaude, P. and Marchal, M., 1980. A classification of volcanic and plutonic rocks using R1R2-diagram and major-element analyses — Its relationships with current nomenclature. Chemical Geology, 29(1): 183-210.

Devaney, J.R. and Williams, H.R., 1989. Evolution of an Archean subprovince boundary: a sedimentological and structural study of part of the Wabigoon-Quetico boundary in northern Ontario. Canadian Journal of Earth Sciences, 26(5): 1013-1026.

Drummond, M., Defant, M. and Kepezhinskas, P., 1996. Petrogenesis of slab-derived trondhjemite–tonalite-dacite/adakite magmas. Geological Society of America Special Papers, 315: 205-215.

Duncan, A., Erlank, A., Marsh, J. and Cox, K., 1984. Regional geochemistry of the Karoo igneous province.

Edwards, G. and Sutcliffe, R., 1980. Archean granitoid terranes of the western Superior Province, Ontario, Program with Abstracts, pp. 50.

Edwards, G.R. and Stauffer, M.R., 1999. Polyphase deformation and crustal evolution in the Pipestone Lake area of the Archean Wabigoon Subprovince, Superior Province, Canada. Canadian Journal of Earth Sciences, 36(3): 459-477.

Ermanovics, I., McRitchie, W. and Houston, W., 1979. Petrochemistry and tectonic setting of plutonic rocks of the Superior Province in Manitoba, Trondhjemites, Dacites and Related Rocks. Elsevier Amsterdam, pp. 323-362.

Fenwick, K.G., 1976. M2297 Finlayson Lake, Rainy River District, Map, 2000 Series. Ontario Ministry of Northern Development and Mines, Ontario Geological Survey, pp. 52B13, Finlayson Lake, Freeborn, Ontario, Canada, Schwenger, Steeprock Lake.

Foley, S., Tiepolo, M. and Vannucci, R., 2002. Growth of early continental crust controlled by melting of amphibolite in subduction zones. Nature, 417(6891): 837-840.

Fralick, P. and Davis, D.W., 1999. The Seine-Coutchiching problem revisited: Sedimentology, geochronology and geochemistry of sedimentary units in the Rainy Lake and Sioux Lookout areas. Lithoprobe Report #70, Lithoprobe Secrectariate, University of British Columbia, p 66-75.

Fralick, P., Hollings, P. and King, D., 2008. Stratigraphy, geochemistry, and depositional environments of Mesoarchean sedimentary units in western Superior Province: Implications for generation of early crust. In: K.C. Condie and V. Pease (Editors), When Did Plate Tectonics Begin on Planet Earth. Geological Society of America Special Papers, pp. 77-96.

Fralick, P. and King, D., 1996. Mesoarchean evolution of western Superior Province: evidence from metasedimentary sequences near Atikokan, Western Superior Transect, Second Annual Workshop, Lithoprobe Secretariat, University of British Columbia, Vancouver, British Columbia, pp. 29-35.

Fralick, P., Purdon, R.H. and Davis, D.W., 2006. Neoarchean trans-subprovince sediment transport in southwestern Superior Province: sedimentological, geochemical, and geochronological evidence. Canadian Journal of Earth Sciences, 43(7): 1055-1070.

Frost, B.R., Barnes, C.G., Collins, W.J., Arculus, R.J., Ellis, D.J. and Frost, C.D., 2001. A geochemical classification for granitic rocks. Journal of petrology, 42(11): 2033-2048.

Galley, A., Breemen, O.v. and Franklin, J., 2000. The relationship between intrusion-hosted Cu-Mo mineralization and the VMS deposits of the Archean Sturgeon Lake mining camp, northwestern Ontario. Economic Geology, 95(7): 1543-1550.

Gardiner, N.J., Hickman, A.H., Kirkland, C.L., Lu, Y., Johnson, T. and Zhao, J.-X., 2017. Processes of crust formation in the early Earth imaged through Hf isotopes from the East Pilbara Terrane. Precambrian Research, 297(Supplement C): 56-76.

Geological Survey of Canada, 2013. Canadian Geochronology Knowledgebase. In: N.R.C. Earth Science Sector (Editor).

Goldich, S. and Fischer, L.B., 1986. Air abrasion experiments in U-Pb dating of zircon. Chemical Geology: Isotope Geoscience section, 58(3): 195-215.

Griffin, W.L., Wang, X., Jackson, S.E., Pearson, N.J., O'Reilly, S.Y., Xu, X. and Zhou, X., 2002. Zircon chemistry and magma mixing, SE China: In-situ analysis of Hf isotopes, Tonglu and Pingtan igneous complexes. Lithos, 61(3–4): 237-269.

Halla, J., van Hunen, J., Heilimo, E. and Hölttä, P., 2009. Geochemical and numerical constraints on Neoarchean plate tectonics. Precambrian Research, 174(1): 155-162.

Hamilton, M.A., Davis, D.W. and Kamo, S.L., 2007. OGS base sample geochronology report—2007; unpublished report of the Jack Satterly Geochronology Laboratory, Department of Geology, University of Toronto, Earth Sciences Centre, 22 Russell Street, Toronto, Ontario, 50p.

Hamilton, W.B., 1998. Archean magmatism and deformation were not products of plate tectonics. Precambrian Research, 91(1): 143-179.

Harris, N.B.W., 1976. The significance of garnet and cordierite from the Sioux Lookout region of the English River gneiss belt, Northern Ontario. Contributions to Mineralogy and Petrology, 55(1): 91-104.

Heaman, L.M. and Easton, R.M., 2006. Preliminary U/Pb geochronology results from the Lake Nipigon Region Geoscience Initiative; Ontario Geological Survey, MRD-191.

Henry, P., Stevenson, R.K. and Gariepy, C., 1998. Late Archean mantle composition and crustal growth in the Western Superior Province of Canada: Neodymium and lead isotopic evidence from the Wawa, Quetico, and Wabigoon subprovinces. Geochimica Et Cosmochimica Acta, 62(1): 143-157.

Henry, P., Stevenson, R.K., Larbi, Y. and Gariépy, C., 2000. Nd isotopic evidence for Early to Late Archean (3.4–2.7 Ga) crustal growth in the Western Superior Province (Ontario, Canada). Tectonophysics, 322(1–2): 135-151.

Herzberg, C., 2014. Early Earth: Archaean drips. Nature Geosci, 7(1): 7-8.

Herzberg, C. and Rudnick, R., 2012. Formation of cratonic lithosphere: An integrated thermal and petrological model. Lithos, 149: 4-15.

Hollings, P. and Wyman, D., 1999. Trace element and Sm-Nd systematics of volcanic and intrusive rocks from the 3 Ga Lumby Lake Greenstone belt, Superior Province: evidence for Archean plume-arc interaction. Lithos, 46(2): 189-213.

Hollings, P., Wyman, D. and Kerrich, R., 1999. Komatiite-basalt-rhyolite volcanic associations in Northern Superior Province greenstone belts: significance of plume-arc interaction in the generation of the proto continental Superior Province. Lithos, 46(1): 137-161.

Hynes, A. and Song, Z., 2006. Variable unroofing in the western Superior Province—metamorphic evidence and possible origin. Canadian Journal of Earth Sciences, 43(7): 805-819.

Irvine, T.N. and Baragar, W.R.A., 1971. A guide to the chemical classification of the common volcanic rocks. Canadian Journal of Earth Sciences, 8(5): 523-548.

Johnson, T.E., Brown, M., Gardiner, N.J., Kirkland, C.L. and Smithies, R.H., 2017. Earth's first stable continents did not form by subduction. Nature, 543(7644): 239-242.

Kamo, S., 2004. U-Pb geochronological investigations of rocks from the Lac des Iles area, northwestern Ontario, the Michipicoten greenstone belt, Wawa, and the Tomiko terrane, Mattawa, Ontario; unpublished report of the Jack Satterly Geochronology Laboratory, Department of Geology, University of Toronto, Earth Sciences Centre, 22 Russell Street, Toronto, Ontario.

Kemp, A. and Hawkesworth, C., 2013. Growth and differentiation of the continental crust from isotope studies of accessory minerals. In: R. Rudnick (Editor), Treatise on Geochemistry. The Crust. The Crust, vol. 12, second ed. Elsevier Science, Oxford.

Ketchum, J.W.F. and Davis, D.W., 2001. U-Pb geochronological results from the Abitibi greenstone belt, Sachigo subprovince, and Onaman-Tashota greenstone belt, Superior Province, Ontario; Unpublished report for the Ontario Geological Survey, 2001, 24p. .

Krogh, T., Harris, N. and Davis, G., 1976. Archean rocks from the eastern Lac Seul region of the English River Gneiss Belt, northwestern Ontario, part 2. Geochronology. Canadian Journal of Earth Sciences, 13(9): 1212-1215.

Kuno, H., 1966. Lateral variation of basalt magma type across continental margins and Island Arcs. Bulletin Volcanologique, 29(1): 195-222.

Kwok, Y.-Y., Amelin, Y., Kamo, S.L. and Davis, D.W., 2000. Report on U-Pb geochronology of rocks from the Onaman greenstone belt. Unpublished report to the Ontario Geological Survey, 38p. .

Lafrance, B., DeWolfe, J.C. and Stott, G.M., 2004. A structural reappraisal of the Beardmore-Geraldton Belt at the southern boundary of the Wabigoon subprovince, Ontario, and implications for gold mineralization. Canadian Journal of Earth Sciences, 41(2): 217-235.

Langford, F.F. and Morin, J.A., 1976. Development of the Superior Province of Northwestern Ontario by merging island arcs. American Journal of Science, 276(9): 1023-1034.

Laurent, O., Martin, H., Moyen, J.F. and Doucelance, R., 2014. The diversity and evolution of late-Archean granitoids: Evidence for the onset of "modern-style" plate tectonics between 3.0 and 2.5 Ga. Lithos, 205: 208-235.

Lewis, D., Kamo, S.L. and Lodge, R.W.D., 2012. New geochemical and geochronological results from the Rowan Lake area, northwestern Ontario. Summary of Field Work and Other Activities 2012, Ontario Geological Survey, Open File Report 6280, p. 9-1 to 9-10.

Lin, S., Parks, J., Heaman, L.M., Simonetti, A. and Corkery, M.T., 2013. Diapirism and sagduction as a mechanism for deposition and burial of "Timiskaming-type" sedimentary sequences, Superior Province: Evidence from detrital zircon geochronology and implications for the Borden Lake conglomerate in the exposed middle to lower crust in the Kapuskasing uplift. Precambrian Research, 238: 148-157.

Lodge, R.W.D., Gibson, H.L., Stott, G.M., Hudak, G.J., Jirsa, M.A. and Hamilton, M.A., 2013. New U–Pb geochronology from Timiskaming-type assemblages in the Shebandowan and Vermilion greenstone belts, Wawa subprovince, Superior Craton: Implications for the Neoarchean development of the southwestern Superior Province. Precambrian Research, 235: 264-277.

Ludwig, K., 2009. SQUID 2: A User's Manual, rev. 12 Apr, 2009. Berkeley Geochron. Ctr. Spec. Pub. 5 110 p.

Martin, H. and Moyen, J.-F., 2002. Secular changes in tonalite-trondhjemite-granodiorite composition as markers of the progressive cooling of Earth. Geology, 30(4): 319-322.

Martin, H., Moyen, J.-F., Guitreau, M., Blichert-Toft, J. and Le Pennec, J.-L., 2014. Why Archaean TTG cannot be generated by MORB melting in subduction zones. Lithos, 198–199: 1-13.

Martin, H., Moyen, J.F. and Rapp, R., 2010. The sanukitoid series: magmatism at the Archaean-Proterozoic transition. Earth and Environmental Science Transactions of the Royal Society of Edinburgh, 100: 15-33.

Melnyk, M., Davis, D.W., Cruden, A.R. and Stern, R.A., 2006. U–Pb ages constraining structural development of an Archean terrane boundary in the Lake of the Woods area, western Superior Province, Canada. Canadian Journal of Earth Sciences, 43(7): 967-993.

Morrison, D.A., Davis, D.W., Wooden, J.L., Bogard, D.D., Maczuga, D.E., Phinney, W.C. and Ashwal, L.D., 1985. Age of the Mulcahy Lake intrusion, northwest Ontario, and implications for the evolution of greenstone-granite terrains. Earth and Planetary Science Letters, 73(2): 306-316.

Moser, D.E., 1994. The geology and structure of the mid-crustal Wawa gneiss domain: a key to understanding tectonic variation with depth and time in the late Archean Abitibi–Wawa orogen. Canadian Journal of Earth Sciences, 31(7): 1064-1080.

Moyen, J.-F., 2011. The composite Archaean grey gneisses: Petrological significance, and evidence for a non-unique tectonic setting for Archaean crustal growth. Lithos, 123(1–4): 21-36.

Moyen, J.-F. and Martin, H., 2012. Forty years of TTG research. Lithos, 148: 312-336.

Ontario Geological Survey, 2011. 1: 250 000 Scale Bedrock Geology of Ontario-Revision 1, MRD 126-REV-1. Ontario Geological Survey.

Pan, Y., E. Fleet, M. and Heaman, L., 1998. Thermo-tectonic evolution of an Archean accretionary complex: U–Pb geochronological constraints on granulites from the Quetico Subprovince, Ontario, Canada. Precambrian Research, 92(2): 117-128.

Pan, Y. and Fleet, M.E., 1993. Polymetamorphism in the Archean Hemlo – Heron Bay greenstone belt, Superior Province: P–T variations and implications for tectonic evolution. Canadian Journal of Earth Sciences, 30(5): 985-996.

Pan, Y. and Fleet, M.E., 1999. Kyanite in the western Superior Province of Ontario; implications for Archean accretionary tectonics. The Canadian Mineralogist, 37(2): 359-373.

Parmenter, A.C., Lin, S.F. and Corkery, M.T., 2006. Structural evolution of the Cross Lake greenstone belt in the northwestern Superior Province, Manitoba: implications for relationship between vertical and horizontal tectonism. Canadian Journal of Earth Sciences, 43(7): 767-787.

Patiño Douce, A.E., 1997. Generation of metaluminous A-type granites by low-pressure melting of calc-alkaline granitoids. Geology, 25(8): 743-746.

Peate, D.W., 1997. The Paraná-Etendeka Province. Large igneous provinces: Continental, oceanic, and planetary flood volcanism: 217-245.

Percival, J.A., 1989. A regional perspective of the Quetico metasedimentary belt, Superior Province, Canada. Canadian Journal of Earth Sciences, 26(4): 677-693.

Percival, J.A. and Helmstaedt, H., 2004. Insights on Archean continent—ocean assembly, western Superior Province, from new structural, geochemical and geochronological observations: introduction and summary. Precambrian Research, 132(3): 209-212.

Percival, J.A., McNicoll, V., Brown, J.L. and Whalen, J.B., 2004. Convergent margin tectonics, central Wabigoon subprovince, Superior Province, Canada. Precambrian Research, 132(3): 213-244.

Percival, J.A., Sanborn-Barrie, M., Skulski, T., Stott, G.M., Helmstaedt, H. and White, D.J., 2006. Tectonic evolution of the western Superior Province from NATMAP and Lithoprobe studies. Canadian Journal of Earth Sciences, 43(7): 1085-1117.

Percival, J.A., Skulski, T., Sanborn-Barrie, M., Stott, G.M., Leclair, A.D., Corkery, M.T. and Boily, M., 2012. Geology and tectonic evolution of the Superior Province, Canada. Tectonic Styles in Canada: The Lithoprobe Perspective, Special Paper, 49: 321-378.

Percival, J.A. and West, G.F., 1994. The Kapuskasing uplift: a geological and geophysical synthesis. Canadian Journal of Earth Sciences, 31(7): 1256-1286.

Percival, J.A. and Williams, H.R., 1989. Late Archean Quetico accretionary complex, Superior province, Canada. Geology, 17(1): 23-25.

Perkins, D. and Chipera, S.J., 1985. Garnet-orthopyroxene-plagioclase-quartz barometry: refinement and application to the English River subprovince and the Minnesota River valley. Contributions to Mineralogy and Petrology, 89(1): 69-80.

Poulsen, K.H., Borradaile, G.J. and Kehlenbeck, M.M., 1980. An inverted Archean succession at Rainy Lake, Ontario. Canadian Journal of Earth Sciences, 17(10): 1358-1369.

Rapp, R.P., Norman, M.D., Laporte, D., Yaxley, G.M., Martin, H. and Foley, S.F., 2010. Continent Formation in the Archean and Chemical Evolution of the Cratonic Lithosphere: Melt–Rock Reaction Experiments at 3–4 GPa and Petrogenesis of Archean Mg-Diorites (Sanukitoids). Journal of Petrology, 51(6): 1237-1266.

Sanborn-Barrie, M., Parker, J. and Skulski, T., 2001. Three hundred million years of tectonic history recorded by the Red Lake greenstone belt, Ontario. Geological Survey of Canada, Current Research 2001-C19, 14 pp.

Sanborn-Barrie, M. and Skulski, T., 2006. Sedimentary and structural evidence for 2.7 Ga continental arc-oceanic-arc collision in the Savant-Sturgeon greenstone belt, western Superior Province, Canada. Canadian Journal of Earth Sciences, 43(7): 995-1030.

Satkoski, A.M., Bickford, M.E., Samson, S.D., Bauer, R.L., Mueller, P.A. and Kamenov, G.D., 2013. Geochemical and Hf–Nd isotopic constraints on the crustal evolution of Archean rocks from the Minnesota River Valley, USA. Precambrian Research, 224: 36-50.

Schaefer, S.J. and Morton, P., 1991. Two komatiitic pyroclastic units, Superior Province, northwestern Ontario: their geology, petrography, and correlation. Canadian Journal of Earth Sciences, 28(9): 1455-1470.

Shirey, S.B. and Hanson, G.N., 1986. Mantle heterogeneity and crustal recycling in Archean granite-greenstone belts: Evidence from Nd isotopes and trace elements in the Rainy Lake area, Superior Province, Ontario, Canada. Geochimica et Cosmochimica Acta, 50(12): 2631-2651.

Skjerlie, K.P. and Johnston, A.D., 1993. Fluid-absent melting behavior of an F-rich tonalitic gneiss at mid-crustal pressures: implications for the generation of anorogenic granites. Journal of Petrology, 34(4): 785-815.

Skulski, T., Corkery, M., Stone, D., Whalen, J. and Stern, R., 2000. Geological and geochronological investigations in the Stull Lake–Edmund Lake greenstone belt and granitoid rocks of the northwestern Superior Province. Report of activities: 117-128.

Smithies, R.H. and Champion, D.C., 2000. The Archaean High-Mg Diorite Suite: Links to Tonalite–Trondhjemite–Granodiorite Magmatism and Implications for Early Archaean Crustal Growth. Journal of Petrology, 41(12): 1653-1671.

Smithies, R.H., Champion, D.C. and Van Kranendonk, M.J., 2009. Formation of Paleoarchean continental crust through infracrustal melting of enriched basalt. Earth and Planetary Science Letters, 281(3–4): 298-306.

Stern, R.A. and Hanson, G.N., 1991. Archean high-Mg granodiorite: a derivative of light rare earth element-enriched monzodiorite of mantle origin. Journal of Petrology, 32(1): 201-238.

Stern, R.A., Hanson, G.N. and Shirey, S.B., 1989. Petrogenesis of mantle-derived, LILE-enriched Archean monzodiorites and trachyandesites (sanukitoids) in southwestern Superior Province. Canadian Journal of Earth Sciences, 26(9): 1688-1712.

Stevenson, R.K., Henry, P. and Gariepy, C., 2009. Isotopic and geochemical evidence for differentiation and crustal contamination from granitoids of the Berens river subprovince, Superior province, Canada. Precambrian Research, 168(1-2): 123-133.

Stone, D., 2007. Steep Rock Revisited, Summary of Field Work and Other Activities, pp. 10-1 to 10-8.

Stone, D., 2010a. Precambrian geology of the central Wabigoon Subprovince area, northwestern Ontario. Ontario Geological Survey, Open File Report 5422: 130.

Stone, D., 2010b. Precambrian Geology, central Wabigoon Subprovince area, northwestern Ontario. Ontario Geological Survey.

Stone, D., Davis, D.W., Hamilton, M.A. and Falcon, A., 2010. Interpretation of 2009 Geochronology in the Central Wabigoon Subprovince and Bending Lake Areas, Northwestern Ontario.

Stone, D., Kamineni, D.C. and Jackson, M.C., 1992. Precambrian geology of the Atikokan area, northwestern Ontario; . Geological Survey of Canada, Bulletin 405: 106p.

Stone, D., Tomlinson, K., Davis, D., Fralick, P., Hallé, J., Percival, J. and Pufahl, P., 2002. Geology and tectonostratigraphic assemblages, south–central Wabigoon Subprovince, Ontario Geological Survey, Preliminary Map P. 3448.

Stott, G., 1997. The Superior Province, Canada. In: M.J.d. Wit and L.D. Ashwal (Editors), Greenstone Belts. Oxford Clarendon Press, Oxford Monograph on Geology and Geophysics 35, pp. 480-507.

Stott, G. and Corfu, F., 1991. Uchi subprovince. Geology of Ontario. Edited by PC Thurston, HR Williams, RH Sutcliffe, and GM Stott. Ontario Geological Survey, Special, 4(Part 1): 145-238.

Stott, G.M., 2011. A Revised Terrane Subdivision of the Superior Province in Ontario; Ontario Geological Survey, Miscellaneous Release--Data 278.

Stott, G.M., Davis, D.W., Parker, J.R., Straub, K.J. and Tomlinson, K.Y., 2002. Geology and tectonostratigraphic assemblages, eastern Wabigoon Subprovince, Ontario. Ontario Geological Survey Map P3449 and Geological Survey of Canada, Open File 4285; scale 1 : 250 000.

Sun, S.S. and McDonough, W.F., 1989. Chemical and isotopic systematic of oceanic basalts: implication for mantle composition and processes. In: M.J.N. A.D. Sunders (Editor), Magmatic in Oceanic Basins, Special Publication 42. Geology Society of London, pp. 313–345.

Thurston, P., Osmani, I. and Stone, D., 1991. Northwestern Superior Province: review and terrane analysis. Geology of Ontario. Edited by PC Thurston, HR Williams, RH Sutcliffe, and GM Stott. Ontario Geological Survey, Special, 4(Part 1): 81-144.

Tomlinson, K., Davis, D., Stone, D. and Hart, T., 2003. U–Pb age and Nd isotopic evidence for Archean terrane development and crustal recycling in the south-central Wabigoon subprovince, Canada. Contributions to Mineralogy and Petrology, 144(6): 684-702.

Tomlinson, K.Y., Davis, D.W., Percival, J.A., Hughes, D.J. and Thurston, P.C., 2002. Mafic to felsic magmatism and crustal recycling in the Obonga Lake greenstone belt, western Superior Province: evidence from geochemistry, Nd isotopes and U-Pb geochronology. Precambrian Research, 114(3-4): 295-325.

Tomlinson, K.Y., Davis, D.W., Stone, D. and Hart, T.R., 2001. New U and Nd geochronology for volcanic and granitoid rocks of the central Wabigoon Subprovince; in 2001 Western Superior Transect, 7th Annual Meeting, Lithoprobe Secretariat, University of British Columbia, Vancouver, British Columbia.

Tomlinson, K.Y., Hughes, D.J., Thurston, P.C. and Hall, R.P., 1999. Plume magmatism and crustal growth at 2.9 to 3.0 Ga in the Steep Rock and Lumby Lake area, Western Superior Province. Lithos, 46(1): 103-136.

Tomlinson, K.Y., Stevenson, R.K., Hughes, D.J., Hall, R.P., Thurston, P.C. and Henry, P., 1998. The Red Lake greenstone belt, Superior Province: evidence of plume-related magmatism at 3 Ga and evidence of an older enriched source. Precambrian Research, 89(1-2): 59-76.

Tomlinson, K.Y., Stott, G.M., Percival, J.A. and Stone, D., 2004. Basement terrane correlations and crustal recycling in the western Superior Province: Nd isotopic character of granitoid and felsic volcanic rocks in the Wabigoon subprovince, N. Ontario, Canada. Precambrian Research, 132(3): 245-274.

Turek, A., Sage, R. and Schmus, W.V., 1992. Advances in the U-Pb zircon geochronology of the Michipicoten greenstone belt, Superior Province, Ontario. Canadian Journal of Earth Sciences, 29(6): 1154-1165.

Valli, F., Guillot, S. and Hattori, K.H., 2004. Source and tectono-metamorphic evolution of mafic and pelitic metasedimentary rocks from the central Quetico metasedimentary belt, Archean Superior Province of Canada. Precambrian Research, 132(1–2): 155-177.

Vervoort, J.D. and Kemp, A.I.S., 2016. Clarifying the zircon Hf isotope record of crust–mantle evolution. Chemical Geology, 425: 65-75.

Watson, E.B. and Harrison, T.M., 1983. Zircon saturation revisited: temperature and composition effects in a variety of crustal magma types. Earth and Planetary Science Letters, 64(2): 295-304.

Whalen, J.B., McNicoll, V.J., Galley, A.G. and Longstaffe, F.J., 2004a. Tectonic and metallogenic importance of an Archean composite high- and low-Al tonalite suite, Western Superior Province, Canada. Precambrian Research, 132(3): 275-301.

Whalen, J.B., Percival, J.A., McNicoll, V.J. and Longstaffe, F.J., 2002. A Mainly Crustal Origin for Tonalitic Granitoid Rocks, Superior Province, Canada: Implications for Late Archean Tectonomagmatic Processes. Journal of Petrology, 43(8): 1551-1570.

Whalen, J.B., Percival, J.A., McNicoll, V.J. and Longstaffe, F.J., 2004b. Geochemical and isotopic (Nd–O) evidence bearing on the origin of late- to post-orogenic high-K granitoid rocks in the Western Superior Province: implications for late Archean tectonomagmatic processes. Precambrian Research, 132(3): 303-326.

White, D.J., Musacchio, G., Helmstaedt, H.H., Harrap, R.M., Thurston, P.C., van der Velden, A. and Hall, K., 2003. Images of a lower-crustal oceanic slab: Direct evidence for tectonic accretion in the Archean western Superior province. Geology, 31(11): 997-1000.

Wilks, M.E. and Nisbet, E.G., 1988. Stratigraphy of the Steep Rock Group, northwest Ontario: A major Archaean unconformity and Archaean stromatolites. Canadian Journal of Earth Sciences, 25: 370–391.

Williams, H., 1991. Quetico subprovince. Geology of Ontario, Ontario Geological Survey, Special 4(Part 1): 383-403.

Wyman, D. and Kerrich, R., 2010. Mantle plume – volcanic arc interaction: consequences for magmatism, metallogeny, and cratonization in the Abitibi and Wawa subprovinces, Canada. Canadian Journal of Earth Sciences, 47(5): 565-589.

Wyman, D.A., Hollings, P. and Biczok, J., 2011. Crustal evolution in a cratonic nucleus: Granitoids and felsic volcanic rocks of the North Caribou Terrane, Superior Province Canada. Lithos, 123(1–4): 37-49.

Zartman, R.E. and Kwak, L.M., 1990. U-Th-Pb systematics in zircon and titanite. Isotopic Studies of the Eye-Dashwa Lakes Pluton and the Long-term Integrity of Whole-rock and Mineral Systems. At. Energy Can., Ltd., Pinawa, Man., AECL-10120.